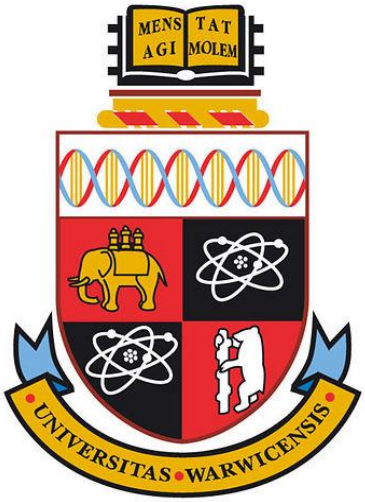

Bovine respiratory syncytial virus modulation of NF-κB p65 mediated innate immune responses

by

Fatoumatta Jobe

A thesis submitted in partial fulfilment of the requirements for the degree of **Doctor of Philosophy** in Biological Sciences

University of Warwick

School of Life Sciences

April 2021

Table of Contents

List of figures and tables

Acknowledgements

First, I would like to thank my supervisor Dr Dalan Bailey for the opportunity to be a part of his group. I truly appreciate him taking over my supervision so far into my studentship and completely turning the project around. His guidance, support and in-depth virology knowledge has really helped make the project a success. Thank you for not only challenging me Dalan, but for being a great mentor and fuelling my passion in virology. I am immensely grateful.

I would also like to thank the rest of my supervisory team (Dr Efrain Guzman, Dr Bruno Frenguelli, and Dr Simon Graham) and advisory panel (Professor Keith Leppard, Dr Julian Seago and Dr Vardis Ntoukakis) for their guidance. I am also grateful to all past and present members of the Viral glycoproteins group: Dr James Kelly, Nazia Thakur, Leanne Logan, Dr Carina Conceição, Dr Stacey Human, Michal Varga, Ahmed Mohamed, and Dr Giulia Gallo, for their help with my work and very stimulating discussions. It was great working in a positive environment. I must also thank Jennifer Simpson for her collaboration on the project.

My most special appreciation goes to my husband, my rock, Pa Alasan Jobe for being my biggest cheerleader. He has always believed in me and provided endless support and love along the way. Our lovely daughter Sainabou ("we have been together for a long time", as she so fondly put it) and delightful son Sidia for giving us so much joy and purpose in life. Special thanks to my friends and family, especially my mum Binta Ceesay 'Ngari jarr mew', my brother Alieu and Sisters Maimuna, Awa, Aji Mariam, Haddijatou and Aminata for their encouragement, support and for always listening.

Finally, to my Dad Ansumana Jarju. My interest in science started because of you. Even though you are no longer with us to see what I achieved, I hope you are proud.

Declaration

This thesis is submitted to the University of Warwick in support of my application for the degree of Doctor of Philosophy. It has been composed by me and has not been submitted in any previous application for any degree.

The work presented (including data generated and data analysis) was carried out by myself, except in the cases outlined below, also explicitly stated in the text:

- Transmission electron microscopy (Figure 4.7A; done by Jennifer Simpson).
- Correlative light and electron microscopy (Figure 4.8 and Figure 5.4; also done by Jennifer Simpson).

Parts of this thesis chapters have now been published in the following:

Jobe F, Simpson J, Hawes P, Guzman E, Bailey D. Respiratory Syncytial Virus Sequesters NF-κB Subunit p65 to Cytoplasmic Inclusion Bodies to Inhibit Innate Immune Signalling. J Virol. 2020 Oct 27;94(22):e01380-20. doi: 10.1128/JVI.01380-20. PMID: 32878896; PMCID: PMC7592213.

Summary

Respiratory syncytial viruses of humans (hRSV) and animals (bovine, bRSV) are the leading cause of lower respiratory tract infections – bronchiolitis and pneumonia – in their respective hosts. They pose serious health risks to young calves, children under 5, the elderly and immunocompromised. RSV is an enveloped, single-stranded negative-sense RNA virus taxonomically classified within the *Orthopneumovirus* genus in the *Pneumoviridae* family. The only available treatment option for hRSV is monoclonal antibody based immunoprophylaxis. There is no approved vaccine for hRSV, while bRSV vaccines are of varying effectiveness.

RSV can suppress the host immune response and prevents the generation of long-term immunity. RSV encodes two accessory proteins (NS1 and NS2) which are well established to block interferon signalling. Previous studies have also shown that the viral SH protein plays a role in pathogenesis by inhibiting the NF-κB pathway, an important regulator of the host innate immune response. However, the exact mechanisms employed are less well characterised. We aimed to understand the role of the RSV SH protein and found that expression reduced NF-κB signalling at the level of both IκBα degradation and subunit p65 nuclear translocation, when wild type virus-infected cells were compared to cells infected with viruses lacking SH expression. However, the differences were minimal, especially when NF-κB transactivation was assessed in cells ectopically expressing SH in the absence of all other viral proteins.

Interestingly however, during these experiments we identified separate RSV-mediated antagonism of the NF-κB pathway, with a mechanism entirely distinct from the NS1, NS2 and SH proteins. In both hRSV and bRSV infected cells we demonstrated that the p65 subunit of NF-κB is sequestered to perinuclear viral inclusion bodies (IBs). These were formed in the cytoplasm of RSV infected cells and were separately confirmed as the sites of viral RNA replication and synonymous with viral inclusion bodies. We also found that captured p65 is unable to translocate to the nucleus following TNF-α stimulation, highlighting the antagonistic nature of this event.

Abbreviations

AEC	Airway epithelial cell
AMPV	Avian metapneumovirus
ANOVA	Analysis of variance
bRSV	Bovine respiratory syncytial virus
bRSV ΔSH	Bovine respiratory syncytial virus lacking the SH protein
BSA	Bovine serum albumin
CCL	Chemokine ligand
CLEM	Correlative light electron microscopy
CPE	Cytopathic effect
CX3CR	Chemokine receptor
DAPI	4, 6-diamidino-2-phenylindole
DC	Dendritic cells
DMEM	Dulbecco's modified eagle's medium
EBOV	Ebola virus
EDTA	Ethylenediaminetetraacetic acid
EGFR	Epidermal growth factor receptor
EM	Electron microscopy
EV	Empty vector
FCS	Foetal calf serum
FRAP	Fluorescence recovery after photo-bleaching
GAPDH	Glyceraldehyde 3-phosphate dehydrogenase
GFP	Green fluorescent protein
HAE	Human airway epithelial cells
HMPV	Human metapneumovirus
HRP	Horse-radish peroxidase
hRSV	Human respiratory syncytial virus
IB	Inclusion body
IBAG	Inclusion body-associated granule
ICAM1	Intercellular adhesion molecule 1
IDR	Intrinsically disordered region
IF	Immunofluorescence
IFN	Interferon

IκBα	I-kappa-B-alpha
IKK	IκB-kinase
IL	Interleukin
IRF	Interferon regulatory factor
ISG	Interferon-stimulated gene
LLPS	Liquid-liquid phase separation
MAVS	Mitochondrial antiviral-signalling protein
MeV	Measles virus
MDBK	Madin-Darby bovine kidney
MOI	Multiplicity of Infection
MPV	Murine pneumonia virus
MuV	Mumps virus
NF-κB	Nuclear factor-kappa-light-chain-enhancer of activated b cells
NiV	Nipah virus
NS	Non-structural protein
ORF	Open reading frames
PAMP	Pathogen-associated molecular pattern
PBS	Phosphate buffered saline
PCR	Polymerase chain reaction
PFA	Paraformaldehyde
PIV	Parainfluenza virus
PRRs	Pattern recognition receptors
PVDF	Polyvinylidene difluoride
RBP	RNA-binding protein
RIG-I	Retinoic acid-inducible gene I
RIPA	Radioimmunoprecipitation assay buffer
RNP	Ribonucleoprotein complex
RT-PCR	Reverse transcriptase polymerase chain reaction
SDS-PAGE	Sodium dodecyl sulphate – Polyacrylamide gel electrophoresis
SH	Small hydrophobic
STAT2	Signal transducer and activator of transcription
TBK1	TANK-binding kinase
TEM	Transmission electron microscopy

TLR	Toll-like receptor
TNFα	Tumour necrosis factor alpha
TRAF	TNF receptor associated factor
VSV	Vesicular stomatitis virus
WB	Western blot

Chapter 1: Introduction

1.1. Orthopneumoviruses

1.1.1. Classification, host range and global impact

Orthopneumoviruses are enveloped viruses taxonomically classified within the *Pneumoviridae* family of non-segmented, negative-sense, single stranded (NNS) RNA viruses - *Mononegavirales* order (Amarasinghe et al., 2019). This genus includes three virus species: *bovine orthopneumovirus* and *human orthopneumovirus*, which until 2016, were known as respiratory syncytial viruses (bovine RSV; bRSV and human RSV; hRSV, respectively) and *murine orthopneumovirus* (previously murine pneumonia virus; MPV) (Rima et al., 2017). A taxonomic reclassification in 2015 by the International Committee on Taxonomy of Viruses (ICTV) promoted the member viruses from the *Pneumovirinae* subfamily of the *Paramyxoviridae* family, to a now distinct *Pneumoviridae* family. The new family contains one other genus, *Metapneumovirus* which classifies related human pathogens including human metapneumovirus (hMPV). Other related virus families that also classify important human pathogens include, but are not limited to, the *Paramyxoviridae* (classifying e.g., measles virus; MeV, mumps virus; MuV, parainfluenza virus type 5; PIV5, Nipah virus; NiV), *Rhabdoviridae* (e.g., rabies virus; RABV), and *Filoviridae* (e.g., ebola virus; EBOV) (Pfaller et al., 2015).

Although orthopneumoviruses are all associated with causing acute respiratory disease, they are restricted to their individual hosts. Studies of these viruses in non-native hosts did not recapitulate disease (Buchholz et al., 2000), despite several genetic and antigenic similarities, as well as orthologous mechanisms of replication and similar pathogenesis (Borchers et al., 2013, Sacco et al., 2014, Taylor, 2017). As implied by their nomenclature, the two important viruses, bRSV and hRSV, target cattle and humans, respectively, and are the leading causes of lower respiratory tract illness in their respective hosts (Nair et al., 2013, Sacco et al., 2014). They infect all ages, but severe respiratory illness associated with bronchiolitis and pneumonia, is more common in calves and infants, the elderly and immunocompromised (Falsey et

al., 2005, Hogan et al., 2016, Smyth and Openshaw, 2006). Globally, hRSV affects almost all children by the age of five, accounting for nearly 33 million cases per year and 3.2 million hospital admissions (Shi et al., 2017). Around 60,000 of the hospitalised under-fives die, with a higher mortality rate in infants under 6 months of age (Shi et al., 2017). In industrialised countries, death primarily occurred in those at high risk of developing severe disease. These include premature babies and infants with chronic lung and heart disease (Hogan et al., 2016, Smyth and Openshaw, 2006). However, 90% of RSV mortality occur in low and middle income countries, in post neonatal infants and often associated with bacterial sepsis and pneumothorax (Geoghegan et al., 2017). Bovine RSV infection is also responsible for significant losses to the cattle farming industry worldwide (Brodersen, 2010, Valarcher and Taylor, 2007).

HRSV was first isolated from chimpanzees (Blount et al., 1956) and then shortly after in young children (Chanock et al., 1957). BRSV, on the other hand, was identified over a decade later based on cross-reactivity with hRSV antibodies (Sacco et al., 2014). Despite decades of research and development efforts, there is no approved vaccine available against hRSV. In contrast, there are several vaccines available against bRSV, the first of which was generated in the 1970s; however, these are only mildly protective (Ellis, 2017). Thus, there is a broad need to develop more efficacious vaccines against bRSV as well as hRSV. Some of the challenges that have been encountered over the years include the historic formalin-inactivated RSV vaccine failure which caused enhanced natural infection in some of the vaccinated children (Fulginiti et al., 1969, Kim et al., 1969). Another challenge is the need to vaccinate young children with pre-existing maternal antibodies and an underdeveloped immune system which may affect the generation of a robust immune response (Murata, 2009). Other challenges include the heterogeneity of RSV subtypes and the incomplete immune response generated against RSV. However, there have been recent advances in the field using a variety of vaccine strategies including live-attenuation of wild type virus, vector-, viral protein sub-unit-, and DNA-based candidates (Murata, 2009, Broadbent et al., 2015, Elawar et al., 2021).

Although several vaccine candidates have recently failed clinical trials (Ruckwardt et al., 2019), there are still promising candidates in development (Shan et al., 2021). For

hRSV, a recently completed phase I study of a live attenuated vaccine candidate RSV/ΔNS2/Δ1313/I1314L showed that the vaccine virus is attenuated and immunogenic in RSV-seronegative children (Karron et al., 2020). Other live-attenuated/chimeric vaccine candidates including deletion of the M2-2 gene which plays a role in the transition from transcription to viral RNA are being explored. LIDΔM2-2 (McFarland et al., 2018) and LID/ΔM2-2/1030s (McFarland et al., 2020a) were both reported safe and immunogenic in children – generating both neutralising and anti-RSV F IgG antibody responses. MEDI-ΔM2-2, previously reported immunogenic in children, albeit with lower safety profiles (Karron et al., 2015), was further modified to D46/NS2/N/ΔM2-2-HindIII (McFarland et al., 2020b). This vaccine virus was highly immunogenic and safe in children (McFarland et al., 2020b). A purified recombinant hRSV F protein vaccine stabilised in the pre-fusion conformation was also reported safe and highly immunogenic in adult men (Langley et al., 2017). Another pre-F vaccine, Ad26.RSV.preF (Williams et al., 2020), and a nanoparticle F vaccine candidate (Glenn et al., 2013, Fries et al., 2017) with promising results are considered potential effective vaccines for the elderly (Shan et al., 2021). Similarly, for bRSV, a F protein vaccine stabilised in the pre-fusion conformation (PreF) was recently reported safe and effective in new-born calves with maternally-derived antibodies (Riffault et al., 2020). In another study, when PreF was assessed in parallel with bRSV lacking the SH gene (ΔSH rBRSV), also in the presence of maternally-derived antibodies, both vaccines were safe and immunogenic although the PreF vaccine induced the most significant protection post challenge (Valarcher et al., 2021). Of note, this is not an exhaustive list and there are other vaccine candidates in development (Elawar et al., 2021, Shan et al., 2021).

Current treatment for hRSV relies on immunoprophylaxis, palivizumab (a monoclonal antibody against the viral fusion protein), although its use is restricted to high risk patients due to its high cost (Groothuis and Nishida, 2002). However, studies show that the antibody does not prevent disease but rather reduces the risk of developing severe disease (Rodriguez et al., 1997). Other biologics in development include ALX-0171, a trimeric nanobody that binds the antigenic site II of RSV F protein with sub-nanomolar affinity (Detalle et al., 2016). Preliminary data shows that ALX-0171 has greater neutralising activity against prototypic RSV subtype A and B strains when

compared to palivizumab (Detalle et al., 2016). Another novel monoclonal antibody nirsevimab (MEDI 8897), targeting prefusion F also exhibits superior neutralisation and stability over palivizumab (Domachowske et al., 2018).

1.1.2. Genome organisation and encoded proteins

Orthopneumoviruses have a linear negative-sense RNA genome, (15,223 nucleotides [nt] in length for hRSV A2 [GenBank accession no. KT992094] and 15,140 nt for bRSV A51908 [GenBank accession no. NC_038272] which encodes genes for 11 proteins from 10 mRNAs. These are, in order from the 3′ end: *NS1*, *NS2*, *N*, *P*, *M*, *SH*, *G*, *F*, *M2*, and *L* (Fig 1.1); and are flanked by 3′ leader and 5′ trailer sequences. This follows the typical genome organisation of mononegaviruses, encoding genes for a nucleoprotein (N), polymerase cofactor (X/P), matrix protein (M), surface glycoprotein (G) and polymerase (L) (Pfaller et al., 2015). Each gene is transcribed into a single mRNA directed by gene start (*gs*) and gene end (*ge*) signals, and short intergenic regions of variable length (1 to 46 nucleotides) (Collins and Melero, 2011). The only exception is the *M2* gene which has two slightly overlapping open reading frames (ORFs). The initiation and regulation of orthopneumovirus transcription and replication is described later in sub-section 1.1.4.2.

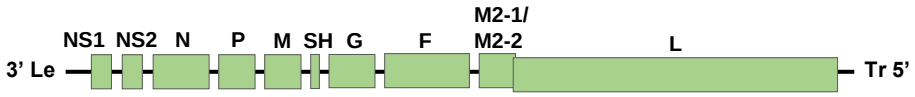

Figure 1.1 Organisation of the *Orthopneumovirus* genome. Schematic depiction of the negative sense single-stranded RNA genome (length is approximately 15,000 nucleotides) showing organisation of the encoded genes (green rectangles). Note that the gene lengths are represented to scale although the intergenic regions are not. The beginning of the *L* gene slightly overlaps with the *M2* gene.

Orthopneumoviruses may be distinguished from related viruses by the presence of four extra genes: *NS1*, *NS2*, *SH* and *M2*. Three of the encoded proteins (non-structural proteins; NS1 and NS2 and small hydrophobic; SH protein) are non-essential for virus replication but function in inhibiting innate immune signalling (Schlender et al., 2000, Spann et al., 2004, Pollock et al., 2017, Taylor et al., 2014, Bitko et al., 2007, Atreya

and Kulkarni, 1999). NS1 and NS2 are not found in any other virus in the *Mononegavirales* order and have been shown to antagonise apoptosis (Bitko et al., 2007) and interferon (IFN)-mediated host responses by targeting both type I and II IFN induction (Schlender et al., 2000, Spann et al., 2004, Spann et al., 2005) and signalling (Lo et al., 2005). The two proteins localise in the cytoplasm, can form homotetramers, and work synergistically or individually (Schlender et al., 2000, Swedan et al., 2009). Specifically, NS2 interacts with a cytoplasmic nucleic acid receptor (RIG-I) inhibiting its interaction with the mitochondrial antiviral-signalling protein (MAVS) (Ling et al., 2009). Similarly, NS1 can inhibit phosphorylation of interferon regulatory factor 3 (IRF-3) by interacting with MAVS (Boyapalle et al., 2012) or by decreasing the levels of IKKε, a key protein kinase that specifically phosphorylates IRF3 (Swedan et al., 2009). The proteins can also decrease levels of other components of the interferon signalling pathway. NS1, and to a lesser extent NS2, mediate a decrease in the levels of TRAF3 in a non-proteasomal mechanism (Swedan et al., 2009). Recently, the NS proteins have also been shown to be involved in formation of an "NS -degradasome" that promotes the degradation of components of IFN induction or signalling, such as, RIG-I and IRF-3 and -7, TBK1 and STAT2 (Goswami et al., 2013). Consequently, activation of the cytotoxic T lymphocyte component of the adaptive immune response is also suppressed (Kotelkin et al., 2006).

The M2 gene which encodes the M2-1 and M2-2 proteins with roles in the regulation of viral RNA synthesis, is unique to members of the *Pneumoviridae* family and the basis for their recent separation from paramyxoviruses (Rima et al., 2017). These are expressed from overlapping ORFs, with expression of the second ORF using a unique mechanism of translation of the mRNA (Ahmadian et al., 2000, Gould and Easton, 2007, Powell, 2010). M2-1 is essential for virus replication and mainly localises in inclusion bodies (IBs) formed in the cytoplasm of infected cells (Rincheval et al., 2017). The details of viral transcription are discussed later, but briefly, once initiated at the 3′ extragenic leader sequence, viral mRNA transcripts are produced sequentially from the 3′ end of the genome in a stop-restart mechanism directed by *gs* and *ge* sequences that flank each gene (Kuo et al., 1996b). M2-1 acts as a transcription factor that prevents the early termination of the transcription machinery at *ge* signals, thus enhancing the transcription of genes towards the 5′ end of the genome (Collins et al., 1995, Collins et al., 1996, Fearns and Collins, 1999b). M2-1 forms tetramers that can

exist in phosphorylated and non-phosphorylated forms (Lambert et al., 1988, Tran et al., 2009). Phosphorylation was found to be important for hMPV replication and pathogenesis (Cai et al., 2016). The phosphorylation status of RSV M2-1 has been suggested to determine its interacting partners, localisation (cytoplasmic or intra-IB) and subsequent function (Richard et al., 2018). Both forms can interact with the P protein. However, interaction of phosphorylated M2-1 in the cytoplasm with P bound to a phosphatase, PP1, facilitates its dephosphorylation and recruitment into IBs, where they regulate viral mRNA transcription (Richard et al., 2018). M2-1 then binds and concentrates with the newly synthesised mRNA, an interaction which displaces P (Blondot et al., 2012, Tran et al., 2009, Cuesta et al., 2000). Phosphorylation then releases M2-1 from the mRNA destined for translation and free M2-1 may then restart the cycle by interacting with P (Richard et al., 2018). Whether M2-1 plays a role in translation remains unclear but an interactomics study has identified that M2-1 interacts with several cellular proteins involved in mRNA metabolism and translation (Bouillier et al., 2019). Separately, a CCCH zinc-binding motif, that usually plays a role in RNA binding, is found in the conserved functionally essential *N*-terminus of both RSV (Hardy and Wertz, 2000, Tang et al., 2001, Zhou et al., 2003) and MPV M2-1 (Cai et al., 2015). The exact role of this motif, other than stabilisation of the tetrameric complex (Esperante et al., 2013), is presently unclear. M2-1 was also shown to play a role in M protein IB localisation and its interaction with the ribonucleoprotein complex (Li et al., 2008, Kiss et al., 2014).

M2-2 is encoded by the second ORF of the M2 gene and unlike M2-1 is an accessory protein, not essential for virus growth. However, deletion of this ORF from hRSV A2 resulted in host range-specific partial attenuation of the virus (Jin et al., 2000a). Its absence also increased viral mRNA transcription and expression of the antigenic proteins (F and G) whilst genome and antigenome replication were reduced in comparison (Bermingham and Collins, 1999, Jin et al., 2000a). This suggests that accumulation of the M2-2 protein, perhaps in later stages of infection when significant viral proteins are expressed, directs RNA synthesis in favour of genome and anti-genome replication by downregulating transcription (Collins et al., 2013). Since both processes use the same machinery and RNA template, a balance is important for efficient virus replication. In effect, M2-2 acts as an RNA synthesis regulatory factor, although the exact mechanism of this switch is not clearly understood. Viruses lacking

the expression of this protein are currently being investigated as live-attenuated vaccine candidates with promising results (McFarland et al., 2020a, McFarland et al., 2018). Recently, hMPV M2-2 protein was found to inhibit innate immune signalling by targeting MAVS (Chen et al., 2016, Kitagawa et al., 2017, Ren et al., 2014, Ren et al., 2012). A similar role has not been reported for orthopneumovirus M2-2 proteins and there is no significant sequence identity between the pneumovirus M2-2 proteins (Collins et al., 2013).

The final extra orthopneumovirus gene, *SH*, encodes one of three surface glycoproteins found in the virus lipid envelope (Fig 1.2). Unlike the unique NS and M2 proteins, SH orthologs are found in some members of the paramyxoviridae family and their role will be discussed in section 1.3. The other encoded proteins, non-glycosylated structural protein M, glycoproteins G and F involved in attachment and entry into host cells, and components of the RNA-dependent RNA polymerase complex (RdRp), N, P and L, will be discussed in the next two sections.

1.1.3. Virion structure and composition

Virions of *Pneumoviridae* family members, are known to be pleomorphic. Detailed morphological analysis has revealed RSV particles consist of spherical, asymmetric, and filamentous structures that share the same composition and similar ultrastructural organisation (Kiss et al., 2014, Liljeroos et al., 2013, Ke et al., 2018). Each type exhibits a wide range of sizes, independent of the cell type used for propagation. Spherical structures (Fig 1.2) typically measure 150-200 nm in diameter (Easton et al., 2004), however, Liljeroos *et al*. have observed spherical particles up to 1 µm in diameter. Particles grown in cell culture predominantly consist of long filaments that measure 0.5-12 µm in length (average 1.5 µm) and a diameter ranging from 100-250 nm (average 130 nm) (Ke et al., 2018).

RSV particles are composed of the viral genome and the structural proteins, including F, G, SH, M, M2-1, N, P and L proteins (Fig 1.2). Molecular interaction studies and electron microscopic analysis have revealed their spatial organisation within the virus particle as well as its architecture. Firstly, the N protein which encapsidates the viral genome, interacts with the L and P proteins to form a helical ribonucleoprotein

complex (RNP) called a nucleocapsid (Easton et al., 2004). The RNP complex is encapsulated by a matrix protein layer formed from polymerisation of the M protein. It has been found that this connection is facilitated by M2-1; forming separate interactions with P (Mason et al., 2003) and M (Li et al., 2008). Because of the abundance of M and the size capacity of the virus particle, more than one RNP complex may be packaged in a virus particle (Kiss et al., 2014).

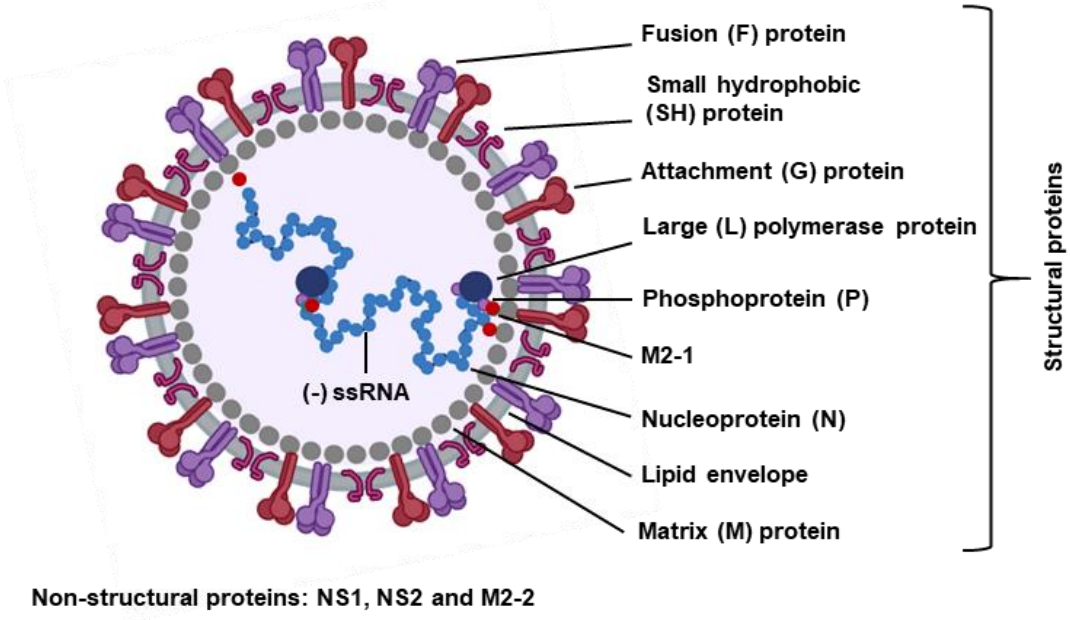

Figure 1.2 The structure of the orthopneumovirus virion. The locations of encoded proteins are shown. The surface glycoproteins, F, G and SH, are anchored in the lipid envelope, underneath which is the matrix (M) layer. The negative sense single-stranded (-ss)RNA genome is tightly encapsidated by the nucleoprotein (N). The N protein interacts with the polymerase (L), and phosphoprotein (P) to form the ribonucleoprotein (RNP) complex. Encapsulation is facilitated by the M2-1 protein interacting with P in the RNP complex and the matrix layer. Created with BioRender.com.

The mature RSV particle consists of the encapsidated RNP wrapped in a lipid envelope from which the surface glycoproteins, F, G and to a lesser extent SH, project (Fig 1.2). F and G are also the major antigenic proteins of the virus, although antibodies against F, especially the pre-fusion form are more neutralising (McLellan et al., 2013). The M protein is important for virus assembly and the formation of mature RSV filaments (Mitra et al., 2012, Shaikh and Crowe, 2013, Liljeroos et al., 2013). Unsurprisingly, the cytoplasmic domains of the F and G proteins interact with M protein at the inner

leaflet of the membrane (Ghildyal et al., 2005, Baviskar et al., 2013), although M may also directly interact with membrane lipids (Henderson et al., 2002, Money et al., 2009).

1.1.4. Viral life cycle

1.1.4.1. Attachment and entry

RSV primarily infects and replicates in ciliated airway epithelial cells via the apical surface (Fig 1.3) (Zhang et al., 2002). Of the proteins contained in the lipid envelope, G and F are involved in host cell attachment and the F protein alone in entry of the nucleocapsid. The SH protein is not involved in this process, and G is also nonessential since deletion of both proteins did not affect virus replication *in vitro* (Karron et al., 1997, Teng et al., 2001, Techaarpornkul et al., 2001, Techaarpornkul et al., 2002). Restriction of the mutant virus in certain cell types and attenuation *in vivo,* however, shows an important role in pathogenesis (Crowe et al., 1996). Earlier studies in cell lines revealed that RSV infection is mediated by G or F protein recognition of glycosaminoglycans (GAGs) containing heparan sulfate on host cell surfaces (Feldman et al., 1999, Feldman et al., 2000, Krusat and Streckert, 1997, Techaarpornkul et al., 2002). However, using more physiologically relevant human airway epithelial (HAE) cells, the absence of heparan sulphate on the cognate target cells of the virus was observed (Zhang et al., 2005a). Subsequently, studies using HAE cells identified other receptors used for virus attachment, for example, G protein binding to CX3R1 (Johnson et al., 2015, Chirkova et al., 2015, Jeong et al., 2015), heparin (Krusat and Streckert, 1997) and annexin II (Malhotra et al., 2003). F protein also binds nucleolin (Tayyari et al., 2011), intercellular adhesion molecule-1 (ICAM-1) (Behera et al., 2001), toll-like receptor 4 (TLR4) (Marr and Turvey, 2012) and epidermal growth factor receptor (EGFR) (Currier et al., 2016). Because of the ubiquitous expression of most of these receptors, there are ongoing discussions to try and explain RSV's specific tropism for airway epithelial cells. Instead of using a single receptor recognition step for entry, RSV makes multiple interactions, possibly in synergy, to enhance infection. Recently, coreceptor usage in RSV entry was reported involving EGFR and nucleolin (Griffiths et al., 2020).

Following attachment, conformational changes in the F protein mediate fusion of the viral and host cell membranes in a pH-independent manner, releasing the RNP (infectious material) into the cytoplasm for replication (Fig 1.3) (McLellan et al., 2013, Walsh and Hruska, 1983, Battles et al., 2016, Krzyzaniak et al., 2013).

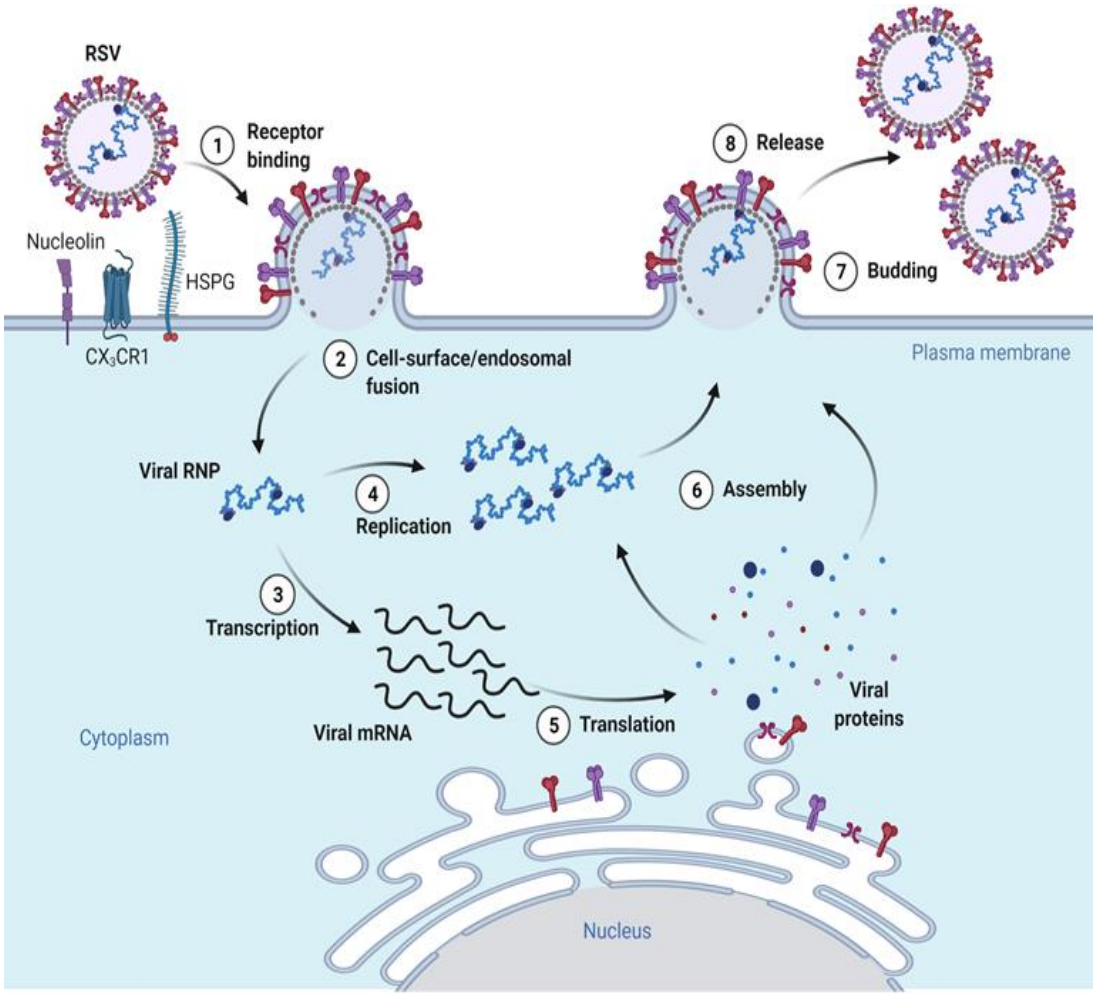

Figure 1.3 Orthopneumovirus life cycle in lung epithelial cells. A schematic illustrating the replication cycle of orthopneumoviruses. (1) The F and G proteins mediate attachment to cell surface receptors, such as, nucleolin, CX3CR1 and heparan sulphate containing proteoglycans (HSPG), *etc*., and (2) F alone mediates entry of the ribonucleoprotein complex (RNP) through fusion of viral and host cell membranes. (3) Transcription of viral mRNA by the encoded polymerase occurs in the cytoplasm using the genome as template. (4) The polymerase also replicates the genome by first making an anti-genome template. (5) Viral mRNA is translated into viral proteins through the ER-golgi system or in the cytoplasm. (6) Viral proteins and genome are transported to the plasma membrane where particle assembly (7) budding and (8) release of mature virions occur. Created with BioRender.com.

The same process also mediates multinucleated syncytium formation by driving infected epithelial cell-cell membrane fusion (Walsh and Hruska, 1983). Although it

is widely accepted that the fusogenic activity of the F protein is required to allow entry at the cell surface, there is evidence supporting the involvement of macropinocytosis (Krzyzaniak et al., 2013) and clathrin-mediated endocytosis (Kolokoltsov et al., 2007). The currently proposed model is that virus-cell fusion can occur either at the cell membrane or in endosomes post macropinocytosis or endocytosis (Tayyari et al., 2011, Krzyzaniak et al., 2013, Battles and McLellan, 2019).

1.1.4.2. Viral genome transcription and replication

RNA synthesis – transcription and replication - occur exclusively in the cytoplasm of infected cells (Fig 1.3) (Walsh and Hruska, 1983, Garcia et al., 1993). The genomic RNA is used as a template for mRNA and antigenome synthesis, and the antigenome as a template for genomic RNA synthesis (Fig 1.4). Both processes are carried out by the polymerase, L protein (the catalytic enzyme), in complex with P and N (RdRp complex), but as already stated, efficient transcription requires an additional transcription factor, M2-1 (Collins et al., 1995, Collins et al., 1996, Fearns and Collins, 1999b). Initiation of transcription requires recognition of the promoter sequence in the extragenic 44-nucleotide 3′ leader sequence (Fearns et al., 2002, Fearns et al., 2000). The bound polymerase moves along the RNA template (towards the 5′ end), presumably removing and replacing the associated N protein subunits, sequentially transcribing each gene into a 5′ capped and 3′ polyadenylated viral mRNA guided by cis-acting signals (Fig 1.4) (Whelan et al., 2004, Kuo et al., 1996a). These signals, *gs* and *ge*, flank coding regions and signal the start and end of mRNA synthesis, respectively (Kuo et al., 1996b). Inefficient termination at the *ge* signal leads to readthrough transcription and the production of polycistronic mRNA (Collins and Wertz, 1983). Intergenic regions are untranscribed and scanned by the polymerase for the next *gs* signal to restart transcription. An overlap between the M2 and L genes means the L *gs* is located upstream of the M2 *ge*. In a process different from what is described above, following the termination of M2 gene transcription, the polymerase scans backwards and begins L gene transcription at the *gs* 68 nucleotides upstream of the termination site (Fearns and Collins, 1999a, Collins et al., 1987). A characteristic feature of non-segmented negative strand RNA genome transcription is early termination at the various gene junctions which results in a gradient of mRNA transcripts (Fig 1.4) (Collins and Wertz, 1983, Kuo et al., 1996a). This effect is

compounded because transcription can only be re-initiated at the 3′ proximal promoter, thus more of the 3′ proximal genes, NS1, NS2 and N, are expressed compared to the M2 and L genes at the 5′ end (Fig 1.4). This is favourable for the virus since the proteins required in large amounts for immune modulation and genome encapsidation are highly expressed.

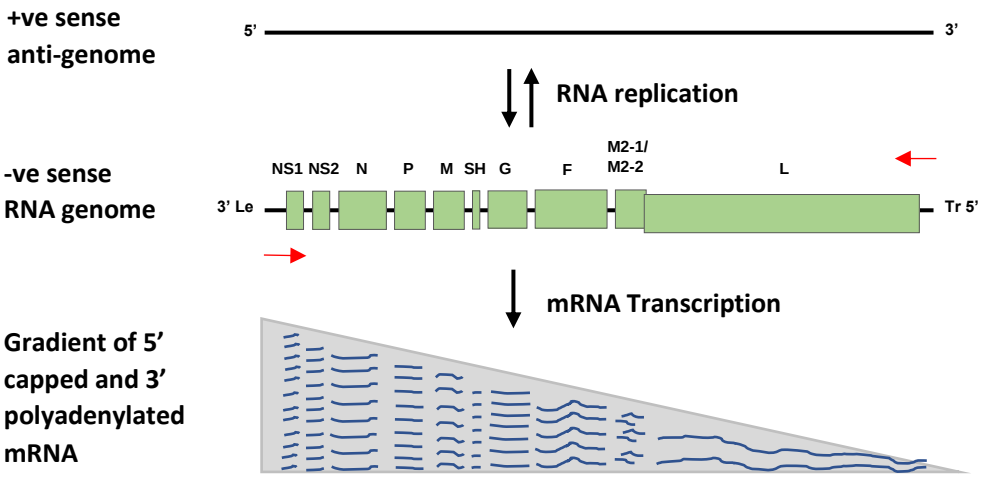

Figure 1.4 A schematic illustrating orthopneumovirus genome replication and mRNA transcription. The RNA genome is negative sense (3′-5′), whereas the anti-genome is positive sense (5′-3′). Genome encoded genes are represented with green rectangles and red arrow heads indicate the directions of mRNA transcription and replication. Transcription occurs along a gradient, resulting in more mRNA expression from 3′ proximal genes than those closer to the end of the genome. Blue lines represent viral mRNAs.

There are two promoters for replication – one in the leader sequence which initiates positive sense antigenome synthesis and another in the 155-nucleotide trailer sequence for genome synthesis using antigenomic RNA as the template (Noton and Fearns, 2015). In both cases, RNA synthesis proceeds along the entire length of the RNA, ignoring cis-acting gene junction signals in the negative strand (Fig 1.4). In addition, both RNAs are co-encapsidated with N as they are synthesised. It is not clear how the polymerase balances transcription and replication, but increased N protein expression was shown to upregulate genome synthesis (Fearns et al., 1997). As already discussed, M2-2 also down regulates transcription in favour of replication (Collins et al., 2013, Bermingham and Collins, 1999). A similar model of RNA synthesis is followed by several other mononegaviruses (Pfaller et al., 2015, Collins et al., 2013, Fearns et al., 2000).

1.1.4.3. Assembly and budding

Viral proteins are synthesised in the cytoplasm using the host translation machinery. Nucleocapsid-associated proteins (N, P, L and M2-1) and M proteins quickly colocalise in inclusion bodies, 6-10 h post infection (Ghildyal et al., 2002, Garcia et al., 1993), where nucleocapsid assembly is thought to also take place. Membrane glycoproteins are expressed in the ER, modified (for example, by glycosylation or proteolytic cleavage) and then transported to the PM via the secretory pathway (Fig1.3) (McLellan et al., 2013). As well as its localisation in inclusion bodies, M is also distributed in the cytoplasm, nucleus and plasma membrane, possibly indicating the multitude of interactions it can form and its role in particle assembly (Ghildyal et al., 2003, Ghildyal et al., 2005, Baviskar et al., 2013, Henderson et al., 2002, Money et al., 2009). M is the major structural protein and was shown to be required for virus assembly and filament extension (Mitra et al., 2012, Ghildyal et al., 2006), thus playing crucial roles in the virus lifecycle. Virus assembly involves several virus-virus and virus-host interactions, although, the exact mechanisms underpinning all these interactions are not clear for RSV. There is strong evidence showing that RSV virions bud from the plasma membrane (PM) of infected cells (Fig 1.3) and at the apical surface of airway epithelial cells during natural infection (Ke et al., 2018, Marty et al., 2004, Shaikh et al., 2012a). However, whether RSV particle assembly occurs at the membrane or begins in the cytoplasm prior to transportation of components to the budding site (Arslanagic et al., 1996), are two working models under debate.

In the first model, the data suggests that virion components may be transported to the PM individually or with their interacting partners. The M protein is involved in nucleocapsid transport from IBs to the PM (Ghildyal et al., 2002, Mitra et al., 2012), an indirect interaction that was recently shown to be facilitated through M2-1 (Kiss et al., 2014, Ke et al., 2018, Li et al., 2008). This was thought to involve traffic along actin filaments (Jeffree et al., 2007, Ulloa et al., 1998), although, a later study showed that host cell cytoskeleton does not play a significant role in filament assembly or release (Shaikh et al., 2012b). M also interacts with the cytoplasmic domains of the envelope glycoproteins, F and G, and likely associates with them during trafficking through the secretory pathway (Meshram et al., 2016, Ghildyal et al., 2005). At the internal surface of the PM, M mediates insertion of the RNP into growing virus

filaments through homo-oligomerisation (Bajorek et al., 2014, Forster et al., 2015, Trevisan et al., 2018) and interactions with the membrane and viral glycoproteins (Marty et al., 2004, Money et al., 2009, Shaikh et al., 2012a, Meshram et al., 2016).

In the alternative model, filament assembly is postulated to start in the cytoplasm following re-internalisation of viral glycoproteins from the membrane by clathrin-mediated endocytosis (Vanover et al., 2017, Arslanagic et al., 1996). The filaments grow in a microtubule and dynein motor protein-dependent manner, and subsequently merge with RNP granules via an unknown mechanism (Vanover et al., 2017). Filaments are then transported to the PM where they fuse with the membrane by a mechanism that is also unclear. The process of filament maturation is however complex and involves the formation of lipid rafts (McDonald et al., 2004), membrane curvature and actin-dependent outward budding, leading to extension and acquisition of a lipid envelope (Shaikh and Crowe, 2013, El Najjar et al., 2014). The final budding step and subsequent release of progeny virions was also shown to involve the Rab11 endosomal pathway (Utley et al., 2008). Nevertheless, the process appears inefficient, and most RSV filaments remain associated with the membrane.

1.1.5. Disease and pathogenesis

Orthopneumoviruses are transmitted between hosts through aerosols or via self-inoculation following contact with infected surfaces. Following exposure, signs, and symptoms of infection – commonly, fever, cough and rhinorrhea – develop after an incubation period that varies between 2 and 8 days (Easton et al., 2004, Collins et al., 2013). Infection and replication primarily occur in the upper respiratory tract but may spread to the lower airways, which may cause a more severe disease characterised by bronchiolitis and pneumonia. RSV pathogenesis is not well understood, which is further complicated by a large variability in disease severity observed between different individuals. Interestingly, it was recently reported that RSV susceptibility is enhanced by mucosal neutrophilic inflammation (Habibi et al., 2020). The presence of inflammation at the time of virus exposure caused a delayed onset response which caused a large influx of immune cells, and enhanced cytokine secretion. In contrast, the absence of inflammation induced early immune activation that prevents the development of symptomatic disease (Habibi et al., 2020). RSV pathogenesis is also

thought to be enhanced by viral, environmental and other host factors although the contribution of these factors to disease also varies between different individuals (van Drunen Littel-van den Hurk and Watkiss, 2012).

Broadly, the pathogenesis of viral respiratory infection is usually a combination of morphological and functional changes caused by virus replication (cytopathic effect, cpe), and immunopathology induced by the immune response to the virus (Newton et al., 2016, van Drunen Littel-van den Hurk and Watkiss, 2012). Successful replication and spread depends on the ability of the virus to evade the host immune system. RSV encodes several non-essential genes – NS1, NS2, G and SH genes – identified using reverse genetics techniques - that inhibit the immune response, enhancing pathogenesis. Evidence of their roles was provided by full or partial virus attenuation observed when these genes are deleted (Fuentes et al., 2007, Russell et al., 2015, Tripp et al., 1999, Valarcher et al., 2003, Whitehead et al., 1999). Their mechanisms of immune modulation will be further discussed in subsection 1.2.3. BRSV infection is often associated with secondary bacterial infections leading to high severity bovine respiratory disease complex in infected herds (Taylor, 2017, Valarcher and Taylor, 2007). The contributions of strain heterogeneity and viral load on pathogenesis are contentious, with some groups reporting correlations where others found none (Borchers et al., 2013).

Although the F protein induces syncytia formation, RSV is known to be minimally cytopathic. Lab-adapted strains induce more cpe than that observed in infected tissues (Johnson et al., 2007, Zhang et al., 2002). Thus, the induced host inflammatory response appears to play a major role in pathogenesis. In that regard, development of symptoms and viral load were shown to correlate with the expression of antiviral mediators such as, interferon-α (IFN-α), IFN-γ, CXCL10, and IL-15, the chemokines CCL3 (MIP-1α) and CCL5 (RANTES), and the anti-inflammatory cytokine IL-10, and tumor necrosis factor-α (TNF-α) (Habibi et al., 2020). These proinflammatory cytokines and chemokines transiently produced by airway epithelial cells (AECs), macrophages and dendritic cells (DCs) promote the recruitment of a large number of innate (neutrophils, eosinophils, monocytes, macrophages, DCs) and adaptive (memory T cells, TH1 cells and NK cells) immune cells from the general circulation to the sites of infection causing mucosal oedema (Lay et al., 2013). Activation of the

recruited cells also leads to further cytokine expression, inducing responses that can cause damage and small airway obstruction. An exaggerated immune response to natural infection was first observed in infants and children administered a formalin-inactivated hRSV (FI-RSV) vaccine in the 1960s (Fulginiti et al., 1969, Kim et al., 1969). Virus exposure caused a more severe disease in the RSV-naive vaccinees (>80%) which was later associated with an immune response biased towards Th2 responses (Prince et al., 1986, Graham et al., 1993). A skew of the Th1/Th2 cytokine response towards Th2 cytokines (IL-4, IL-5, IL-10, IL-13) and IgE produces an allergy-like inflammation that is also seen in unvaccinated children but at a much smaller proportion (5%) (Collins et al., 2013, Becker, 2006). However, the exact mechanisms underlying the induction of enhanced disease severity, especially in otherwise healthy children, are not fully understood.

Other well defined contributing host risk factors include premature birth, young age, under-developed or damage airways, chronic lung or heart disease, male gender, immunodeficiency, a weakened immune system due to old age, *etc* (van Drunen Littel-van den Hurk and Watkiss, 2012, Buchwald et al., 2020). Single nucleotide genetic polymorphisms (SNPs) in genes encoding components of the immune system have also been shown to enhance disease severity (Miyairi and DeVincenzo, 2008). These include SNPs in surfactant proteins, cell surface adhesion molecules, receptors such as TLR4 (Awomoyi et al., 2007, Tal et al., 2004), TLR2 and 9 (Alvarez et al., 2018) CX3CR (Amanatidou et al., 2006) and IFNAR, type I IFNs and signalling proteins (Janssen et al., 2007, Siezen et al., 2009), amongst others. SNPs in CCL5 and NOS2 have also been associated with the presence of bronchiolitis (Alvarez et al., 2018).

Environmental factors that increase risk of infection include cold weather, exposure to cigarette smoke and other air pollutants that impair lung function, increased virus exposure in day care settings and multiple sibling households *etc*., (Taleb et al., 2018, Collins and Graham, 2008). Children from disadvantaged socioeconomic backgrounds are also at increased risk of early-life RSV-related hospitalisation (Fitzpatrick et al., 2021)

1.2. Innate immune response to RSV infection

1.2.1. Innate immune recognition of RSV and cellular responses

Once the physical barriers to infection have been overcome, virus detection in AECs, alveolar macrophages and intraepithelial DCs induces an antiviral state before activation of the more specific adaptive response. RSV's distinct pathogen-associated molecular patterns (PAMPs) are detected through multiple mechanisms involving pattern recognition receptors (PRRs): toll-like receptors (TLRs), retinoic acid-

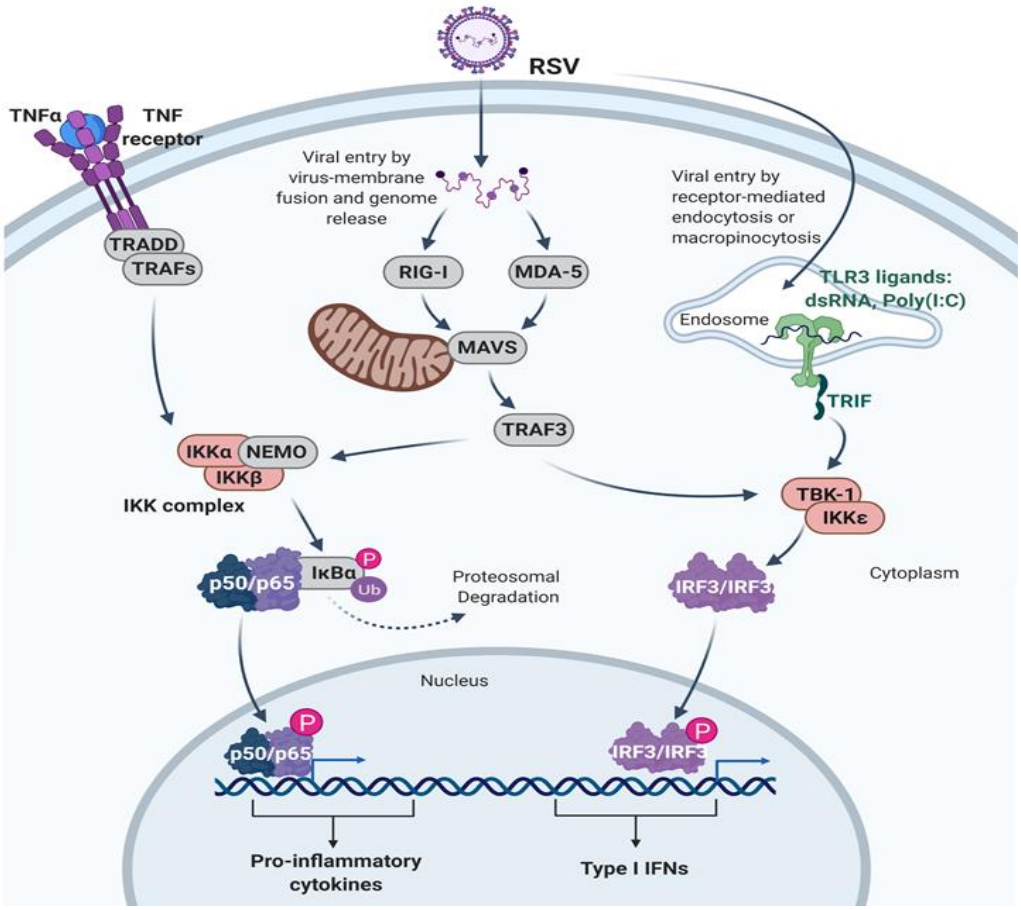

Figure 1.5 The activation of NF-κB and IRF3 transcription factors. RSV pathogen-associated molecular patterns (PAMPs), such as, single- or double-stranded viral RNA, activate cellular pattern recognition receptors (RIG-I, MDA-5 or TLR3, *etc*.). Signalling from these receptors through their adaptor proteins activate cytoplasmic kinases including the IKK complex or TBK-1. The kinases may also be activated by signals from TNF and poly(I:C). Activated IKK complex results in phosphorylation and degradation of IκBα and the release of NF-κB (p50/p65) transcription factors. The released p50/p65 enters the nucleus and induces the transcription of pro-inflammatory cytokine genes. Similarly, activated TBK-1 phosphorylates IRF3 dimers which then enter the nucleus and induce the expression of type I interferon genes. Created with BioRender.com.

inducible gene I (RIG-I) like receptors (RLRs) (Fig 1.5), and nucleotide-binding oligomerization domain (NOD)-like receptors (NLRs) (Kim and Lee, 2014, Kumar et al., 2011). Several studies have shown that RSV activation of innate immune signalling via TLRs involves interactions with TLR2, 3, 4, 6 and 7 (Kim and Lee, 2014, Kumar et al., 2011, Zeng et al., 2012). Cell surface TLRs, TLR4/CD14 complexes are activated by the F protein (Awomoyi et al., 2007, Haeberle et al., 2002, Haynes et al., 2001, Kurt-Jones et al., 2000) and TLR2/TLR6 heterodimers via an unknown mechanism (Murawski et al., 2009). Endosomal TLR3 and TLR 7, activated by double- and single-stranded RNA, respectively, have also been shown to be activated by RSV infection (Liu et al., 2007, Rudd et al., 2005, Huang et al., 2009, Lukacs et al., 2010). Activation signals are transmitted through the adaptor proteins MyD88 and/or TRIF leading to activation of the kinases TBK1/IKKε and IKKα/IKKβ (IKK complex) (Kumar et al., 2011, Zeng et al., 2012). RSV may also induce these kinases through intracellular PRRs - RIG-I, MDA-5 and Nod2 (Liu et al., 2007, Loo et al., 2008, Yoboua et al., 2010, Sabbah et al., 2009) that interact with the adaptor, mitochondrial antiviral-signalling protein (MAVS; Fig 1.5).

Multiple transcriptional networks can then be activated - nuclear factor-κB (NF-κB) transcription factors are activated through the IKK complex and the interferon regulatory factors (IRF3 and 7) through TBK1/IKKε (Baum and Garcia-Sastre, 2010, Liu et al., 2007, Kumar et al., 2011). These critical transcription factors induce the expression of proinflammatory cytokines including, tumour necrosis factor alpha (TNFα), interleukin-1 (IL-1), IL-6, IL-8, type I interferons (IFNs) (IFN-α/β) and type III IFNs (IFN-λ) (Haeberle et al., 2002, Murawski et al., 2009, Russell et al., 2015). These regulate host cell innate responses and induce responses such as apoptosis in infected cells thereby controlling virus replication and spread (Everett and McFadden, 1999). They also induce the expression of chemokines such as CXCL8, CXCL10, CCL2 and CCL5 (McNamara et al., 2005, Carpenter et al., 2002, Valarcher and Taylor, 2007) that promote the recruitment and activation of various effector cells in the airways, in particular, neutrophils (McNamara et al., 2003). Furthermore, the IFNs act to induce the expression of IFN-stimulated genes (ISGs) – antiviral effectors such as, PKR, IFIT1, Mx1, Viperin, OAS, amongst others - that also contribute to the antiviral state (Lazear et al., 2019). Together, the cytokines triggered by RSV play important roles in the host defense but interestingly also contribute to RSV

pathogenesis, as discussed above. These cytokines and activated antigen presenting cells subsequently induce an RSV specific humoral and adaptive cellular responses that clear the infection. However, the immune responses are short-lived, making RSV re-infections common throughout life (Habibi et al., 2015).

1.2.2. NF-κB signalling

NF-κB is a superfamily of five ubiquitous transcription factors - p65 (RelA), RelB, c-Rel, p50 and p52 - that play a key role in the host innate response to infection (Hayden and Ghosh, 2008). The most extensively studied of these are p65/p50 dimers but they can be found in various homo- and hetero-dimers. In the absence of stimulus, these are sequestered in the cytoplasm bound to a family of inhibitors, called inhibitors of κB (IκB) (Mitchell et al., 2016). As discussed in sub-section 1.2.1, detection of virus PAMPs by PRRs activates signal transduction cascades that result in phosphorylation and activation of the IκB kinase complex (IKKα/IKKβ; Fig 1.5) (Mitchell et al., 2016, Oeckinghaus et al., 2011). This can then phosphorylate IκBα/β/ε causing their release from p65/p50 and subsequent degradation through the ubiquitin-proteasome pathway (Chen et al., 1995). Free NF-κB p65/p50 complex is also activated by phosphorylation, at subunit p65. Various phosphorylation sites have been identified including Ser276, Ser529, Ser536 and Ser311 (Hayden and Ghosh, 2008). These induce NF-κB translocation into the nucleus where it binds target genes containing 9-10 base pair DNA sequences in the promoter (called κB sites) to induce or repress their expression (Mitchell et al., 2016, Oeckinghaus et al., 2011, Hayden and Ghosh, 2008).

These events are not only activated by virus PAMPs but may also be initiated by cytokine receptors, in particular, TNFα (Fig 1.5) and IL-1 receptors, in steps which are better characterised. Despite decades of research, the molecular mechanism by which RSV induces NF-κB activation is not fully understood. RSV activation of TLR2 and F protein interaction with TLR4/CD14 complex were shown to activate NF-κB signalling through MyD88 (Kurt-Jones et al., 2000, Segovia et al., 2012b). RSV was also recently shown to induce phosphorylation of p65 at Ser536, downstream of the RIG-I/MAVS/TRAF6/IKKβ pathway (Yoboua et al., 2010). In another study, phosphorylation at Ser276 was shown to occur downstream of reactive oxygen species signalling and MSK1 activation in RSV infected cells (Jamaluddin et al., 2009).

Involvement of the non-canonical pathway following RIG-I activation - NIK/IKKα complex/p100 processing to p52 – by RSV was also observed (Liu et al., 2008). In addition, differential effects of RSV and TNFα on IκBα regulation (Fiedler and Wernke-Dollries, 1999) and NF-κB activation (Carpenter et al., 2002) suggest different mechanisms of signalling and involvement of distinct NF-κB dimers. Thus, RSV seems to trigger multiple mechanisms of NF-κB signalling to induce proinflammatory cytokine and chemokine expression and innate responses.

1.2.3. RSV modulation of the immune response

To overcome this ubiquitous first line of defence, viruses have evolved various inhibitors to modulate innate immune signalling pathways. Viral immune evasion mechanisms include the targeting of receptors, adaptor proteins and/or intracellular kinases of the signalling pathways or indeed directly targeting the transcription factors and their regulators (Chiang and Liu, 2018, Deng et al., 2018). In this regard, RSV is no exception. The non-essential NS1, NS2, G and SH proteins modulate the innate immune response, thus impacting activation of the adaptive/RSV-specific immune response.

1.2.3.1. NS1 and NS2 proteins

BRSV and hRSV NS1 and NS2 proteins were shown to antagonise IFN-mediated host responses by targeting both type I and III IFN induction (Schlender et al., 2000, Spann et al., 2004, Spann et al., 2005) and signalling through the JAK-STAT pathway (Lo et al., 2005). Mechanistically, NS2 interacts with RIG-I inhibiting its interaction with MAVS (Ling et al., 2009). Similarly, NS1 can inhibit phosphorylation and activation of IRF-3 by interacting with MAVS (Boyapalle et al., 2012). NS1 also interacts with TRIM25 inhibiting TRIM25-mediated ubiquitination of RIG-1, thereby suppressing antiviral signalling (Ban et al., 2018). Recently, the NS proteins have also been shown to be involved in the formation of an "NS-degradasome" that promotes the degradation of components of IFN induction or signalling, including RIG-I, IRF-3, IRF-7, TBK1 and STAT2 (Goswami et al., 2013). NS1 and NS2 have also been shown to interfere with signalling downstream of MAVS, disrupt the activation and function of IRF and NF-κB transcription factors, and interfere with IFN induction as well as the function

of some ISG products (Sedeyn et al., 2019). Consequently, activation of the adaptive immune response is also suppressed (Kotelkin et al., 2006, Sedeyn et al., 2019). Unsurprisingly, deletion of the NS1 and/or NS2 proteins caused virus attenuation *in vivo*, which was attributed to the induction of a more robust IFN response compared to wild type virus (Valarcher et al., 2003).

1.2.3.2. Attachment (G) glycoprotein

G may also have a role in modulating innate immune signalling as its deletion enhanced the proinflammatory response and cytokine expression (Arnold et al., 2004, Tripp et al., 1999). G also contains a CX3C motif which mimics the chemokine, CX3CL1, and inhibits pulmonary migration of immune cells by blocking CX3CL1-CX3CR1 interactions (Harcourt et al., 2006, Tripp et al., 2001). G is also highly variable between strains making it less important as a vaccine antigen (Melero et al., 1997, Cui et al., 2013). In addition, the secreted truncated form of G (soluble G) acts as a decoy that inhibits antibody-mediated neutralisation of the virus (Bukreyev et al., 2008).

1.2.3.3. Small hydrophobic (SH) protein

The third membrane glycoprotein, SH, was found to inhibit NF-κB activation (Pollock et al., 2017, Taylor et al., 2014), although the exact mechanism of this antagonism is yet to be characterised. Deletion of bRSV and hRSV SH slightly enhanced apoptosis and increased the expression of NF-κB induced proinflammatory cytokines IL-1β and TNF-α (Fuentes et al., 2007, Taylor et al., 2014, Russell et al., 2015). The resulting partial attenuation of mutant hRSV (Bukreyev et al., 1997, Whitehead et al., 1999, Russell et al., 2015) and bRSV (Taylor et al., 2014) in mice and chimpanzees demonstrates the contribution of SH to RSV pathogenesis. In addition, inhibition of apoptosis may delay antigen presentation and activation of the adaptive response required to clear the infection.

1.2.3.4. RSV inclusion body

hRSV has also been shown to employ an additional mechanism of innate immune antagonism whereby MAVS and MDA-5 are sequestered into inclusion bodies (IBs),

likely through interaction with the RSV nucleoprotein (N protein) (Lifland et al., 2012). Other cellular proteins involved in the cellular response to viral infection such as, p38 mitogen-activated protein kinase (MAPK) and O-linked N-acetylglucosamine transferase (OGT) have also been shown to be recruited into IBs (Fricke et al., 2013).

Together, these immunomodulatory mechanisms allow successful replication and spread of the virus, enhancing virulence as a result. They may also contribute to the incomplete and short-lived protective immunity generated by both bRSV and hRSV, (Borchers et al., 2013, Collins and Melero, 2011, Guzman and Taylor, 2015), although the actual basis for this remains unclear. Of note, there is a need to further understand the mechanisms of immune regulation employed by RSV. In this PhD project, I therefore aim to characterise the immunomodulatory functions of the SH protein and RSV IBs, to improve our understanding of RSV innate immune antagonism.

1.3. The small hydrophobic protein

1.3.1. Sequence and structure

The small hydrophobic (SH) protein - 73 (strain A51908) or 81 (strain 391-2) amino acids in length in bRSV and 64 (subgroup A) or 65 (subgroup B) in hRSV - forms a single-pass type II transmembrane glycoprotein (Collins and Mottet, 1993, Gan et al., 2012, Gan et al., 2008). SH amino acid sequences are highly conserved among hRSV strains (Chen et al., 2000, Tapia et al., 2014) but less so between orthopneumoviruses (Fig 1.6A) (Samal and Zamora, 1991, Taylor, 2017). Structural studies of hRSV SH revealed an α-helical transmembrane domain extending from residues 18 to 43 (Gan et al., 2012), flanked by a intracellular/intravirion *N*-terminal domain (a short α-helix), and a larger *C*-terminal ectodomain which forms an extended β-hairpin (Fig 1.6B) (Li et al., 2014, To and Torres, 2018). During infection, SH production occurs via the secretory pathway, similarly to the F and G surface glycoproteins (McLellan et al., 2013). SH accumulates in membranes of the ER/Golgi complex and also in the plasma membrane, although it is incorporated into RSV filaments at much lower levels compared to F and G (Rixon et al., 2004, Triantafilou et al., 2013). Four different

forms of hRSV SH are present in infected cells: the primarily expressed full length non-glycosylated SH_0 (7.5 kDa), an N-terminally truncated SH_t (4.8 kDa) produced following translation initiation at the second start codon in the ORF, an *N*-glycosylated form of SH_0 - SH_g (13-15 kDa) (Collins and Mottet, 1993, Olmsted and Collins, 1989), which is subsequently modified with the addition of polylactosaminoglycan, producing SH_p (21-30 kDa) (Anderson et al., 1992).

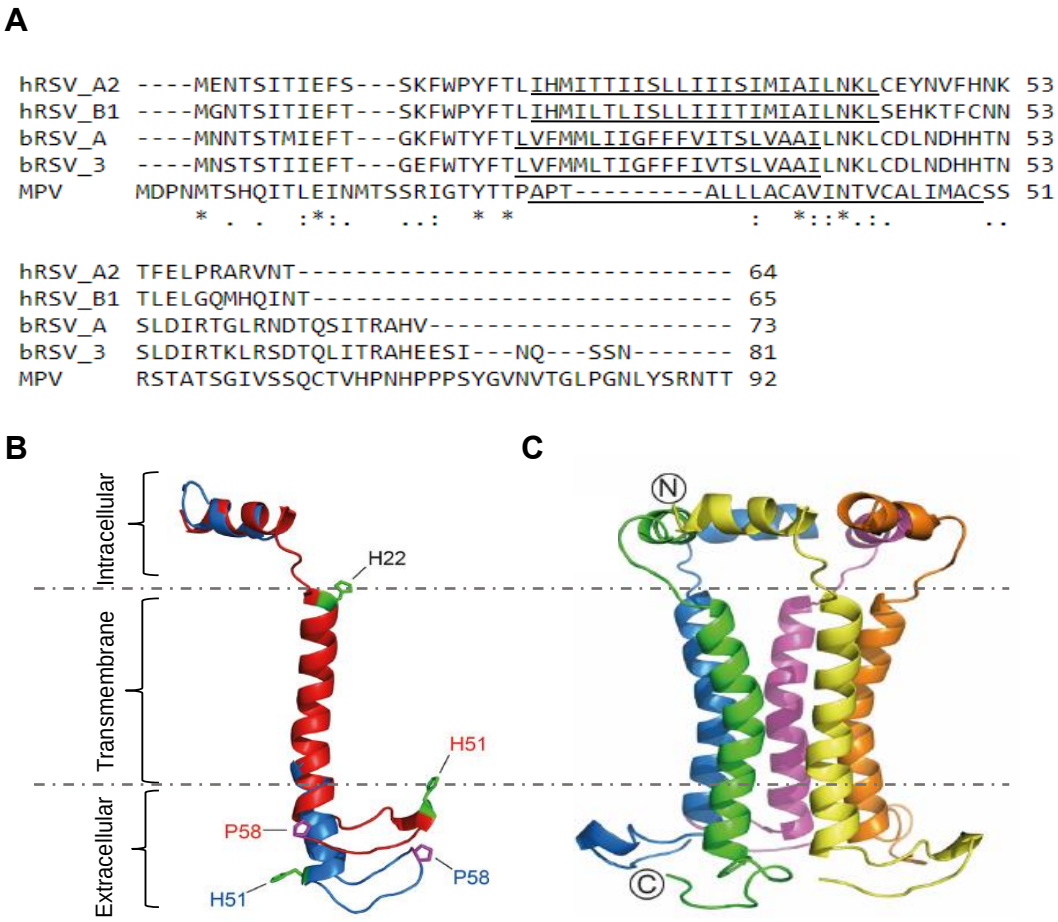

Figure 1.6 Orthopneumovirus SH protein. (A) Multiple alignment of SH protein sequences of orthopneumoviruses (hRSV subgroup A strain A2 and subgroup B strain B1; bRSV strains A51908 and 391-2; and murine orthopneumovirus strain 15). Transmembrane domains are underlined. (B) Overlay of two structural models of hRSV SH protein in dihexanoylphosphatidylcholine-dilauroylphosphatidylcholine (DHPC-DLPC) bicelles (blue) and dodecylphosphocholine (DPC) micelles (red) obtained by NMR studies (Li et al., 2014). Side chains indicated in green and purple are for comparison of the two structures. (C) Side-view of the proposed pentameric structure (Gan et al. 2012 and Surya et al. 2015). Colors here indicate different monomers.

These multiple forms are conserved for hRSV and bRSV SH (Anderson et al., 1992), despite low sequence identity between the two species (Fig 1.6A) (Taylor, 2017, Samal and Zamora, 1991). However, to date, there are no reports on the significance

of the maintenance of these variants. Interestingly, they can oligomerise in different combinations to form multimeric complexes in synthetic and biological membranes, the most abundant of which was a pentameric oligomer with ion-channel activity (Fig 1.6C) (Gan et al., 2012, Collins and Mottet, 1993, Carter et al., 2010).

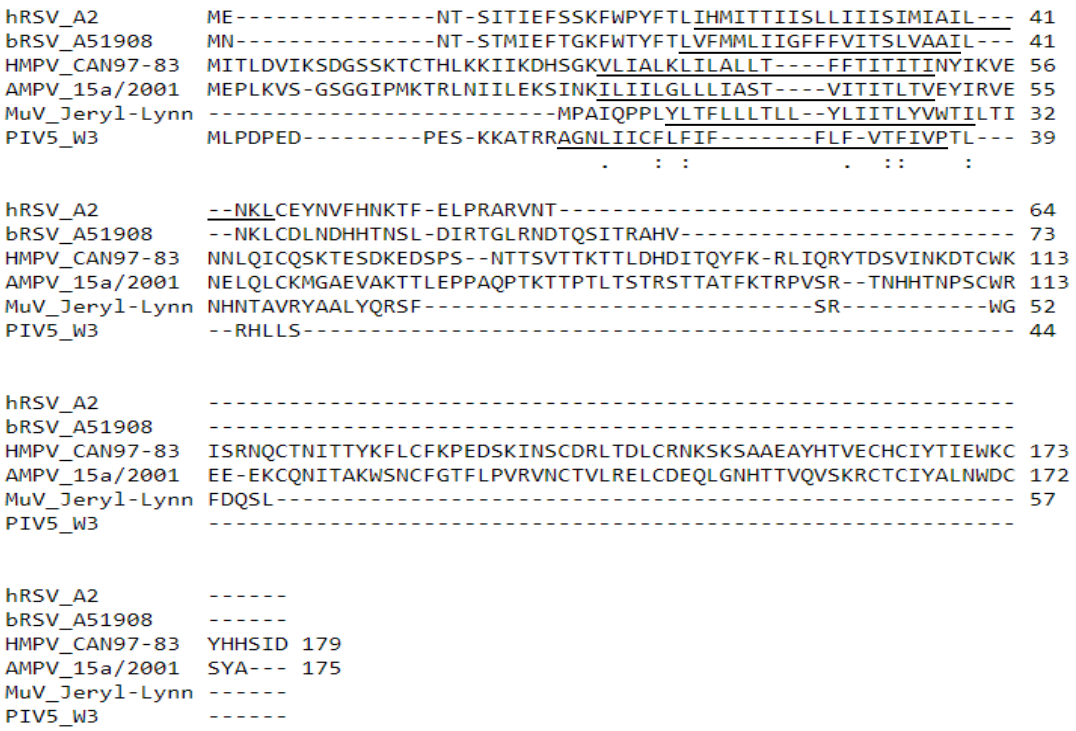

Figure 1.7 Multiple sequence alignment of SH proteins from selected mononegaviruses. Multiple sequence alignment of SH proteins of hRSV (A2) and bRSV (A51908) and orthologs in human metapneumovirus (HMPV; CAN97-83), avian metapneumovirus (AMPV; 15a/2001), mumps virus (MuV; Jeryl-Lynn) and parainfluenza virus 5 (PIV5; W3). Transmembrane domains are underlined.

SH proteins of similar properties are found in all other members of the pneumoviridae family (murine orthopneumovirus, HMPV and AMPV) and some members of the paramyxoviridae family (MuV, PIV5, Newcastle disease virus and J paramyxovirus) (Rima et al., 2017) but there is extensive sequence divergence between the species (Fig 1.7). Like RSV SH, they are type II membrane proteins, except for MuV SH, which is a type I membrane protein, and have relatively short lengths.

1.3.2. Role in infection and disease

SH is an accessory protein, dispensable for virus propagation *in vitro*. However, previous research has shown that both bRSV and hRSV SH inhibit the NF-κB pathway

and the induction of apoptosis to modulate the host response to infection (Fuentes et al., 2007, Taylor et al., 2014, Russell et al., 2015). In a study using bovine monocytes and Madin-Darby bovine kidney (MDBK) cells, infection with a virus in which the *SH* gene was deleted (bRSV ΔSH) enhanced apoptosis and the expression of pro-inflammatory cytokines, TNFα and IL-1β, compared to those infected with wild type bRSV (Taylor et al., 2014). Interestingly, Taylor et al. also observed no significant differences in the replication of the wild type and mutant bRSV although ΔSH hRSV was previously reported to replicate more efficiently than the wild type in some cell types (Whitehead et al., 1999, Jin et al., 2000b). Similar effects on NF-κB pathway activation and the induction of apoptosis were observed in another study of hRSV SH, where an inhibition of TNFα signalling was also observed (Fuentes et al., 2007). Interaction of SH with a critical regulator of apoptosis, B-cell associated protein 31 (BAP31) suggests a mechanism of inhibition in wild type RSV infected cells (Li et al., 2015). By comparing bRSV to ΔSH virus infected cells, or by ectopic expression of bRSV SH, we recently showed that SH modulates NF-κB by inhibiting phosphorylation of the p65 subunit and the degradation of the inhibitor IκBα (Pollock et al., 2017).

In *in vivo* studies, deletion of SH caused partial or full attenuation of the virus, depending on the experimental model of infection. For bRSV, similar replication profiles were observed in the upper respiratory tract (URT) of calves but the ΔSH virus was attenuated in the lower respiratory tract (LRT) (Taylor et al., 2014). In addition, the ΔSH virus induced significantly less pulmonary inflammation compared to the wild type although both were immunogenic and induced protection in calves immunised 6 months prior to challenge with virulent bRSV. Bukreyev *et al*. and Russell *et al*. also observed site-specific attenuation of hRSV ΔSH in the respiratory tract of mice (Bukreyev et al., 1997, Russell et al., 2015). These studies show that the SH protein plays a role in RSV pathogenesis by modulating the immune response and highlight the need to understand the molecular mechanisms by which it subverts the immune response.

As described in section 1.7, SH proteins of related viruses have also been shown to modulate NF-κB activity downstream of TNFα signalling (Fuentes et al., 2007, Bao

et al., 2008, Lin et al., 2003, Wilson et al., 2006, Parks and Alexander-Miller, 2013, Xu et al., 2011, Abraham et al., 2018, Li et al., 2011) even though they have low sequence homology (Fig 1.7). Similar to bRSV ΔSH, when cells were infected with rPIV5, rPIV5 ΔSH or rPIV5 with its SH gene replaced with that from hRSV strain A2 or B1 (rPIV5ΔSH-RSV A2 SH or rPIV5ΔSH-RSV B1 SH) (all with similar growth rates), only rPIV5 ΔSH infected cells were induced to undergo apoptosis (Fuentes et al., 2007). This indicates that, like bRSV, the SH proteins of hRSV and PIV5 inhibit apoptosis (an antiviral response) in infected cells. In addition, hRSV and PIV5 SH also inhibited nuclear localisation of NF-κB subunit p65 (Fuentes et al., 2007, Lin et al., 2003). Ectopic expression of hRSV (Fuentes et al., 2007) and bRSV (Pollock et al., 2017) SH proteins were both able to inhibit TNFα-induced NF-κB activation similarly to PIV5 (Fuentes et al., 2007), MuV (Wilson et al., 2006), and J paramyxovirus (JPV) SH (Li et al., 2011), expressed in the context of virus infection. The increase in expression of the NF-κB regulated genes, TNFα, in cells infected with PIV5 ΔSH (Lin et al., 2003) and JPVΔSH (Abraham et al., 2018, Li et al., 2011), plus IL-6, and IL-8 in hMPV ΔSH infected cells (Wilson et al., 2006) further shows the effect of SH on NF-κB activation. Separately, the SH protein of HMPV was shown to inhibit IFN signalling by targeting STAT1 expression and phosphorylation (Dinwiddie and Harrod, 2008, Hastings et al., 2016). In summary, the SH proteins encoded by several mononegaviruses appear to contribute to viral pathogenesis by modulating antiviral responses such as apoptosis induction, NF-κB activation and IFN signalling. Their mechanisms of action are currently unknown, except for MuV SH which was recently reported to interact with TNFR1/IL-R1/TLR3 complexes in the plasma membrane of infected cells, thereby interfering with NF-κB activation (Franz et al., 2017).

SH protein modulation of innate immune signalling has also been observed in antigen presenting cells (APCs) - dendritic cells (DCs) and macrophages (Guzman and Taylor, 2015). NF-κB activation in DCs up-regulates the expression of several pro-inflammatory cytokines and chemokines; proteins essential for antigen processing, presentation, and activation of the adaptive immune response, in particular, T-cell activation. The SH protein of bRSV was shown to block phosphorylation of NF-κB p65 in bovine monocytes and DCs (Pollock et al., 2017). Furthermore, RSV infection of monocyte-derived DCs significantly reduces their ability to activate CD4+ T Cells (de Graaff et al., 2005). This effect was also observed in HMPV infected human DCs

and shown to involve the SH protein (Le Nouen et al., 2014). SH was also shown to inhibit IFN induction downstream of TLR7/MyD88/TRAF6 signalling in HMPV infected plasmacytoid DCs. Thus, the presence of SH interferes with the biological role of DCs, the ultimate consequence of which may be an impairment in initiating the more specific adaptive response. Similar to infection of AECs, the mechanism and significance of this modulation on DC function requires further investigation.

1.3.3. SH viroporin structure and function

Chemical cross-linking analysis first highlighted the formation of various oligomers (di-, tri-, tetra-, and pentamers, *etc*.) of RSV SH (Collins and Mottet, 1993). Electron microscopy of SH in liposomes suggested the formation of pentameric or hexameric pore-like structures (Carter et al., 2010) and further analysis confirmed the adoption of pentameric structures in various lipidic membranes (Gan et al., 2008, Gan et al., 2012, Araujo et al., 2016, Li et al., 2014). These structures were also shown to alter membrane permeability to cations and small molecules (Perez et al., 1997, Gan et al., 2008), providing evidence of ion channel activity that could be inhibited by the presence of a small molecule inhibitor, pyronin B (Li et al., 2014). Structural models of the pentamer show circular arrangements of the monomeric units forming a central funnel-shaped channel (Li et al., 2015, Li et al., 2014). Interestingly, these structural and functional features are shared with a group of short viral membrane proteins with ion channel activity called viroporins (Gonzalez and Carrasco, 2003, Wang et al., 2011). Various orthologues have been shown to be expressed by a range of different viruses, for example, positive sense single-stranded RNA viruses - coronavirus E (Wilson et al., 2004) and 3a (Lu et al., 2006) proteins, and picornavirus 2B (Lama and Carrasco, 1992); segmented negative sense RNA virus - influenza A virus M2 (Pinto et al., 1992); retrovirus - HIV-1 Vpu (Ewart et al., 1996), and others (Wang et al., 2011). They are non-essential viral proteins that alter host cell plasma/intracellular membrane permeability by forming ion-selective oligomeric structures. Their function enhances virus growth by promoting processes such as virus entry, genome replication, glycoprotein transport, particle assembly and release (Gonzalez and Carrasco, 2003, Wang et al., 2011).

Unlike well characterised viroporins, such as M2 homo-tetramers that form proton-selective ion channels (Pinto et al., 1992) to promote virus uncoating in endosomes (Mould et al., 2000), the biological role of SH viroporins are unclear. As more evidence emerges on their ability to form viroporins (Gan et al., 2008, Gan et al., 2012, Araujo et al., 2016), other studies have reported that this activity plays a role in IL-1β secretion (Segovia et al., 2012a, Triantafilou et al., 2013). Prior to their secretion, IL-1β and IL-18, expressed following NF-κB activation require cleavage into active forms by caspase-1 (Farag et al., 2020). Caspase-1 on the other hand is activated downstream of multiprotein complexes known as inflammasomes which are induced by infection or cellular stress. Segovia *et al.* showed that in RSV infected cells, IL-1β expressed via the TLR2/MyD88/NF-κB pathway was processed and secreted following inflammasome activation induced by reactive oxygen species production and potassium efflux (Segovia et al., 2012a). This was later shown to involve the activity of SH viroporins located in Golgi lipid rafts (Triantafilou et al., 2013). However, the exact mechanism and role of this function requires further study, especially since RSV lacking SH induces higher levels of IL-1β when compared to wild type (Russell et al., 2015, Taylor et al., 2014).

Similar to RSV SH (Segovia et al., 2012a, Triantafilou et al., 2013), the ion channel activities of coronavirus E (Nieto-Torres et al., 2014), influenza virus M2 (Ichinohe et al., 2010), and hepatitis C virus (HCV) P7 (Farag et al., 2017, Negash et al., 2013, Shrivastava et al., 2013) proteins were shown to induce NLRP3 inflammasome activation and the subsequent maturation of pro-IL-1β to the active form (Farag et al., 2020). Interestingly, some of the other reported roles for RSV SH have also been associated with other viroporins. For example, the coronavirus, SARS-CoV, E protein that also forms homopentameric ion channels, is a virulence factor important for virus pathogenesis. Deletion of the protein (rSARS-CoV-ΔE) increased apoptosis in infected cells (DeDiego et al., 2011) and also led to attenuation of the virus *in vivo* (DeDiego et al., 2014). However, in the case of rSARS-CoV-ΔE infections, attenuation was associated with inhibit of NF-κB-mediated inflammation (DeDiego et al., 2014) contrary to the increased responses observed in ΔSH virus infected cells (Fuentes et al., 2007, Taylor et al., 2014).

1.4. Inclusion bodies

1.4.1. RSV inclusion bodies and liquid organelles

Human RSV infection is characterised by the formation of intracytoplasmic granules known as inclusion bodies (IBs; Fig 1.8) (Fricke et al., 2013, Lifland et al., 2012, Rincheval et al., 2017). These have been consistently observed both *in vitro* and *in vivo* (Norrby et al., 1970, Neilson and Yunis, 1990, Garcia et al., 1993, Lifland et al., 2012, Rincheval et al., 2017, Fricke et al., 2013), and are structurally and functionally similar to inclusions formed by several other viruses classified within the *Mononegavirales* order. This includes IBs induced by rabies virus infection termed Negri bodies (Lahaye et al., 2009, Nikolic et al., 2016, Nikolic et al., 2017), hMPV (Cifuentes-Munoz et al., 2017), MeV (Zhou et al., 2019), NiV (Ringel et al., 2019), and Ebola virus (Hoenen et al., 2012), and likely represent an essential component of the cellular cycle of many negative-sense RNA viruses. Recently, IBs were also observed in IAV infected cells, negative strand RNA viruses with a segmented genome (Alenquer et al., 2019).

Interestingly, viral IBs also share many characteristics with biomolecular condensates called liquid organelles (Nevers et al., 2020). These form by liquid-liquid phase separation, LLPS, a process which favours macromolecular-macromolecular over macromolecular-water interactions (Banani et al., 2017, Uversky, 2017, Nevers et al., 2020, Alberti et al., 2019). The resulting structures have high molecular density, are composed of RNA and proteins (mostly RNA-binding proteins, RBPs), and also lack surrounding membranes, unlike classical organelles. These organelles are not exclusive to pathogens; cellular examples of biomolecular condensates include stress granules and P-bodies that form in the cytoplasm, and nucleoli and Cajal bodies found in the nucleus (Gomes and Shorter, 2019, Banani et al., 2017). They can be identified by their liquid-like properties based on the following criteria: spherical shape, ability to rapidly undergo fusion and fission, and their high fluidity/dynamic state when assessed by fluorescence recovery after photobleaching (FRAP) (Gomes and Shorter, 2019, McSwiggen et al., 2019, Alberti et al., 2019).

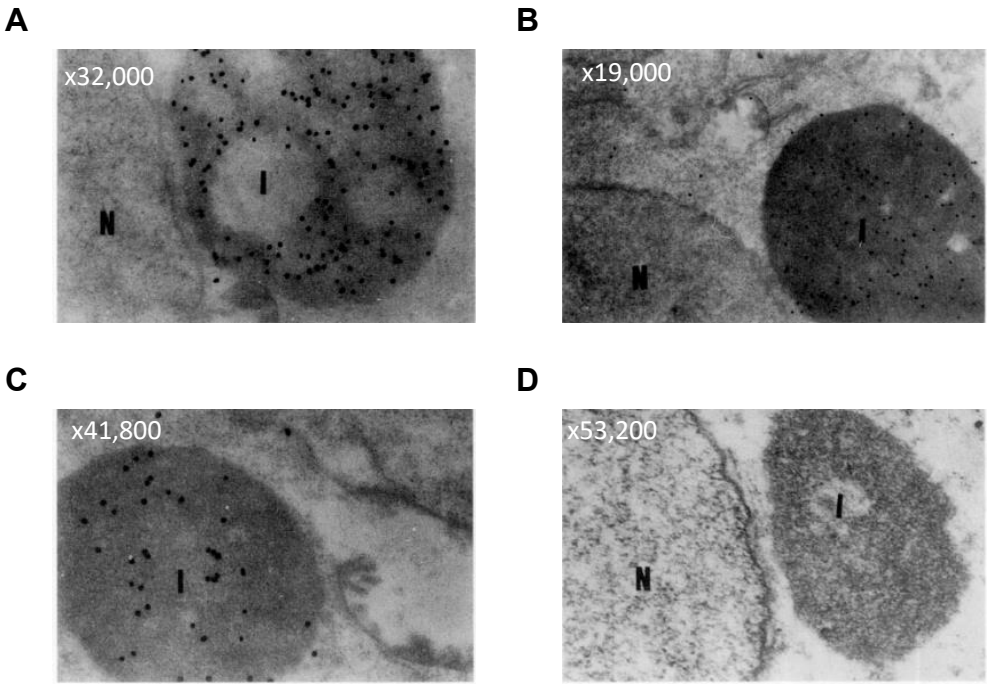

Figure 1.8 Inclusion bodies in RSV infected Hep-2 cells identified by immuno-electron microscopy. Inclusion bodies were immunogold labelled with mAbs against (A) P, (B) N, (C) M2-1 and (D) M proteins. N indicates cell nuclei and I cytoplasmic inclusions. Figure adapted from (Garcia et al., 1993).

Recent studies have provided insight into the process of phase separation - the mechanism underlying liquid organelle formation and maintenance. Alberti *et al.* noted that all proteins and nucleic acids have the propensity to undergo LLPS under specific physicochemical conditions but that only a subset of protein sequences can support LLPS in the conditions present in a cell, under physiological conditions (Alberti et al., 2019). These authors, and others, have further suggested that proteins containing specific molecular signatures including multiple folded domains, intrinsically disordered regions (IDRs) and RNA-binding domains can form multiple protein-protein and protein-RNA interactions. (Banani et al., 2017, Alberti et al., 2019, Kato et al., 2012, Lin et al., 2015, Uversky, 2017). These motifs are found in proteins with low sequence complexity and those that contribute to initiating nucleation have been termed “scaffolds” (Banani et al., 2017). At high cellular concentration, the multivalent interactions formed enable the proteins to transition from a dispersed state, assembling into granules of high molecular density (Banani et al., 2017, Uversky, 2017). Once formed, the recruitment of proteins into the granules is also thought to be governed by the same molecular signatures (Lin et al., 2015, Alberti et al., 2019). Although the different types of liquid organelles have similar biophysical properties

their protein composition and functions differ (McSwiggen et al., 2019, Banani et al., 2017). As a result, they can be identified by differential markers, for example, TIA1 in stress granules, nucleolin in the nucleolus, TTP in P-bodies *etc*., (Uversky, 2017). However, how cells control this differential composition is not fully understood.

1.4.2. Assembly of RSV IBs

With regards to viral IBs – biomolecular condensates formed in the context of virus infection – several have been shown to have liquid-like properties based on the criteria currently used for defining liquid organelles. These include cytoplasmic inclusions induced in RSV (Rincheval et al., 2017), MeV (Zhou et al., 2019), VSV (Heinrich et al., 2018), rabies (Nikolic et al., 2017) and ebola (Hoenen et al., 2012) virus infected cells, formed through the process of LLPS (Alberti et al., 2019, Nevers et al., 2020). However, the exact mechanism of their formation is less well characterised. RSV IBs appear in the cytoplasm at around 6h post infection, as viral proteins are expressed and grow in size as infection proceeds (Fricke et al., 2013, Lifland et al., 2012, Rincheval et al., 2017). Although they colocalise all proteins of the polymerase complex (Fig 1.8), for RSV, rabies and measles viruses, the N and P proteins are the minimum components essential for their formation in the absence of infection (Lifland et al., 2012, Nikolic et al., 2017, Rincheval et al., 2017, Zhou et al., 2019). Co-expression of the N and P proteins alone results in the formation of IB-like structures (pseudo-IBs) with similar properties to the viral inclusions. For VSV, the minimal system requires the presence of L (Heinrich et al., 2018). Viral IBs are essentially condensates of RNA and protein as proven by the large amounts of nucleocapsids and viral mRNA contained in these structures (Fig 1.9).

The minimal system however does not rule out the involvement of RNA interactions in formation of the structures as cellular RNA may be used in the absence of virus infection. More recently, the N and P proteins of RSV (Galloux et al., 2020b) and MeV (Guseva et al., 2020) were shown to induce liquid droplets outside of the cellular environment, thus showing they are the main drivers of viral phase separation. However, there was a discrepancy between the two viruses in cells as the formation of pseudo-IBs by RSV N and P required N:RNA interaction (Galloux et al., 2020b); however, the MeV proteins did not (Guseva et al., 2020, Zhou et al., 2019). Guseva *et*

al. further showed that although RNA is dispensable for MeV N:P phase separation, it preferentially colocalises to and triggers assembly of nucleocapsid-like particles within the structures formed.

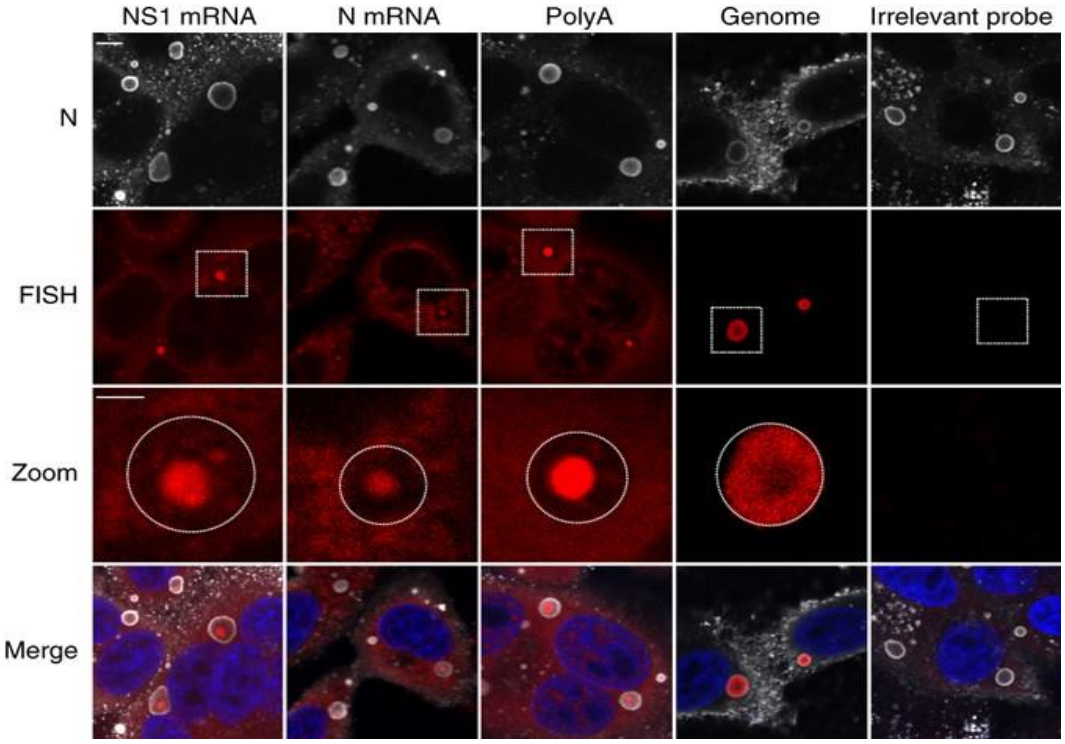

Figure 1.9 Locations of the N protein and viral RNAs in RSV infected cells. Hep-2 cells infected with RSV for 24 h were stained for the N protein to identify inclusion bodies (IBs; top panel). NS1 mRNA, N mRNA, polyadenylated RNA (PolyA) or viral genomic RNA, detected by Fluorescence in situ hybridization (FISH) colocalised with IBs. Scale bar in top panel 5 µm; in zoom panel 2 µm. IB boundaries are represented by circles. Figure taken from (Rincheval et al., 2017).

Similar to cellular proteins involved in inducing LLPS, assembly of ectopically expressed N and P proteins into inclusions has been shown to involve oligomerisation and intrinsically disordered domains within these viral proteins (Zhou et al., 2019, Nikolic et al., 2017, Galloux et al., 2020a). The higher degree of intrinsic disorder within P proteins of RSV (Gilman et al., 2019, Pereira et al., 2017), MeV and rabies virus (Nevers et al., 2020, Longhi et al., 2017) suggests it has a greater propensity to phase separate but the involvement of N shows there are crucial mechanisms provided by this protein. Mechanistically, for RSV, the central oligomerisation domain and C-terminal domain (an intrinsically disordered region) of P, plus the ability of N to interact with both P and RNA, were shown to be required for pseudo-IB formation

(Galloux et al., 2020b). Despite sequence variability, similar intrinsically disordered and oligomerisation domains are present in rabies and MeV P proteins (Nevers et al., 2020), and were also shown to be required for pseudo-IB formation (Nikolic et al., 2017, Zhou et al., 2019).

Therefore, it appears that the N and P proteins and RNA (depending on the virus) are the "scaffolds" required for IB formation. Thus, as the concentrations of the viral proteins increase during infection, oligomerisation of P, multiple interactions facilitated by the intrinsically disordered regions of N and P (Pereira et al., 2017) and interactions with viral RNA (Galloux et al., 2015) could act in synergy to initiate phase separation and nucleation of the IB. These may then mature and grow in size as they further colocalise newly synthesised viral RNA and protein. Of note, several other viral protein-protein and protein-RNA interactions which could contribute towards maturation exist in IBs. For instance, the viral nucleocapsid which concentrates in IBs (Fig 1.8 and Fig 1.9), is composed of genomic RNA, N, L and P proteins (Fig 1.2) (Easton et al., 2004). M2-1 also can form multiple interactions - with P (Mason et al., 2003, Richard et al., 2018), M (Li et al., 2008) and viral mRNA (Rincheval et al., 2017). However, the process of maturation appears to be a complex and regulated process as indicated by the organisation of the condensates into multi-phasic structures. Rincheval *et al.* recently demonstrated the presence of sub-compartments within RSV IBs with distinct protein and RNA composition, biophysical properties and functions termed inclusion body associated granules; IBAGs (Rincheval et al., 2017). M2-1 and newly synthesised viral mRNA, presumably interacting, mainly localised to these IBAGs (Rincheval et al., 2017). This is similar to the distinct, coexisting liquid phases that make up the nucleolus (Feric et al., 2016). The IBAGs are dynamic structures, and their contents are subsequently released to the cytoplasm. However, further investigation is required to understand the mechanism underlying the evolution of biomolecular condensates from a single phase to sub-compartments carrying out distinct functions.

1.4.3. Function of RSV IBs

The formation of membrane-less liquid organelles allow cells to spatially compartmentalise specific cellular processes whilst allowing biomolecule exchange

with the cyto-/nucleoplasm (Banani et al., 2017, Gomes and Shorter, 2019). Viruses also appear to use biomolecular condensation for a multitude of virus-virus/virus-host interactions with the advantage of increasing the efficiency of replication. Prominent examples include IBs which are essentially replication complexes and sites of nucleocapsid assembly (Nevers et al., 2020), and also lipid rafts where particle assembly takes place (McDonald et al., 2004). The functional compartmentalisation of viral proteins and replication intermediates into inclusion bodies also minimises their interaction with factors of the host immune response. The exact role of IBs induced during infection was previously unclear and initially thought of as "aggregates of viral nucleocapsids" (Garcia et al., 1993). Recent evidence shows it is a common mechanism used by several mononegaviruses and further demonstrates their involvement in processes such as viral RNA replication and host immune modulation (Nevers et al., 2020).

1.4.3.1. Viral RNA replication and transcription

Analysis of hRSV infected cells by immunofluorescence (IF) microscopy shows concentration of several viral proteins within IBs including N, P, L, M2-1, M and NS2 (Carromeu et al., 2007, Garcia et al., 1993, Lindquist et al., 2010, Brown et al., 2005, McDonald et al., 2004, Ghildyal et al., 2002). Most of these viral proteins are directly/indirectly associated with the nucleocapsid, explaining their colocalization within the structure. Interestingly, all of the proteins involved in transcription and replication (N, P, L and M2-1) co-localise in the IBs, whereas the surface glycoproteins are excluded. Recent identification of viral genomic RNA and mRNA within the IB (Fig 1.9) strongly suggests that these organelles are functional and are the primary site for viral RNA replication and transcription within the infected cell (Rincheval et al., 2017). Interestingly, distinct spatial organisations were observed between viral genomic and mRNA. As already noted above, mRNA concentrated in IBAGs whereas genomic RNA mostly localised towards the boundary of the IB (Fig 1.9). Further study is required to understand the significance of this organisation. Similarly, IBs produced in rabies (Lahaye et al., 2009) and ebola (Hoenen et al., 2012) virus infected cells were also shown as the sites of RNA replication and transcription. However, this does not appear to be a universal trend since viral RNA replication of Nipah virus (NiV) was recently shown to occur outside both its structurally distinct

IB populations (Ringel et al., 2019).

1.4.3.2. Innate immune antagonism

As discussed in sub-section 1.2.3, a number of host cell proteins have been shown to interact with or co-localise within RSV induced IBs. These include antiviral proteins MAVS and MDA5 (Lifland et al., 2012), and signalling proteins involved in the cellular response to viral infection – p38 mitogen-activated protein kinase (MAPK) and O-linked *N*-acetylglucosamine transferase (OGT) (Fricke et al., 2013). In addition, the chaperone protein, HSP70 that protects cells from stress, has also been observed within RSV IBs (Brown et al., 2005). MDA5 and MAVS sequestration into IBs were shown to result in a reduction of IFNβ mRNA induction (Lifland et al., 2012). Similarly, sequestration of p38 MAPK and OGT suppressed MK2 activity and stress granule assembly. This is distinct from the known RSV mechanisms of inhibition, for example, encoded by the SH and NS proteins (detailed in sub-section 1.2.3). RSV Recruitment of these key signalling proteins into IBs following RSV infection appears to be an additional mechanism of immune antagonism whereby their roles are inhibited through sequestration. However, whether these integrate with the scaffolds during the process of IB formation or associate with the granules as they mature, remains to be elucidated. Of note, viral IBs are induced in the early stages of infection, at a time when activation of innate immune signalling pathways is crucial. Thus, the use of IBs for innate immune antagonism is an important phenomenon for enhancing virus fitness during infection. Currently, it is unclear how broad this mechanism for regulating host antiviral responses is for viruses that induce cytoplasmic IBs. Much of what is currently known is on RSV IBs (Lifland et al., 2012, Fricke et al., 2013, Brown et al., 2005), although cellular WD repeat-containing protein 5 (Zhou et al., 2019, Ma et al., 2018), heat shock protein 72 (Zhang et al., 2005b) and actin-modulating protein cofilin (Koga et al., 2015) were also observed in measles virus IBs. Localisation of WD repeat-containing protein 5 in IBs was shown to enhance virus infection (Ma et al., 2018). It is therefore essential that further research is conducted to determine the scope of this strategy of immune modulation and to examine the implications for host responses to infection.

1.5. Aims of the study

RSV modulates the NF-κB signalling pathway during infection, but the underlying mechanisms of this modulation are not fully understood. The SH proteins of hRSV and bRSV are accessory proteins, dispensable for growth in cell culture and with poorly characterised functional roles. However, several reports have suggested a broad role in virus pathogenesis. This is based on virus attenuation observed in *in vivo* experiments using viruses lacking SH, bRSV ΔSH (Taylor et al., 2014) and hRSV ΔSH (Russell et al., 2015, Fuentes et al., 2007). This is further supported by evidence of similar responses with SH deletion mutants of related viruses such as, HMPV, MuV (Wilson et al., 2006) and PIV5 (Fuentes et al., 2007). These studies further showed that attenuation is associated with enhanced NF-κB-related responses, such as increased apoptosis and expression of NF-κB regulated proinflammatory cytokines and chemokines (Fuentes et al., 2007, Taylor et al., 2014, Russell et al., 2015). However, the molecular mechanism of NF-κB antagonism has not been fully explored, except for MuV SH (Franz et al., 2017). At the time of writing, I am aware of only one report showing the effect of RSV SH on NF-κB signalling (Pollock et al., 2017). However, in this study, Pollock *et al* investigated steps in the signalling cascade and downstream responses but failed to define the specific mechanism of inhibition mediated by SH. Within my PhD project, I aim to identify the specific molecular mechanism by which RSV SH inhibits the NF-κB signalling pathway using bRSV SH as model.

Separately, inclusion bodies induced in RSV infected cells have been shown to play a role in modulating the host immune response. A novel mechanism of NF-κB targeting was observed whereby the p65 subunit was sequestered into punctate structures in the cytoplasm of bRSV infected cells. The aim of this aspect of my PhD is to investigate this finding by characterising the p65 granules and uncovering the implications of this phenotype for activation of the NF-κB signalling pathway. Broad conservation of this viral modulation of p65 activity between orthopneumoviruses was also investigated by comparing bovine and human RSV. Finally, formation of cytoplasmic inclusion bodies is a characteristic feature of hRSV infection (Fricke et al., 2013, Garcia et al., 1993, Lifland et al., 2012, Rincheval et al., 2017). These form by liquid-liquid phase

separation and have been shown to play a role in compartmentalising virus genome replication and mRNA transcription, as well as nucleocapsid assembly (Richard et al., 2018, Rincheval et al., 2017). However, to date, there is no evidence on the formation of these structures in bRSV infected cells. Thus, the final aim of my PhD was to investigate the formation of inclusion bodies in bRSV infected cells and assess their role in the virus life cycle by exploring the spatio-temporal organisation of viral RNA and protein synthesis.

The NF-κB pathway is an important regulator of the host immune response to infection. I hypothesise that RSV targets NF-κB signalling through multiple mechanisms to inhibit the innate immune response.

Chapter 2: Materials and methods

2.1. Cells and cell culture

Table 2.1 Eukaryotic cell lines used in this study.

Cell	Description	Source
Vero	monkey kidney epithelial cells	The Pirbright Institute's Central Services Unit (CSU)
MDBK	Madin-Darby bovine kidney cells	
293T	human embryonic kidney cells	
Hep-2	human epithelial type 2 cells	
THP-1	human monocyte-like cells	
BEAS-2B	human bronchial epithelial cells	ATCC

MDBK, Vero, 293T and Hep-2 cells were maintained in cell culture flasks (Corning) containing complete medium (Dulbecco's modified Eagle's medium [DMEM; Gibco, Life Technologies] supplemented with 10% heat-inactivated foetal calf serum [FCS; TCS Biologicals], 1% sodium pyruvate solution [Sigma], and 1% penicillin/streptomycin [P/S; 10000 U/ml; Life Technologies]) at 37°C in a 5% CO_2 atmosphere. Beas-2B and THP-1 cells were maintained as above in LHC basal medium (ThermoFisher) or RPMI-1640 medium (Gibco), respectively, supplemented with 10% FCS and 1% P/S. All adherent cells (MDBK, Vero, 293T, Hep-2 and Beas-2B) were passaged when >80% confluent. Before splitting, cell culture medium was removed, and cells detached from the flask after washing once with PBS using 0.25% trypsin-EDTA solution (Life Technologies) for 5 to 10 mins. Cells were then resuspended 1:10 to 1:20 in complete medium and allowed to proliferate. Suspension THP-1 cells were passaged into new culture flasks when cell density reached $1x10^6$ cells/ml, at $5x10^5$ cells/ml.

2.2. Virus work

2.2.1. Virus propagation

Wild type recombinant bRSV (rbRSV) and deletion mutant rbRSVs ΔSH, ΔNS1, ΔNS2, and ΔNS1/2 were produced by reverse genetics from rbRSV strain A51908

variant Atue51908 (GenBank accession no. AF092942) (Schlender et al., 2000, Buchholz et al., 1999, Karger et al., 2001). BRSVs were propagated in Vero cells whereas hRSV subtype A (A2 strain) was grown in Hep-2 cells. A day prior to infection, $5x10^6$ cells were seeded into T175 cm^3 tissue culture flasks and incubated at 37°C in a 5% CO_2 atmosphere. 24 h later, cells were washed once with PBS infected with virus diluted in 10 ml serum-free DMEM for an MOI of 0.01 and returned to the incubator. Following 90 min virus adsorption, unbound virus was removed, and cells further incubated in 15 ml virus-free media containing 2% FCS and 1% P/S. At 3 days post infection (dpi), when cytopathic effect was pronounced, infected cells were harvested by scraping into the medium and transferred into 50 ml Falcon tubes kept on ice. Viruses were then extracted and purified as described below.

2.2.2. Virus concentration and purification by ultracentrifugation

The virus/cell suspensions from 2.2.1 were vortexed for 20 secs and then sonicated as follows: 70% Amp, pulsed 1 sec on, 1 sec off, for 20 secs followed by 10 secs (BRANSON Digital Sonifier). Virus supernatants were made by centrifugation in a Beckman Coulter centrifuge at 2900 *xg* for 20 min at 4ºC to remove cell debris. $MgSO_4$ (Sigma) was added to virus supernatants at a 100 mM final concentration. 50% (w/v) polyethylene glycol (PEG) 6000 (Sigma) in NT buffer (100mM $MgSO_4$, 150 mM NaCl (Sigma), 1mM EDTA (Invitrogen), 50 mM Tris-HCl (Sigma), pH 7.5) and serum-free DMEM were also added to make final concentrations of 10% and 2.3% (v/v), resp. Virus particles were precipitated for 90 mins at 4ºC on a magnetic stirrer and then pelleted at 2900 *xg* for 20 min at 4ºC. Supernatants were discarded and the pellets re-suspended in 700 µl ice cold NT buffer.

A day before virus purification, discontinuous sucrose gradients were prepared by sequential layering and freezing at -80ºC of 60, 45 and 30% sucrose (Sigma) in NT buffer in Ultra-Clear 14x95 mm centrifuge tubes (Beckman Coulter UK Ltd). Gradients were allowed to thaw at 4ºC and then layered with PEG precipitated virus samples. Tubes were balanced by topping up with NT buffer and then centrifuged at 4ºC in a SW-32 rotor for 1.5 h at 32,000 rpm. For all viruses, two bands were visible: at the 30-45% and 45-60% interface (Fig A1.A), except for the ΔNS viruses due to poor yield (Fig A1.D). Both bands were collected, aliquoted, snap frozen in liquid nitrogen and stored at -80ºC. The presence of viral F and SH proteins in the fractions

were analysed by western blot prior to use (Fig A1.B, Fig A1.C and Fig A1.D) and titres of all virus stocks determined in Vero cells by TCID50 assay using the Reed-Müench method.

2.2.3. Virus quantification by TCID50 assay

On the day of virus titration, $1x10^4$ cells per well in 100 µL DMEM with 2% FCS and 1% P/S were seeded into flat-bottom 96 well plates (Thermo Scientific). Virus stocks were serially diluted 1:10 in 2% FCS DMEM in round-bottom 96 well plates (Thermo Scientific), enough to make 4x replicate infections. 50 µL of each dilution was transferred onto the cells to generate a set of 4 columned replicates and the plates incubated at 37°C in a 5% CO_2 atmosphere. Virus titres were calculated 5-7 dpi when cytopathic effect was pronounced.

2.2.4. Virus infections

For the single step growth curves, $1x10^5$ MDBK or Vero cells were seeded in DMEM with 2% FCS and 1% P/S per well in 6 well plates (Thermo Scientific) and incubated at 37°C. The next day, cell monolayers were washed once with PBS, infected with wild type bRSV or ΔSH at an MOI of 2 in serum-free medium and incubated at 37°C and 5% CO2. The inoculum was removed 90 mins later, cells were washed 2x with PBS, and finally replaced with DMEM containing 2% FCS and 1% P/S and returned to the incubator. Viruses were then harvested by snap freezing at 3, 6, 16, 24, 48 and 72 h p.i, and virus titres later determined by TCID50 end point assay. For virus growth in THP-1 cells, $1x10^5$ cells prepared in serum-free RPMI medium were infected with wild type bRSV or ΔSH at an MOI of 2 and incubated at 37°C and 5% CO2 for 90 mins with rotation. Inoculum was removed by pelleting cells at 500 *xg* for 5 min before washing twice in PBS and incubating in RPMI with 10% FCS and 1% P/S. Viruses were harvested by snap freezing at 0 and 72 h p.i and nascent virus titrated by TCID50 assay.

For all other investigations, cells were seeded a day prior to reaching approximately 70-80% confluency on the day of infection. Cell monolayers were left uninfected/mock infected or infected with virus stocks diluted in serum-free medium for the desired MOI at 37°C and 5% CO2. Cells were infected for 90 min before inoculum was removed and replaced with medium containing 5% FCS and 1% P/S.

For western blot analysis, THP-1 cells were prepared on the day of infection and infected in tubes with rotation. Inoculum was removed by pelleting cells at 500 *xg* for 5 mins and then re-suspending in medium containing 10% FCS and 1% P/S. For immunofluorescence (IF) microscopy, THP-1 cells were adhered to coverslips pre-treated with Corning Cell-Tak (Fisher Scientific) after antibody labelling.

2.3. Antibodies and dyes

Antibodies used in this study include primary (commercial and in-house generated) and secondary (commercial) antibodies, and are detailed in Tables 2.2 and 2.3, respectively.

Table 2.2 Primary antibodies generated against RSV and cellular proteins.

Antibody	**Source**	**Validation/approved application**	**Application**
Mouse monoclonal anti-RSV F (mAb19)	(Taylor et al., 1992)	Radioimmunoassay and IF	WB (1/200); IF (1/400)
Mouse monoclonal anti-RSV N (mAb89)	(Taylor et al., 1984)		WB (1/1000); IF (1/400)
Mouse monoclonal anti-RSV P (mAb12)	(Taylor et al., 1984)		WB (1/500); IF (1/100)
Mouse monoclonal anti-RSV M (mAb105)	Geraldine Taylor, The Pirbright Institute		IF (1/100)
Mouse monoclonal anti-RSV M2-1 (mAb91)			IF (1/100)
Rabbit polyclonal anti-bRSV SH	Ingenasa	WB	WB (1 µg/ml); IF (1/1000)
Rabbit polyclonal anti-hRSV SH	BH Labs	WB	WB (1/1000); IF (1/400)

Rabbit monoclonal anti-NF-kB p65 (D14E12)	Cell Signaling Technology	WB, IF, IP, CHIP assay, *etc.*	WB (1/1000); IF (1/800)
Rabbit monoclonal anti-phospho-NF-kB p65 (Ser536) (93H1)		WB, IF, IP, *etc*.	WB (1/1000)
Mouse monoclonal anti-IKappaBalpha (L35A5) (Amino-terminal antigen)		WB, IF, IP, *etc.*	WB (1/1000)
Rabbit monoclonal anti-phospho-IKappaBalpha (S32) (14D4)		WB, IF, IP, *etc*	WB (1/1000)
Rabbit monoclonal anti-IRF3 (D614C)		WB, IF and IP	IF (1/100)
Rabbit anti-alpha tubulin	Abcam	WB	WB (1/10000); IF(1/1000)
Rabbit monoclonal anti-GAPDH	Cell Signaling Technology	WB, IF, IP, *etc*	WB (1/1000)
Rabbit polyclonal anti-FLAG		WB, IF, IP, CHIP assay, *etc.*	WB (1/1000); IF (1/200)
Rabbit anti-beta Actin	Abcam	WB, IF and IHC	WB (1/5000); IF (1/500)
Mouse monoclonal anti-V5 tag	Thermo Fisher	WB, IF, IP, ELISA, CHIP assay, *etc.*	WB (1/5000); IF (1/5000)
Rabbit monoclonal anti-Calnexin	Cell Signaling Technology	WB, IF and IHC	IF (1/100)
Rabbit monoclonal anti-AIF		WB, IP, IF and IHC	IF (1/100)
Mouse anti-G3BP	BD Biosciences	WB and IF	IF (1/100)

Rabbit monoclonal anti-eIF4G	Cell Signaling Technology	WB, IF, IHC, *etc*.	IF (1/100)
Rabbit monoclonal anti-eIF4A1		WB	IF (1/100)

Table 2.3 Secondary antibodies and dyes.

Antibody	**Source**	**Application**
Goat polyclonal anti-rabbit IgG (heavy and light chain), HRP-linked antibody	Cell Signaling Technology	WB (1/2000)
Horse polyclonal anti-mouse IgG (heavy and light chain), HRP-linked antibody		WB (1/2000)
Goat polyclonal anti-mouse IgG (H+L), Alexa Fluor 488	Life Technologies	IF (1/2000)
Goat polyclonal anti-rabbit IgG (H+L), Alexa Fluor 488		IF (1/2000)
Goat polyclonal anti-mouse IgG (H+L), Alexa Fluor 568		IF (1/2000)
Goat polyclonal anti-rabbit IgG (H+L), Alexa Fluor 568		IF (1/2000)
Goat polyclonal anti-mouse IgG2a, Alexa Fluor 647		IF (1/2000)
Goat polyclonal anti-mouse IgG2a, Alexa Fluor 488		IF (1/2000)
Goat polyclonal anti-mouse IgG2b, Alexa Fluor 568		IF (1/2000)
4, 6-diamidino-2-phenylindole (DAPI)	Invitrogen	IF (1/10000)
Vectashield Antifade mounting medium with DAPI	Vectorlabs	Neat

2.4. Molecular techniques

Table 2.4 Outsourced plasmids.

Name	Description	Source
pcDNA3.1(+)	Mammalian constitutive expression vector with CMV promoter.	Invitrogen
pcDNA6 bRSV SH-V5/His	Expresses the bRSV SH protein	(Pollock et al., 2017)
pcDNA3.1 hRSV SH	Expresses the hRSV SH protein	Provided by Jane McKeating; University of Birmingham
pcDNA3.1 bRSV N	Expresses codon-optimised bRSV N protein	Bio Basic Inc
pcDNA3.1 hRSV N	Expresses codon-optimised hRSV N protein	Bio Basic Inc
pcDNA3.1 BST2-FLAG	Expresses FLAG-tagged bone marrow stromal antigen 2 (BST2)	(Kelly et al., 2019)
pcDNA3.1 HA-p65	Expresses HA-tagged NF-κB subunit p65	Provided by Carlos Maluquer de Motes; University of Surrey
pCI MC159	Expresses the MC159 protein of molluscum contagiosum virus	Provided by Chris Netherton, The Pirbright Institute and used with permission from Joanna Shisler, University of Illinois (Randall et al., 2012)
pCEP MC005	Expresses the MC005 protein of molluscum contagiosum virus	Provided by Gareth Brady; The University of Dublin
pTRAF2	Expresses human TRAF2	

NF-κB-Fluc	Expresses firefly luciferase under the control of NF-κB response elements	
pGL3 renilla luciferase (TK-renilla)	Constitutively expresses renilla luciferase	

2.4.1. Diagnostic reverse transcriptase (RT) PCR

Production of ΔNS1, ΔNS2, and ΔNS1/2 bRSV were previously described (Schlender et al., 2000, Buchholz et al., 1999). RT-PCR was used to confirm deletion of the genes by comparing PCR fragments from the mutant viruses to that produced from wild type bRSV. Vero cells were infected with the viruses at an MOI of 2 and total RNA extracted 24 h later using TRIzol reagent (ThermoFisher Scientific) by following the manufacturer's instructions. RNA extracts were resuspended in 30 µL molecular biology grade H_2O and quantified using a NanoDrop spectrophotometer.

Single-stranded cDNA were generated from the RNA extracts using SuperScript II reverse transcriptase (Invitrogen) following the manufacturer's instructions. Each reaction contained 1µg vRNA and forward or reverse primers (Table 2.5) which amplify from the gene start (Gs) region of NS1 to the beginning of the N gene. The single strand cDNA were then used as templates for amplification in PCR with *Taq* DNA polymerase (New England BioLabs), also following the manufacturer's instructions.

Table 2.5 Primers for RT-PCR

Description	**Sequence (5′ to 3′)**
Binds the NS1 G_S region of the bRSV genome	ACGCGAAAAAATGCGTATAACAAACCTGTACATCCA
Binds the beginning of the bRSV *N* gene	GAGCCATTTTTGTATTTGCCCCACATTTCA

2.4.2. Cloning into pcDNA3.1

2.4.2.1. Oligonucleotides

To design oligos, the *SH* gene sequence was targeted from bRSV Snook strain; *N* and *P* gene sequences from bRSV A51908 (NC_038272) and hRSV A2 (KT992094); and NF-κB p65 coding sequence from (NM_021975). Forward and reverse oligonucleotides specific for the 5′ and 3′ ends, respectively, of the coding sequences were designed and purchased from Sigma (Table 2.6). Forward primers (For) were tailed with additional nucleotides to facilitate restriction enzyme digest (TTATT), followed by a restriction enzyme recognition site (underlined) and a Kozak consensus sequence (GCCACCATG; coloured blue) upstream of the complementary sequence to the 5′ end of the gene ORFs. Reverse primers were synthesised with a stop codon (TCA; coloured green), a restriction enzyme recognition site (underlined) and tail nucleotides (TATTA) downstream of the complementary sequence to the 3′ end of the gene ORFs. The coding sequence for a FLAG tag (coloured brown) was included in reverse primers and any desired mutations (coloured red) incorporated in both For and Rev primers.

Table 2.6 Primers for cloning RSV and host genes into pcDNA3.1

Sequence (5′ to 3′)	**Target gene ORF**
For: TTATTAAGCTTGCCACCATGAACAATACATCTACCAT AATAGAG Rev: TATTAGAATTCTCAGTTGCTTGA TTGGTTGATGGATCC	bRSV SH
For: TTATTAAGCTTGCCACCATGAACAATACATCTACCAT AATAGAG Rev: TATTAGAATTCTCATTTATCATCATCATCTTTATAATC GTTGCTTGATTGGTTGATGGATCC	bRSV SH-FLAG
For: TTATTAAGCTTGCCACCATGTTAGCCTTTATGATGTTA Rev:	bRSV SH-FLAG (ΔN1-19)

TATTAGAATTCTCATTTATCATCATCATCTTTATAATC GTTGCTTGATTGGTTGATGGATCC	
For: TTATTAAGCTTGCCACCATGACTGGTGAATTTTGGAC T Rev: TATTAGAATTCTCATTTATCATCATCATCTTTATAATC GTTGCTTGATTGGTTGATGGATCC	bRSV SH-FLAG (ΔN1-10)
For: TTATTAAGCTTGCCACCATGAACAATACATCTACCAT AATAGAG Rev: TATTAGAATTCTCATTTATCATCATCATCTTTATAATC TATTGCTGCCACTAATGA	bRSV SH-FLAG (ΔC41-82)
For: TTATTAAGCTTGCCACCATGAACAATACATCTACCAT AATAGAG Rev: TATTAGAATTCTCATTTATCATCATCATCTTTATAATC GATGTCTAGACTATTTGT	bRSV SH-FLAG (ΔC58-82)
For: CTTACTTTACATTAGCCGCCATGATGTTAACCATAGG Rev: CCTATGGTTAACATCATGGCGGCTAATGTAAAGTAAG	bRSV SH-FLAG (F22A)
For: GTGACTTCAACGATCATGCCACAAATAGTCTAGACAT C Rev: GATGTCTAGACTATTTGTGGCATGATCGTTGAAGTCA C	bRSV SH-FLAG (H51A)
For: TTATTGGTACCGCCACCATGGAAAAATTTGCACCTGA GT Rev: TATTAGGATCCTCAGAAATCTTCAAGTGATAGATC	bRSV P

For: TTATTGGTACCGCCACCATGGAAAAGTTTGCTCCTGA ATTCCATGGAGAAGATGC Rev: TATTAGGATCCTCAGAAATCTTCAAGTGATAGATCAT TGTCAC	hRSV P
For: TTATTGGTACCGCCACCATGGACGAACTGTTCCCCCT CATCTTCCCGGCAGAGC Rev: TATTAGGATCCGGAGCTGATCTGACTCAGCAGGGCTG AGAAGTCC	NF-κB p65

2.4.2.2. Isolation of total RNA from RSV infected cells

Vero cells were infected with hRSV or bRSV at an MOI of 2 and total RNA extracted 24 h later as already described in 2.4.1.

2.4.2.3. Reverse transcription

Single-stranded cDNA were generated from RSV RNA extracts (produced in 2.4.2.2) using SuperScript II reverse transcriptase (Invitrogen) following the manufacturer's instruction. Each reaction contained 1µg vRNA and primers specific for the 5′ and 3′ ends of b/hRSV *P* genes (Table 2.6).

2.4.2.4. Polymerase chain reaction (PCR)

The open reading frame (ORF) of full-length *SH* was amplified from a plasmid encoding bRSV SH snook strain (pcDNA6 bRSV SH-V5/His; (Pollock et al., 2017) using oligos flanked by *HindIII* and *EcoR1* restriction sites (Table 2.6) and KOD Hot Start DNA polymerase (EMD Millipore) following the manufacturer's instructions. FLAG-tagged and truncation mutants of *SH* were generated by amplifying the desired regions using oligos also flanked by *HindIII* and *EcoR1* restriction sites and incorporating the FLAG encoding sequence. F22A and H51A mutants were made by overlap extension PCR using primers incorporating the mutations. The ORFs of b/hRSV *P* were amplified from cDNA generated in 2.3.2.3 and NF-κB p65 amplified

from pcDNA3.1-HA-p65 (kindly provided by Carlos Maluquer de Motes, University of Surrey) using oligos flanked with *KpnI* and *BamHI* restriction sites. Each PCR reaction contained 10% (v/v) 10X Buffer for KOD Hot Start DNA Polymerase, 1.5 mM $MgSO_4$, 0.2 mM of each dNTP, 0.3 µM of each primer, 0.02 U/µL KOD Hot Start DNA Polymerase all in a final volume of 50 µL. PCR reactions were run for 30 cycles in a thermal cycler (Applied Biosystems).

2.4.2.5. Restriction enzyme digestion and isolation of DNA fragments

PCR products were purified using GFX PCR DNA and gel band purification kit (Merck) and digested in a 50 µL reaction containing 10% (v/v) 10X buffer (CutSmart; New England Bio-Labs) and 15 units of each enzyme. 5 µg pcDNA3.1 was digested in separate reactions also containing 10% (v/v) 10X buffer (CutSmart; New England Bio-Labs) and 15 units of each enzyme pair. Digests were incubated for 2 h at 37ºC. Vectors were then dephosphorylated using Antarctic phosphatase (New England Bio-Labs) by following the manufacturer's instructions.

DNA gel loading buffer was then added to digested inserts and vector and separated by agarose gel electrophoresis. Inserts were separated out using 1% (w/v) agarose (Sigma) gels and vectors on 2% (w/v) gels prepared in 1x Tris-borate EDTA (TBE; ThermoFisher Scientific) and stained with SYBR Safe DNA gel stain (Invitrogen). Electrophoresis was run at 100 V for 40-60 min in 1x TBE running buffer. DNA fragments were visualised on a UV transilluminator, relevant bands extracted using GFX PCR DNA and gel band purification kit and eluted in 30 µL H_2O.

2.4.2.6. Ligation of DNA fragments

Ligation reactions were prepared with 5 µL vector DNA, 7.5 µL insert DNA, 10% (v/v) ligation buffer, 1 µL T4 DNA ligase in a 20 µL reaction volume. A negative control containing no insert DNA was also prepared and the reactions incubated at 16ºC overnight.

2.4.2.7. Isolation of plasmid DNA and quality control

5 µL of each ligation mix was used to transform 50 µL of HB101 competent cells (Promega) and the mixture spread out onto agar plates containing 100 µg/ml ampicillin (Sigma). Plates were then incubated at 37ºC overnight in an inverted position.

Following successful transformation, 10 colonies were picked from each plate and grown in 5 mL LB-medium containing 100 µg/ml ampicillin at 37ºC overnight in a shaking incubator. Plasmid DNA were prepared from 4 mL of the overnight cultures using QIAprep miniprep kit (Qiagen) and eluted in 50 µL elution buffer (EB; 10 mM Tris-Cl). The presence of DNA inserts was confirmed by digesting 8 µL of isolated plasmids with 5 units of each enzyme in a 15 µL reaction followed by agarose gel electrophoresis. Sequences were confirmed by conventional sanger sequencing performed by GATC Biotech. Larger preparations of clones containing the right sequences were made using a QIAprep maxiprep kit (Qiagen).

Table 2.7 Primers for sequencing genes inserted into pcDNA3.1

Description	**Sequence (5′ to 3′)**
Forward primer: binds 3' region of CMV promoter in pcDNA3.1	CGCAAATGGGCGGTAGGCGTG
Reverse primer: binds 5' region of BGH polyA signal in pcDNA3.1	CCTCGACTGTGCCTTCTA

2.4.3. Transfections

Plasmids were transfected into cells using TransIT-X2 (Geneflow). Plasmid DNA were prepared in Opti-MEM (ThermoFisher Scientific), TransIT-X2 added (4 µL per 2 µg DNA) and then incubated at room temperature for 20 mins. Transfection mix was added dropwise to cells at 70-90% confluency and incubated at 37ºC and 5% CO_2 for the required times to allow protein expression.

2.4.4. SDS-PAGE and western blotting

Following virus infection, transient transfection or stimulation, growth medium was removed, and cells washed once with PBS. Cell extracts were prepared by lysing in 100 µl (1 x10^5 cells) or 200 µl (2 x10^5 cells) 1X SDS sample buffer (Laemmli; Bio-Rad) supplemented with β-mercaptoethanol (Sigma), Complete mini-EDTA-free protease inhibitors (Roche) and 1 mM sodium orthovanadate (New England Bio-Labs). Samples from virus growth and replication time points were prepared by adding 2X sample buffer in a 1:1 ratio. Cell extracts were denatured by boiling at 100ºC for 5 mins, with 20 µl separated by SDS PAGE using 1X running buffer (25 mM Tris,

192 mM glycine, and 0.1% (w/v) SDS, pH 8.3; Bio-Rad) on an 8-12% (v/v) polyacrylamide gel made with reagents from Bio-Rad. PageRuler plus prestained protein ladder (ThermoFisher Scientific) was included for molecular weight estimation. Electrophoresis was run at 30 mA for 15 min followed by 50 mA for 50-60 mins using a Mini-protean tetra system (Bio-Rad).

For western blotting, proteins were transferred to polyvinylidene difluoride (PVDF) membranes (Bio-Rad) with the Trans-blot Turbo blotting system (Bio-Rad) using 1X transfer buffer (25 mM Tris, 192 mM glycine, pH 8.3; Bio-Rad) and 20% (v/v) methanol following the manufacturer's instructions (30 min at 25 V). After blocking for 1 hr with 5% (w/v) semi-skimmed milk in PBS with 0.1% Tween 20 (mPBS-T) and washed thoroughly in PBS-T, the membranes were probed with primary antibodies overnight at 4^{o}C, washed three times with PBS-T and probed with the corresponding horseradish peroxidase-conjugated secondary antibodies (CST) in 5% mPBS-T. Protein bands were detected using Clarity Western ECL substrate (Bio-Rad) and imaged with Bio-Rad ChemiDoc^{TM} MP Imaging System. Data analysis and quantification of phospho-p65 band volumes were performed using ImageLab (Bio-Rad.

2.4.5. Coimmunoprecipitation.

A total of 1×10^5 293T cells cultured overnight in 12-well plates were transfected with pcDNA3.1-empty vector (pEV) or pcDNA3.1-p65 (pP65) using the TransIT-X2 reagent (Geneflow) as described in 2.4.3. After 24 h, cells were infected with bRSV at an MOI of 1 or mock infected and incubated for another 24 h. Cells were then lysed on ice for 10 mins with 200 µL radioimmunoprecipitation assay (RIPA) lysis buffer (EMB Millipore), transferred to sterile 1.5 mL tubes and cell debris removed by centrifugation (at 4°C, max speed for 10 mins). Immunoprecipitation was performed with protein A- or G-coated magnetic beads Cell Signaling technology; CST) according to the manufacturer's instructions. Cell lysates were precleared with beads and 60 µL incubated with rabbit anti-p65 (CST) or mouse anti-N protein antibodies overnight at 4°C with rotation. Lysates containing rabbit antibodies were then incubated with protein A-coated magnetic beads and those with mouse antibodies incubated with protein G-coated magnetic beads for 20 min at room temperature with rotation. Following five washes with PBS-T, immunoprecipitates were eluted with 40

µL 1X Laemmli sample buffer supplemented with β-mercaptoethanol (Sigma) and complete mini-EDTA-free protease inhibitors (Roche). 8 µL 4X sample buffer was added to 25 µL cell lysates as input control. All samples were subjected to SDS-PAGE (30 µL loaded per well on a 12% polyacrylamide gel) and western blot analysis as already described in 2.4.4.

2.5. Fluorescent and bright-field microscopy techniques

2.5.1. Cell viability assay

Viability of transfected cells was tested using CellTiter-Blue cell viability assay (Promega) following the manufacturer's instructions.

2.5.2. Luciferase reporter assay

A total of 2×10^5 293T cells seeded onto 24-well plates were co-transfected with 100 ng of a NF-κB FLuc reporter which expresses the firefly luciferase gene under the control of five NF-κB repeated transcription factor binding sites and 10 ng of the TK-ren control plasmid (both kindly provided by Gareth Brady; The University of Dublin) using Transit-X2 (Geneflow) as described in 2.4.3. For studying the effect of the SH protein, reporter plasmids were transfected together with 100 ng of empty vector (EV; pcDNA3.1), or plasmids expressing MC159, MC005, bRSV SH, SH-FLAG or hRSV SH. Separately, infections with virus (bRSV or hRSV) at an MOI of 1 were done 6 h prior to transfection of reporter plasmids. A total of 24 h post transfection, cells were left untreated or stimulated with 20 ng/ml hTNF-α for 4 or 16 hours. Cells were then lysed with 120 µL reporter lysis buffer (Promega) for 1 h at 4°C on a rocking platform and plates stored at -20°C overnight to enhance lysis. Thawed lysates were used to determine firefly and renilla luciferase activities on a Glomax luminometer using the luciferase assay system (Promega) and coeleterazine (Promega), respectively. Firefly data were normalized to renilla which was used as an internal control of transfection.

2.5.3. Confocal immunofluorescence microscopy

Cells grown on glass coverslips (13 mm in diameter) in 24 well plates were washed once in PBS then fixed with 4% paraformaldehyde (PFA; Sigma) in PBS for 15 min. Fixed cells were permeabilized with 0.2% Triton X-100 in PBS for 5 min and blocked

with 0.5% bovine serum albumin (BSA) (Sigma) in PBS. Cells were incubated in primary antibodies prepared in PBS with 0.5% BSA at the dilutions indicated in Table 2.2, overnight at 4°C on a rocking platform. They were then washed 3X with PBS and incubated with Alexa Fluor secondary antibodies (Life Technologies) prepared in PBS with 0.5% BSA at the dilutions indicated in Table 2.3, for 1 h at room temperature on a rocking platform. Cells were then washed 3X with PBS and coverslips mounted on microscope slides with Vectashield (Vector labs) containing 4′,6-diamidino-2-phenylindole (DAPI) for nuclei staining. Slides were stored in the dark at 4ºC before imaging. Fluorescence was imaged on a Leica TCS SP5 confocal microscope using 405-nm, 488-nm, and 568-nm laser lines for the appropriate dyes and a 63× oil immersion objective. Images were acquired at random in a single Z-position in the median section of the cells, unless otherwise stated and analysed using the Leica LAS AF Lite software.

2.5.4. Quantitation of bRSV-induced p65 puncta and IBs

Mock- or bRSV-infected MDBK cells were fixed in 4% PFA (Sigma) at 6, 16, 24 and 48 h p.i. and labelled according to the immunofluorescence method described in 2.5.3. Images were taken at a single Z-plane in the median section of the cells or at multiple Z-position, 0.5 μm apart, by confocal microscopy and max intensity Z-stacks of 8 planes made using the Leica LAS AF Lite software. Quantifications of p65 puncta were performed on images collected from a single Z-plane using the line and area region of interest analysis tool. N- and p65-positive structures in max intensity Z-stacks were quantified using the area region of interest tool. Acquired data were then processed in GraphPad Prism 7 and parametric one-way analysis of variance (ANOVA) and Tukey's multiple comparison tests performed.

2.5.5. 5-Ethynyl uridine (EU) labelling

To detect newly synthesised viral RNA, cells infected for 24 h and growing on coverslips were incubated with or without medium supplemented with 20 μg/ml actinomycin D (Act D) to inhibit cellular transcription for 1 h. Cells were then incubated with medium containing 1 mM 5EU and 20 μg/ml Act D for another hour. Medium was then washed off and cells fixed in 4% PFA for 15 min. Cells were then washed once with PBS and permeabilized with 0.2% Triton X-100 for 5 min. They were both supplemented with 0.125 U/ml RNase inhibitor (Promega). Incorporated

5EU was labelled using the Click-IT RNA imaging kit (Invitrogen) following the manufacturer's protocol. Following that step, immunofluorescence staining was done as described in 2.5.3.

2.5.6. Transmission electron microscopy

Cells seeded onto Thermanox coverslips (Thermo Scientific) were fixed at 24 h and 48 h p.i in phosphate-buffered 2% glutaraldehyde (Agar Scientific) for 1 hour and the rest of the protocol carried out by Jennifer Simpson (The Pirbright Institute bioimaging group). Briefly, glutaraldehyde fixation was followed by 1 hour in aqueous 1% osmium tetroxide (Agar Scientific). The following dehydration steps were performed in an ethanol series: 70% for 30 min, 90% for 15 min, and 100% 3X for 10 min. Subsequently, a transitional step of 10 min in propylene oxide (Agar Scientific) was undertaken before infiltration with a 50:50 mix of propylene oxide and epoxy resin (Agar Scientific) for 1 hour. After a final infiltration of 100% epoxy resin for 1 hour, the samples were embedded and polymerized overnight at 60°C. Next, 80-µm-thin sections were cut, collected onto copper grids (Agar Scientific), and grid stained using Leica EM AC20 before being imaged at 100 kV in a FEI Tecnai 12 TEM with a TVIPS F214 digital camera.

2.5.7. Correlative light electron microscopy

Cells seeded onto gridded glass coverslips (MatTek) were fixed at 24 h and 48 h p.i in 4% PFA (Sigma) and labelled according to the described immunofluorescence method (2.5.3). Cells were then handed to Jennifer Simpson who performed the rest of the protocol. Briefly, selected grid squares were imaged on a Leica TCS SP8 confocal microscope using 405-nm, 488-nm, and 568-nm laser lines for the appropriate dyes. The cells were then fixed in phosphate-buffered 2% glutaraldehyde (Agar Scientific) for 1 hour followed by 1 hour in aqueous 1% osmium tetroxide (Agar Scientific). Following 15 min in 3% uranyl acetate (Agar Scientific), the cells were dehydrated in an ethanol series, as follows: 70% for 30 min, 90% for 15 min, and 100% 3X for 10 min. After infiltration of 100% epoxy resin for 2 hours, the samples were embedded and polymerized overnight at 60°C. The glass coverslips were removed with liquid nitrogen and the appropriate grid squares located. Next, 80-µm-thin sections were cut, collected onto copper grids (Agar Scientific), and grid stained using a Leica EM AC20

instrument. The specific cells imaged in the confocal were identified and imaged at 100 kV in a FEI Tecnai 12 TEM with a TVIPS F214 digital camera.

2.6. Statistics

GraphPad Prism 7 was used to perform unpaired T tests or parametric one-way analysis of variance (ANOVA) and Tukey's multiple comparison tests.

2.7. Ethics statement

This research did not use any primary human or animal tissue.

Chapter 3: The role of bRSV SH protein in NF-κB activation

3.1. Introduction and aims.

As discussed in chapter 1, the RSV SH protein forms a single-pass, type II membrane glycoprotein, suggested to assemble into pentameric viroporins (Gan et al., 2012, Carter et al., 2010). Although its exact role in the virus lifecycle is not fully defined, previous studies using deletion mutants have demonstrated a role in inhibiting the inflammatory response in infected cells. Both bRSV and hRSV lacking the *SH* gene (bRSV ΔSH and hRSV ΔSH) induced higher levels of proinflammatory cytokines (TNFα and IL-1β) and apoptosis relative to wild type viruses (Taylor et al., 2014, Fuentes et al., 2007, Abraham et al., 2018, Russell et al., 2015). Furthermore, the mutant viruses were partially attenuated *in vivo*, although replication *in vitro* was comparable to the wild type viruses (Taylor et al., 2014, Russell et al., 2015). These responses were attributed to inhibition of the NF-κB pathway (Pollock et al., 2017) – a key regulator of the antiviral response that also induces expression of several proinflammatory cytokines. Thus, we hypothesised that there is a specific domain within the SH protein that inhibits a step in the NF-κB signalling pathway thereby preventing the correct modification of components, such as NF-κB subunit p65 or IκBα.

We aimed to test this hypothesis by comparing the effects of recombinant bRSV ΔSH and wild type bRSV infection on activation of the NF-κB pathway in epithelial cells, macrophages, and dendritic cells, using western blotting, immunofluorescence microscopy and reporter gene assay analyses. Specifically, we planned to examine IκBα degradation, NF-κB subunit p65 phosphorylation, p65 nuclear translocation and NF-κB transactivation in virus infected cells and in response to TNFα stimulation. In addition, the impact of ectopic overexpression of full length and mutant bRSV SH would also be assessed using the same techniques, to identify the role of specific domains within the SH protein. Experimental protocols would initially be established in epithelial and monocyte cell lines to uncover examples of significant inhibition. This would subsequently be followed up with analyses in more physiologically relevant primary bovine antigen presenting cells. Bovine RSV would be used as the

model virus throughout this study, however, hRSV and ectopic hRSV SH expression were to be included as controls where relevant. Understanding NF-κB modulation by RSV will improve our basic knowledge on how such infections interact with the host immune system. This is also important for developing future strategies to control RSV.

3.2. Results

3.2.1. Comparison of wild type and ΔSH bRSV replication.

To confirm the suitability of bRSV ΔSH as a tool for studying SH protein function, the *in vitro* replication fitness of this recombinant virus was evaluated and compared to wild type virus. Previous studies have shown that deletion of the *SH* gene does not significantly impact virus replication (Karger et al., 2001). Firstly, virus growth was compared in three different cell lines: MDBK (bovine kidney epithelial line), Vero (monkey kidney epithelial line) and THP-1 (human monocytic line) cells. To assess virus replication in the epithelial cells, Vero and MDBK cells were infected with recombinant bRSV (wild type and ΔSH) at a MOI of 2 and growth monitored. Viruses were harvested by making cell lysates in the growth medium to collect both cell-associated virus and virus released into the supernatant at 3, 6, 16, 24, 48 and 72 h p.i. Virus titres were then determined by TCID50 end point assay. In MDBK cells, bRSV ΔSH replicated faster in the early stages of infection when compared to wild type bRSV although there were no significant differences in the final titres (Fig 3.1A). Both viruses replicated to similar mean titres of 10^5 TCID50/ml by 72 hours post infection in MDBK (Fig 3.1A) and in Vero cells (Fig 3.1B). A separate experiment was set up, in Vero cells only, as described above to monitor cytopathic effect (cpe) by syncytia formation over a 6-day period. Cpe was observed earlier in cells infected with the mutant virus when compared to wild type bRSV (Fig B.1). At 72 h p.i., there were larger and more syncytiated cells in rBRSV ΔSH infected cells, however by day 6, both viruses had caused significant cpe in all cells. To conclude, although bRSV ΔSH replicates faster in the early stages of infection in MDBK cells, when compared to the wild type virus, both viruses grew to equivalent titres in Vero and in MDBK cells.

Although ciliated airway epithelial cells are the primary target of RSV, immune cells, such as macrophages and dendritic cells, which are major contributors in RSV-induced inflammation (Goritzka et al., 2015, Valarcher and Taylor, 2007), may also become

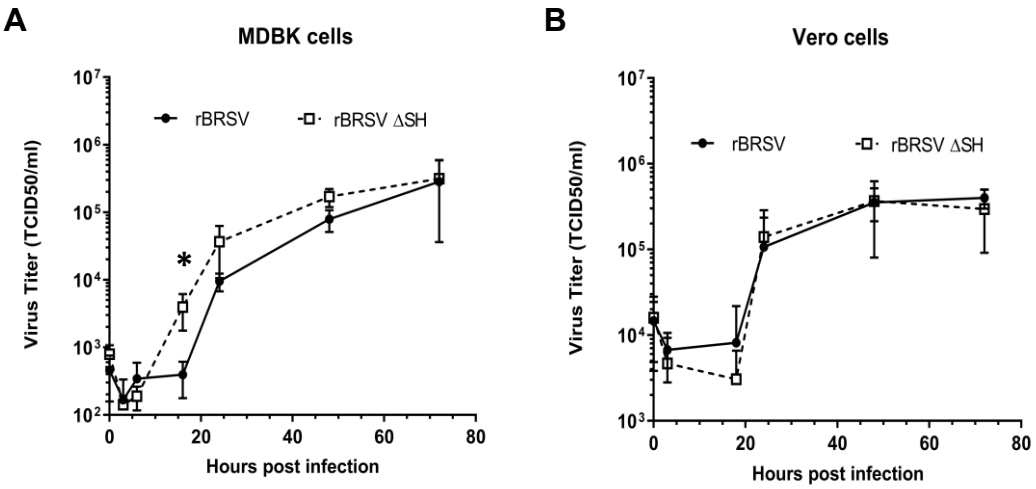

Figure 3.1 SH protein deletion does not reduce the efficiency of bRSV replication in epithelial cells. (A) MDBK (**B)** Vero cells were infected with wt bRSV or ΔSH at an MOI of 2. Viruses were harvested by snap freezing at 3, 6, 16, 24, 48 and 72 h p.i, and virus titres determined by TCID50 end point assay. Graphs show means ± SD of triplicate infections from the same experiment. Data are representative of n=2 independent experiments. Statistical significance was determined by unpaired T test. *p<0.05.

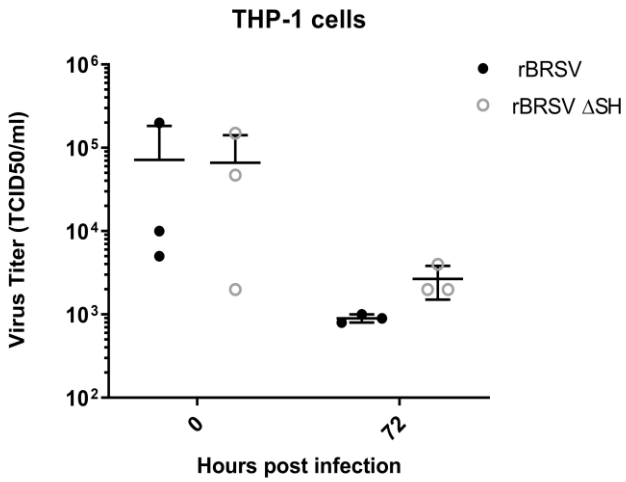

Figure 3.2 THP-1 cells are not permissive to recombinant bRSV replication. THP-1 cells were infected with wt bRSV or ΔSH at an MOI of 2. Viruses were harvested by snap freezing at the indicated times p.i, and virus titres determined. Graph shows means ± SD of triplicate infections from the same experiment and are representative of two independent experiments.

infected (Panuska et al., 1990, Jones et al., 2006). Furthermore, the increased IL-1β response observed in monocytes infected with bRSV ΔSH (Taylor et al., 2014) and hRSV ΔSH infected macrophages (Russell et al., 2015) suggests SH also has an effect on NF-κB in these cells. Due to the unavailability of a relevant bovine immune cell line, I used the human monocyte-like THP-1 line (Tsuchiya et al., 1980) in order to optimise experimental conditions for downstream analysis in primary bovine antigen presenting cells. Although THP-1 cells are routinely used as a model for primary monocytes (Bosshart and Heinzelmann, 2016, Qin, 2012), their susceptibility to RSV infection is unclear. Russell *et al*. have shown limited transcription of RSV-encoded RNA in these cells using GFP-expression (Russell et al., 2015), however the production of nascent virus was not explored. To examine this, THP-1 cells were infected at an MOI of 2 (equivalent to that used to infect epithelial cells) and virus growth determined at 72 h p.i. by TCID50 end point assay. The 0 h p.i. titres represent cell adsorbed virus which were collected following thorough washing of cells 2 h after incubation with inoculum. The significant differences in the titres compared to the values obtained in Fig 3.1 is likely due to increased virus-cell contact. Infection of THP-1 cells were carried out in suspension with gentle rotation whereas the epithelial cells were adherent. The titres obtained at 72 h p.i. include both cell-associated virus and virus released in the supernatant. Assessment of virus growth over the time course of the experiment, comparing titres at 0 h p.i. to 72 h p.i. (Fig 3.2), indicates a failure in the replication cycle. In summary, this data suggests that THP-1 cells are not permissive to bRSV replication.

3.2.2. Viral glycoprotein production in Vero and THP-1 cells

Although I did not observe nascent RSV production in THP-1 cells (Fig 3.2), the previously observed expression of virus-encoded GFP (Russell et al., 2015) indicates that they can support transcription of the RSV genome, and possibly protein synthesis. Thus, I examined how the observed nascent virus production (in Vero), or lack thereof (in THP-1 cells), correlated with viral protein synthesis. Vero and THP-1 cells were infected with virus and then at 0, 3, 6, 18, 24, 48, and 72 h p.i., examined for expression of bRSV F and SH proteins using western blot analysis. As observed with the growth analysis (Fig 3.1 and Fig 3.2), there was significant expression of the assessed viral proteins in Vero cells (Fig 3.3A), especially in the later stages of infection, but not in THP-1 cells (Fig 3.3B). In Vero cells, similar patterns of F protein expression were

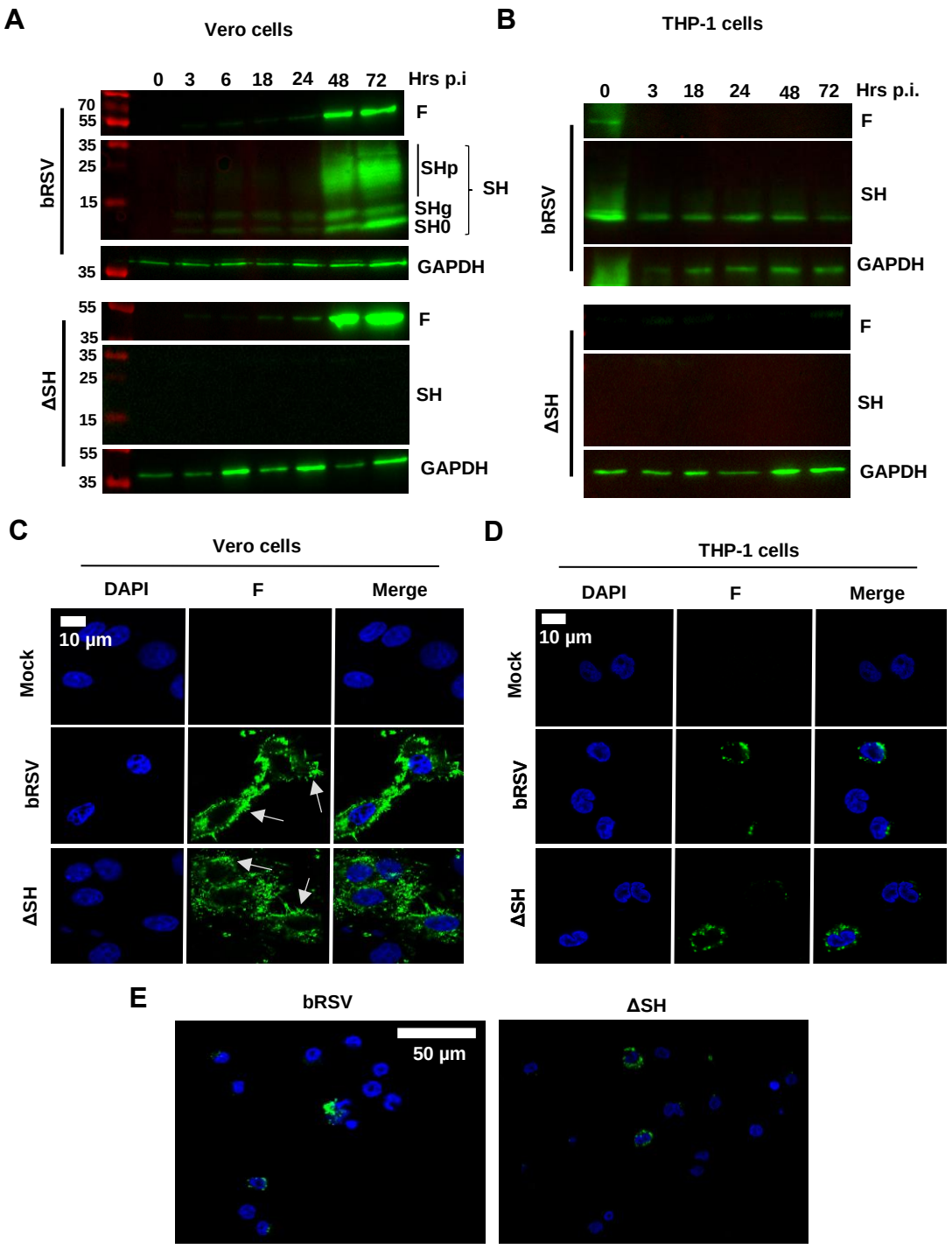

Figure 3.3 Viral protein expression by western blot and immunofluorescence analyses. (A) Vero and **(B)** THP-1 cells were mock infected or infected at an MOI of 2 with bRSV or bRSV ΔSH viruses. Cells were lysed at the indicated times and analysed by immuno-blotting using antibodies against the indicated proteins. GAPDH was detected as a sample loading control. Data are from a single experiment. **(C)** Vero and **(D)** THP-1 cells were mock infected or infected at an MOI of 2 with bRSV or bRSV ΔSH. At 24 h p.i., cells were fixed and immuno-stained with anti-RSV F antibodies (green). Nuclei were stained with DAPI (blue), and images obtained using a Leica TCS SP5 confocal microscope. White arrow heads indicate virus filaments projecting from the plasma membrane. **(E)** Lower magnification images of D to highlight low infection rates. Images are representative of n=4 independent experiments.

seen in both wt and bRSV ΔSH infected cells, peaking at 72 h p.i. (Fig 3.3A).
SH protein was only detected in wt bRSV infected cells and not in cells infected with the mutant virus (Fig 3.3A), confirming deletion of the gene. Previous studies have demonstrated that several forms of human RSV SH protein are expressed in virus infected cells: glycosylated forms SH_g (13-15 kDa) and SH_p (21-30 kDa), and non-glycosylated forms SH_0 (7.5 kDa; full length) and SH_t (4.8 kDa; truncated) (Anderson et al., 1992). I observed the expression of all of these forms of SH in bRSV infected Vero cells, except for the truncated SH_t form (Fig 3.3A). Of the forms of SH detected, significant levels of expression were apparent from 24 h p.i., increasing as infection progressed. Immunofluorescence (IF) microscopy was also carried out to examine the expression of bRSV F in cells infected with virus for 24 h. Similar patterns of F protein expression were observed between the two viruses (Fig 3.3C). Notably, in Vero cells, the increase in F and SH protein expression (Fig 3.3) correlated with the increase in nascent virus production (Fig3.1B).

In contrast, THP-1 cells infected with an equivalent amount of virus appeared to show no expression of F and very low levels of SH by western blot analysis (Fig 3.3B), also correlating with the unproductive infection observed in Fig 3.2. However, when F protein expression was examined by IF microscopy, reasonably high levels of expression were observed, albeit only in a few cells (Fig 3.3D), approximately <5% of cells per field of view (Fig 3.3E). Of note, IF analysis represents a more sensitive assay compared to western blotting since signals are reported at the level of individual cells and less influenced by background from uninfected cells. However, these results, together with the poor virus recovery from THP-1 cells, confirms the low permissivity of these cells.

Interestingly, two populations of F protein were observed by IF in Vero cells – an intracellular, presumably endoplasmic reticulum (ER) or secretory pathway-associated population and a filamentous plasma membrane-associated population (Fig 3.3C). This finding was consistent with previously reported data which shows that F protein is expressed in the ER and rapidly transported through the secretory pathway to lipid rafts in the plasma membrane, where it is incorporated into virus filaments (Rixon et al., 2004). Evidently, several F protein-stained filaments were seen projecting from the plasma membrane of infected Vero cells (white arrowhead; Fig

3.3C), possibly showing incorporation of F into mature virions at sites of assembly. Of note, this was not apparent in infected THP-1 cells. F protein could be seen predominantly distributed in the cytoplasm with a notable lack of projecting filaments at the cell surface (Fig 3.3D. There appears to be a lack of virus assembly in THP-1 cells although the preceding steps in the viral life cycle, i.e., genome replication, transcription etc. require further investigation. In summary, these data indicate that bRSV might exhibit abortive infection in THP-1 cells, and that deletion of the SH gene does not affect replication of the virus in permissive cells.

3.2.3. Characterisation of transiently expressed SH protein

To assess the suitability of transient overexpression of SH as a tool to study the function of this protein, I examined whether overexpressed and endogenously expressed SH behave similarly. The synthesis and sub-cellular localisation of overexpressed SH were analysed and compared to SH expressed in virus infected cells. Firstly, 293T cells were transfected with plasmid expressing bRSV SH (pcDNA3.1-SH) and the expressed SH forms analysed by western blotting. Cell lysates were prepared for reducing SDS PAGE at 24 h post transfection (p.t.), in Laemmli lysis buffer with and without the addition of beta-mercaptoethanol (β-ME) and denatured at a range of temperatures to assess instances of multimerisation. The three different monomeric forms of SH (SH_0, SH_g and SH_p) previously observed in bRSV infected cells (Fig 3.3A) were also detected following transient overexpression (Fig 3.4A). This was unaffected by the presence of β-ME or the denaturation temperature, confirming the absence of interchain di-sulphide linkages in the multimeric complex. When the various conformations of SH were investigated by preparation of transfected cells in RIPA lysis buffer, a ladder of bands was observed at lower reducing temperatures (Fig 3.4B). These are possibly representative of multimeric versions rather than protein aggregations. One of the multimeric units, with an indicated molecular weight of 40-50 kDa, could correspond to a pentameric complex, a previously proposed conformation for human RSV SH (Gan et al., 2008, Gan et al., 2012). The three monomeric forms of SH were still seen when the lysate was fully denatured at 100ºC. The disappearance of the putative pentamer at 100ºC denaturation correlated with detection of SH_0 and thus suggests the pentamer is made of non-glycosylated SH. However, this requires further analysis.

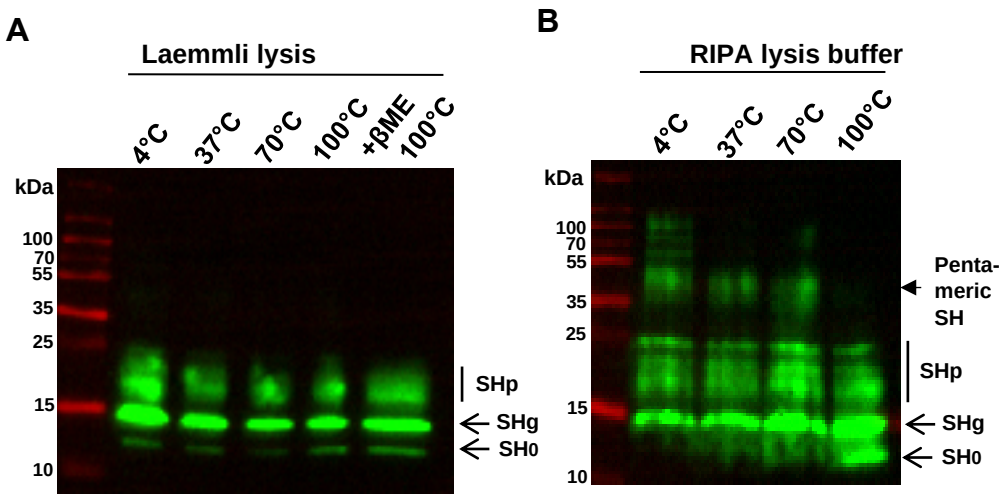

Figure 3.4 SH protein analysis by SDS PAGE. 293T cells were transfected with plasmid expressing bRSV SH. 24 h p.t., cells were **(A)** lysed in Laemmli sample buffer with and without β-mercaptoethanol (β-ME) or **(B)** in RIPA lysis buffer. Lysates were denatured at varying temperatures for 5 mins each and run on a 15% SDS-PAGE gel. The proteins were then transferred to PVDF membranes and probed with polyclonal anti-SH antibody. The data are from a single experiment.

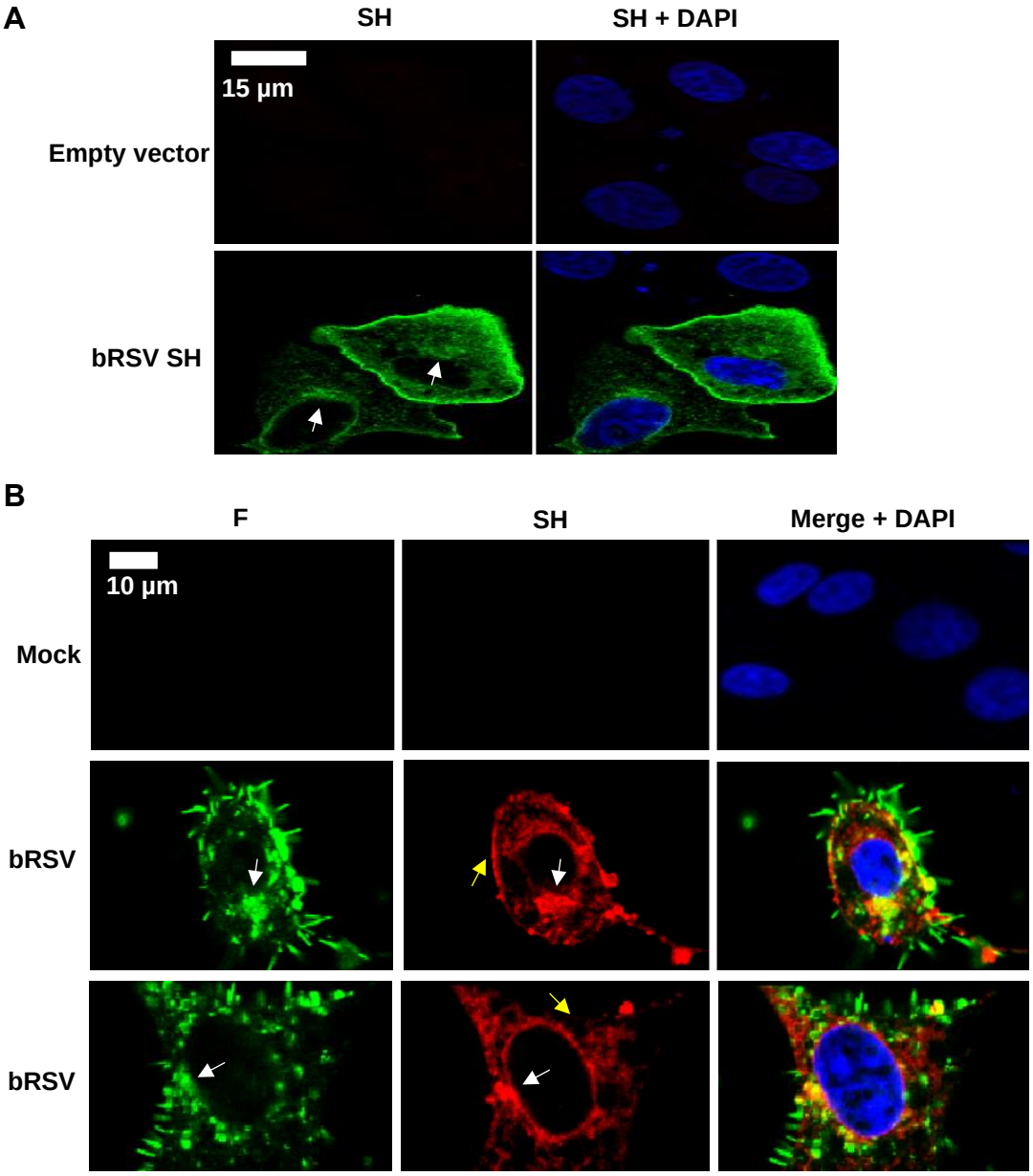

Figure 3.5 Comparing localisation of nascent and transiently expressed SH by immunofluorescence staining. **(A)** Vero cells were transfected with 1µg empty vector (pcDNA3.1) or plasmid expressing wild type bRSV SH. **(B)** Vero cells were mock infected or infected with wild type bRSV at an MOI of 1. 24 h later, cells in **(A)** were fixed and immuno-stained with anti-SH antibody (green). Cells in **(B)** were immuno-stained with anti-RSV F (green) or polyclonal anti-SH antibody. Nuclei were stained with DAPI (blue) and images obtained using a Leica TCS SP5 confocal microscope. Two representative images of infected cells are presented in B. White arrow heads indicates indicate ER regions and yellow indicate plasma membranes. Images are representative of n=2 independent experiments.

Next, the subcellular localisation of overexpressed SH was examined and compared to SH expressed following virus infection. Vero cells were transfected with plasmids expressing bovine RSV SH or infected with wild type bRSV. Using IF microscopy the location of the SH protein was compared in the two conditions 24 h afterwards. As an integral membrane protein, SH is expected to associate with the ER as well as intracellular and plasma membranes, which was consistent with my findings. SH could be seen distributed throughout the cytoplasm of transfected (Fig 3.5A) and infected (Fig 3.5B) cells, with significant localisation in the plasma membrane and peri-nuclear region (white arrow), presumably ER (Rixon et al., 2004). However, some infected cells showed more significant plasma membrane staining (middle panel of Fig 3.5B; yellow arrows) than others (bottom panel), similar to the trend observed in transfected cells (Fig 3.5A). This might be dependent on the amount of SH expressed and how much has been transported through the secretory pathway to the cell surface. As already noted in Fig 3.3C, F protein can be seen incorporated into putative virus filaments projecting from the plasma membrane. There was a notable absence of SH in these filaments, correlating with the previously reported reduced levels of SH that have been observed incorporating into mature virions, especially when compared to the F/G glycoproteins (Triantafilou et al., 2013, Rixon et al., 2004). Nevertheless, ectopically expressed SH showed a similar sub-cellular localisation to SH expressed in virus infected cells demonstrating that transient SH expression can theoretically be used to investigate the functional roles of RSV SH.

3.2.4. Generation and analysis of SH mutants

As discussed in chapter 1, the SH protein consists of three domains – an N-terminal intracellular domain, a transmembrane domain and a larger C-terminal ectodomain. In order to identify specific domains within SH involved in NF-κB regulation, a series of SH mutants were generated, using full length SH as the basis (Fig 3.6A). The following full and partial N- and C-terminus truncations were generated: ΔN1-19, ΔN1-10, ΔC41-82, and ΔC58-82. In addition, two critical residues were selected for mutation - F22 which has a structural role contributing to SH pentamerisation, and H51 which has been shown to be important for ion channel activity (Li et al., 2014). In order to disrupt their activities, these residues were mutated to alanine (Fig 3.6A). A FLAG epitope was added to the C-terminus of full length and all SH mutants because the existing SH antibody binds to unknown epitopes and because anti-FLAG

antibodies were readily available for immunostaining analysis. All fragments, generated by primer specific PCR amplification, were cloned into the pcDNA3.1 backbone and successful cloning verified by conventional Sanger sequencing.

Expression from the constructs was then analysed by western blotting at 24 h post transfection and compared to existing plasmids expressing bRSV and hRSV SH. A plasmid expressing FLAG-tagged bone marrow stromal antigen 2 (BST2-FLAG), used in a previous study (Kelly et al., 2019) was included as a positive control for tag detection. The three different forms of SH were only readily detected in cells transfected with wild type SH expression plasmids (Fig 3.6B and C). Interestingly, the addition of the FLAG tag significantly reduced the expression of all forms, especially the SH_0 and SH_p variants. The alanine mutants showed similar levels of expression when compared to SH-FLAG. However, neither of the C-terminal deletions were detected using the SH antibody (Fig 3.6C). Deletion of all of the ecto-domain (ΔC41-82) completely abrogated expression whereas the partial deletion (ΔC58-82) was minimally detected using an anti-FLAG antibody (white arrow). In contrast, ΔN mutants were expressed and detected by both FLAG and SH antibodies although the predicted glycosylated SH_p form was lost. To summarise, this data indicates that C-terminal tagging affects either the expression or stability of the SH protein and that the extra-membrane C-terminal domain is possibly essential for SH protein stability.

Viroporins alter the function of cellular membranes and their activity is known to be associated with increased toxicity in virus infected cells (Gonzalez and Carrasco, 2003). As a putative viroporin, I examined whether ectopic overexpression of bRSV SH was toxic to cells using a CellTiter-Blue viability assay. The assay indicates the viability of cells by measuring their ability to convert a redox dye (resazurin) into a fluorescent end product (resorufin). Given the impact of FLAG-tagging observed by western blotting (Fig 3.6B and Fig 3.6C), the toxicity of SH-FLAG was also examined. A dose-response assay was carried out by titrating amounts of plasmids expressing wt and SH-FLAG into 293T cells and measuring fluorescence. Wild type SH expression reduced viability to 87% when cells were transfected with 1 μg DNA and 76% when 2 μg DNA was used (Fig 3.6D). In comparison, SH-FLAG expression did not reduce cell viability. This might be a result of limited activity or lack of function due to the

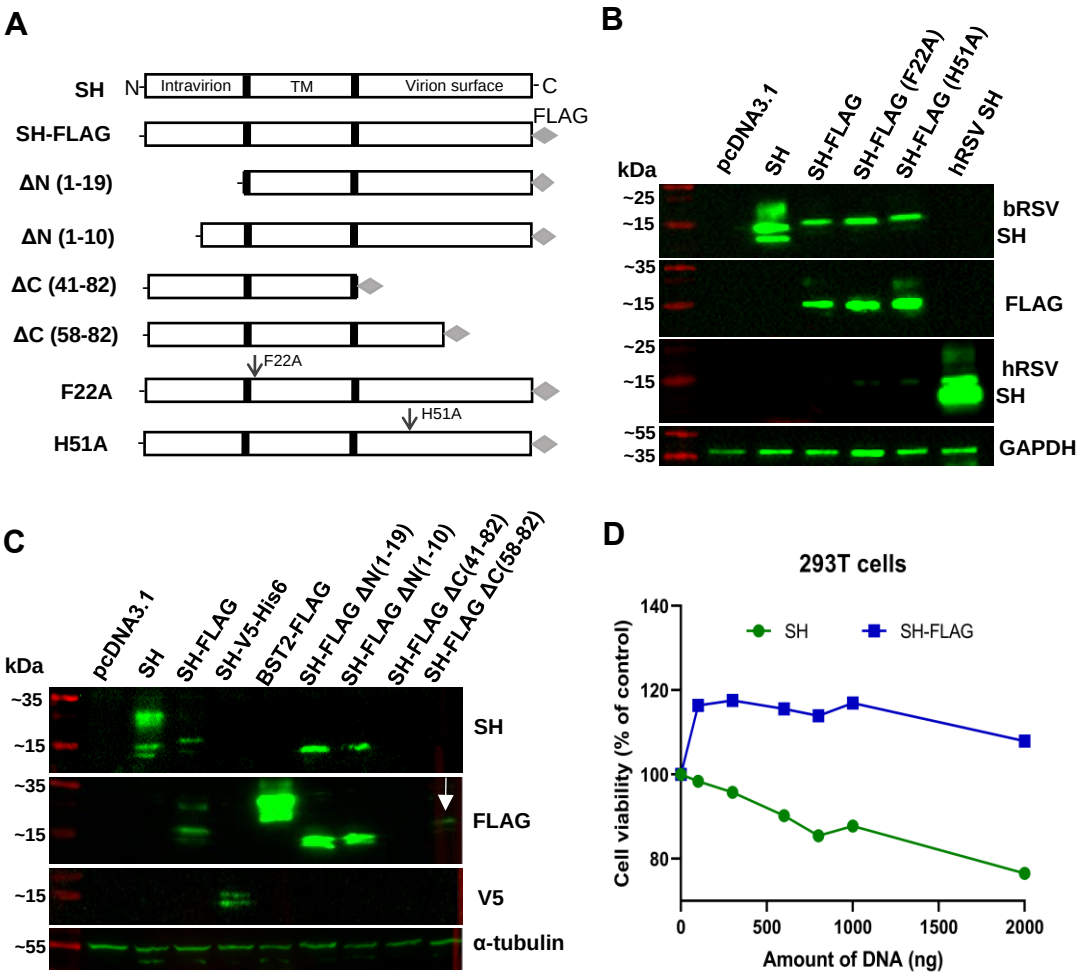

Figure 3.6 Generation and analysis of bRSV SH mutants. (A) Schematic of the bRSV SH mutants generated in this study. C-terminal FLAG tags are represented by grey diamonds. **(B)** Vero and **(C)** 293T cells were transfected with 1μg empty vector (pcDNA3.1) or plasmids expressing wild type bRSV SH, the indicated SH constructs or hRSV SH. BST2-FLAG expression construct was included as a FLAG expression control. 24 h p.t., cells were lysed, proteins separated by SDS-PAGE and then immuno-blotted using antibodies against the indicated proteins. GAPDH in (B) and α-tubulin in (C) were detected as sample loading controls. **(D)** 293T cells were transfected with increasing amounts of the plasmids expressing bRSV SH or SH-FLAG. 24 hours later, cells were incubated with CellTiter-Blue reagent for 3 h at 37ºC and then fluorescence at 560/590nm recorded. Background fluorescence was subtracted from all values and cell viability calculated as percentage fluorescence compared to the no plasmid control. Images are representative of n=1 independent experiments.

low levels of expression and absence of the various molecular weight isoforms (Fig 3.6B and Fig 3.6C). Importantly, these data suggest there is a level of toxicity associated with wild type SH expression, especially when high levels of the protein are expressed. To acknowledge this, low levels of DNA were used in future experiments with SH overexpression in order to minimize the effects of toxicity. The data also suggests differences in functionality between wild type SH and SH-FLAG which was acknowledged by including both constructs in future investigations and experiments.

3.2.5. The effect of the SH protein on NF-κB p65 activation

The NF-κB signalling pathway may be activated by several stimuli including TNFα, IL-1, bacterial and viral antigens, *etc*. Firstly, TNFα was validated as an NF-κB signalling agonist and used to establish appropriate time-points for analysis. Vero and THP-1 cells were lysed in the absence of infection at 0, 10, 30, 60, and 120 mins post 20 ng/ml TNFα treatment. Cell lysates were then analysed for degradation of the NF-κB inhibitor, IκBα (Chen et al., 1995), and the subsequent phosphorylation of released NF-κB (Mitchell et al., 2016) by western blotting. Alpha-tubulin was used as a sample loading control. The levels of total IκBα were lowest at 30 mins post TNFα stimulation in Vero cells (Fig 3.7A) and at 10 mins in THP-1 cells (Fig 3.7B), indicating degradation in response to agonist treatment. As IκBα levels reduced, phosphorylation of p65 (P-p65) increased and then gradually reduced over the time course of the investigations in THP-1 cells. However, phosphorylation of p65 preceded IκBα degradation in Vero cells with the highest levels detected at 10 mins post stimulation, highlighting small differences in signalling between Vero and THP-1 cells. At 60 mins post stimulation, there was an apparent increase in the levels of IκBα in both cells. The IκBα gene is one of the immediate targets induced following NF-κB p65 activation and translocation into the nucleus (Sun et al., 1993). Thus, the reduction and subsequent increase in IκBα levels is a significant marker of NF-κB signalling in cells, as well as the phosphorylation of p65. The return of IκBα to basal levels and association with free p65 switches off the NF-κB response in a negative feedback loop (Mitchell et al., 2016, Oeckinghaus et al., 2011).

Next, the role of the SH protein in NF-κB activation was examined in the context of bRSV infection. Vero cells were infected with wt or ΔSH bRSV at an MOI of 2 and

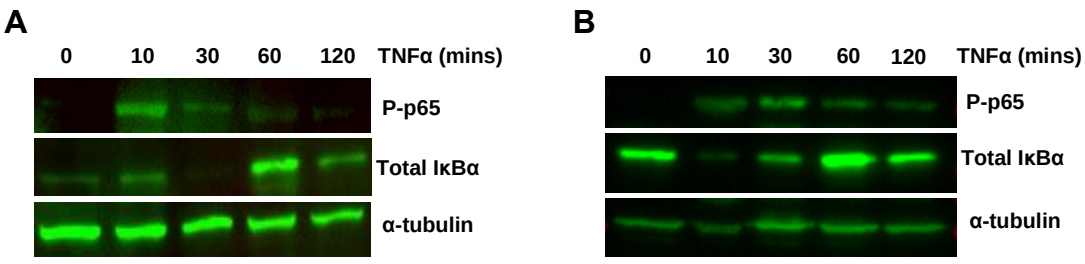

Figure 3.7 Time course of TNFα-induced NF-κB p65 phosphorylation and IκBα degradation. **(A)** Vero and **(B)** THP-1 cells were left untreated (0) or stimulated with 20 ng/ml TNFα for the indicated times. Cells were then lysed and analysed by western blotting for the phosphorylation of p65 (P-p65) using a phospho-specific form of the antibody as well as for IκBα degradation. Alpha-tubulin was detected as a loading control. Vero data representative of n=3 independent experiments, and THP-1 n=1.

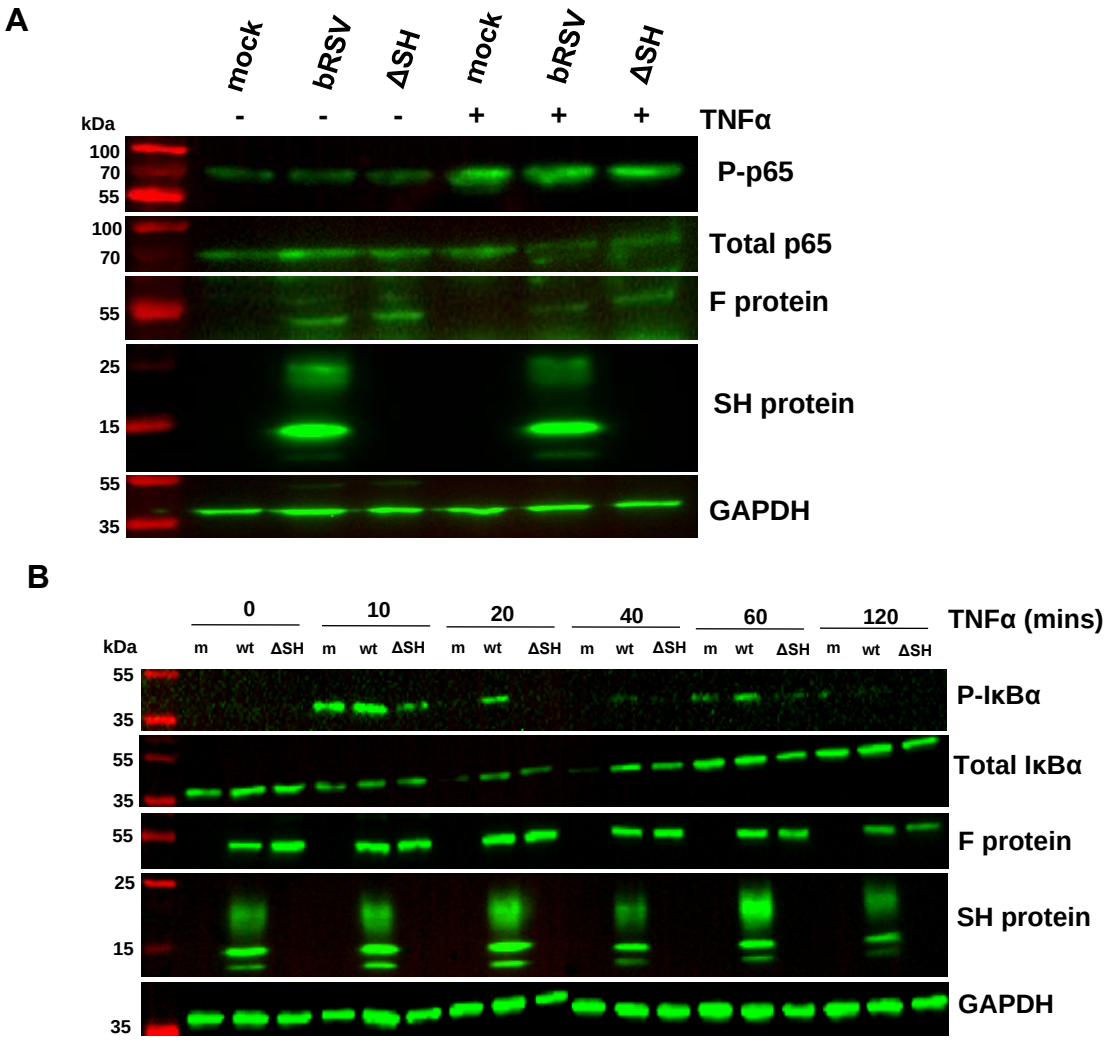

Figure 3.8 bRSV blocks IκBα degradation but not phosphorylation of p65. (A) Vero cells were mock infected or infected with bRSV or bRSV ΔSH at an MOI of 2. 24 h later, cells were stimulated with 20 ng/ml hTNFα for 10 mins or left untreated. Cells were then lysed and analysed by western blotting for phosphorylation of p65 (P-p65) using a phospho-specific form of the antibody, total p65, RSV F and SH protein. **(B)** Vero cells infected with virus for 24 h were left untreated or stimulated with 20 ng/ml hTNFα for 10, 20, 40, 60 and 120 mins. Following cell lysis, immuno-blotting was done for P-IκBα, total IκBα, RSV F and SH protein. GAPDH was detected as a loading control. Data are representative of n=2 independent experiments.

then examined for phosphorylation of NF-κB subunit p65 and IκBα turnover by western blotting. Stimulation of mock infected cells with TNFα (Fig 3.8A, compare mock [-] to mock [+ TNFα]) increased levels of P-p65, as observed in Fig 3.7. However, there was no significant difference in the level of p65 phosphorylation when cells were infected with either virus (Fig 3.8A), suggesting that the presence of SH did not influence NF-κB activation. In what is also a well characterised response (Mercie et al., 1998, Schmitz, 1995), degradation of IκBα was observed over a time course of TNFα treatment in mock (m) infected cells (Fig 3.8B). This is preceded by its phosphorylation (P-IκBα; compare "m" plus 10 mins TNFα treatment to 20 and 40 mins). Interestingly, there was a reduction in the level of total IκBα degradation in virus infected cells when compared to mock infected cells (Fig 3.8B, 20 and 40 mins), indicating that the turnover of IκBα following TNFα stimulation was inhibited, even though p65 phosphorylation seemed unaffected. Importantly, there were no significant differences between wild type and ΔSH infected cells, although there were clear differences in P-IκBα levels. The role of the SH protein on NF-κB activation could not be investigated in THP-1 cells by western blotting following virus infection due to the aforementioned poor permissivity of these cells.

3.2.6. The effect of the SH protein on NF-κB p65 activation and sub-cellular localisation

Although virus infection did not inhibit TNFα-induced phosphorylation of p65, when compared to mock infected cells, the reduced IκBα degradation did suggest interference with NF-κB activation. IF microscopy of Vero cells, mock infected or infected with virus at an MOI of 1 for 24 h, was performed to assess how SH expression affects p65 nuclear translocation (which occurs downstream of phosphorylation in the signalling cascade). Analysis of mock infected cells confirmed that p65 is normally located in the cytoplasm, translocating to the nucleus when activated by TNFα treatment (Fig 3.9A). Unexpectedly, infection caused p65 to coalesce into perinuclear intracytoplasmic puncta that were only present in infected cells, as indicated by RSV F expression (Fig 3.9B). These puncta were present in both wt and bRSV ΔSH infected cells and apparently reduced the level of p65 nuclear translocation, when compared to mock infected cells. The percentage of cells showing any level of nuclear p65 staining (Fig 3.9C) were manually counted and the nuclear

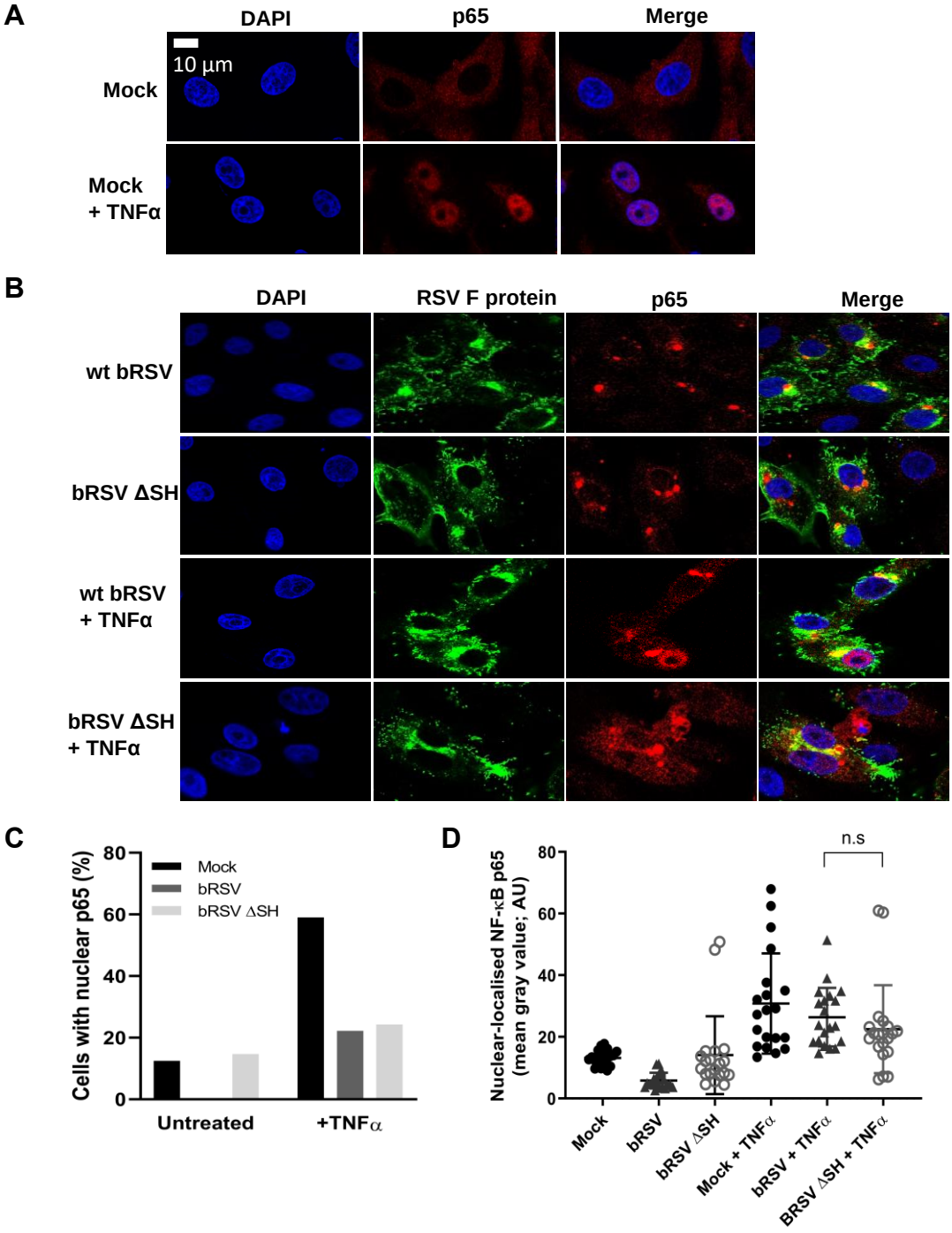

Figure 3.9 bRSV blocks NF-κB p65 nuclear translocation in Vero cells. Vero cells were **(A)** uninfected (mock), or **(B)** infected with wt bRSV or ΔSH at an MOI of 1 for 24 h. Cells were then left untreated or stimulated with 20 ng/ml hTNFα for 30 mins, fixed and immunostained with anti-RSV F (green) or anti-NF-κB p65 (red) antibodies. Cell nuclei were stained with DAPI (blue), and images obtained using a Leica TCS SP5 confocal microscope. Images are representative of data from a single experiment. **(C)** Percentage of cells with nuclear localised p65. **(D)** Quantification of nuclear NF-κB p65 signal intensity was done using the quantify tool of Leica LAS AF Lite software as described in the methods. Nuclear p65 signal intensities are shown for twenty cells per condition (based on the number of infected cells in the images collected); with means ± SD also indicated. Statistical significance was determined by ANOVA as described in the methods, n.s: non-significant.

p65 signal intensities (Fig 3.9D) quantified using the area region of interest analysis tool of the Leica LAS AF Lite software. Due to a limited number of infected cells in the images collected for some of the conditions, only twenty cells were analysed for each condition. Analysis of infected cells in the absence of TNFα stimulation showed comparable levels of basal p65 nuclear translocation between mock and ΔSH infected cells. There was a reduction observed in cells infected with wt bRSV, possibly reflecting the previously reported differences in the response to the two viruses at the signalling level (Taylor et al., 2014). Although the difference was not highly significant, the increased nuclear translocation seen in bRSV ΔSH infected cells could theoretically contribute to enhancing the cytokine response during infection. On the other hand, analysis of TNFα stimulated cells showed a ~40% reduction in the number of cells with nuclear p65 when infected with virus (Fig 3.9C), with most of the p65 remaining in the observed perinuclear puncta (Fig 3.9B). These responses were observed independently of SH expression. The average nuclear p65 signal intensity was also reduced in cells infected with both viruses (Fig 3.9D) indicating an inhibition of p65 nuclear translocation. In summary, SH expression appeared to have a minimal effect on NF-κB activation in unstimulated cells, this was negated in TNF-stimulated cells; however, other mechanisms for inhibition also appear to be at play.

Unlike western blot analysis, IF microscopy allowed analysis of the NF-κB response to RSV infection in THP-1 cells, despite the low percentage of infected cells observed. As already described for Vero cells, TNFα stimulation of mock infected cells induced p65 nuclear translocation (Fig 3.10A). On average, infection induced nuclear translocation in 11% of wild type bRSV infected cells and around 32% when infected with bRSV ΔSH (Fig 3.10B and C). In contrast to Vero cells, infection increased TNFα-induced p65 nuclear translocation from 62% in mock infected to 91 and 93% in wt and ΔSH bRSV infected cells, respectively. However, there were no p65 puncta observed in these cells, possibly leading to the enhanced nuclear translocation observed. Since infection induced p65 puncta in the highly permissive Vero cells, the lack of sequestration in THP-1 cells may also be linked to the absence of productive infection observed in these cells, however that will require further experimental analysis. In summary, the data shows that bRSV infection reduced NF-κB activation in Vero but not in THP-1 cells, with a moderate effect potentially being elicited

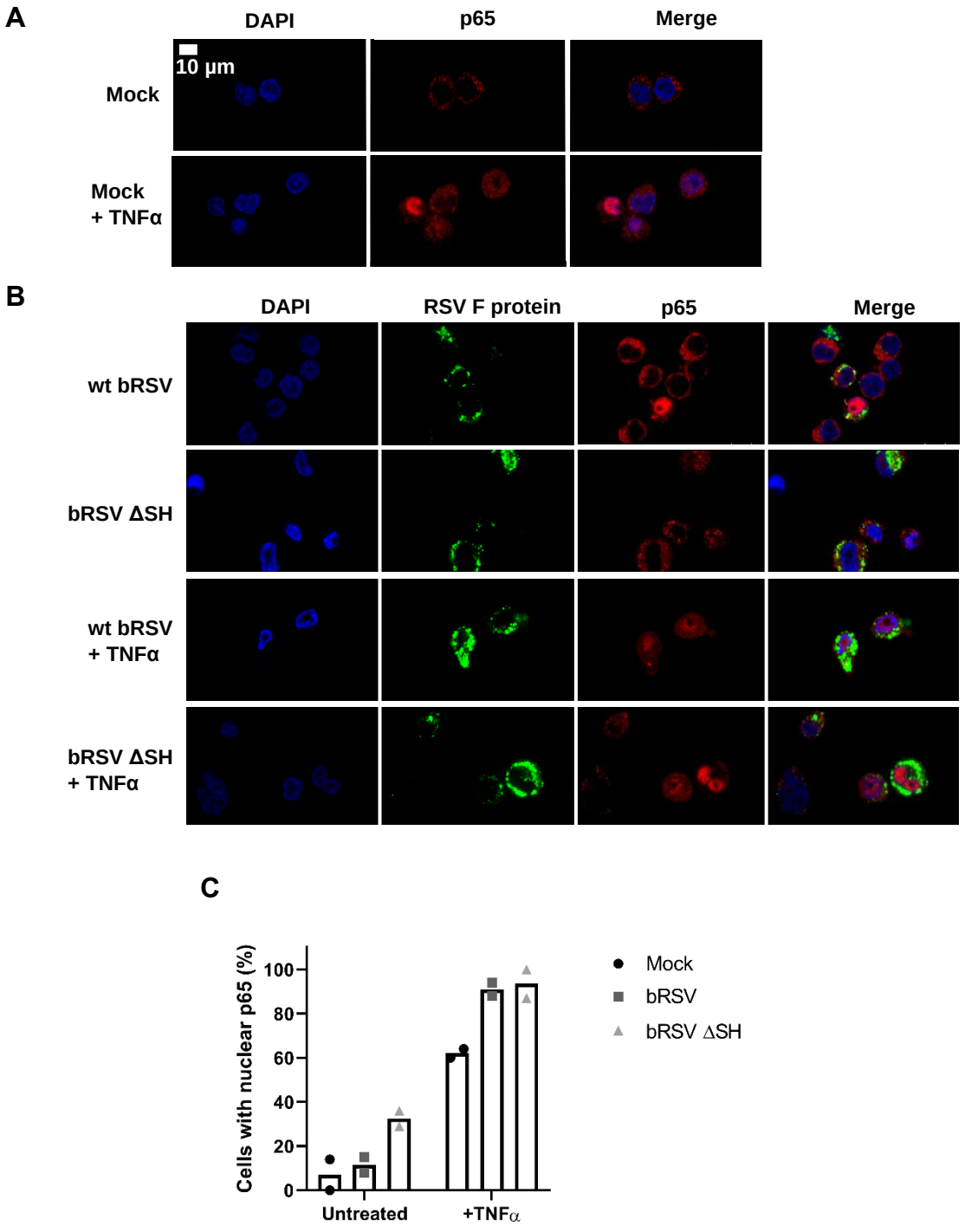

Figure 3.10 bRSV does not block NF-κB p65 nuclear translocation in monophagocytic cells. THP1 cells were **(A)** uninfected (mock), or **(B)** infected with wt bRSV or ΔSH at an MOI of 1 for 24 h. Cells were then left untreated or stimulated with 20 ng/ml hTNFα for 30 mins, fixed and immunostained with anti-RSV F (green) or anti-NF-κB p65 (red) antibodies. **(C)** Percentage of infected cells with nuclear-localised p65. Images are representative of n=2 independent repeats.

by the viral SH protein. Separately, in Vero cells, it is clear bRSV specifically inhibited TNFα-induced IκBα degradation and p65 nuclear translocation, thereby modulating NF-κB signalling via an alternative mechanism, independent of the SH protein.

3.2.7. Effect of SH overexpression on NF-κB p65 activation

To further evaluate if the SH protein has a direct role in inhibiting NF-κB activation, transiently transfected cells were examined, in the absence of virus infection to allow specific focus on the function of this protein. First phosphorylation of p65 was analysed by western blotting following SH overexpression. 293T cells were transfected with plasmids expressing wt SH, SH fused to a FLAG tag (SH-FLAG) or empty vector as a control. NF-κB activation was stimulated with TNFα treatment at 24 h post transfection, then cells were lysed and analysed for the levels of P-p65 and SH. TNFα treatment induced phosphorylation of p65 in the control as well as cells expressing wt SH and SH-FLAG (Fig 3.11A). Normalisation of P-p65 band volumes to GAPDH shows an increase in P-p65 levels in the presence of SH and SH-FLAG when compared to cells transfected with the empty vector (Fig 3.11B). This data further indicates that SH has a no effect on NF-κB activation.

The effect of SH overexpression on p65 nuclear translocation was then investigated by IF microscopy. Vero cells were transfected with empty vector, plasmids expressing full length SH-FLAG or the N-terminal truncation mutants (ΔN1-10 and ΔN1-19; both with FLAG tags). Of note, due to antibody cross-reactivity issues, antibodies against untagged SH could not be used in co-staining analyses with the anti-p65 antibody. Cells were stimulated with TNFα at 24 h p.i., fixed and then the localisation of p65 examined. As previously described, in control cells, TNFα treatment induced p65 translocation from the cytoplasm to the nucleus (Fig 3.12). When expressing SH-FLAG, in the absence of NF-κB stimulation, p65 remained cytoplasmic. However, following TNFα stimulation, varying degrees of p65 nuclear translocation were observed in both SH expressing and non-expressing cells. Similar results were also seen in cells transfected with both partial and full N-terminal deletion mutants. Thus, the role of SH overexpression on p65 nuclear translocation could not be inferred from this data, especially considering the poor expression of the flag-tagged constructs, as observed by western blotting.

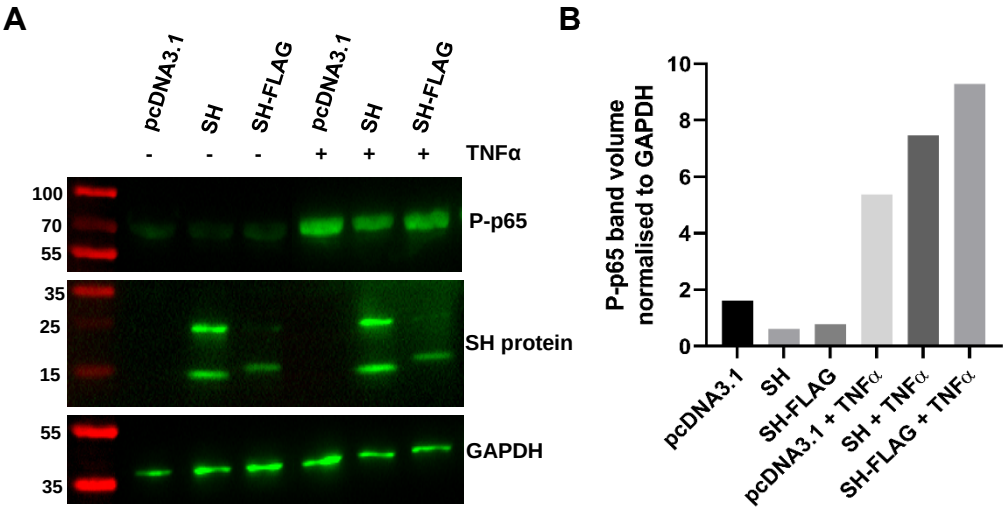

Figure 3.11 Ectopic expression of bRSV SH does not inhibit NF-κB p65 phosphorylation. (A) 293T cells transfected with empty vector (pcDNA3.1) or plasmids expressing bRSV SH or SH-FLAG were left untreated or stimulated with 20 ng/ml hTNFα for 10 mins at 24 h post transfection. Cells were then lysed and analysed by western blotting for phosphorylation of p65 using phospho-specific forms of the antibody and RSV SH. GAPDH was detected as a loading control. **(B)** The graph shows phospho-p65 band volumes, obtained using the Image Lab software, normalised to GAPDH. Data is representative of n=3 independent repeats.

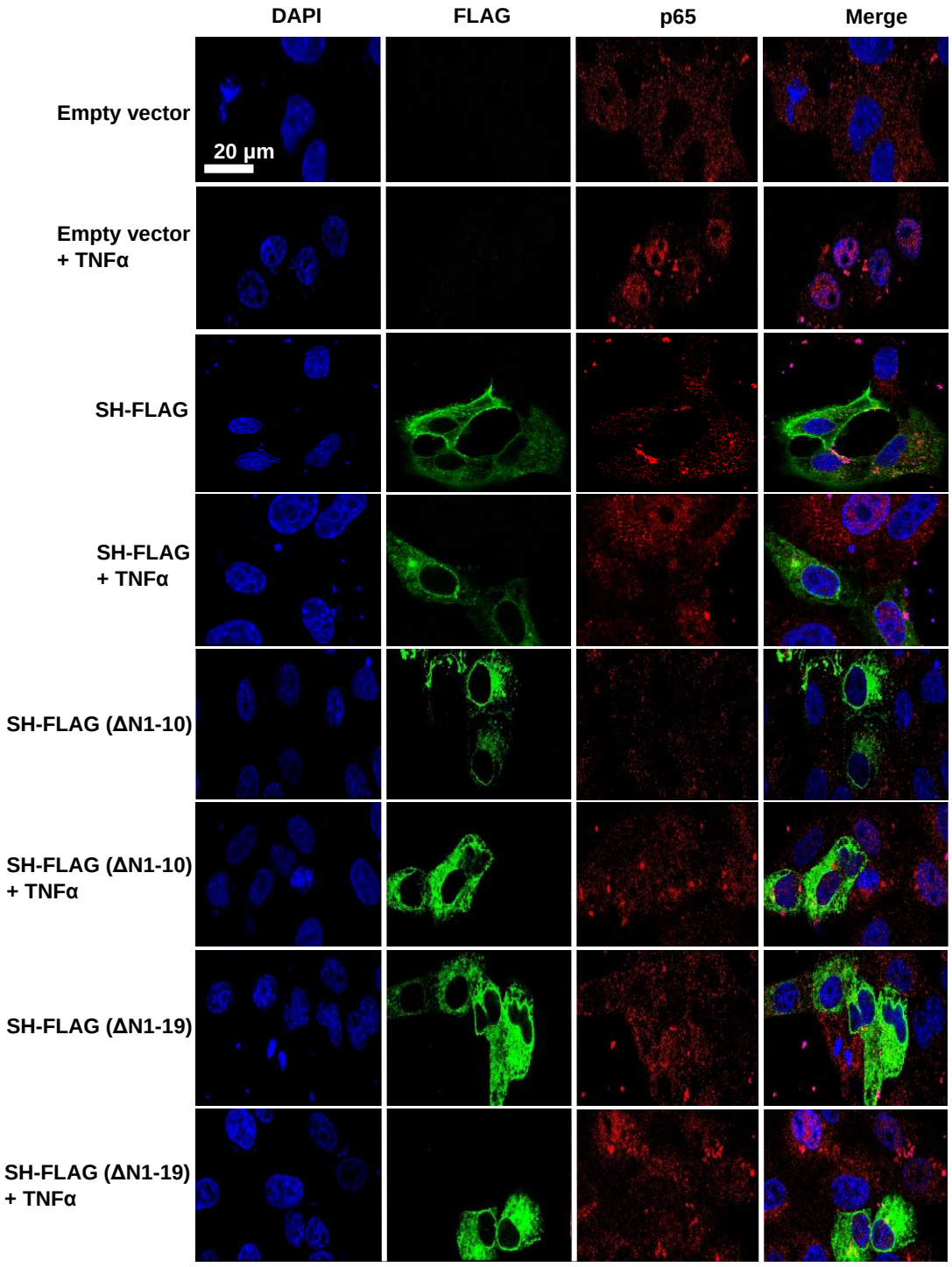

Figure 3.12 Ectopic expression of bRSV SH does not inhibit TNFα-induced NF-κB p65 nuclear translocation. Vero cells were transfected with empty vector (pcDNA3.1) or plasmids expressing bRSV SH-FLAG or mutants from which residues 1-10 or 1-19 where deleted. 24 h post transfection, cells were left untreated or stimulated with 20 ng/ml hTNFα for 20 mins. Cells were then fixed and immuno-stained with anti-FLAG (green) or anti-NF-κB p65 (red) antibodies. Cell nuclei were stained with DAPI (blue), and images obtained using a Leica TCS SP5 confocal microscope. Data is representative of n=2 independent repeats.

3.2.8. The effect of the SH protein on NF-κB induction

Finally, a luciferase reporter gene assay was used to assess the effect of SH expression on NF-κB transactivation. This provides a more quantitative approach, when compared to western blotting and IF microscopy techniques, and also evaluates a different step in NF-κB signalling. In this system, an NF-κB reporter plasmid (NF-κB Fluc) which expresses the firefly luciferase gene under the control of five repeated NF-κB transcription factor binding sites was employed. 293T cells were transfected with the reporter plasmid and plasmids encoding bRSV SH (with and without a FLAG tag) or hRSV SH. As controls, cells were also transfected with empty vector, plasmids encoding known viral inhibitors of NF-κB (MC159 and MC005) (Biswas and Shisler, 2017, Biswas et al., 2018, Brady et al., 2017) or cellular TRAF2, overexpression of which strongly induces NF-κB (Rothe et al., 1995). MC159 and MC005 are encoded by Molluscum contagiosum virus, a poxvirus with a double stranded DNA genome. NF-κB activation (detected as luciferase activity) was then stimulated with bovine (b) or human (h) TNFα treatment, or TRAF2 transfection. Bovine TNFα induced strong activation of NF-κB (Fig 3.13A); a 6-fold induction (Fig 3.13B), which was significantly reduced in the presence of the inhibitors MC159 and MC005. Expression of neither bRSV or hRSV SH significantly reduced the level of induction observed. MC005 and MC159 also significantly inhibited NF-κB activation following hTNFα (Fig 3.13C and D) and TRAF2 (Fig 3.13E) stimulation, respectively. However, bRSV SH expression did not significantly alter hTNFα-induced luciferase activity (Fig 3.13C and D). Similarly, TRAF2 overexpression increased luciferase activity in EV-transfected cells (a mean induction of 26-fold) which was reduced to about 23-fold in cells expressing bRSV SH, 19-fold in SH-FLAG cells and 20-fold in hRSV SH cells (Fig 3.12E). All reductions in the presence of RSV SH proteins were non-significant, unlike the established inhibitor, MC159. Overall, the data presented here suggests that RSV SH does not significantly inhibit NF-κB activation, confirming the immunoblotting and IF microscopy data.

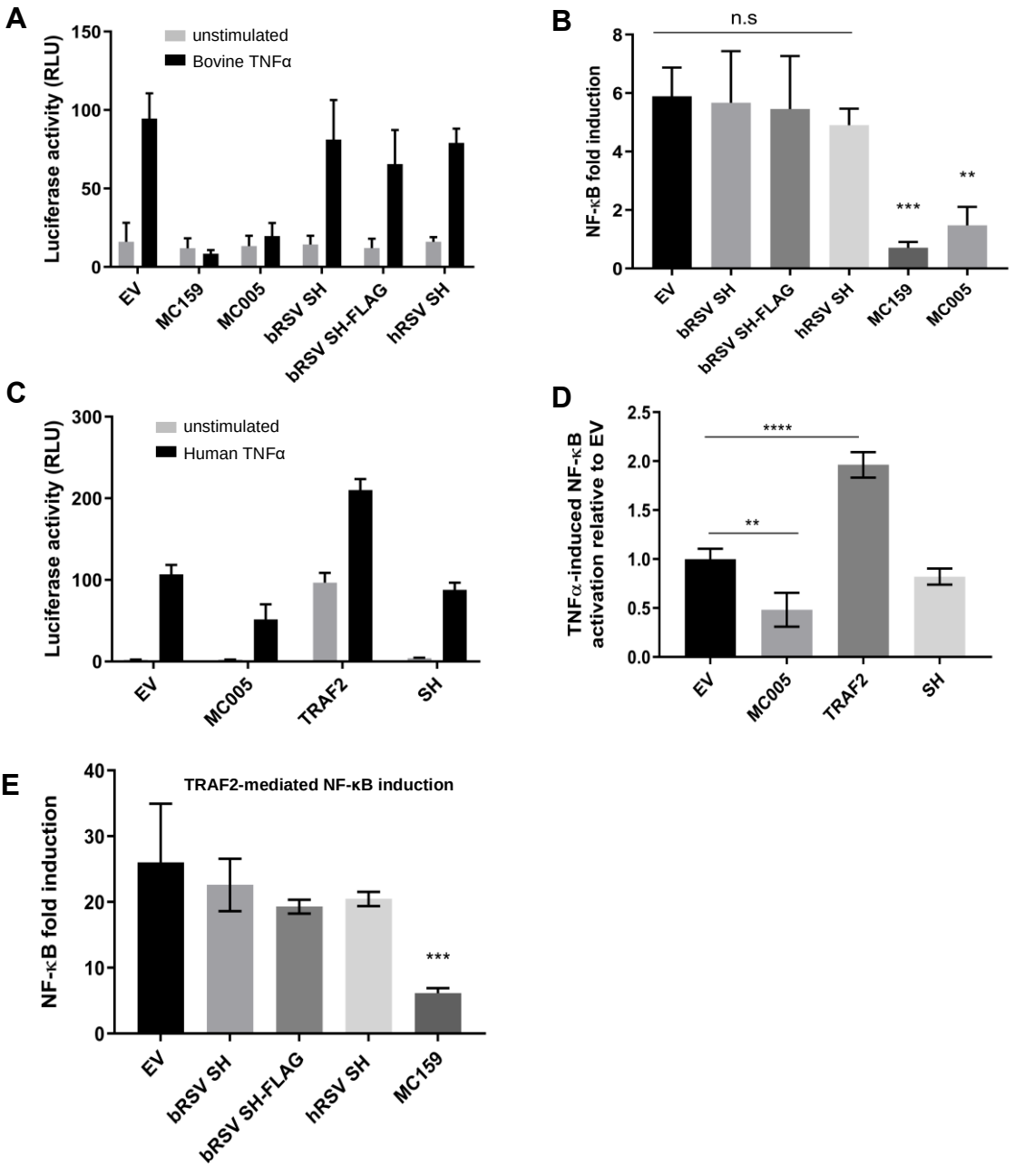
A
Luciferase activity (RLU)
150
100
50
0
unstimulated
Bovine TNFα
EV
MC159
MC005
bRSV SH
bRSV SH-FLAG
hRSV SH
B
n.s
NF-κB fold induction
8
6
4
2
0
***
**
EV
bRSV SH
bRSV SH-FLAG
hRSV SH
MC159
MC005
C
Luciferase activity (RLU)
300
200
100
0
unstimulated
Human TNFα
EV
MC005
TRAF2
SH
D
TNFα-induced NF-κB activation relative to EV
2.5
2.0
1.5
1.0
0.5
0.0
****
**
EV
MC005
TRAF2
SH
E
TRAF2-mediated NF-κB induction
NF-κB fold induction
40
30
20
10
0
***
EV
bRSV SH
bRSV SH-FLAG
hRSV SH
MC159

Figure 3.13 Ectopic SH overexpression does not significantly inhibit TNFα- and TRAF2-mediated NF-κB activation by luciferase reporter assay. (A) 293T cells were transfected with 100 ng NF-κB FLuc reporter and 10 ng TK-renilla luciferase together with 100 ng of empty vector (EV; pcDNA3.1), or plasmids expressing MC159, MC005, bRSV SH, SH-FLAG or hRSV SH and incubated at 37ºC. At 24 h p.t., cells were left unstimulated or stimulated for 4 h with 20 ng/ml bTNFα. Cells were then lysed and analysed for firefly and renilla luciferase activities. **(B)** Graph shows fold induction of NF-κB. **(C)** 293T cells were prepared as already described in A, except cells were co-transfected with plasmids expressing the indicated proteins and stimulated for 4 h with 20 ng/ml hTNFα. **(D)** Graph shows the level of NF-κB activation relative to EV transfected cells. **(E)** 293T cells were transfected with 100 ng empty vector or plasmids expressing MC005, TRAF2 or bRSV SH. 6 h later, cells were additionally transfected with 100 ng NF-κB FLuc reporter and 10 ng TK-renilla luciferase with and without 20 ng of the TRAF2 expression plasmid. Cells were lysed 24 h later and analysed for firefly and renilla luciferase activities. All graphs depict means ± SD of three replicates from the same experiment. Statistical significance was determined by ANOVA as described in the methods, $**p<0.01$; $***p<0.001$ $****p<0.0001$. Data is representative of n=3 independent repeats, except for (E), where n=2.

3.3. Discussion

Several viruses encode antagonists that target the NF-κB pathway as a mechanism of escape from the immune response (Deng et al., 2018). Although the exact role of the SH protein of orthopneumoviruses and related negative sense RNA viruses is unclear, it has a putative role in inhibiting NF-κB activation during infection. Several studies have observed reduction in NF-κB downstream responses, in particular, expression of proinflammatory cytokines and chemokines, and induction of apoptosis, when cells are infected with wt virus and compared to SH-deficient viruses (Bao et al., 2008, Fuentes et al., 2007, Pollock et al., 2017, Russell et al., 2015, Taylor et al., 2014). Using bRSV as a model virus, the molecular mechanism by which RSV SH protein suppresses NF-κB activation was investigated at various levels in this signalling pathway. I found that although bRSV infection did not significantly impact p65 phosphorylation (Fig 3.8A) and IκBα degradation (Fig 3.8B) in Vero cells, the presence of SH somewhat reduced the level of p65 nuclear translocation in both Vero (Fig 3.9) and THP-1 (Fig 3.10) cells. Interestingly, infection inhibited TNFα-mediated IκBα degradation (Fig 3.8B), and p65 nuclear translocation in Vero cells (Fig 3.9) but not in THP-1 cells (Fig 3.10); in responses that were elicited independently of the SH protein. However, in the absence of infection, the SH proteins of both hRSV and bRSV had limited/non-significant roles in NF-κB pathway activation, at least in the cell lines I used, and at the timepoints investigated.

Unlike, the F surface glycoprotein, the role of the SH protein is undefined. Both human and bovine RSV SH proteins were previously suggested to have roles in membrane fusion, presumably affecting virus entry and syncytium formation (Heminway et al., 1994, Samal and Pastey, 1997). However, these findings were contradicted by efficient growth of mutant viruses lacking SH expression in cell culture (Karron et al., 1997, Techaarpornkul et al., 2001), which also demonstrated that SH does not play a significant role in entry, virus-host cell membrane/cell-cell fusion, or successful completion of the virus lifecycle. Similarly, the SH protein of the closely related HMPV was also shown to inhibit the fusogenic activity of F (Masante et al., 2014) and virus entry into host cells with no significant impact on the efficiency of virus growth (Le Nouen et al., 2014). Several other studies have confirmed that RSV SH protein is not essential for replication and is thus dispensable to the virus *in vitro*. Supporting

evidence includes the similar growth profiles of wild type and ΔSH viruses, observed here (Fig 3.1) and previously with bRSV (Taylor et al., 2014), and also hRSV (Russell et al., 2015). In my hands, neither virus grew in the human-monocytic cell line, THP-1 cells (Fig 3.2) and no cpe was observed up to 7 days post infection. These cells seem to exhibit an abortive replication process late in the viral life cycle, as previously shown for alveolar macrophages (Makris et al., 2016), since expression of the F protein when assessed by IF microscopy indicates they at least support transcription of the RSV genome. Nonetheless, in these cells, we were able to assess how SH impacts NF-κB signalling in the absence of productive infection.

Although wild type and SH knockout viruses have comparable growth kinetics, there are inconsistencies in previous reports examining their growth efficiency. One study showed a reduction in the growth of ΔSH bRSV in MDBK cells compared to wild type (Karger et al., 2001), whereas others observed no difference (Taylor et al., 2014). I found that the ΔSH virus grew faster in MDBK cells, but only in the early stages of infection (Fig 3.1). Although I did not observe significant differences in the virus titers in infected Vero cells, ΔSH bRSV presented syncytia earlier in these cells which also grew larger over the time course of the infection. The delay in replication of the wild type virus may be attributable to the repositioning of the *F* gene, in the normally polarised transcription gradient, as a result of *SH* gene deletion (Valarcher and Taylor, 2007). In the mutant we are studying, *SH* gene deletion removes 508 nucleotides upstream of the *F* gene in the single-stranded bRSV ΔSH genome (Karger et al., 2001). Therefore, the relative positions of the two *F* genes may result in more F protein mRNAs being produced in bRSV ΔSH infected cells than wild type bRSV infected cells. As a result, the increased expression of F protein in ΔSH infected cells (evident in Fig 3.3A) could favour increased cell-cell fusion and syncytia formation. Similar observations were made by a study showing that ΔSH hRSV grew better than wild type virus in multiple cell lines (Bukreyev et al., 1997). The authors further observed that although the absence of SH enhanced transcription and replication in most cells, there was a general variability in growth efficiency influenced by the cell line used for virus propagation. Thus, the inconsistencies observed by different studies may also be related to the use of different cell lines. Ultimately, when infection was allowed to proceed long enough, up to 6 days post-infection at MOI 0.1, both viruses caused similar levels of cell death in Vero cells.

Differences were also observed at the signalling level which may have implications for virus pathogenesis. Despite the similar growth profiles, ΔSH bRSV was shown to induce increased apoptosis in infected cells (Fuentes et al., 2007, Taylor et al., 2014) similar to ΔSH mutants of other negative sense RNA viruses. These include PIV5 (Lin et al., 2003, Wilson et al., 2006), hMPV(Bao et al., 2008), MuV (Parks and Alexander-Miller, 2013), and JPV (Abraham et al., 2018). Although induction of apoptosis was not quantified here, this is in line with the enhanced cpe observed in ΔSH infected Vero cells. Apoptosis and cytokine expression are important immune responses induced in the early stages of infection and regulated by the critical transcription network, NF-κB. TNFα signalling also induces apoptosis in infected cells through the activation of caspases as a way of restricting virus replication and spread (Fuentes et al., 2007, Mitchell et al., 2016, Taylor et al., 2014). These studies show that the SH protein is required to block TNFα-induced NF-κB responses during virus infection. A delay in the onset of apoptosis gives the viruses a better chance of completing its life cycle, releasing infectious virions, and spreading to neighbouring cells with a suppressed antiviral response. In the absence of this inhibition, early apoptosis will release viral antigens that can stimulate the more specific adaptive immune response before the infection overwhelms the immune system. Thus, it is not surprising that NF-κB suppression is a common adaptation strategy used by not only RSV and related viruses, but by a plethora of other viruses via different strategies (Deng et al., 2018).

In a positive feedback mechanism, signalling from NF-κB-induced TNFα activates the NF-κB pathway in a series of well characterised events leading to TNFα production. We decided to use TNF-α to stimulate NF-κB pathway activation in our experiments in order to identify break points in the signalling cascade. Using Vero and THP-1 cells, I was able to confirm TNFα-mediated activation of NF-κB by detecting critical events such as degradation of IκBα and phosphorylation of NF-κB subunit p65 (Ser536), using antibodies specific for the phospho protein (Fig 3.7). Subsequent, translocation of p65 from the cytoplasm into the nucleus was also observed in both Vero (Fig 3.9A) and THP-1 (Fig 3.10A) cells. In comparison to TNFα stimulation (mock + TNFα), I did not observe significant activation of NF-κB signalling in wild type or ΔSH bRSV infected Vero cells at 24 h p.i. by western blotting (Fig 3.8) or IF analysis (Fig 3.9).

This was a surprising observation since other studies have reported more robust activation of NF-κB in response to RSV infection (Carpenter et al., 2002, Yoboua et al., 2010, Bitko et al., 2004, Fink et al., 2008) which could indicate that the cell line and viral strain play a role in RSV-mediated NF-κB activation. With regards to the human monocytic THP-1 cells, previous work by Ennaciri et al. showed that hRSV initiates a protein kinase C (PKC)-dependent signalling cascade in these cells leading to NF-κB activation, through the p65 subunit (Ennaciri et al., 2007). Similarly, I found that bRSV infection induced NF-κB activation in THP-1 cells with a slightly stronger response observed in the absence of SH (Fig 3.10). Quantification of nuclear p65 signals in infected Vero cells also revealed a reduction in the level of p65 nuclear translocation in the presence of the SH protein (Fig 3.9; compare bRSV to bRSV ΔSH). Although the effect of SH on NF-κB activation in both epithelial and monocytic cell lines was statistically non-significant, the slight reduction observed might result in the modulation of cytokines and immune responses regulated by NF-κB during RSV infection (Bitko et al., 1997, Tian et al., 2002).

Interestingly, in Vero cells, infection caused p65 to condense into perinuclear intracytoplasmic puncta that were only present in infected cells (Fig 3.9B). This response was observed independently of the SH protein indicating that bRSV may employ additional mechanisms for NF-κB inhibition which remain uncharacterized. These bRSV-induced p65 puncta were not present in infected THP-1 cells. This observation, together with the robust induction of NF-κB signalling in these cells, strongly suggests the lack of activation observed in RSV infected Vero cells is a direct consequence of p65 aggregation into the perinuclear puncta. Furthermore, I also demonstrate that as a result, activation of NF-κB p65 (at the level of nuclear translocation) is suppressed in infected Vero cells, even with exogenous TNFα stimulation (Fig 3.9). The absence of this suppression in response to TNFα in THP-1 cells (Fig 3.10) further confirms the role of p65 aggregation in inhibition of NF-κB signalling. Thus, this appears to be a novel mechanism by which RSV inhibits activation of the NF-κB signalling pathway through sequestration of the p65 subunit into intracytoplasmic puncta. Of note, it is currently not clear what proportion of the punctate p65 is phosphorylated or IκBα associated, the elucidation of which might explain the partial protection of IκBα from degradation seen following TNFα treatment (Fig 3.8, mock versus bRSV +TNFα).

As already stated, SH does not appear to have a role in the novel mechanism of NF-κB inhibition identified during the course of this study. In the context of infection, SH had a limited effect on NF-κB signalling when examined by IF microscopy; however, this was not obvious from the immunoblotting analyses. Although this may be significant for viral pathogenesis *in vivo* it posed a challenge for the identification of the specific molecular mechanism of inhibition. Similar results were also obtained with ectopic expression of SH. When NF-κB transcriptional activity was assessed using a firefly luciferase reporter assay, I observed a significant induction in 293T cells which was only slightly reduced in the presence of bRSV and hRSV SH, with the changes being statistically insignificant (Fig 3.13). Transient SH overexpression also did not inhibit p65 phosphorylation in response to exogenous TNFα (Fig 3.11). Of note, we observed that IF microscopy provided a more sensitive approach in this context since in these experiments we could focus on individual infected/transfected cells allowing direct comparison between SH expressing and non-expressing cells under the same conditions. In assays such as western blot and luciferase assays, the signal from non-expressing cells can easily mask signals seen in SH-expressing cells especially if the infection/transfection efficiency is poor. Nevertheless, examination of transfected cells by IF microscopy produced variable results that were therefore inconclusive in this particular experiment (Fig 3.12). Of note, only FLAG-tagged mutants could be assessed, due to antibody cross-reactivity, and these constructs were already shown to express significantly worse than the wt protein (Fig 3.6).

I was able to detect three main species (SH_0, SH_g and SH_p) (Anderson et al., 1992, Olmsted and Collins, 1989) of both bRSV and hRSV SH proteins in Western blot. SH_0 was previously shown to be the most abundant species in virus infected cells (Olmsted and Collins, 1989) although I have seen comparable levels of SH_p in bRSV infected cells. However, when a FLAG or V5-His6 tag was fused to the *C*-terminus of full length or truncation mutants, the presumed SH_p expression was lost in transfected cells (Fig 3.6). SH_p contains a polylactosaminoglycan modification with glycosylation sites in the *C*-terminus, at position Asn63 in the 73 aa SH from strain A51908 and position Asn77 in the 81aa SH in strain 391-2 (The UniProt, 2017). Thus, it seems extension of the *C*-terminus may disrupt glycosylation or stability of this protein species. In

addition, I observed significantly reduced expression when approximately half of the *C*-terminus was deleted, and complete deletion of the *C*-terminus (Δ41-82) was detrimental to expression of the protein. This may be due to the fact that the *C*-terminus is critical for membrane anchorage during the expression of type-II membrane proteins. Similarly, the different species produced by wild type SH expression were not present in the *N*-terminus or in the two alanine mutants (Fig 3.6). Thus, no further analyses were carried out with the generated SH mutants due to the aforementioned poor expression and inconsistent results obtained by IF microscopy (Fig 3.12). It will however be interesting to see how these modifications affect oligomerisation of SH into viroporins and their ability to interfere with NF-κB activation. This will enable elucidation of the key features and functional domains of the SH protein responsible for NF-κB pathway inhibition and for discrimination of the impact of viroporin activity. Perhaps, considering the challenges encountered in this study, a better approach will be found in the context of infection in *in vivo* experiments.

Viral antagonists of the NF-κB pathway are known to target various components of the signalling pathway. MuV SH protein was recently shown to inhibit NF-κB activation at the receptor level by interacting with TNF, IL-1 and TLR3 receptor complexes at the plasma membrane of infected cells, thereby inhibiting their activation (Franz et al., 2017). Different mechanisms of NF-κB inhibition have been observed in various virus families. For example, the non-structural 2C proteins of enteroviruses recruit protein phosphatase 1 to IKKβ thereby antagonizing its phosphorylation and inhibiting TNFα-mediated NF-κB activation (Li et al., 2016). The hepatitis C virus non-structural protein NS3 binds to LUBAC which ubiquitinates NEMO (an important step in IKK activation) thus inhibiting its activation (Chen et al., 2015). The molluscum contagiosum virus (MCV) MC005 protein competitively disrupts formation of the IKK complex by directly binding NEMO (Brady et al., 2017). MCV interestingly encodes multiple NF-κB antagonists with different mechanisms of inhibition. MC159 binds NEMO and competitively inhibits its interaction with the cellular inhibitor of apoptosis 1 (cIAP1), an E3 ligase that polyubiquitinates NEMO (Biswas and Shisler, 2017, Randall et al., 2012). MC160 reduced phosphorylation of the IKK complex subunits and also induced degradation of IKKα (Beaury et al., 2017, Nichols and Shisler, 2006, Nichols and Shisler, 2009). Interestingly, MC159 may also

enhance NF-κB activation when expressed at low levels (Challa et al., 2010, Murao and Shisler, 2005). Others may act further downstream at the level of IκBα and p65, such as, human immune-deficiency virus Vpu protein (Sauter et al., 2015, Langer et al., 2019) which also encodes a viroporin (Gonzalez, 2015), porcine epidemic diarrhoea virus non-structural protein 1 (Zhang et al., 2017), Orf virus ORFV 121 (Diel et al., 2011, Khatiwada et al., 2017), pox virus MC132 (Brady et al., 2015), amongst others.

Aside from MuV SH, not much is known about the mechanism of SH protein inhibition of NF-κB (Franz et al., 2017). Multiple sequence alignment with other SH proteins (Fig 1.7) shows very little sequence homology except for in the transmembrane domains. However, all are type II membrane proteins except for mumps virus SH, which is a type I. Although they differ in sequence, their mechanisms of inhibition are hypothesised to relate to their membrane localisation (Deng et al., 2018, Franz et al., 2017). There is up to 13% SH sequence variability between bRSV strains and they share 38-44% identity with hRSV SH proteins (Valarcher and Taylor, 2007). As it has been successfully applied for MuV SH (Franz et al., 2017), an RSV SH interactome analysis by co-immunoprecipitation may identify NF-κB pathway interacting partners and elucidation of the mechanism of inhibition.

In conclusion, I report that the bRSV SH protein is not a significant antagonist of the NF- κB pathway. Reduction of TNFα-mediated NF-κB signalling independent of SH in Vero cells indicates that other mechanisms of NF-κB inhibition are also employed by RSV. This may be related to the sequestration of the p65 subunit into cytoplasmic puncta and is the subject of the investigations detailed in chapter 4. While SH reduced p65 activation in infected THP-1 cells, the lack of inhibition of TNFα-mediated activation suggests other pathways of NF-κB activation may be targeted by RSV SH, at least in these cells.

Chapter 4: Investigating RSV modulation of NF-κB subunit p65

The material presented in this chapter has been peer reviewed and published in the Journal of Virology:
Jobe F, Simpson J, Hawes P, Guzman E, Bailey D. Respiratory Syncytial Virus Sequesters NF-κB Subunit p65 to Cytoplasmic Inclusion Bodies to Inhibit Innate Immune Signaling. J Virol. 2020 Oct 27;94(22):e01380-20. doi: 10.1128/JVI.01380-20. PMID: 32878896; PMCID: PMC7592213.

4.1. Introduction and aims

Inhibition of NF-κB signalling is one of many strategies employed by viruses to prevent innate immune activation and antiviral activity (Chiang and Liu, 2018, Deng et al., 2018). RSV encodes two accessory proteins, NS1 and NS2, which are well established interferon antagonists, inhibiting interferon-mediated antiviral responses (Lo et al., 2005, Schlender et al., 2000, Spann et al., 2004, Spann et al., 2005). Previous studies have suggested that the SH protein is involved in inhibiting NF-κB activation (Pollock et al., 2017, Taylor et al., 2014). However, following the investigations carried out in chapter 3, the individual importance of SH in this antagonism remains unclear. Importantly, from these investigations I discovered that bRSV infection induced NF-κB subunit p65 sequestration into intra-cytoplasmic bodies and that the sensitivity of NF-κB in these cells to TNFα stimulation was reduced relative to mock infected cells (Fig 3.9B). Similarly, studies by Lifland *et al* have shown that sequestration of the immune-mediators MAVS and MDA-5 into cytoplasmic bodies is a mechanism of innate immune antagonism employed by hRSV (Lifland et al., 2012). Thus, in the work described in this chapter, I aimed to characterise the p65 puncta induced in response to wild type bRSV infection and to further investigate the impact of this sequestration on NF-κB activation. I hypothesised that the inhibition of NF-κB activation observed was a direct consequence of its sequestration into intra-cytoplasmic puncta. This would represent a novel mechanism of RSV-mediated antagonism of the NF-κB pathway, distinct from other known viral mechanisms of NF-κB inhibition.

4.2. Results

4.2.1. Wild type bRSV infection inhibits NF-κB subunit p65 activation but not IRF3

Virus infection and replication within the cell triggers pattern recognition receptors (PRRs), including toll-like receptors (TLRs) and cytoplasmic nucleic acid receptors (RIG-I and MDA-5), which in turn induce NF-κB- and IRF-dependent signalling (Baum and Garcia-Sastre, 2010, Liu et al., 2007, Yoboua et al., 2010). As discussed in chapter 1, NF-κB and IRF are two families of transcription factors that regulate the host innate responses. To demonstrate that bRSV infection reduced activation of the NF-κB pathway, Vero cells were mock infected or infected with wild type bRSV at an MOI of 2. 24 h later, cells were left untreated or stimulated with TNFα for 10 or 20 mins, and then cell lysates prepared and assessed for the levels of p65 (total and transiently phosphorylated) and IκBα by western blotting. Infection without TNFα treatment did not significantly alter levels of protein detected despite demonstrable viral protein (bRSV F) production (Fig 4.1A). As previously observed (in chapter 3; Fig 3.7), TNFα treatment of mock-infected cells resulted in an increase in p65 phosphorylation and a decrease in total IκBα – the result of proteasomal degradation (Chen et al., 1995). When cells were infected with bRSV, the reduced levels of P-p65 and IκBα degradation (Fig 4.1A), especially at 10 mins post TNFα stimulation, indicated a reduction in the level of NF-κB activation. The reduced IκBα degradation in bRSV infected cells was consistently observed in all replicates (n=3), however, p65 phosphorylation was either equivalent or only slightly reduced when levels were compared in mock and virus infected cells.

Separately, a luciferase reporter assay, as described in section 3.2.8, was used to assess NF-κB transactivation. 293T cells were infected with bRSV at an MOI of 1. Infection was allowed to proceed for 6 h before being transfected with the NF-κB reporter and subsequently treated (at 18 h p.t.) with or without TNFα. Again, infection alone did not result in any significant activation of the reporter (Fig 4.1B, black bars and bRSV F western blot), confirming that even in the presence of active viral replication there is little to no activation of the NF-κB signalling pathway in bRSV-infected cells. Indeed, activation of the NF-κB reporter was only seen following addition of 20 ng/ml

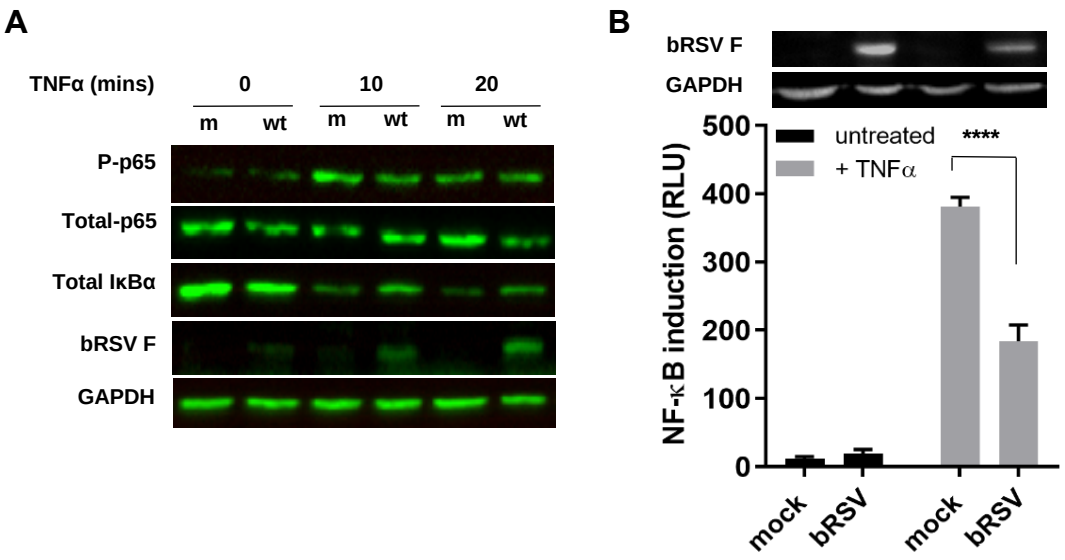

Figure 4.1 Wild type bRSV infection reduces NF-κB p65 activation. (A) Vero cells mock infected (m) or infected with bRSV (wt) at an MOI of 2 for 24 h were left untreated or stimulated with 20 ng/ml hTNFα for 10 or 20 mins. Cells were then lysed and analysed by western blotting for phosphorylation of p65 using phospho-specific forms of the antibody, total p65, IκBα and RSV F. GAPDH was detected as a loading control. **(B)** 293T cells were mock infected or infected with bRSV at an MOI of 1. At 6 h p.i., cells were transfected with 100 ng NF-κB FLuc reporter and 10 ng TK-renilla luciferase and incubated at 37ºC. At 18 h p.t., cells were left untreated or stimulated for 16 h with 20 ng/ml hTNFα. Cells were then lysed and analysed for firefly and renilla luciferase activities. Graph depicts means ± SD of three replicates from the same experiment. As controls, the levels of RSV F and GAPDH were analysed by western blotting on a fourth replicate. Statistical significance was determined by ANOVA as described in the methods, ****p<0.0001. Data is representative of n=2 independent repeats.

of exogenous hTNFα; however, this activation was significantly less than those seen in uninfected cells (Fig 4.1B, grey bars).

Next, I re-examined NF-κB activation in infected cells by IF microscopy, this time in parallel with IRF3 signalling, given the established role of these pathways in the cell's innate immune response and the clearance of viral infection (Fig 1.5). Vero cells were mock infected or infected with bRSV at a MOI of 1 for 24h and then left untreated or stimulated with TNFα or poly(I:C). Cells were then fixed and immuno-stained for bRSV F as a marker for infection as well as for the NF-κB subunit p65 or, separately, IRF3. IF analysis of mock-infected cells confirmed that both transcription factors are normally located in the cytoplasm (Fig 4.2). When the NF-κB and IRF3 pathways were stimulated in mock-infected cells with agonist treatment (hTNFα and poly[I:C], respectively), both the NF-κB subunit p65 and IRF3 translocated from the cytoplasm to the nucleus, as expected (Fig 4.2 top panel; inset zooms). However, although infection with bRSV induced similar levels of IRF3 nuclear translocation (bottom right panel), significantly the NF-κB subunit p65 remained cytoplasmic, coalescing into intracytoplasmic puncta, mostly perinuclear and present only in infected cells (bottom left panel). Fluorophore intensity profile analysis was then performed to assess the relative accumulation of both p65 and IRF3 in infected and/or stimulated cells. For IRF3, poly(I:C) stimulation of infected cells enhanced its nuclear translocation, relative to uninfected cells (bottom right – inset zoom). However, IF and intensity profile analysis revealed that, even with TNFα stimulation, p65 nuclear translocation in bRSV infected cells was absent and that most p65 remained in the observed perinuclear puncta (bottom left – inset zoom). bRSV can infect a broad range of host cells *in vitro* – growing to similar titres in both Vero and MDBK cells (Fig 3.1). To examine this apparent innate immune antagonism in bovine cells, similar infections were performed in MDBK cells. These experiments confirmed an equivalent sequestration of p65 into perinuclear puncta following bRSV infection, as well as a related insensitivity to TNFα stimulation (Fig 4.3), indicating a conserved mechanism of antagonism active in both primate and ruminant cells.

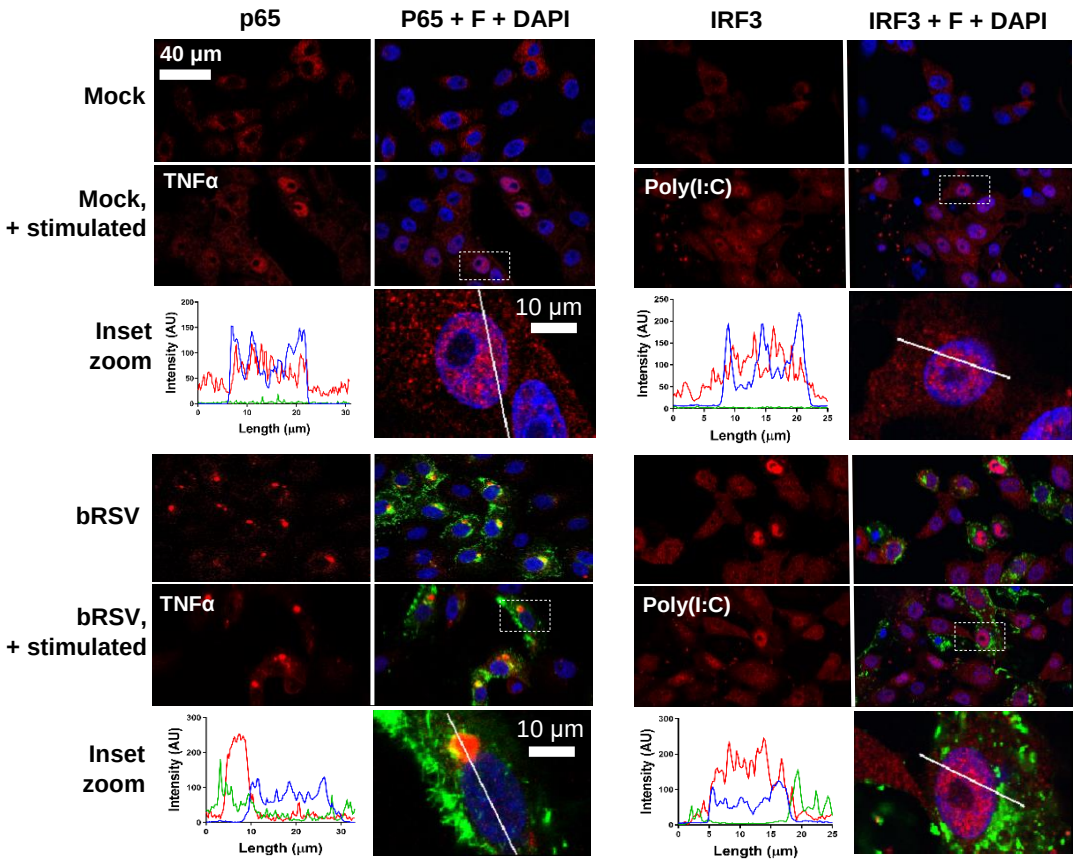

Figure 4.2 bRSV infection induces IRF3, but not NF-κB p65 nuclear translocation. Vero cells, uninfected (mock), or infected with bRSV at an MOI of 1 for 24 h, were left untreated, stimulated with 20 ng/ml hTNFα for 30 mins or transfected with 2.5 µg/ml poly(I:C) and incubated for 6 hrs at 37ºC. Cells were then fixed and immunostained with anti-RSV F (green) and anti-NF-κB p65 or anti-IRF3 (red) antibodies. Cell nuclei were stained with DAPI (blue) and images obtained using a Leica TCS SP5 confocal microscope. The boxed areas are shown magnified in the panels below (inset zoom). Graphs show fluorescent line intensity profiles along the respective white lines within these inset zooms. Data is representative of n=2 independent repeats.

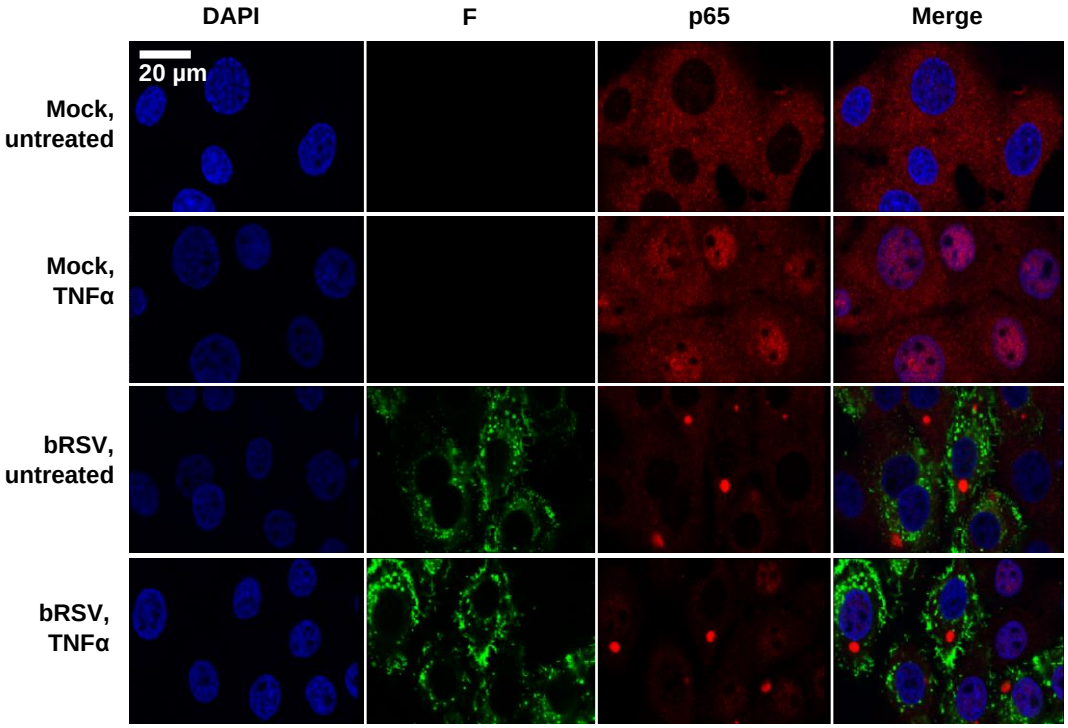

Figure 4.3 bRSV infection reduces NF-κB p65 nuclear translocation in MDBK cells. MDBK cells mock infected or infected with bRSV at an MOI of 1 for 24 h were left untreated or stimulated with 20 ng/ml hTNFα for 30 mins. Cells were then fixed and immuno-stained with anti-RSV F (green) or anti-NF-κB p65 (red) antibodies. Cell nuclei were stained with DAPI (blue) and images obtained using a Leica TCS SP5 confocal microscope. Images are representative of n=3 independent repeats.

4.2.2. Characterisation of NF-κB p65 aggregates induced in response to bRSV infection

To define the kinetics of p65 sequestration over time, Vero and MDBK cells were infected at an MOI of 1 and fixed at different times post infection. Cells were then fixed, permeabilised, and the distribution of p65 and RSV F analysed by IF. p65 puncta were present in infected cells from 16 h p.i. which correlated with significant levels of F expression (Fig 4.4 and 4.5A). Although there was no specific colocalization of F and p65, by 24 h p.i., all infected cells contained at least one p65 puncta with none being observed in nearby uninfected cells. The cross-sectional area of the punctate structures present at each time point was also measured. Visible aggregates measured above 3 μm^2 with the average size increasing as infection progressed (Fig 4.5B). At 48 h p.i., p65 aggregations had a mean area of 22.18 μm^2 but smaller puncta (<10 μm^2) were also observed, most likely the result of nascent infections in nearby cells. Using fluorophore line of interest analysis, I was also able to assess the ratio of cytoplasmic- to puncta-localised p65 as well as the increasing diameter of these aggregates. As infection proceeded, the intensity of p65 in the puncta increased as the level of dispersed p65 in the cytoplasm decreased (Fig 4.5C; 'p65 in puncta' vs. 'p65 outside puncta'), implying movement of p65 into the puncta.

Recent work has demonstrated that hRSV infection induces the formation of inclusion bodies (IB) which contain components of the RNA polymerase complex and ribonucleoprotein (RNP), notably N and P (Rincheval et al., 2017). IBs, also known as viroplasms, are compartments within the host cell cytoplasm where viral replication occurs. However, similar IBs have not been identified, or functionally characterised, in bRSV-infected cells. To examine the presence and sub-cellular localisation of IBs relative to the observed p65 puncta, Vero cells were infected and fixed at 6, 16, 24 and 48 h p.i. along with mock infected cells for IF analysis. Cells were then co-immunostained for p65 and bRSV N protein. As expected, neither p65 puncta nor bRSV N were detected in mock infected cells (Fig 4.6A). Aggregations of RSV N were observed from 6 h p.i.; growing into large intracytoplasmic organelles more characteristic of IBs as infection progressed from 24 h p.i. Although there was some degree of cytoplasmic signal for N outside of the IBs, most of the IF signal was found within these structures. The sub-IB localisation was similar to that previously

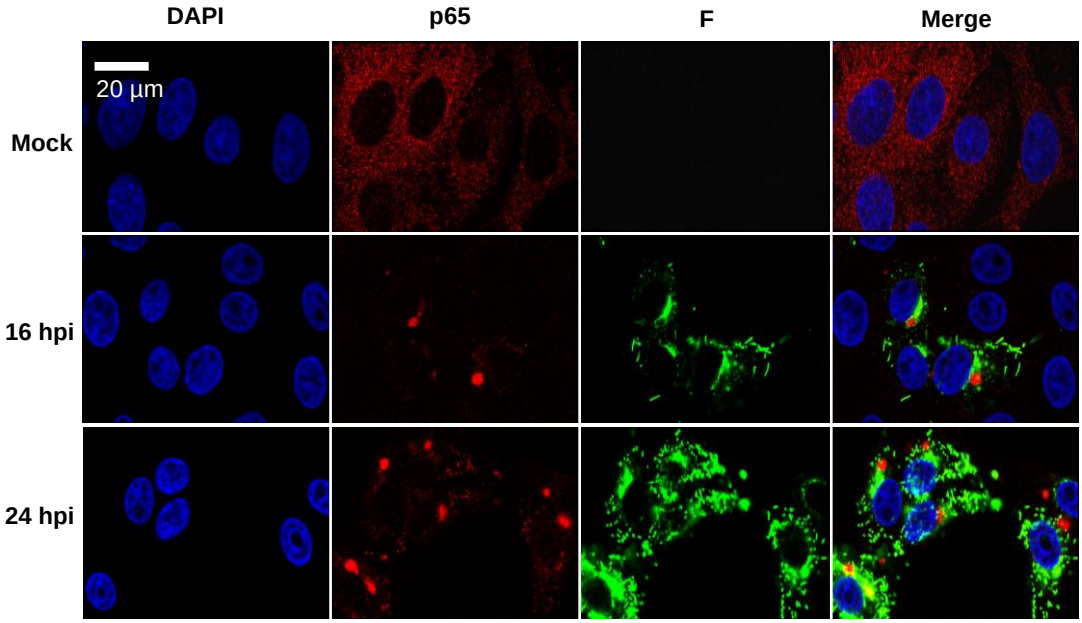

Figure 4.4 Time course of NF-κB p65 puncta formation in bRSV infected Vero cells. Vero cells were mock infected or infected with bRSV. At the indicated times p.i., cells were fixed and immuno-stained with anti-NF-κB p65 (red) and anti-RSV F (green) antibodies. Nuclei were stained with DAPI (blue) and images obtained using a Leica TCS SP5 confocal microscope. Images are representative of n=4 independent repeats.

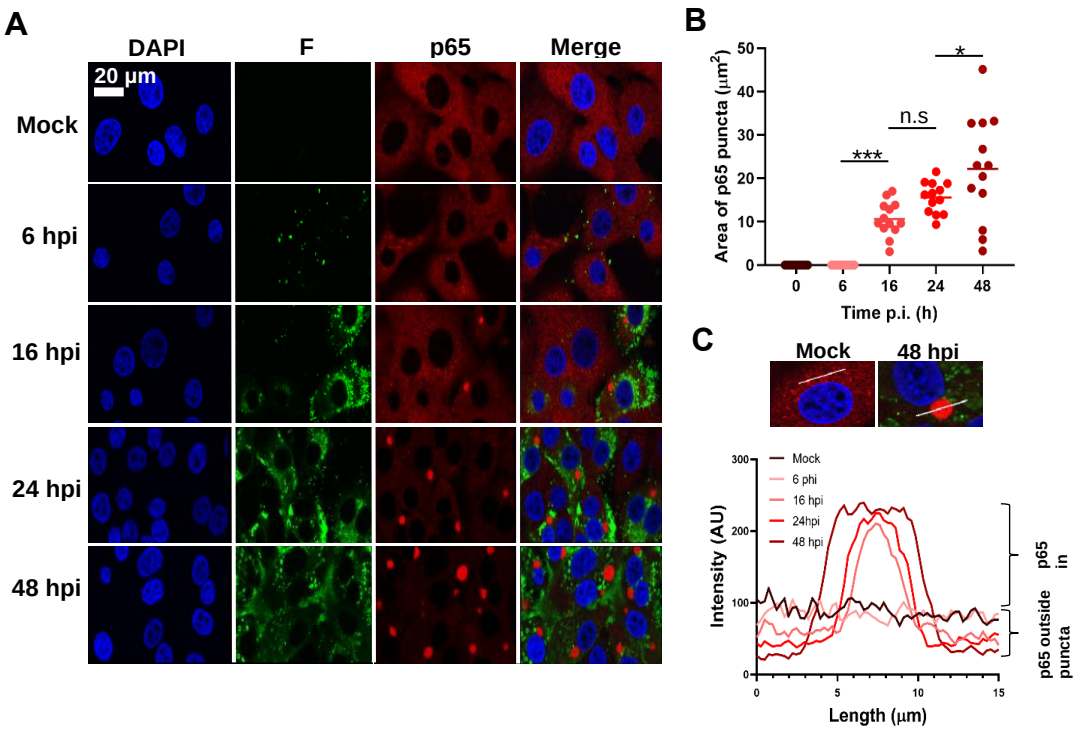

Figure 4.5 bRSV replication induces the recruitment of NF-κB subunit p65 into intra-cytoplasmic bodies. (A) MDBK cells were mock infected or infected with bRSV. At the indicated times p.i. cells were fixed and immuno-stained with anti RSV F (green) and anti-NF-κB p65 (red) antibodies. Nuclei were stained with DAPI (blue) and images obtained using a Leica TCS SP5 confocal microscope. **(B and C)** Quantification of p65 puncta size and intensity in A obtained using the quantify tool of Leica LAS AF Lite software as described in the methods. **(B)** Cross-sectional area of thirteen p65 puncta (selected randomly) per time point and mean area are indicated. Statistical significance determined by ANOVA as described in the methods, n.s: non-significant; *p<0.05; ***p<0.001. **(C)** Graph showing the line intensity profiles along chosen 15 µm lines of interest (example micrographs: 15 µm drawn across a puncta, or, across the cytoplasm in mock cells) of an average of five puncta per time point. Images are representative of data from a single experiment

described for hRSV N, being found on the periphery of the organelle (Rincheval et al., 2017). Significantly, the larger N positive IBs were, in the majority of cases, also p65 positive identifying, for the first time, that this NF-κB component was being recruited to RSV IBs in infected cells.

To examine this in detail, I next characterised the number, size and p65 status of N-positive IBs in infected cells, observing that they were numerous and mostly localised in the median section of the cell. Images were obtained from multiple planes in this section to assemble max intensity z-stacks to aid quantification. From 16 h p.i., N and p65 positive IBs were evident throughout the cell in a conserved pattern consisting of a single large and perinuclear IB with multiple smaller inclusions more evenly distributed through the cytoplasm (Fig 4.6B). Using z-stacks, I quantified the number per cell (counting 18 cells per sample, per timepoint) and cross-sectional area of N and/or p65 positive structures >0.1 μm^2, observing these both increasing as infection progressed. The average number of IBs >0.1 μm^2 grew from 1.7 per cell at 6 h p.i., to 23.8 at 24 h p.i. (Fig 4.6C). Their mean area also increased to 8.99 μm^2 by 24 h p.i. (Fig 4.6D), significantly influenced by the presence and growth of the larger IB. p65 positive IBs were detected from 16 h p.i.; however, p65 was only detected in larger IBs (>1.39 μm^2) (Fig 4.6D) with up to 4 of these being evident per cell (Fig 4.6C). In conclusion, although multiple N-positive IBs are present in infected cells it is predominantly the larger IBs which contain the sequestered p65. Together, these data suggest that bRSV infection induces the formation of IBs in the cytoplasm of infected cells - organelles which are also involved in sequestering cellular proteins to effect immunomodulation. To my knowledge, this represents an entirely novel mechanism of viral inhibition of NF-κB signalling, since it is the sequestration of signalling components to a viral organelle, rather than the competitive interaction or degradation commonly seen (Deng et al., 2018, Goswami et al., 2013), which leads to the innate immune antagonism witnessed in Fig 4.1 and 4.2.

4.2.3. bRSV infection induces membrane-less IBs in infected cells and alters the cellular ultrastructure.

IBs and IB-like structures form by liquid-liquid phase separation (LLPS) which favours macromolecular-macromolecular over macromolecular-water interactions (Alberti et al., 2019, Murthy and Fawzi, 2020, Mudogo et al., 2019). The resulting

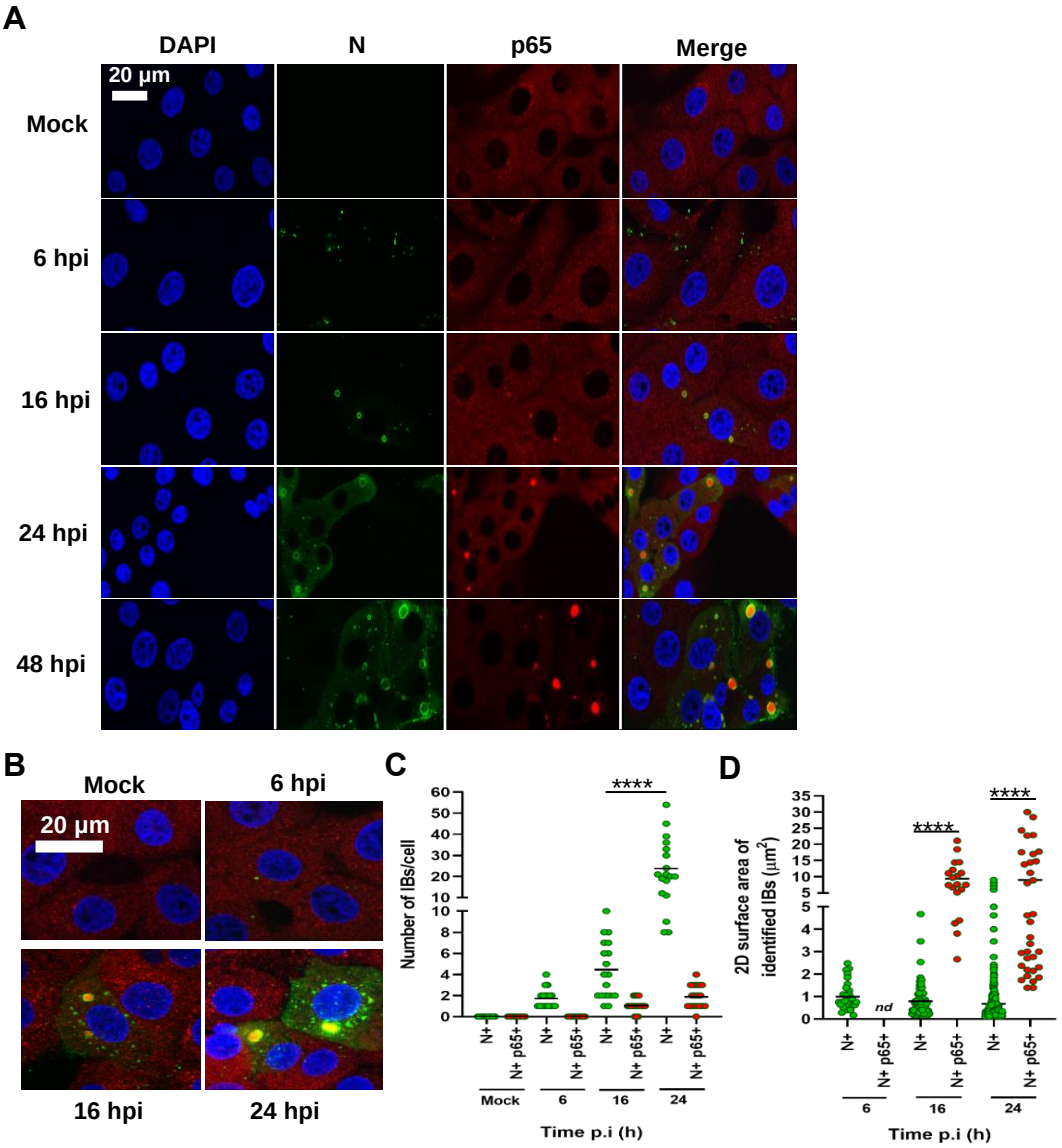

Figure 4.6 bRSV-induced NF-κB p65 intra-cytoplasmic bodies colocalize with N protein. (A) MDBK cells were mock infected or infected with bRSV. At the indicated times p.i. cells were fixed and immuno-stained with anti RSV N (green) and anti-NF-κB p65 (red) antibodies. Cell nuclei were stained with DAPI (blue) and images obtained using a Leica TCS SP5 confocal microscope. **(B)** Images are max intensity z-stacks of 8 planes 0.5 µm apart. Cytoplasmic bodies (area >0.1 µm2) from the z-stacks were quantified in a total of 18 infected cells per time point as detailed in the methods. **(C)** Number of N, and N and p65, positive bodies per cell at the indicated time points. **(D)** Cross-sectional area of identified N, and N and p65, positive IBs. Circles on the graphs are coloured according to their IB properties: green with green edges; N positive, red with green edges; N and p65 positive. Statistical significance determined by ANOVA as described in the methods, ****p<0.0001. Images are representative of data from a single experiment

biomolecular condensates are not usually surrounded or compartmentalised by a membrane, distinguishing them from many other organelles found in the cytoplasm (Mudogo et al., 2019, Perez-Pepe et al., 2018). The mechanism of viral IB formation is not well understood but the cytoplasmic modifications induced are thought to require both viral and cellular components (Moshe and Gorovits, 2012). They function to concentrate viral and host cell proteins required for efficient replication as well as protecting replication intermediates from the host innate immune response. To examine the ultrastructural properties of the bRSV IBs, standard transmission electron microscopy (TEM) of infected cells was performed with technical support from Jennifer Simpson, a microscopy expert in The Pirbright Institute Bioimaging group. For this, I infected Vero cells with bRSV at an MOI of 1 and fixed the cells at 24 and 48 h p.i., at which point they were handed to Jennifer for TEM analysis. She also provided data interpretation support along with Philippa Hawes, Bioimaging group leader. From this analysis, granular structures with high electron density, characteristic of RNA virus inclusion bodies, were identified at both timepoints, often in close proximity to the nucleus (Fig 4.7A). Smaller structures (1-2 µm in diameter) were predominately rounder in nature when compared to their larger (>3 µm in diameter), more pleomorphic counterparts (Fig 4.7A).

These structures are similar to those previously reported for the rhabdoviruses, rabies virus and vesicular stomatitis virus (Lahaye et al., 2009, Nikolic et al., 2017, Heinrich et al., 2018), supporting our conclusion that bRSV also forms membrane-less IBs in infected cells. As expected, these structures were not visibly membrane-bound or directly associated with sub-cellular organelles; however, rough endoplasmic reticulum (RER; black arrows) and mitochondria (M in Fig 4.7A) were frequently found in close proximity. Identification of ER and mitochondria using anti-calnexin and anti-AIF antibodies, respectively, by IF analysis further revealed changes in the cellular distribution of these organelles. As both structures occupy the perinuclear region, the ER network is seen excluded from the regions containing the dominant IB (Fig 4.7B). This is unlike the replication complexes of positive strand RNA viruses which are composed of several double-membrane vesicles or spherules derived from diverse organelle membranes (den Boon and Ahlquist, 2010, Harak and Lohmann, 2015, Nevers et al., 2020). Mitochondria, on the other hand, were often seen condensed around the dominant IB in the perinuclear region (Fig 4.7B). Microtubule-

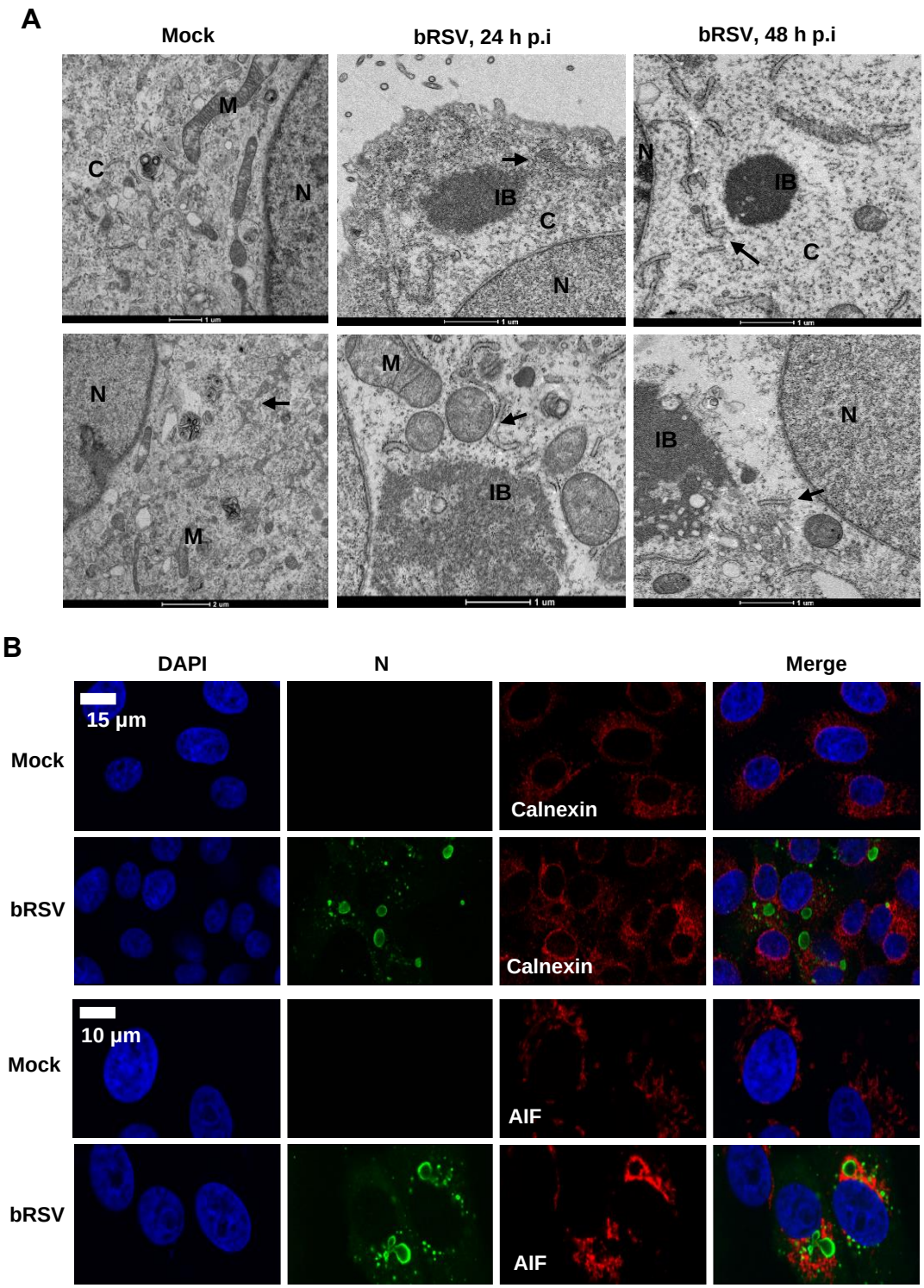

Figure 4.7 Ultrastructural analysis of bRSV infected cells shows membrane-less intra-cytoplasmic structures and changes to cellular ultrastructure. (A) High power transmission electron microscopy (TEM) of mock or bRSV infected Vero cells fixed in glutaraldehyde at 24 and 48 h p.i and prepared for TEM as detailed in the methods. N, nucleus; M, mitochondria; C, cytoplasm; IB, inclusion body and ER indicated with black arrows. Two representative images are shown per time point. Scale bars correspond to 1 µm. **(B)** Vero cells, mock infected or infected with bRSV were fixed at 24 h p.i., and co-immunostained with anti-bRSV N (green) and anti-calnexin/AIF (red) antibodies. Images in A are representative of n=3 independent repeats, and in B, n=2.

dependent mitochondrial redistribution to a perinuclear position has been shown to favour RSV infection by decreasing mitochondrial respiration, loss of mitochondrial membrane potential and increased reactive oxygen species production (Hu et al., 2019b).

To examine the sub-IB localisation of RSV N and p65 in relation to the ultrastructural analysis of IBs, correlative light electron microscopy (CLEM) was performed, again with support from Jennifer Simpson. This is a powerful technique that allows examination of the ultrastructural detail of cells/cellular structures by TEM, in combination with immunofluorescence microscopy. It is a relatively new technique that is increasingly used to study virus-host interactions (Bykov et al., 2016). Here, I infected Vero and MDBK cells at an MOI of 1 on gridded coverslips and fixed the cells at 24 and 48 h p.i. for analysis, firstly by confocal microscopy using N and p65 antibodies to immunolabel these proteins (Fig 4.8). At this point samples were handed over to Jennifer for further analysis. The same cells, examined by IF, were identified by grid reference, then isolated, embedded, and sectioned with their ultrastructure subsequently analysed by TEM. Importantly, these CLEM data confirmed that the electron dense granular structures seen by TEM (Fig 4.7A) are synonymous with the N and p65 stained IBs seen in IF microscopy. An overlay of the two images confirmed that bRSV IBs had retained the electron dense granular structure characteristic of liquid organelles in both Vero and MDBK cells, even with the chemical permeabilization required for IF antibody labelling (Fig 4.8). CLEM data also confirmed that p65 and N proteins localise to the IB, with p65 present within the structure and N around the periphery.

4.2.4. bRSV IBs are dynamic structures and are distinct from stress granules.

Previous reports have demonstrated that IBs can rapidly change their size due to fusion or fission events whilst remaining spherical in nature - a characteristic feature of these liquid organelles and one of the criteria used for their identification (Alberti et al., 2019, Nikolic et al., 2017). Rabies virus inclusion bodies, termed negri bodies, have been shown to rapidly dissolve and reform in response to hypotonic shock, also demonstrating the dynamic nature of these structures and their sensitivity to their physicochemical environment (Nikolic et al., 2016, Nikolic et al., 2018). To assess the

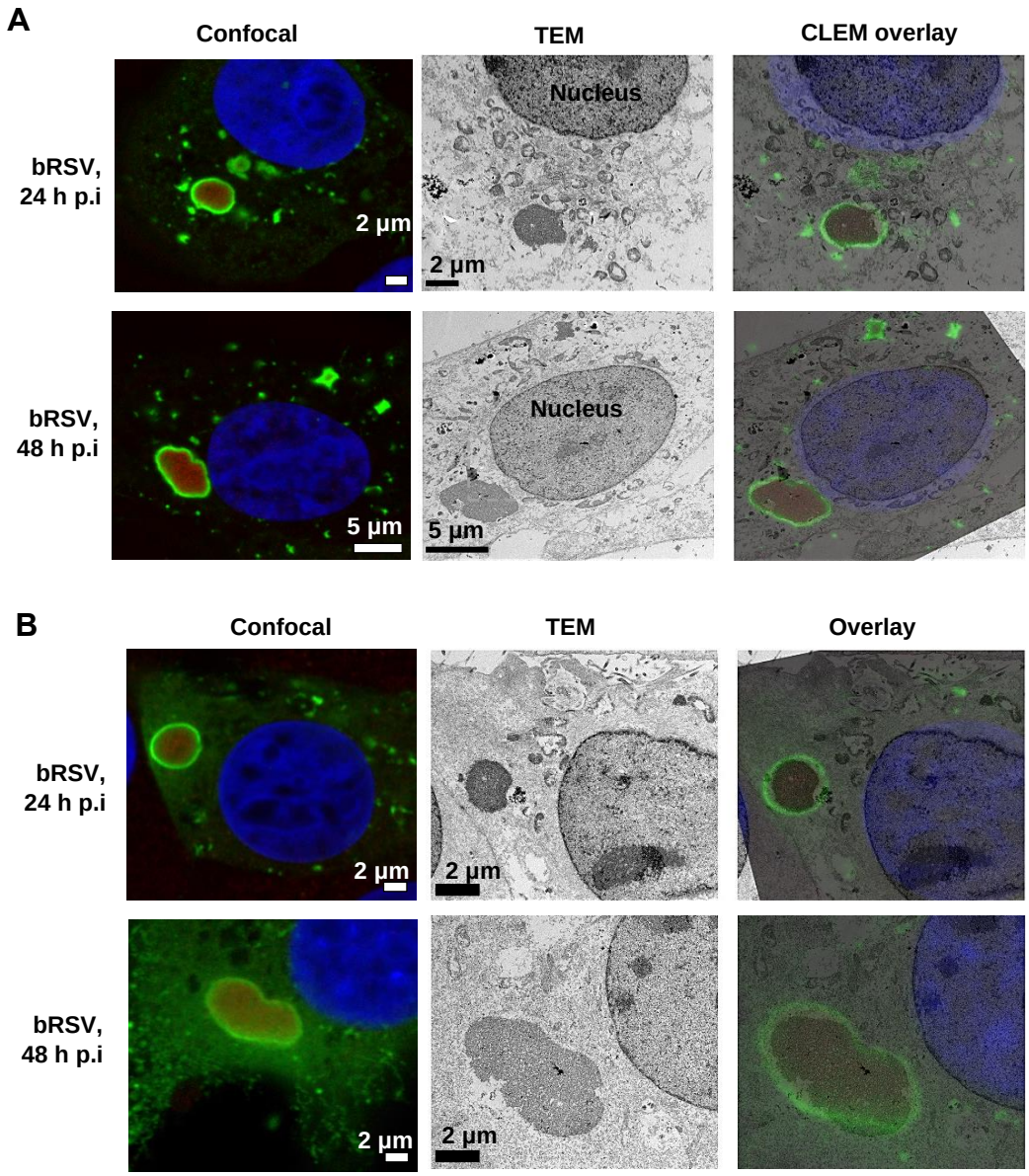

Figure 4.8 Correlative Light and Electron Microscopy (CLEM) confirms p65 recruitment into RSV inclusion bodies. Correlative light electron microscopy (CLEM) of confocal microscopy immunostaining and TEM showing bRSV IBs. **(A)** Vero and **(B)** MDBK cells infected with bRSV at MOI 1 were fixed at 24 or 48 h p.i., stained with antibodies against RSV N (green), NF-κB p65 (red) and nuclei stained with DAPI. Following confocal imaging, cells were fixed in glutaraldehyde, sectioned and visualised by TEM. Confocal (left) and TEM (middle) images of the same cells were overlayed (right) as CLEM images. Images are representative of data from a single experiment

sensitivity of bRSV IBs to hypotonic shock, Vero cells, infected with bRSV for 24 h, were incubated with DMEM (diluted to 20% in H_2O) for 20 mins. Cells were then

fixed and immunostained for N protein only or N and p65. Many smaller IBs showed evidence of dissolution following hypotonic shock (Fig 4.9A; iv); however, unlike rabies virus negri bodies, the larger bRSV IBs remained intact following this significant period of cellular osmotic shock (Fig 4.9A; iii). Of note, incubation beyond 20 minutes was not possible because of the associated cytotoxicity. In addition, a large percentage of the sequestered p65 in these larger IBs remained tightly associated with the intact structure (Fig 4.9B). Recently, Zhou et al., demonstrated that larger measles IBs had slower rates of fluorescence recovery after photobleaching (FRAP), relative to their smaller counterparts, postulating that these structures had acquired a more gel-like property (Zhou et al., 2019). At 24 h p.i., the p65-positive IB structures were mostly spherical, becoming larger and more irregularly shaped by 48 h p.i., possibly as a result of transition into a more gel-like status (Fig 4.8). The acquisition of this gel-like status, which are also less likely to exchange molecules with the surrounding cytoplasm, has been linked to aging of phase separated organelles - a continuum which ends with the formation of irreversible aggregates (Shin et al., 2017). Therefore, the insensitivity of large bRSV IBs to osmotic shock, and the maintenance of p65 within the IB even under these harsh conditions, is perhaps the result of them acquiring gel-like status, a property which may be linked to the age and size of individual IBs within infected cells.

Furthermore, the p65 puncta/IBs observed in bRSV infected cells were visually similar to protein and mRNA aggregations that form in cells in response to cellular stress and viral infections, so-called stress granules (SG). A wide range of viruses have been shown to either induce or inhibit SG formation to their advantage (White and Lloyd, 2012); however, there are contradictory findings on SG induction by RSV (Fricke et al., 2013, Lindquist et al., 2010, Hanley et al., 2010, Lindquist et al., 2011). To examine the potential relationship between these structures and SGs, I induced SG formation in bRSV infected cells with sodium arsenite treatment and performed co-immunostaining for p65 and G3BP1 (a SG marker) in fixed cells. Although I was able to successfully stimulate the production of SGs in Vero cells, the analysis showed that the p65 puncta were entirely distinct from these granules (Fig 4.9C). Tangentially, this

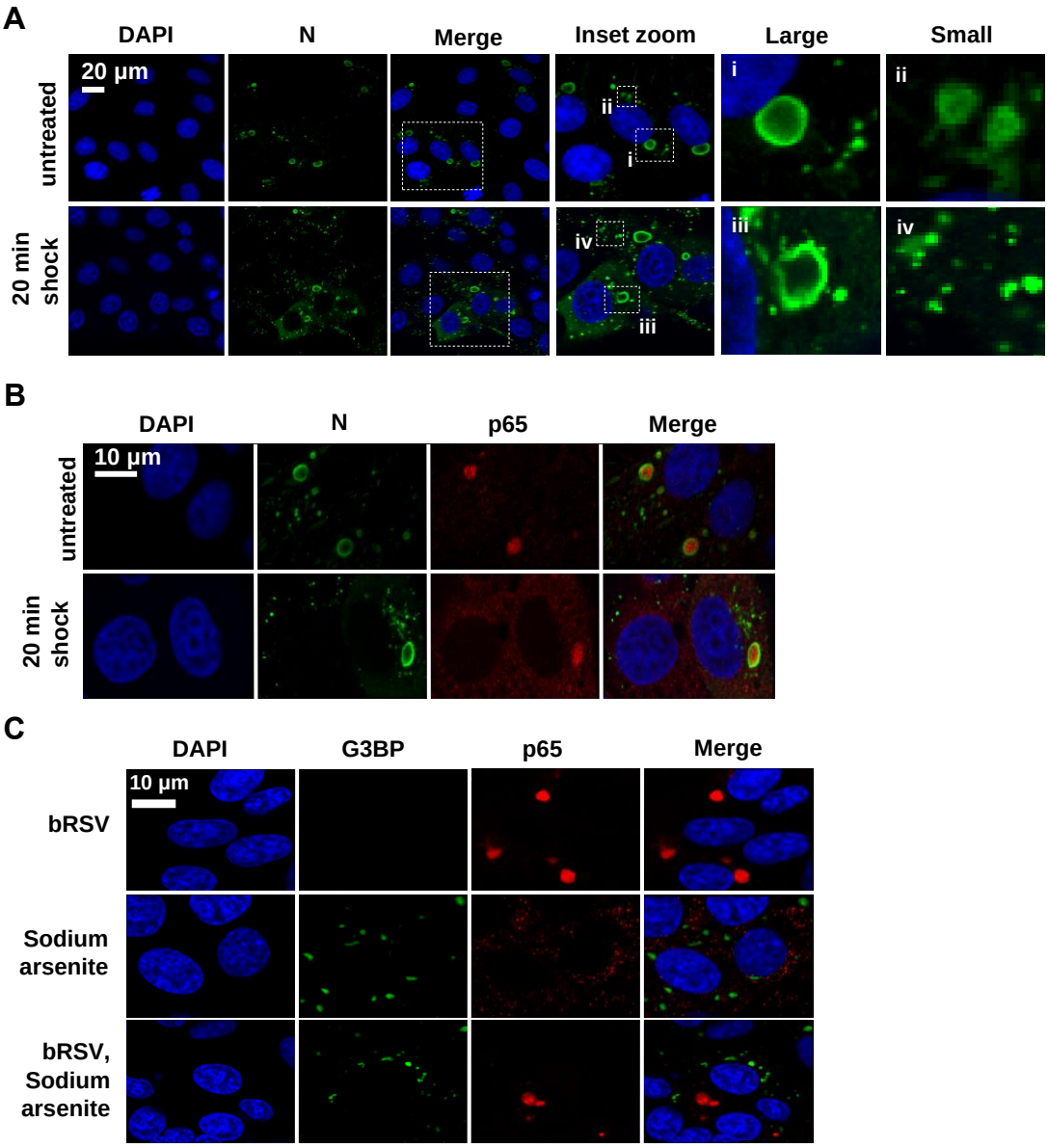

Figure 4.9 P65 IBs are dynamic structures and distinct from stress granules. (A/B) Vero cells were infected with bRSV at an MOI of 1 and incubated at 37ºC for 24 h. Hypotonic shock was applied for 20 mins before the cells were fixed. Confocal analysis was performed following immuno-staining for bRSV N (green), and nucleus stained with DAPI (and p65 for B). Inset zooms demonstrate the observed effects of hypotonic shock on large (i and iii) and small (ii and iv) IBs – representative images shown. **(C)** Vero cells were infected with bRSV or mock infected. At 24 h p.i., cells were treated with 500 µM Sodium arsenite or mock treated for 1 hr. Cells were then fixed and immuno-stained with anti-G3BP1 (green) and anti-NF-κB p65 (red) antibodies. Nuclei were stained with DAPI (blue) and images obtained using a Leica TCS SP5 confocal microscope. Images are representative of n=4 independent repeats. Images are representative of n=2 independent repeats.

experiment also demonstrated that bRSV infection does not significantly induce SG formation, at least in this cell type and at the time point examined.

4.2.5. Role of RSV-encoded immunomodulatory proteins on p65 sequestration into IBs.

As a central regulator of the innate immune response, several viruses target NF-κB signalling to inhibit its activation (Deng et al., 2018). Furthermore, the sub-optimal natural immune response to RSV indicates the employment of immune antagonistic strategies by the virus. However, further work is required to unveil the encoded mechanisms specifically targeting NF-κB. As already discussed, NF-κB p65 capture into RSV IBs blocks its nuclear translocation and transcriptional activation (Fig 4.1 and Fig 4.2). In order to examine a potential role for the established bRSV-encoded immunomodulatory proteins - NS1, NS2 (Schlender et al., 2000) and SH (Pollock et al., 2017, Taylor et al., 2014) in the formation of p65 positive IBs, this phenomenon was investigated in cells infected with virus lacking the expression of these proteins. Mutant viruses [ΔNS1, ΔNS2, ΔNS1/2 (a double knockout) and ΔSH (Buchholz et al., 1999, Taylor et al., 2014, Karger et al., 2001, Schlender et al., 2000)] were obtained from Geraldine Taylor, at the Pirbright Institute, then grown in and titrated on Vero cells. Immunoblotting bRSV ΔSH infected cells with an anti-SH antibody and comparing them to wt bRSV infected cells confirmed deletion of SH (Fig 3.3A).

Since I did not have access to anti-NS antibodies, the genotype of these mutants was confirmed by RT-PCR. Total RNA was extracted from cells infected with bRSV ΔNS1, ΔNS2 and ΔNS1/2, or from wild type bRSV infected cells as control. RT-PCR was performed with primers targeting the region encoding the NS genes, amplifying from the gene start (Gs) region of NS1 to the beginning of the N gene. The right expected product sizes were obtained for ΔNS1 and ΔNS2, confirming deletion of the respective genes (Fig 4.10A). No band was seen in the double knockout possibly due to the expected band size of 101 bp being too small to visualise. Having confirmed the genotypes of the viruses, Vero cells were then infected for 24 h, fixed and co-immunostained for p65 and the RSV F protein. IF analysis of these samples identified p65 puncta in all infected cells (Fig 4.10B), suggesting that these bRSV-encoded immunoantagonists do not play a significant role in either the formation of IBs or the sequestration of p65 to these structures. Thus, these RSV-encoded immune antagonists

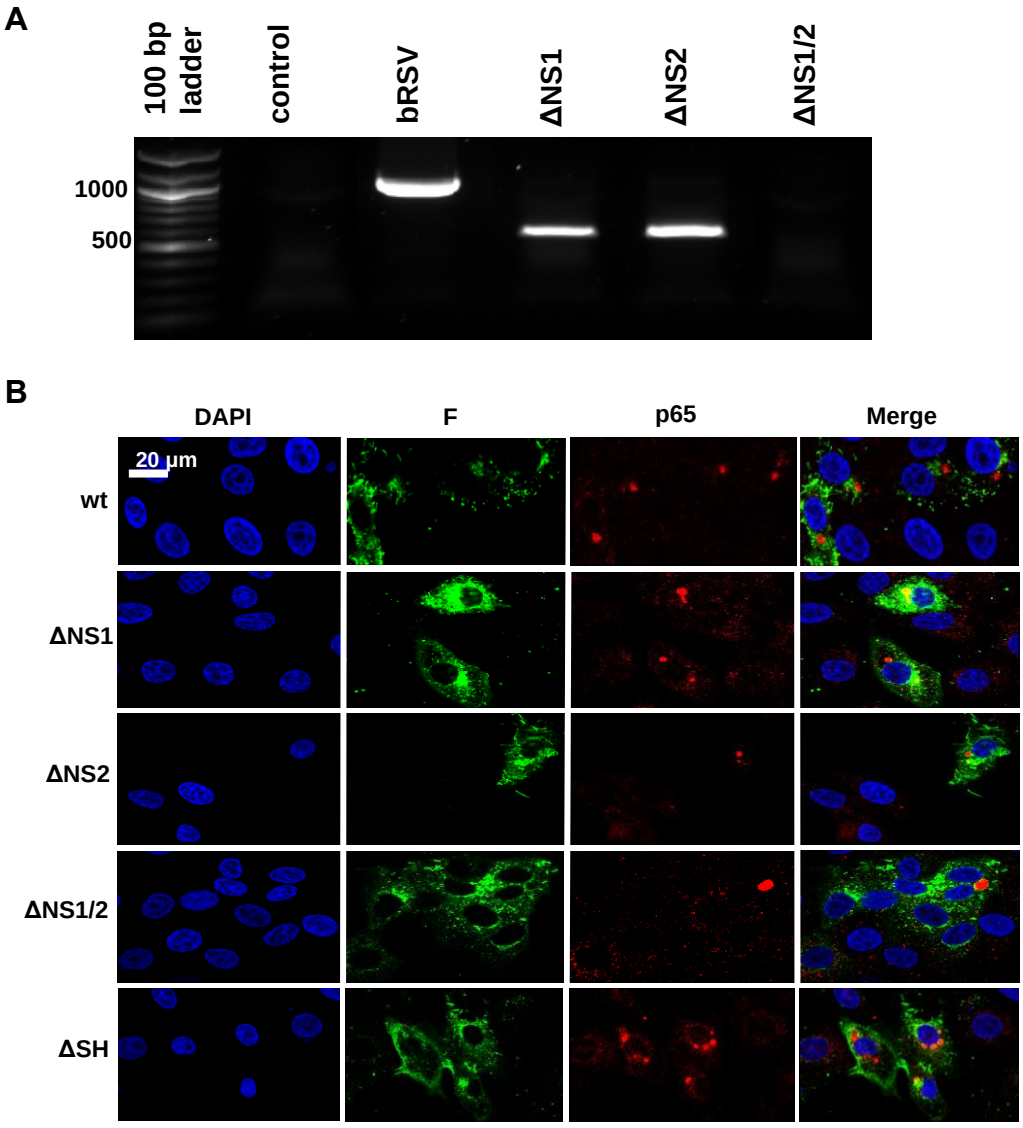

Figure 4.10 NF-κB subunit p65 co-localises with viral inclusion bodies independently of RSV-encoded immunomodulators. (A) Confirmation of NS gene deletion**.** Total RNA was extracted from Vero cells infected with the indicated viruses at 24 h p.i. and subjected to reverse transcriptase PCR using primers that amplify from the gene start (Gs) region of NS1 to the beginning of the N gene. Expected product sizes: wt, 1120 base pairs (bp); ΔNS1,594 bp; ΔNS2, 627 bp; and ΔNS1/2, 101 bp. **(B)** Vero cells were infected with wt bRSV, ΔNS1, ΔNS2, ΔNS1ΔNS2 or ΔSH bRSV. 24 h p.i., cells were fixed and immunostained with rabbit anti-NF-κB p65 (red) and mouse anti-RSV F (green) antibodies. Cell nuclei were stained with DAPI (blue) and images obtained using a Leica TCS SP5 confocal microscope. Data in A is from a single experiment. Images in B are also representative of data from a single experiment

are not exclusively responsible for modulating the innate immune response.

4.2.6. Co-expression of bRSV N and P proteins induces the formation of IB-like structures which can sequester p65

In the absence of infection, ectopic co-expression of many *Mononegavirales* N and P proteins has been shown to result in the formation of IB-like structures (Lifland et al., 2012, Nikolic et al., 2017, Rincheval et al., 2017, Zhou et al., 2019, Garcia et al., 1993) – a finding which has been linked to their potential to induce LLPS independently of viral infection. Although this has been related to the presence of intrinsically disordered regions within the N and P proteins, the exact mechanisms underlying viral IB formation remains uncharacterised. Recently, the central oligomerisation domain and C-terminal domain (an intrinsically disordered region) of P, plus the ability of N to interact with both P and RNA, were shown to be required for pseudo-IB formation (Galloux et al., 2020a). However, whether the infection independent pseudo-IBs retain all the properties of viral IBs is not entirely clear. For hRSV it was shown that IB-associated granules (IBAGs) do not form within these visually orthologous bodies (Rincheval et al., 2017); however, the recruitment of MDA5 and MAVS to the pseudo IBs, following N and P overexpression, was maintained (Lifland et al., 2012). To address similar questions for bRSV IBs, and to examine the related sequestration of p65, Vero cells transiently transfected with plasmids expressing bRSV N (pN) and bRSV P (pP) were fixed and stained at 24 h post transfection and examined by IF. As has been reported previously, expression of N or P alone did not lead to the formation of IB-like structures; however, co-expression did, resulting in the formation of inclusions up to 6.9 μm^2 in area (Fig 4.11). Examination of the sub-cellular localisation of p65 in this system also confirmed that the N- and P-induced inclusions were proficient in sequestering p65, independent of viral replication, with a pattern of expression mirroring that seen in infected cells (Fig 4.11; inset zoom and fluorescent line of interest analysis). This data confirms that the N and P proteins are central to IB nucleation and possibly involved in recruiting p65 or at least create the conditions favouring p65 localisation. In summary, our results indicate that p65 recruitment into bRSV IBs is maintained even in IB-like structures formed after N and P overexpression.

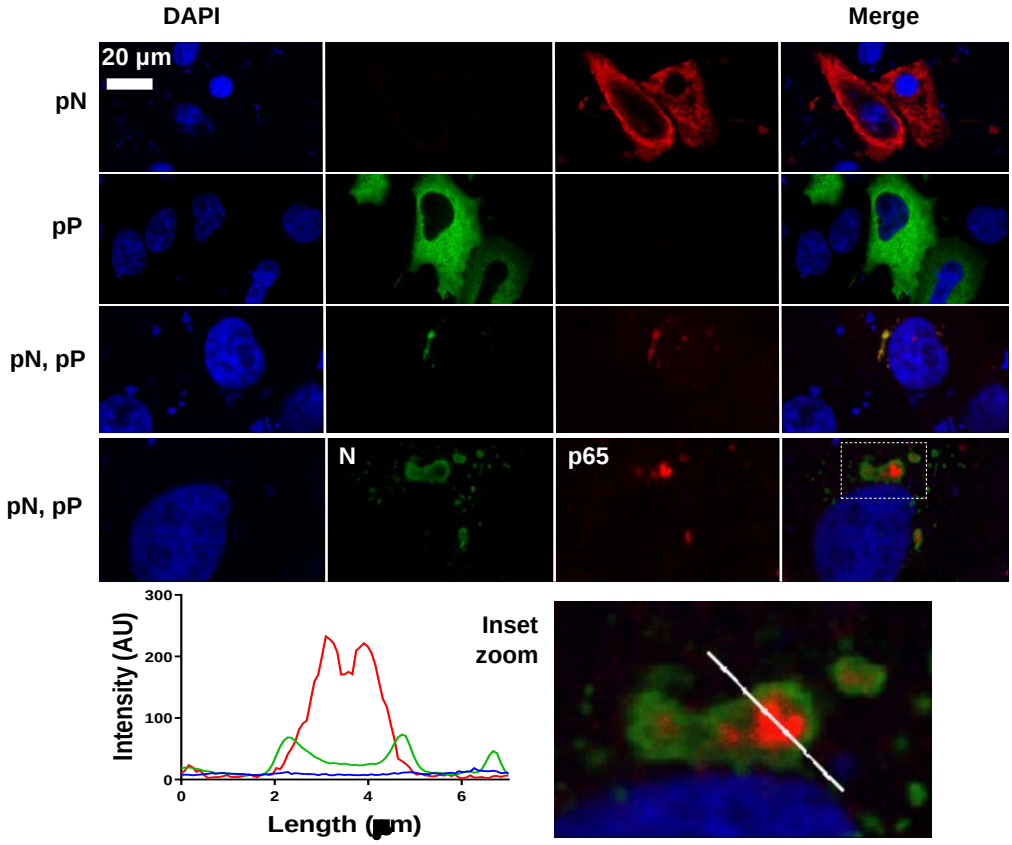

Figure 4.11 Co-expression of bRSV N and P proteins induces the formation of IB-like structures which can sequester p65. Vero cells were co-transfected with equimolar concentrations of plasmids expressing bRSV N (pN) and/or P (pP) proteins as indicated. Following 24 h incubation, cells were fixed and stained with anti-RSV N (green/red) and anti-RSV P (green) or anti-NF-κB p65 (red) antibodies. Bottom panel shows a higher magnification of the boxed area. Graphs shows fluorescent intensity profiles along the indicated white line. Images are representative of n=3 independent repeats.

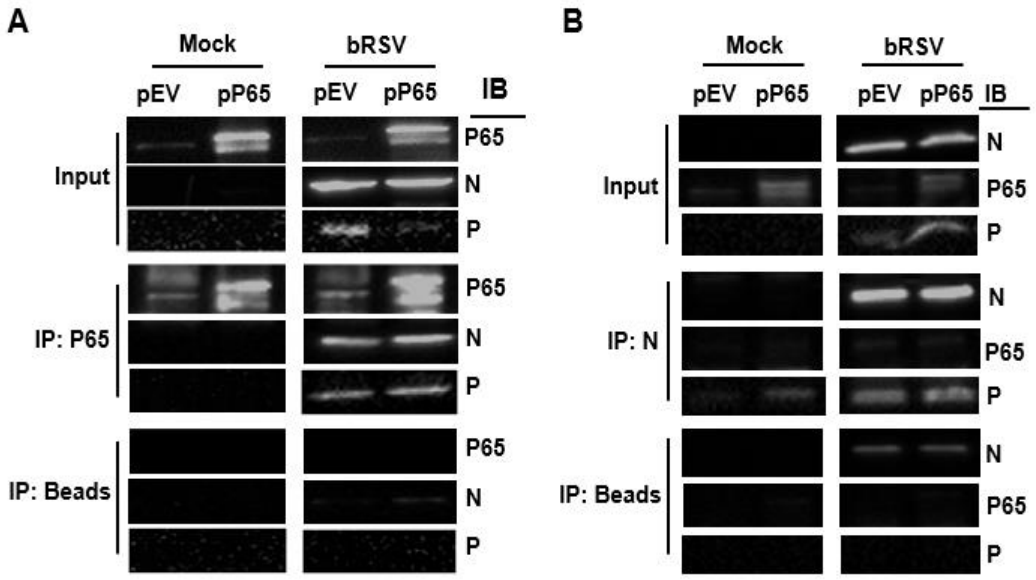

Figure 4.12 P65 interacts with RSV N and P in a co-immunoprecipitation assay. 293T cells were transfected with plasmids expressing NF-κB p65 (pP65) or empty vector (pEV) and 6 h later infected with bRSV at MOI 1. At 24 h p.i., cell lysates were immunoprecipitated (IP) with **(A)** anti-p65 antibody, **(B)** RSV N antibody or beads alone as a control. Pull-downs were analysed by SDS-PAGE and immuno-blotting (IB) using anti-p65, anti-N or anti-P antibodies. Data in A is representative of n=2 independent repeats, and n=1 in B.

4.2.7. Co-immunoprecipitation analysis suggests p65-RSV N interaction

As discussed in section 4.2.2, p65 sequestration into IBs was observed at 16 h p.i., a time point at which significant viral proteins were expressed (Fig 4.5 and Fig 4.6). As infection progressed and IBs grew larger, so did the size of the p65 puncta, directly correlating infection with p65 aggregation. In order to define the mechanism of p65 recruitment into, and sequestration within the bRSV IBs, several models were considered: (i) p65 being transported from the cytoplasm into IBs by direct interaction with viral proteins, (ii) p65 non-specifically captured during retrograde transport from the cytoplasm, along the cytoskeleton, into the nucleus; a process that could be facilitated by the perinuclear positioning of the IBs, or (iii) p65 being non-specifically captured by random diffusion, dependent on the physicochemical properties of the phase separated structure and that of the recruited/excluded proteins.

To investigate the first model, I assessed the interaction of p65 with N and P. The focus on these two viral proteins was due to the finding that p65 was also recruited into the pseudo-IBs formed following ectopic N and P co-expression (Fig 4.11). 293T cells were mock-infected or infected with bRSV. At 24 h p.i, endogenous p65 or p65 expressed from a plasmid (pP65), and N protein were immunoprecipitated from cell lysates using an anti-p65 or anti-RSV N antibody, respectively. When these immuno-precipitates were analysed by western blotting, both bRSV N and P were found to co-immunoprecipitate (co-IP) with endogenous or overexpressed p65 in infected cell lysates, providing evidence of direct interactions being maintained post-lysis (Fig 4.12A). Experiments with beads alone did show a small amount of co-IP N protein; however, this was markedly lower than in the p65 antibody experiment, background signal which may be the consequence of the high levels of N protein in infected cells at 24 h p.i. In converse, when N protein was immunoprecipitated from the cell lysates, P co-IP was maintained but there was no significant co-IP of p65 with N protein (Fig 4.12B). One explanation for this discrepancy may be anti-N antibody interference with the interaction. However, the recruitment of p65 to IBs, if viral protein-dependent, may be due to indirect interactions with the N and/or P proteins. Since RSV N and P are known to interact, yet the IB does not form without both proteins being expressed together, more detailed characterisation of this interaction is required to define the true binding partner.

4.2.8. Disruption of the cytoskeleton does not inhibit IB formation or p65 recruitment, but the microtubule network is required for intracellular movement of viral components and efficient replication

To successfully complete their lifecycle, viruses rely on a functional transport system to move viral components, such as, RNP and newly synthesised viral genome and proteins around the cell, between the entry, replication, and assembly sites. For viruses that form perinuclear replication complexes, these retrograde and anterograde movements are facilitated by the microtubule network and microtubule motor proteins, such as, dynein (Ploubidou and Way, 2001). In order to investigate the role of the cytoskeleton in viral-IB formation and non-specific p65 sequestration, infected cells were examined in the presence of inhibitors that disrupt the cellular transport system. Vero cells were infected with bRSV at MOI 1. Inoculum was removed 2 h later and replaced with media containing 10 ug/ml nocodazole (NCZ; prevents microtubule assembly), 2 uM taxol (prevents microtubule depolymerisation) or 2.5 uM cytochalasin B (CytoB; inhibits actin polymerisation) and then incubated for another 24 h. Cells were then fixed and co-immunostained for RSV N and α-tubulin/actin or RSV F and p65. N-positive IBs were seen in both untreated and in cells treated with the different cytoskeleton inhibitors, demonstrating that bRSV IB formation, like rabies virus IBs (Nikolic et al., 2017, Oksayan et al., 2012), is not dependent on the cytoskeleton (Fig 4.13A and B). As previously observed (Fig 4.6B), the dominant bRSV IBs were localised towards the centre of the cell, next to the nucleus, and there were no significant differences observed in their size in all cases (Fig 4.13C).

This is contrary to the effect of NCZ observed on rabies virus IB morphogenesis – producing one/two IBs that are significantly larger than that produced in control cells (Lahaye et al., 2009, Nikolic et al., 2017). Common to both viruses, the smaller IBs that arise later in infection, at 24 h p.i., can be seen in all cells, except in the presence of NCZ when microtubules are depolymerised. Furthermore, when microtubule depolymerisation was inhibited by taxol treatment, the number of IBs per cell significantly increased from an average of five in control cells to fifteen (Fig 4.13D), indicating the importance of the microtubule network on IB dynamics. However, taxol treatment caused nuclear fragmentation possibly due to the induction of apoptosis.

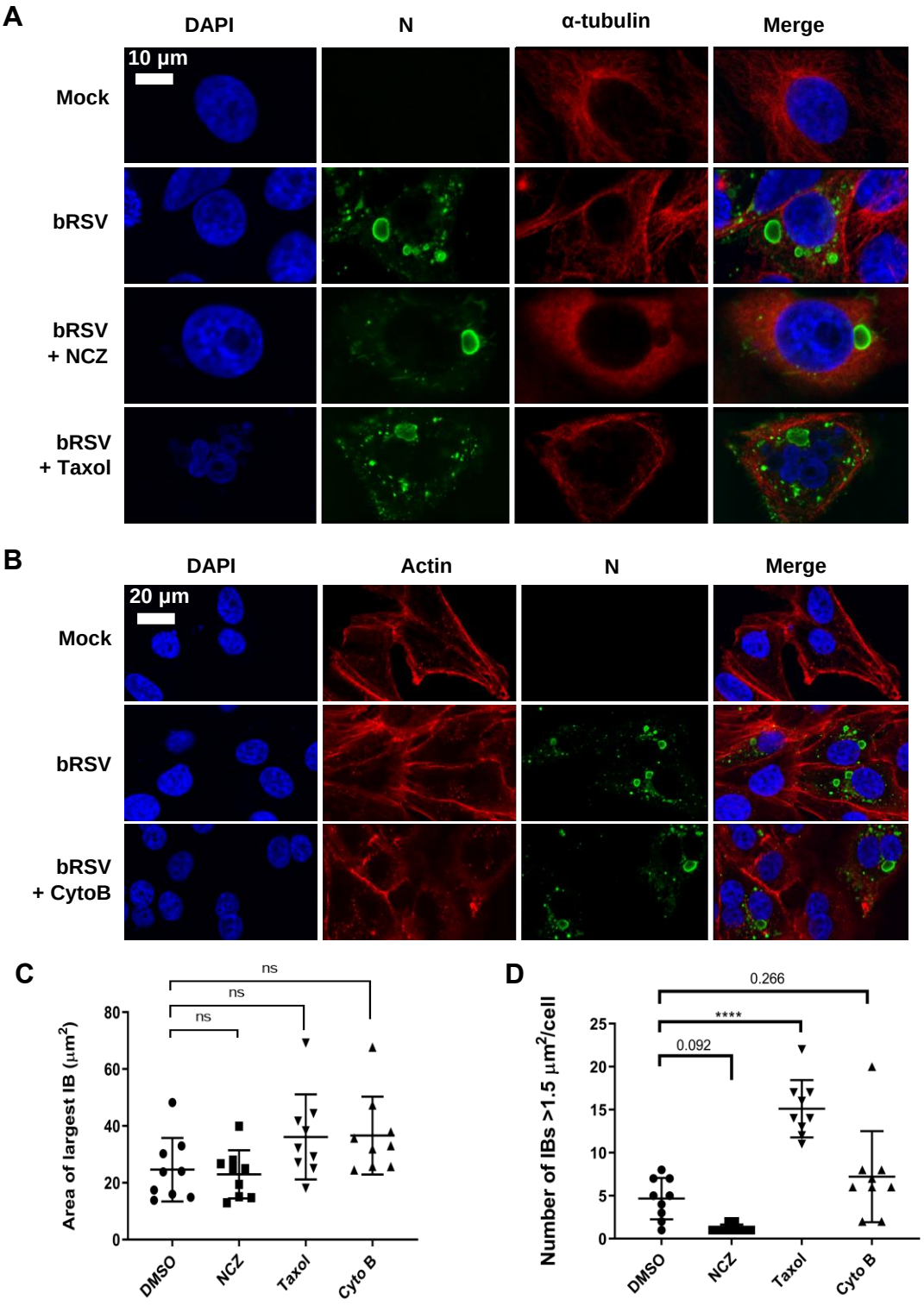

Figure 4.13 bRSV IB dynamics, but not its formation is dependent on the microtubule network. Vero cells were mock infected or infected with bRSV at an MOI of 1. 2 h later, inoculum was removed, and cells incubated with media containing vehicle or **(A)** 10 ug/ml nocodazole, 2 uM taxol, or **(B)** 2.5 uM cytochalasin B for another 24 h. Cells were then fixed and immuno-stained with anti RSV N (green) and anti-α tubulin antibodies (red) and actin stained with phalloidin. Cell nuclei were stained with DAPI (blue) and images obtained as already described. (**C)** Cross-sectional area of the largest IB in nine selected cells. **(D)** Total number of IBs larger than 1.5 µm². Statistical significance determined by ANOVA as described in the methods, n.s: non-significnt; ****p<0.0001. Data is representative of n=2 independent repeats.

CytoB which disrupts actin filaments did not significantly affect the size or number of IBs. This data demonstrates that the dominant IB is possibly established by the RNP of the incoming virus in a process independent of the cellular cytoskeleton. As infection progresses, the smaller ones either fragment from the main IB growing larger elsewhere in the cell, or form from nascent viral material with the ability to fuse into larger bodies, both processes depending on the microtubule network. Consistent with the latter hypotheses, Nikolic *et al*., used live cell imaging to show that rabies virus RNPs are ejected from the main IB and transported along the microtubule network, giving rise to smaller IBs – in a process inhibited by NCZ treatment (Nikolic et al., 2017).

I also found that disruption of the microtubule network did not affect p65 recruitment into the IB but altered the transportation of RSV F protein into virus filaments in the plasma membrane (Fig 4.14A). Microtubule depolymerisation increased the proportion of F protein in the cytoplasm, most likely associated with ER membranes (Fig 4.14B). Line of interest plots also show an uncharacteristic clustering of F at the IB periphery further indicating a breakdown in the anterograde transport system. Since my findings show that microtubule-dependent anterograde transport has little effect on IB formation and p65 recruitment, further investigations are required to assess whether p65 is directly captured by viral proteins into IBs or localised by random diffusion. The effect of these changes on virus replication was then analysed in Vero and MDBK cells. Cells were infected with recombinant bRSV expressing green fluorescent protein (GFP) as a separate transcriptional unit (bRSV-GFP) and virus replication monitored by quantifying fluorescence on an Incucyte real-time live-cell imager (Fig 4.15). When virus replication was compared to untreated cells, both microtubule inhibitors significantly reduced virus replication, particularly in MDBK cells, whereas actin inhibition had a limited effect. Taken together, the data shows that neither RSV IB formation nor its p65 status is dependent on the actin/microtubule network. However, microtubule architecture, but not actin, is important for the maturation of RSV IBs and the progression of infection.

4.2.9. The sequestration of the NF-κB subunit p65 to cytoplasmic IBs is a conserved mechanism of orthopneumovirus immunomodulation

Having established structural and functional similarity between bRSV and hRSV IBs,

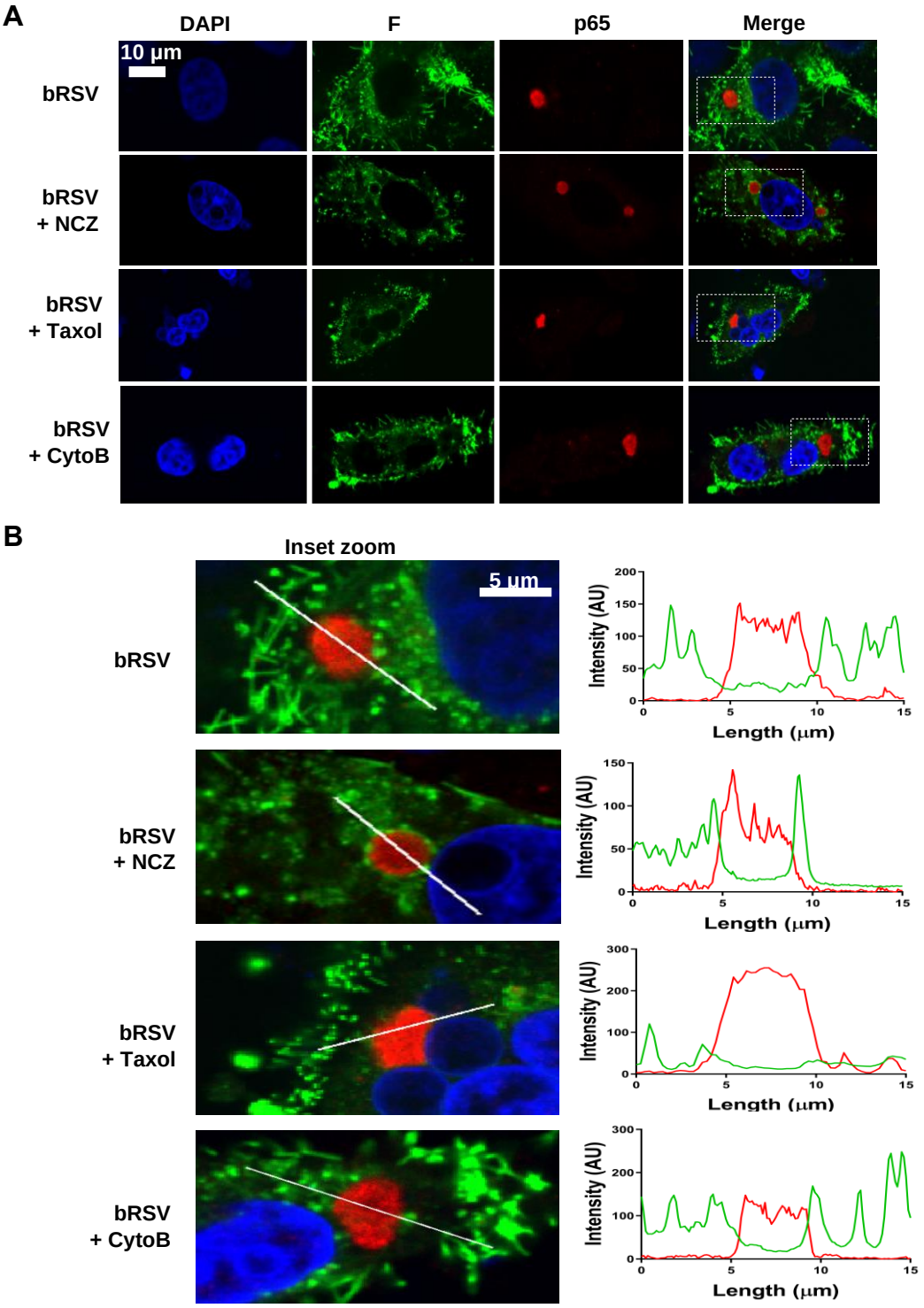

Figure 4.14 The microtubule network is not essential for p65 IB localization but plays a role in RSV F transport to the plasma membrane. (A) Vero cells were mock infected or infected with bRSV at an MOI of 1. 2 h later, inoculum was removed, and cells incubated with media containing vehicle, 10 ug/ml nocodazole, 2 uM taxol, or 2.5 uM cytochalasin B for another 24 h. Cells were then fixed and immuno-stained with anti RSV F (green) and anti-p65 antibodies (red). Cell nuclei were stained with DAPI (blue) and images obtained as already described. **(B)** Magnification of boxed areas in A and line of interest plots. Images are representative of data from a single experiment

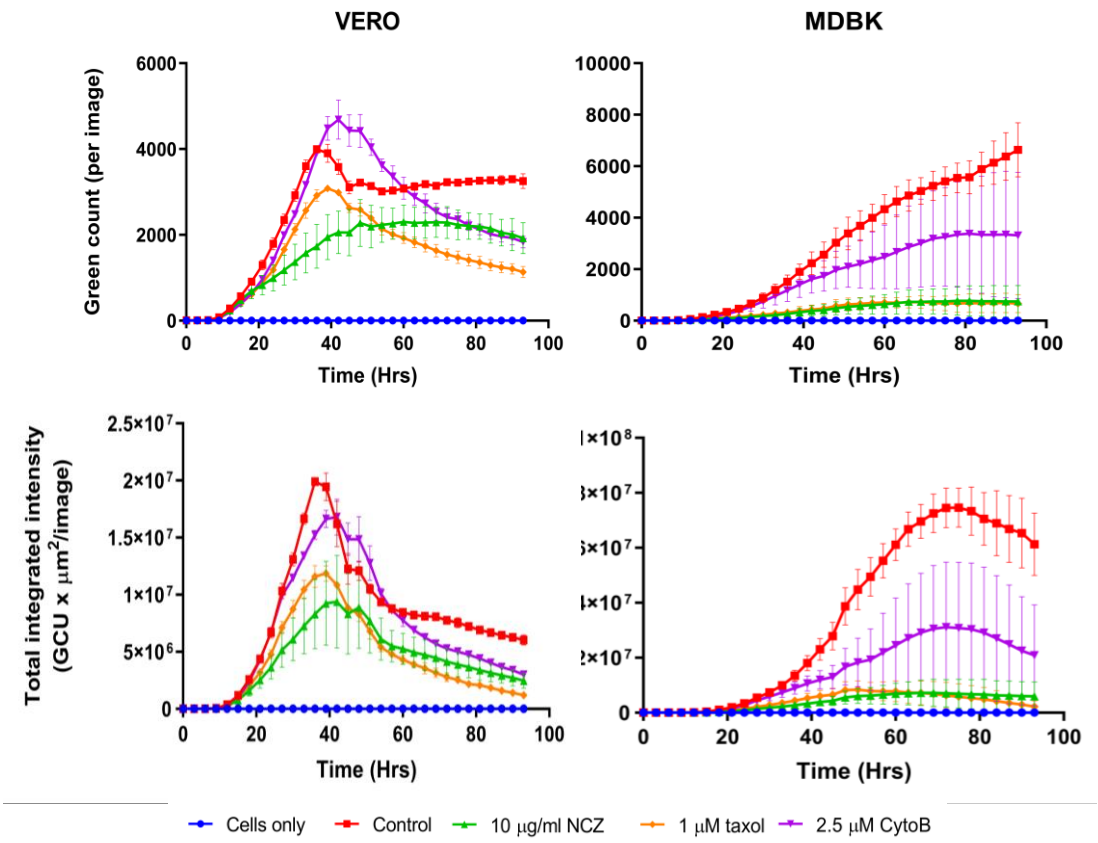

Figure 4.15 Microtubule disruption limits bRSV replication. Vero and MDBK cells were mock infected or infected with bRSV-GFP at an MOI of 1. 2 h later, inoculum was removed, and cells incubated with media containing vehicle, 10 ug/ml nocodazole, 2 uM taxol, or 2.5 uM cytochalasin B and virus replication monitored over 96 h with GFP as a marker using an Incucyte imager. Graphs show means ± SD of triplicate infections from one experiment.

I finally examined the regulation and sub-cellular localisation of the NF-κB subunit p65 in hRSV infected cells. Beginning with the NF-κB luciferase reporter assay, I uncovered a pattern of signalling inhibition similar to bRSV. 293T cells were infected with hRSV at an MOI of 1 and then transfected with the NF-κB reporter at 6 h p.i. 18 h later, cells were left untreated or stimulated with hTNFα for another 16 h before being lysed and analysed for NF-κB transactivation. Infection with hRSV in the presence of the NF-κB reporter did not lead to robust activation when compared to mock infected cells, highlighting a lack of activation of this pathway in infected cells (Fig 4.16A, black bars). Again, similar to bRSV, infected 293T cells (24 h with hRSV) which were stimulated for 16h with hTNFα induced significantly less NF-κB transactivation, when compared to equivalently treated mock-infected cells (Fig 4.16, grey bars). This correlated well with an examination, by IF, of hRSV replication in Vero cells, with and without hTNFα treatment, where again I did not observe significant levels of p65 nuclear translocation (Fig 4.16B). Indeed, as observed in bRSV infected cells, p65 was recruited into intra-cytoplasmic puncta. These puncta were subsequently shown to also be synonymous with viral IBs (Fig 4.17) in a set of experiments which also confirmed that IB formation and the recruitment of p65 is host cell independent. bRSV or hRSV infected MDBK (bovine) or Hep2 (human) cells demonstrated the presence of p65-containing IBs in all scenarios, highlighting that the mechanisms underpinning RSV IB formation, and the sequestration of p65 to these bodies, are likely highly conserved. This examination of host-range specificity was concluded with a more physiologically relevant model of the human bronchial epithelium, BEAS-2B cells. These are derived from normal human tissue taken following autopsy of a non-cancerous individual, identifying again the formation of IBs and sequestration of p65, regardless of RSV species (Fig 4.17). Finally, I confirmed that IB-like structures formed by ectopic hRSV N and P co-expression recruited p65 to their core (Fig 4.18). Taken together, these data indicate that the formation of IBs during viral replication, together with the sequestration of the transcription factor NF-κB subunit p65 to these bodies, is a common feature of orthopneumoviruses.

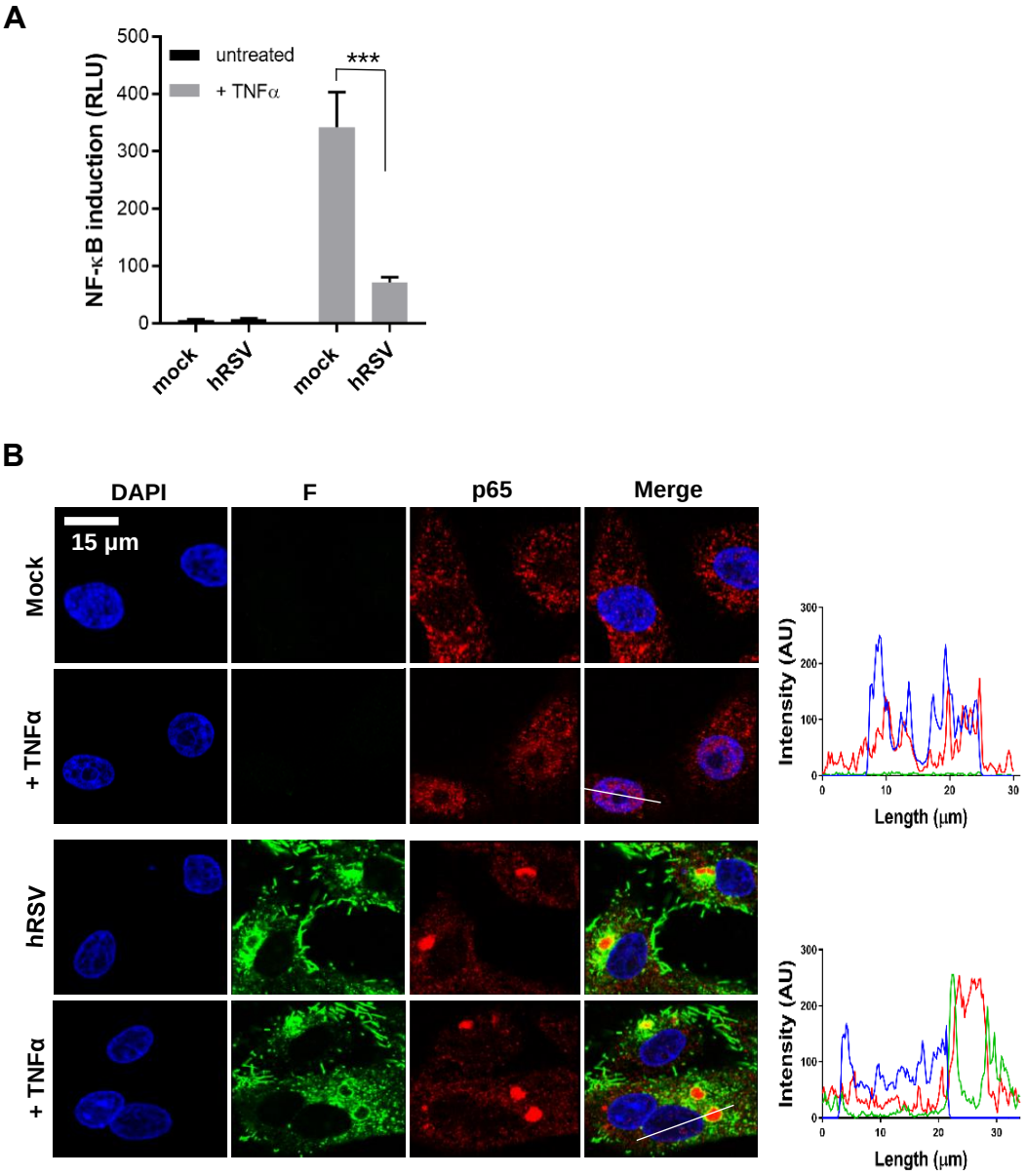

Figure 4.16 hRSV IBs antagonise NF-κB p65 activation similarly to bRSV. (A) 293T cells were mock infected or infected with hRSV at an MOI of 1. At 6 h p.i., cells were transfected with 100 ng NF-κB FLuc reporter and 10 ng TK-renilla luciferase and incubated at 37ºC. At 18 h p.t., cells were left untreated or stimulated for 16 h with 20 ng/ml hTNFα. Cells were then lysed and analysed for firefly and renilla luciferase activities. Graph depicts means ± SD of three replicates from the same experiment. Statistical significance determined by ANOVA as described in the methods, ****p<0.0001. **(B)** Vero cells mock infected or infected with hRSV at an MOI of 1 for 24 h were left untreated or stimulated with 20 ng/ml hTNFα for 30 mins. Cells were then fixed and immuno-stained with anti-RSV F (green) or anti-NF-κB p65 (red) antibodies. Cell nuclei were stained with DAPI (blue) and images obtained using a Leica TCS SP5 confocal microscope. Graphs show line fluorescent intensity profile along the indicated white lines. Images are representative of data from n=2 independent experiments.

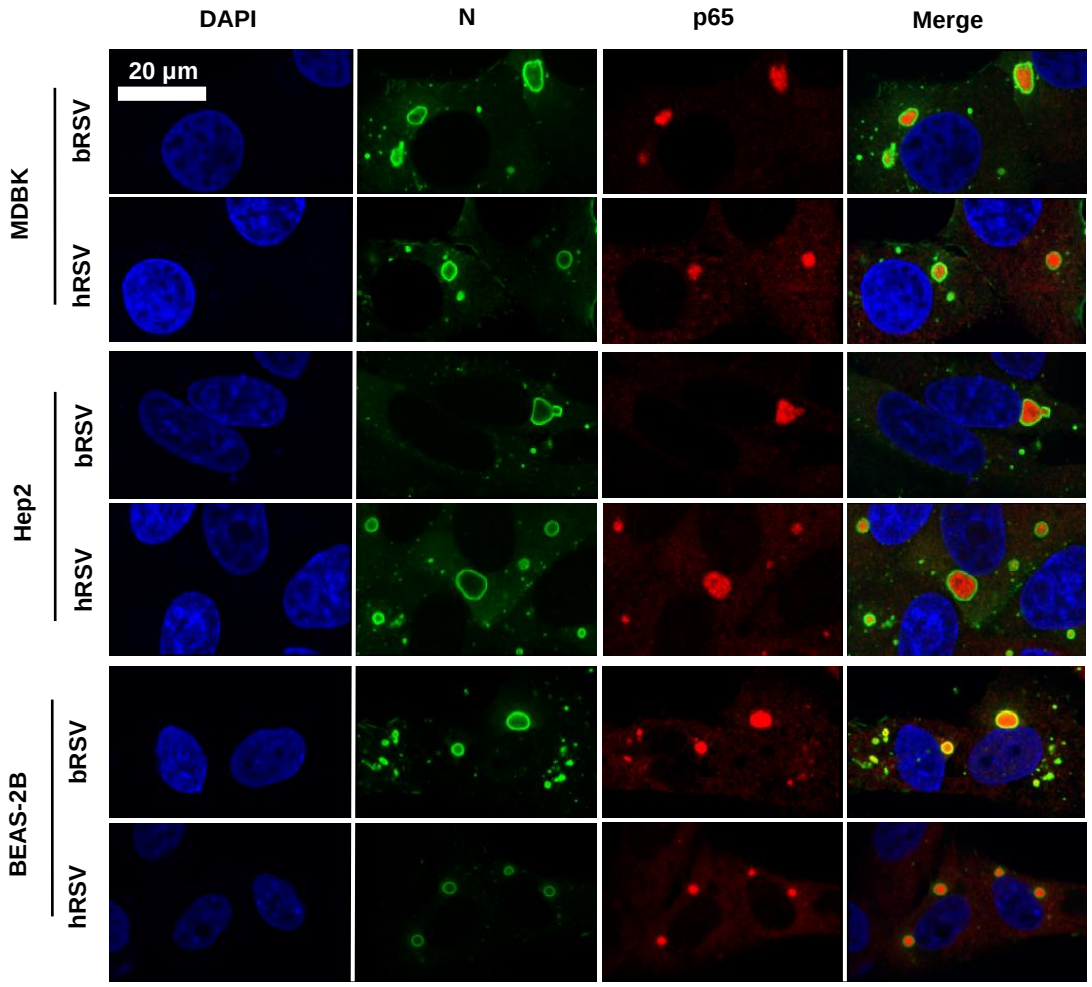

Figure 4.17 The sequestration of the NF-κB subunit p65 to cytoplasmic IBs is a conserved mechanism of orthopneumovirus immunomodulation. (A) MDBK, Hep2 and BEAS-2B cells were infected with b/hRSV for 24 hrs, fixed and immuno-stained for RSV N (green) or NF-κB p65 (red). Cell nuclei were stained with DAPI (blue), and confocal analysis performed as already described. Images are representative of data from a single experiment

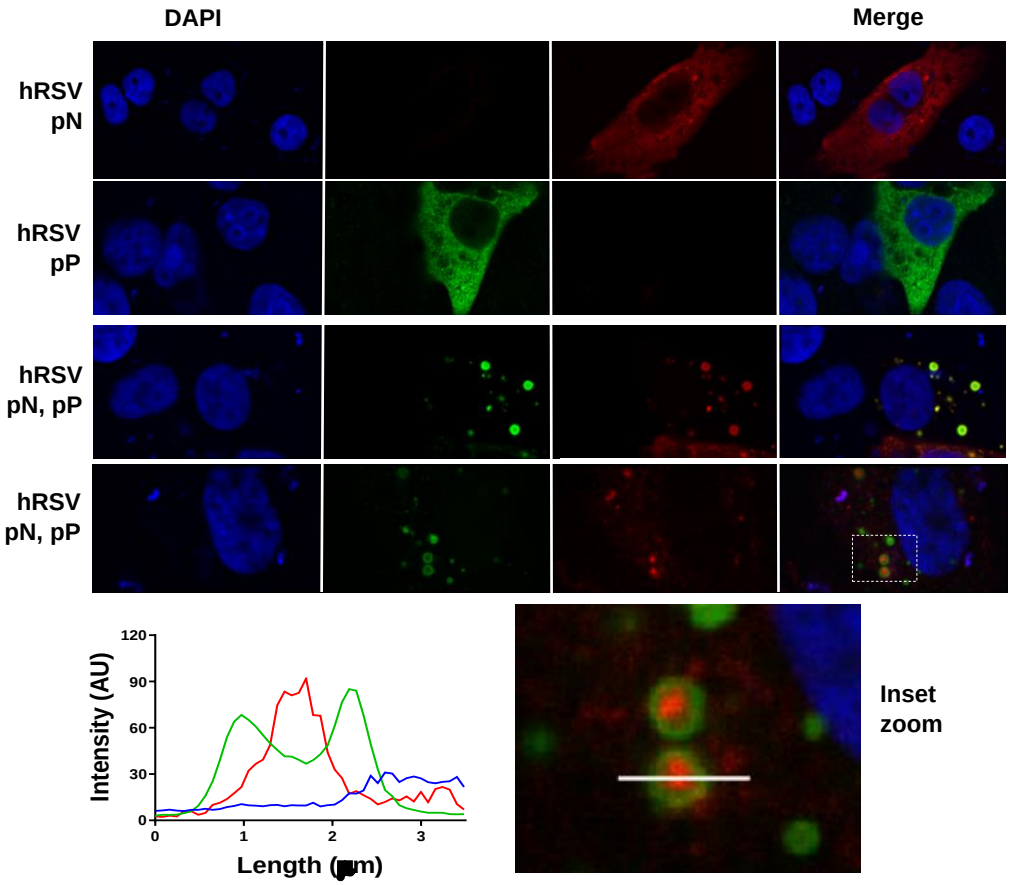

Figure 4.18 Co-expression of hRSV N and P proteins induces the formation of IB-like structures which can sequester p65. Vero cells were co-transfected with equimolar concentrations of plasmids expressing hRSV N (pN) and/or P (pP) proteins as indicated. Following 24 h incubation, cells were fixed and stained with anti-RSV N (green/red) and anti-RSV P (green) or anti-NF-κB p65 (red) antibodies. Cell nuclei were stained with DAPI (blue) and confocal analysis performed. The bottom panels show a higher magnification of the boxed area and a graph with the fluorescent intensity profiles along the indicated white line. Images are representative of data from n=2 independent repeats.

4.3. Discussion

The NF-κB family of transcription factors are involved in several cellular responses including inflammation, stress responses, cellular growth, *etc*., and play an important role in the innate immune response to infection (Mitchell et al., 2016). Recognition of viral pathogen-associated molecular patterns (PAMPs) by RIG-I, MDA5 or NOD2 can lead to activation of transcription factors including NF-κB through the IKK complex or IRFs through TBK-1/IKKε (Hemmi et al., 2004, Mitchell et al., 2016, Sun and Lopez, 2016, Sedeyn et al., 2019). These transcription factors elicit responses that lead to the clearance of RSV infection and establishment of a memory response (Guzman and Taylor, 2015, Sun and Lopez, 2016). However, RSV generates a short-lived immune response *in vivo* which might be a consequence of various immune-evasion strategies involving the SH, NS1, NS2 and G proteins (Kotelkin et al., 2006, Ling et al., 2009, Lo et al., 2005, Taylor et al., 2014, Arnold et al., 2004, Tripp et al., 1999, Sedeyn et al., 2019). As a key innate immune pathway, NF-κB signalling is often a target for viral antagonism (Deng et al., 2018); however, to date, RSV modulation of its activation has remained less well defined. To address this, we monitored NF-κB p65 activation in RSV-infected cells at multiple steps in the signalling pathway, namely, IκBα degradation, p65 phosphorylation (at Ser536), p65 nuclear translocation, and more broadly NF-κB transactivation. We present a novel mechanism of immune evasion wherein RSV infection results in the sequestration of the NF-κB subunit p65 into viral inclusion bodies (Fig 4.6 and Fig 4.16). This is a process independent of the known RSV immunomodulatory proteins – NS1, NS2, and SH (Fig 4.10B) – and was confirmed in BEAS-2B bronchial epithelial cells (Fig 4.17); a more physiologically relevant model of infection. Furthermore, the phenomenon was maintained regardless of the host cell origin implying it is a conserved mechanism of immune regulation. I also demonstrate that as a result, activation of NF-κB subunit p65 is suppressed in infected cells, even with exogenous TNF-α stimulation (Fig 4.1, Fig 4.2, and Fig 4.16). In contrast, there was no aggregation of IRF3, and nuclear translocation of this transcription factor was successfully stimulated by both RSV infection and agonist treatment.

Although small IBs (≤2.5 μm2) were observed as early as 6 h p.i., they did not colocalize with detectable levels of p65 (Fig 4.6). However, this may reflect a

technical limitation of our IF or alternatively that IBs need to grow in size before they can begin to sequester p65. It is currently not clear what proportion of the IB-sequestered p65 is IκBα associated, the elucidation of which might explain the partial protection of IκBα from degradation seen following TNF-α treatment (Fig 4.1A, mock versus bRSV +TNF-α). The phosphorylation status of the sequestered p65 is also not clear, neither is its accessibility to cellular kinases. Thus, although IBs are fluid and allow exchange with the cytoplasm, the directionality of p65 movement remains to be elucidated. Interestingly, the lack of p65 activation prior to IB formation and p65 aggregation, highlights that RSV may employ additional mechanisms for NF-κB inhibition which remain uncharacterized. However, other groups have reported more robust activation of NF-κB in response to RSV infection (Bitko et al., 2004, Carpenter et al., 2002, Yoboua et al., 2010) which could indicate that the cell line, viral strain and level of inoculum purity play a role in RSV-mediated NF-κB activation. This being said, the sequestration of p65 appears to be an orthopneumovirus-conserved strategy active in physiologically relevant cells, such as BEAS-2B cells. This mechanism of innate immune antagonism is also emerging as a common strategy utilized by RSV and possibly other viruses that induce IB formation. Recent data shows the recruitment of a range of cellular proteins into RSV IBs, most of which are involved in the antiviral response. MAVS and MDA5 were both found to be recruited into RSV IBs as a mechanism of suppressing IFN signalling (Lifland et al., 2012). Similarly, p38 MAPK and OGT sequestration into RSV IBs suppressed MAPK-activated protein kinase 2 signalling and stress granule formation, respectively, enhancing virus replication (Fricke et al., 2013). HuR, another component of stress granules, heat shock protein Hsp70 and actin, were also observed within RSV IBs (Lindquist et al., 2010, Brown et al., 2005). It is likely other host cell proteins that are yet to be identified also localise in RSV IBs. However, whether the closely related HMPV or other viruses such as measles, Ebola, Nipah, or rabies that also induce IB formation, adopt similar mechanisms of immunomodulation remains to be determined.

The insensitivity of NF-κB signalling to exogenous TNFα stimulation suggests the modest activation seen in response to RSV infection is a consequence of the observed p65 sequestration. However, the roles of the known immunomodulators – SH, NS1, and NS2 – cannot be excluded at this time since these were previously shown to target

NF-κB. The SH proteins of bRSV and hRSV contribute to virus pathogenesis by inhibiting NF-κB responses (Fuentes et al., 2007, Russell et al., 2018, Taylor et al., 2014, Wilson et al., 2006). This was shown to involve suppression of p65 phosphorylation and IκBα degradation using bRSV SH, although the exact mechanism is still unclear. However, the observation of p65 puncta in bRSV ΔSH infected cells that were also insensitive to TNFα stimulation (Fig 3.9), shows that this accessory protein does not play a central role in this mechanism of p65 antagonism. On the other hand, NS2, and to a lesser extent NS1, were shown to enhance nuclear translocation and activation of NF-κB (Spann et al., 2005). Although I observed formation of p65 puncta in viruses lacking expression of these proteins (Fig 4.10), their influence on TNFα-mediated p65 activation was not assessed here. Considering the observations reported by Spann *et al*. (Spann et al., 2005), I did not find that infection with the NS deletion mutants enhanced p65 nuclear translocation when compared to wild type bRSV infected cells. This may however represent mechanistic differences between the NS proteins of hRSV and bRSV.

Unlike effects observed on NF-κB, there is strong evidence that the targeting/downregulation of key signalling molecules by the NS proteins of both bRSV and hRSV suppresses IRF3 activation, subsequent type I and III interferon induction and also interferon signalling (Sedeyn et al., 2019). Interaction of NS1 with MAVS was shown to inhibit phosphorylation and activation of IRF3 by competitively blocking MAVS activation by RIG-I (Boyapalle et al., 2012). This mechanism of inhibition may also be elicited via NS2, through direct binding to RIG-I (Ling et al., 2009). Several other studies have also shown that the NS1 and NS2 proteins of these viruses target multiple levels in interferon induction and signalling to suppress the antiviral response (Spann et al., 2004, Goswami et al., 2013, Swedan et al., 2009, Spann et al., 2005, Ren et al., 2011). Therefore, it was surprising to see activation of IRF3 using wild type virus encoding both NS1 and NS2 proteins (Fig 4.2). However, most of the studies showing inhibition by these proteins use NS deletion mutants, observing enhanced responses in their absence. Thus, the activation observed here does not indicate absence of inhibitory responses from these proteins. Assessment of IRF3 transcriptional responses, for example, by reporter assay or gene expression analysis might provide a more definitive approach to examine activation compared to nuclear translocation. The effect of the NS proteins may also be assessed in this way

by comparing wild type to deletion mutants or by using ectopic expression. Although IRF and NF-κB are activated downstream of similar pathways, they primarily regulate distinct responses; IRF mainly regulates interferon induction, whereas NF-κB is mostly involved in proinflammatory cytokine expression. Importantly, crosstalk between the IRF and NF-κB pathways implies that members of one pathway may regulate the other (Iwanaszko and Kimmel, 2015). Therefore, analysis of transcriptional activity may also help to examine the effect of p65's sequestration into IBs on IRF3 transactivation. The data presented in Fig 4.2 shows specific targeting of NF-κB subunit p65, similar to the mechanism by which IRF3 is targeted by NS1 (Ren et al., 2011), albeit via different mechanisms. Thus, this shows that RSV encodes multiple mechanisms to suppress antiviral responses induced in the early stages of virus infection.

Formation of cytoplasmic IBs is a characteristic feature of infection with several negative strand RNA viruses. Showing similarities to membrane-less cellular organelles, IBs are essentially biomolecular condensates thought to form by LLPS. These structures have liquid-like properties with a spherical shape induced by surface tension. They are also highly fluid and can undergo fusion and fission (Gomes and Shorter, 2019, McSwiggen et al., 2019, Alberti et al., 2019). Based on these criteria, we postulate that bRSV IBs have properties of liquid compartments similar to IBs induced in the cytoplasm of hRSV (Galloux et al., 2020a, Rincheval et al., 2017), HMPV (Cifuentes-Munoz et al., 2017), MeV (Zhou et al., 2019), VSV (Heinrich et al., 2018) and rabies virus (Nikolic et al., 2017) infected cells and several other mononegaviruses. Electron micrograph analysis of bRSV infected cells showed greater electron density in the IBs than in the cytoplasm (Fig 4.7 and Fig 4.8), which is a characteristic of biomolecular condensates. Importantly, we also observed that they are membrane-less and mostly spherical, although larger IBs tend to have a more pleomorphic structure. In order to definitively identify the bRSV IBs as liquid organelles, fluorescence recovery after photobleaching (FRAP) experiments could be performed to assess the acquisition of tagged N or P over time. In addition, the fusion and fission of these organelles could be monitored in real time. However, the dissolution of the smaller IBs in response to hypotonic shock still provides strong evidence for the phase-separated nature of these structures (Fig 4.9A). The stability of larger IBs to extended periods of hypotonic shock was surprising – a finding we

attribute to the larger IBs gaining hydrogel- or even aggregate-like status (Banani et al., 2017). This might also explain the loss of their spherical nature, as the biophysical constraints on this organelle might be relaxed by this transition.

We observed that formation of IBs in infected cells was initiated with aggregation of the N protein (at 6 h p.i.), as soon as sufficient viral proteins were expressed (Fig 4.6). As the infection proceeded, we observed growth of the IBs in both number and size. As a minimum, the N and P proteins are essential for the formation of 'pseudo-IBs' (Fig 4.11 and Fig 4.18). Ectopic expression of these proteins resulted in the formation of IB-like structures (pseudo-IBs) as has been reported for HMPV (Derdowski et al., 2008), rabies (Nikolic et al., 2017) and measles (Zhou et al., 2019) viruses in cells, and more recently for hRSV both in cells and *in vitro* (Galloux et al., 2020a). Our pseudo-IBs were also mostly spherical and at 24 h post-transfection, measured up to 6.9 μm^2, which is considerably less than that of the conventional IBs observed in infected cells. We hypothesize that both pseudo-IBs and viral IBs form by biomolecular condensation but that their maturation into larger structures is dependent on other factors present only in infected cells. Interestingly, these data and our CLEM analysis confirmed previous IF data from the field that the IB boundary is surrounded by N protein. However, Lifland *et al.* suggested that this is an artefact of disrupted antibody epitope accessibility to N since they observed even distribution of GFP-tagged N protein throughout the IB (Lifland et al., 2012); however, we would only note that we used an antibody developed in-house for this staining. In addition, Galloux et al., observed concentration of mCherry tagged N on the periphery of IBs formed in cells, similar to our observations in Fig 4.11 and Fig 4.18, and in pseudo-IBs reconstituted *in vitro* (Galloux et al., 2020a), questioning the artefactual nature of this organisation. The exact mechanism of viral IB formation is unknown but the process of phase separation in general is thought to be initiated by scaffold proteins that mostly contain multiple folded domains, IDRs, and RNA-binding domains (Banani et al., 2017, Kato et al., 2012, Lin et al., 2015). These enable the proteins to form multivalent (macromolecule-macromolecule) interactions of low affinity resulting in phase-separation and subsequent recruitment of client molecules. Indeed, RSV N and P proteins encode "scaffold" characteristics – an RNA-binding domain in N (Ruigrok and Crépin, 2010), IDRs in N and P (Whelan et al., 2016), and the ability of both proteins to oligomerise (Esneau et al., 2019, Galloux et al., 2012, Galloux et

al., 2015) – that could initiate IB nucleation when present in high concentration. Using mutagenesis studies, Galloux *et al.* found that the central oligomerisation and C-terminal IDR of P, and the P and RNA-binding domains of N are crucial for IB formation (Galloux et al., 2020a, Galloux et al., 2012).

Although the N and P proteins are permanent components of IBs, these structures are fluid and undergo unrestricted exchange of certain macromolecules with the cytoplasm. Using fluorescence tracking, previous studies have demonstrated movement of viral proteins and RNA between the IB and the dispersed cytoplasm, as well as fusion and fission of distinct IBs (Rincheval et al., 2017, Zhou et al., 2019, Heinrich et al., 2018, Nikolic et al., 2017). Banani et al., also noted that the composition of biomolecular condensates is dynamically controlled, with constitutive and transient components that are both selective (Banani et al., 2017). We propose that, once nucleated, recruitment of "clients" into RSV IBs may involve low-affinity interactions with N and/or P and that maintenance within the IB is enhanced by the same physicochemical properties which induce LLPS, such as the presence of IDRS and RNA-binding domains. However, the observation that the pseudo-IBs could also recruit p65 suggested a direct interaction between p65 and RSV N or P, and we confirmed N-p65 interaction by co-IP (Fig 4.12). Interestingly, our IF data were somewhat contradictory, with the staining patterns and line intensity profiles showing p65 concentrated in the middle of IBs with N and P at the periphery, separating the IB contents from the cytoplasm. It is possible that during sequestration, exchange of biomolecules such as p65 across the boundary requires transient N interactions, or with other IB-localised viral proteins in other cases. Evidently, the RSV P protein has been shown to bind and recruit M2-1 to IBs (Richard et al., 2018). P contains a high degree of intrinsic disorder and also M2-1, to a certain extent (Whelan et al., 2016), however the recruitment was shown to involve direct interaction. Lifland et al. also suggested that MAVS and MDA5 are recruited into IBs by interacting with N and P in a macromolecular complex (Lifland et al., 2012). Similarly, host cell Hsp70 was recruited into rabies virus Negri bodies by directly interacting with N (Lahaye et al., 2012, Lahaye et al., 2009). Therefore, recruitment of clients into IBs may be facilitated by IDRs that enable N and P proteins to form multiple interactions.

Although further work is required to identify the exact mechanism of IB population and the contributing factors, we postulate that the RNA-binding properties of these proteins may also be an important factor. Of note, several cellular proteins shown to localise in RSV IBs contain RNA-binding domains (Kato et al., 2012) including MDA5 (Lifland et al., 2012), HuR (Lindquist et al., 2010), PABP and eIF4G (Rincheval et al., 2017). Thus, recognition of viral RNA by RNA-binding domains may be a mechanism by which particular cellular proteins are enriched in IBs (Banani et al., 2017). This is a mechanism used to localise proteins to stress granules (SGs) generated in response to multiple stress stimuli to transiently stall translation (Onomoto et al., 2014). Although we have shown that IBs are distinct from canonical SGs, they share similar characteristics including liquid-like properties, absence of a membrane boundary and are both formed by phase separation. Interestingly, PABP and eIF4G are also SG components (Onomoto et al., 2014). Thus, in addition to localisation by direct interaction with viral proteins, host cell proteins may also be recruited by binding to viral RNA and intermediates of replication. As the site of viral RNA synthesis, IBs are enriched in both genomic and mRNA. Using Herpes Simplex Virus infection as a model, McSwiggen et al., showed that RNA polymerase II and other cellular proteins are recruited into and retained within phase-separated replication complexes by binding to viral DNA via their DNA-binding domains (McSwiggen et al., 2019). It is therefore necessary to assess RNA-binding as a possible mechanism of recruitment and whether any viral RNA-binding protein can be recruited into viral IBs in this way.

It remains to be determined if p65 is actively recruited to IBs by viral proteins or RNA or if its sequestration is a result of the IB's position in the cell and that it captures p65 by an indirect mechanism, perhaps involving trafficking. We observed that IB formation and p65 recruitment occurred independent of microtubule and actin filament networks. However, the higher intensity of p65 in IBs formed in the presence of taxol, which prevents microtubule depolymerisation (Fig 4.14), suggests there is some level of transport along microtubules. In addition, it appears the presence of an intact microtubule network supports virus replication by contributing towards IB maturation and viral protein and RNP trafficking around the cell (Fig 4.13, Fig 4.14, and Fig 4.15). Previously, the microtubule network was shown to facilitate the transport of vRNPs from MuV IBs to the cell surface, enhancing virus production (Katoh et al., 2015b).

Nikolic *et al.* also observed that microtubules had a similar role in the formation and evolution of rabies virus Negri bodies and vRNP transport (Nikolic et al., 2017). For some viruses, vRNP transport may be actin-dependent (Schudt et al., 2013, Schudt et al., 2015), not microtubule. Therefore, in addition to interrogating p65 and N/P interaction, real time fluorescence tracking could be carried out to assess the speed of p65 sequestration in the presence of microtubule, motor protein or other inhibitors of cellular transport. Both investigations could be carried out with wild type and truncated versions of the protein to define the parameters of interaction and sequestration. This will provide better understanding of the process by which viral IBs, and more broadly biomolecular condensates are populated.

Ultrastructural analysis shows significant modification of cellular organisation during RSV infection. Sub-cellular structures, such as the ER (Fig 4.7), microtubules and F-actin were spatially excluded from within IBs (Fig 4.13) but mitochondria which are normally found throughout the cell, were mostly found surrounding the IBs during infection (Fig 4.7). This was also previously observed in hRSV infected cells (Lifland et al., 2012, Hu et al., 2017) and suggest the maintenance of these structures may require energy since mitochondria are central to ATP production. Mitochondrial redistribution around IBs was microtubule/dynein-dependent and shown to gravitate towards the microtubule organising centre (MTOC) (Hu et al., 2019b). Similarly, we also observed that the dominant IBs lie in close proximity to the MTOC although the significance of this observation was unclear at the time. Interestingly, in another study, Hu *et al.* found that the redistribution favours infectious virus production by decreasing mitochondrial respiration and enhancing ROS generation (Hu et al., 2019a). Interestingly, ATP has been shown to play a role in the formation of other biomolecular condensates. In high concentrations, ATP acts as a hydrotrope and inhibits the aggregation of proteins intrinsically prone to LLPS (Patel et al., 2017), such as FUS which contains both an IDR and an RNA-binding domain. This may in part explain why mitochondrial respiration is reduced during infection (that is to allow the formation of RSV IBs) but does not explain the observed condensation around IBs. This subversion is however not unique to RSV. Mitochondrial clustering around virus replication sites has been observed in cells infected with viruses from different families including Enterovirus A71 (Yang et al., 2019), hepatitis B virus (Kim et al., 2007), and hepatitis C virus (Brault et al., 2013), *etc*.

In summary, in this chapter, we show that orthopneumoviruses induce several modifications in the cytoplasm of infected cells including the sequestration of NF-κB subunit p65 into IBs that are also induced during infection. This sequestration impacted activation of NF-κB signalling, which is a significant discovery as inhibition of NF-κB could have a broad impact on the immune response and control of virus infection.

Chapter 5: Functional characterisation of bRSV inclusion bodies

The material presented in this chapter also contributed towards the aforementioned peer-reviewed publication in Journal of Virology:
Jobe F, Simpson J, Hawes P, Guzman E, Bailey D. Respiratory Syncytial Virus Sequesters NF-κB Subunit p65 to Cytoplasmic Inclusion Bodies to Inhibit Innate Immune Signaling. J Virol. 2020 Oct 27;94(22):e01380-20. doi: 10.1128/JVI.01380-20. PMID: 32878896; PMCID: PMC7592213.

5.1. Introduction and aims

Respiratory syncytial viruses, like many negative strand RNA viruses, induce the formation of inclusion bodies/viroplasms in the cytoplasm of infected cells from the early stages of infection. These were previously assumed to be aggregations of excess viral protein, hence the name 'inclusion body', but are now emerging as essential components of the virus lifecycle. Several viral and host proteins concentrate and interact within IBs, carrying out functions that support virus replication and subsequent spread. Studies of the pneumoviruses, RSV (Garcia et al., 1993, Rincheval et al., 2017) and HMPV (Cifuentes-Munoz et al., 2017), and certain paramyxoviruses, MeV (Zhou et al., 2019) and MuV (Katoh et al., 2015a), have shown that these membrane-less organelles contain N, P and L (plus M2-1 in the case of pneumoviruses), viral proteins involved in viral genome replication and mRNA transcription, together with the M protein. These findings, and the presence of nascent viral RNA (genomic, antigenomic and mRNA) within the IBs shows that they are likely replication centres that compartmentalise the processes of virus replication. As a result, not only does this concentration enhance virus replication, it may also protect viral components and replication intermediates from immune recognition. Their role in immunomodulation, sequestering proteins involved in the antiviral response, has recently been reported by us - NF-κB subunit p65 (Jobe et al., 2020) and others - MDA5 and MAVS (Lifland et al., 2012).

Before our publication there was no evidence on the formation of IBs in bRSV infected cells nor, more broadly, any detailed characterisation of their role in the virus life

cycle. In the experiments described in this chapter, I aimed to further characterise the p65 puncta formed in infected cells as IBs, by examining the organisation and function of these structures. I used microscopy techniques to investigate the localisation of bRSV proteins in relation to the IB ultrastructure, as well as the sites of virus genome replication, transcription, and mRNA translation. Considering the close relationship between bRSV and hRSV, and the evolutionary conservation of processes in the lifecycle of the viruses, I hypothesise that bRSV IBs are also replication compartments induced in the cytoplasm of infected cells. Thus, bRSV can be used here as a model virus to functionally characterise orthopneumovirus-induced IBs.

5.2. Results

5.2.1. Cellular localisation of bRSV proteins

P65-positive IBs were only observed in infected cells showing detectable levels of viral (F and N) protein, at 16 h p.i., indicating a correlation between productive infection and IB formation (Fig 4.5 and Fig 4.6). Accordingly, progeny virus was observed a few hours following the establishment of IBs in infected cells, at 24 h p.i. (Fig 3.1). The distribution and sub-cellular localisation of other bRSV proteins were examined in relation to the observed p65 puncta and compared to that observed for the N protein. Vero cells were mock infected or infected with bRSV for 24 h and then fixed for IF analysis. These cells were then co-immunostained for p65 and bRSV N, P, M2-1, M or F proteins. As expected, neither p65 puncta nor bRSV proteins were detected in mock infected cells (Fig 5.1). Also as already described, RSV F did not colocalise with p65 or show evidence of sub-cellular localisation with IB-like structures. In contrast, in infected cells, four of the examined viral proteins (N, P, M2-1 and M) predominately localised to large intracytoplasmic organelles, characteristic of viral inclusion bodies (Fig 5.1; green panels), as already described for N protein in chapter 4. Significantly, the larger N, P, M2-1 or M-positive IBs were, in the majority of cases, also p65 positive (Fig 5.1; red IF panels), as already shown in Fig 4.6D for N-positive IBs. Again, the smaller N-positive IBs were also devoid of p65. The sub-IB localisation of bRSV P was similar to the N protein; concentrating at the periphery of the organelle, forming a boundary that separates it from the cytoplasm (Fig 5.1; zoomed inset and line of interest plots). The significant intra-IB localisation of the M

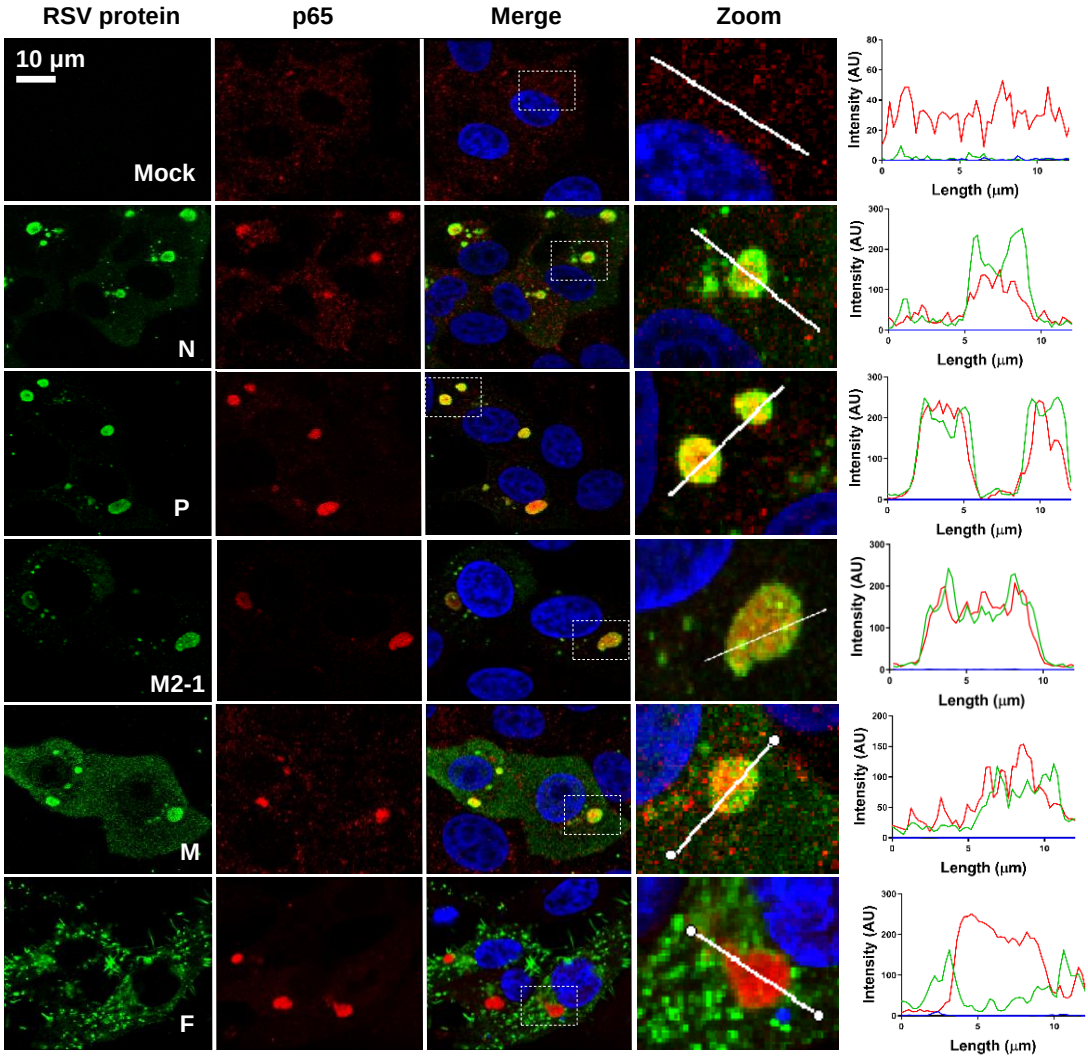

Figure 5.1 RNA-associated proteins N, P and M2-1 co-localise in RSV IBs, along with the matrix, M protein. Vero cells, mock infected, or infected with bRSV for 24 h, were fixed and immunostained with rabbit anti-NF-κB p65 (red) and mouse monoclonal anti-RSV N, P, M2-1, M or F antibodies (green). Nuclei were stained with DAPI (blue) and images obtained using a Leica TCS SP5 confocal microscope. Zoom panel shows magnification of IBs boxed in the merge panel. Graphs shows fluorescent intensity profiles along the indicated white lines drawn across one or two IBs. Images are representative of data from a single experiment

protein at 24 h p.i., as well as its partial nuclear localisation, is consistent with previously reported IF in RSV-infected cells (Ghildyal et al., 2002, Shahriari et al., 2018). However, the role of M in RNA virus IBs reflects an interesting point of divergence; with some viral IBs being M positive (e.g. RSV) and others negative (e.g. rabies) (Lahaye et al., 2009). Although it was not examined here due to the lack of antibodies, the RSV polymerase, L protein, has also been shown to colocalise with N and P at the periphery of the IBs (Carromeu et al., 2007). As these are components of the polymerase complex, their location potentially indicates the site of viral RNA replication and transcription. M2-1, on the other hand, could be seen throughout the IB but mostly concentrated in "pockets" within the IB previously described as inclusion body-associated granules (IBAGs) (Rincheval et al., 2017). The sub-IB organisation of these RSV proteins possibly highlights the structural and functional complexity of these structures.

5.2.2. bRSV IBs are sites of RNA replication

Co-localisation of the RNA-associated proteins, N, P, L and M2-1 in IBs strongly suggests the presence of viral RNA in these structures. Accordingly, hRSV IBs have been shown to be the sites of virus transcription and replication (Rincheval et al., 2017, Carromeu et al., 2007, Fricke et al., 2013). To confirm bRSV IBs are also the site of viral RNA replication, I carried out nascent RNA labelling using 5-ethynyl-uridine (5EU) incorporation. First, MDBK cells were mock infected or infected with bRSV for 24 h and then incubated with vehicle or actinomycin D (Act D) which inhibits cellular transcription for 1 h. 5EU was then added and cells incubated for another 1 h before fixing and detecting the incorporated 5EU. Mock infected cells, incubated with 5EU for 1 h, revealed, as expected, 5EU incorporation into cellular RNA in the nucleus (Fig 5.2; top row). When cellular transcription was inhibited following pre-incubation of mock infected cells with Act D for 1 hr this signal was lost. 5EU labelling performed on bRSV infected cells without Act D treatment did not reveal significant evidence for viral replication in IBs, perhaps due to over-representation of cellular RNA synthesis. However, in the presence of Act D, labelled newly synthesised RNA could only be seen in the N-positive IBs, presumably the result of viral replication.

RSV replication is insensitive to the effects of Act D (de Jong and Harmsen, 1973). This co-localisation of 5EU incorporation and N-protein within IBs provides evidence that bRSV IBs are also the sites of viral RNA replication. A more detailed look at the IBs revealed partial sub-IB organisation to the RNA found within these structures (Fig 5.2B). 5EU concentration was markedly evident in some IBs more than others, most likely depending on the level of RNA expression and the stage of infection. Line of interest graphs of representative images show pockets of RNA concentration in all cases (Fig 5.2B; marked with asterisks), similarly to that observed for M2-1 (Fig 5.1). Using fluorescence in situ hybridization (FISH) experiments, Rincheval et al. showed that genomic RNA colocalised with the hRSV N and P proteins at the periphery, whilst viral mRNA was found to concentrate in functional compartments within IBs, IBAGs that also contain M2-1 (Rincheval et al., 2017). Although, my analysis did not distinguish between genome replication and mRNA transcription, the data highlights the role of bRSV IBs as sites of RNA replication.

5.2.3. Multiple subdomains exist within bRSV IBs

IBAGs have been illustrated as dynamic structures, and their formation shown to depend on viral mRNA synthesis (Rincheval et al., 2017). The authors further showed that they concentrate newly synthesised viral mRNA and the viral M2-1 protein (a transcription termination factor) but not genomic RNA, or the N, P and L proteins. I have also observed accumulation of M2-1 (Fig 5.1) and nascent vRNA (Fig 5.2) into sub-IB domains, albeit separately, but potentially also showing the presence of IBAGs in bRSV IBs. To confirm the presence of IBAGs in bRSV-induced IBs, I immuno-stained infected cells for M2-1 following nascent viral RNA labelling as described in 5.2.2. As a strong marker of IBAG formation, the results showed co-localisation of both components (Fig 5.3A). The intra-IB organisation of vRNA and M2-1 protein into IBAGs, therefore, appears to be a structurally conserved aspect of orthopneumovirus IBs. Tangentially, I examined the potential co-localisation of p65 with these sites of nascent vRNA localisation (IBAGs). Although partial sub-IB localisation signals for p65 were seen, this did not always co-localise with vRNA (Fig 5.3A) or, in subsequent experiments, with M2-1 (Fig 5.3B). This potentially suggest that there are multiple sub-compartments within bRSV IBs, in addition to IBAGs, which carry out a distinct range of functions.

Electron microscopy of infected cells revealed structural similarities between RSV IBs and eukaryotic nucleoli (Fig 5.4A). They exhibit a similar size and shape, with a well-

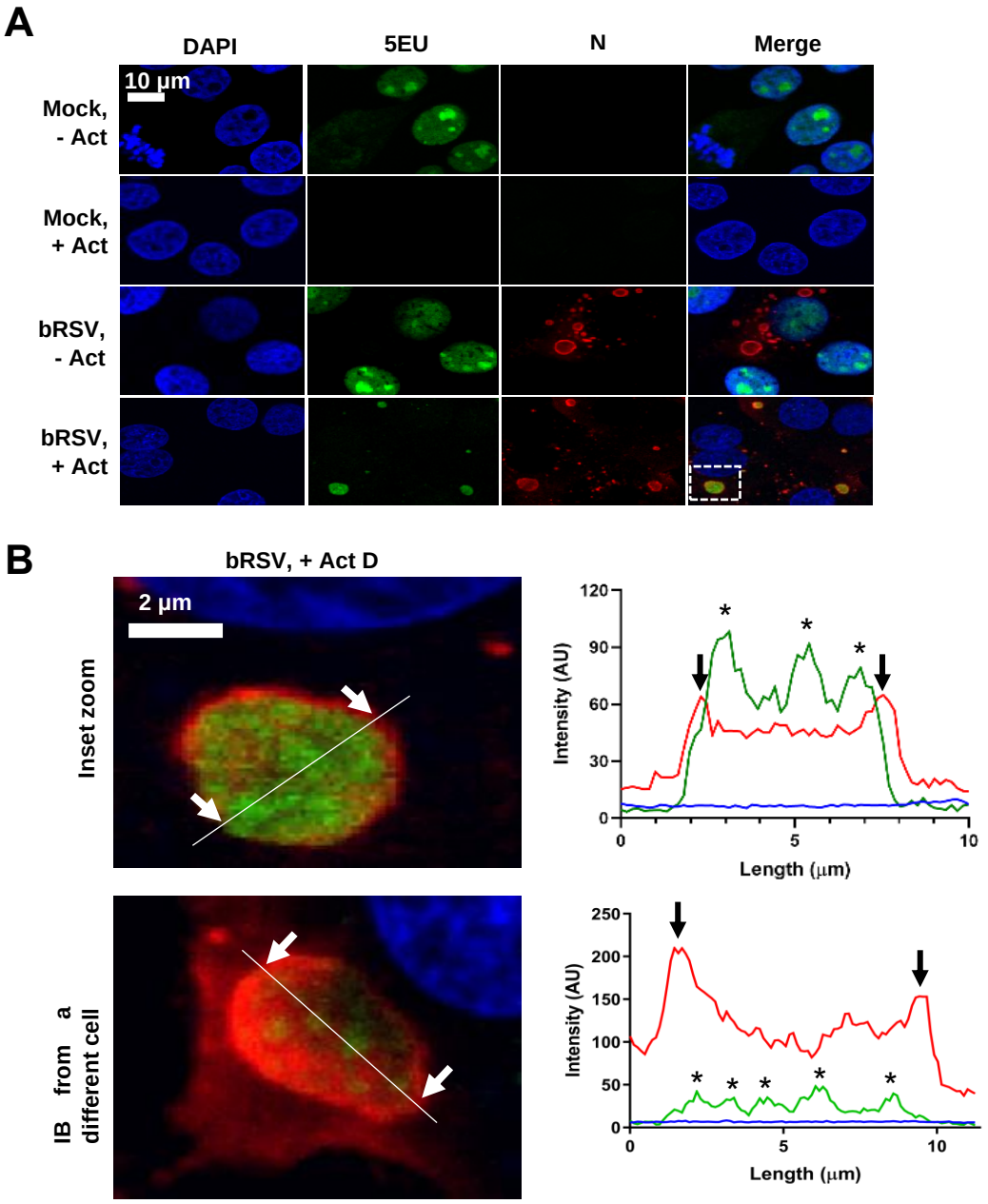

Figure 5.2 5EU staining of nascent RNA shows IBs are sites of viral RNA replication. (A) MDBK cells were mock infected or infected with bRSV. 24 h later, cells were incubated with vehicle or 20 µg/ml actinomycin D (Act D) for 1 h to inhibit cellular transcription. 5-ethynyl uridine (5EU) was then added for another 1 h and the cells fixed. 5EU incorporated into newly synthesized RNA was detected using Alexa Fluor 488-azide (green) as described in the methods. Cells were then immuno-stained with anti-RSV N antibodies (red) and nuclei stained with DAPI (blue). **(B)** Magnified images of representative IBs. "Inset zoom" shows a larger image of the boxed area in A (merge of bRSV, +Act D). Graphs show fluorescent intensity profiles along the indicated white lines drawn across the IBs. Arrows indicate the IB boundary and asterisks indicate areas of increased 5EU staining within the IB. Images are representative of data from n=2 independent repeats.

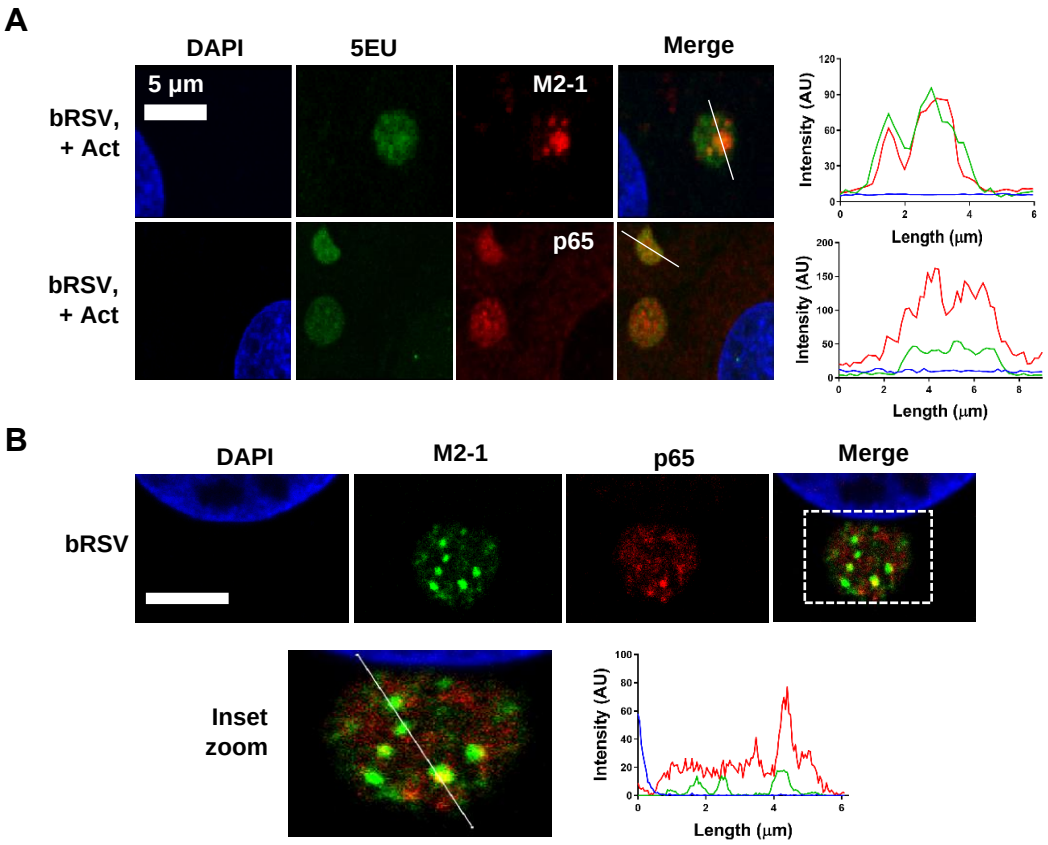

Figure 5.3 NF-κB p65 does not specifically co-localise with M2-1 or nascent viral RNA in IB-associated granules (IBAGs). (A) MDBK cells were infected with bRSV. 24 h later, cells were incubated with 20 µg/ml actinomycin D (Act D) for 1 h to inhibit cellular transcription. 5-ethynyl uridine (5EU) was then added for another 1 h and the cells fixed. 5EU incorporated into newly synthesized RNA was detected using Alexa Fluor 488-azide (green) as described in the methods. Cells were then immuno-stained with anti-M2-1 or anti-NF-κB p65 antibodies (red). Cell nuclei were stained with DAPI (blue) and images obtained using a Leica TCS SP5 confocal microscope. Graphs show fluorescent intensity profiles along the indicated white lines drawn across the IBs. **(B)** Vero cells infected with bRSV for 24 h were fixed and immuno-stained with rabbit anti-NF-κB p65 (red) and mouse anti-M2-1 (green) antibodies. Cell nuclei were stained with DAPI (blue) and images obtained using a Leica TCS SP5 confocal microscope. Bottom panel shows a higher magnification of the boxed area - scale bar corresponds to 4 µm. Graphs shows fluorescent intensity profiles along the indicated white line. Images are representative of data from a single experiment.

defined membrane-less boundary that concentrates N protein in the case of the IBs. Both structures are described in the literature as biomolecular condensates - liquid organelles containing protein and RNA and postulated to form by phase separation (Moshe and Gorovits, 2012, Feric et al., 2016, Alberti et al., 2019, Banani et al., 2017). The composition of liquid organelles is selectively controlled through mechanisms that are not well understood (Banani et al., 2017). Significantly, morphologically similar internal sub-compartments – regions of differing density to the granular structure (black arrows) – were seen in some IBs in common with nucleoli (Fig 5.4A). These sub-compartments were randomly located in both structures, and varied in number and size, indicating a highly dynamic organisation within the structures. Studies of the nucleolar architecture describes these regions as fibrillar centres (one of three nucleolar sub-compartments) where ribosomal RNA synthesis occurs, amongst other functions (Hernandez-Verdun, 2006, Farley et al., 2015). Although not well studied in IBs, I hypothesised that these sub-IB compartments visible by EM are most likely the RNA and M2-1-rich IBAGs that have been described above by IF microscopy (Fig 5.3) and also previously described (Bouillier et al., 2019, Rincheval et al., 2017).

The difference in granularity compared to the rest of the IB is most likely the result of LLPS, facilitating the specialised composition and function of these sites. When assessed by CLEM (as already described in section 4.2.3) at 48 h p.i, the sub-IB compartments did not colocalise with areas of significant p65 staining (Fig 5.4A and bottom panel of B). Areas of N protein localisation (at the IB periphery) were observed to have greater electron density in the electron micrographs (Fig 5.4), highlighting possible structural complexity and specialised functions for this region. In agreement with this observation, Rincheval et al have shown enrichment of RSV genomic RNA in this region using FISH. This data shows that although RSV IBs compartmentalise functions essential to the virus lifecycle, they are highly organised structures, and also present evidence of sub-IB functional compartmentalization.

5.2.4. Cellular proteins involved in the initiation of translation colocalise in IBAGs

Since IBs induced by RSV infection were found to be functional sites of viral RNA synthesis, the next step was to investigate the location of viral protein translation. It

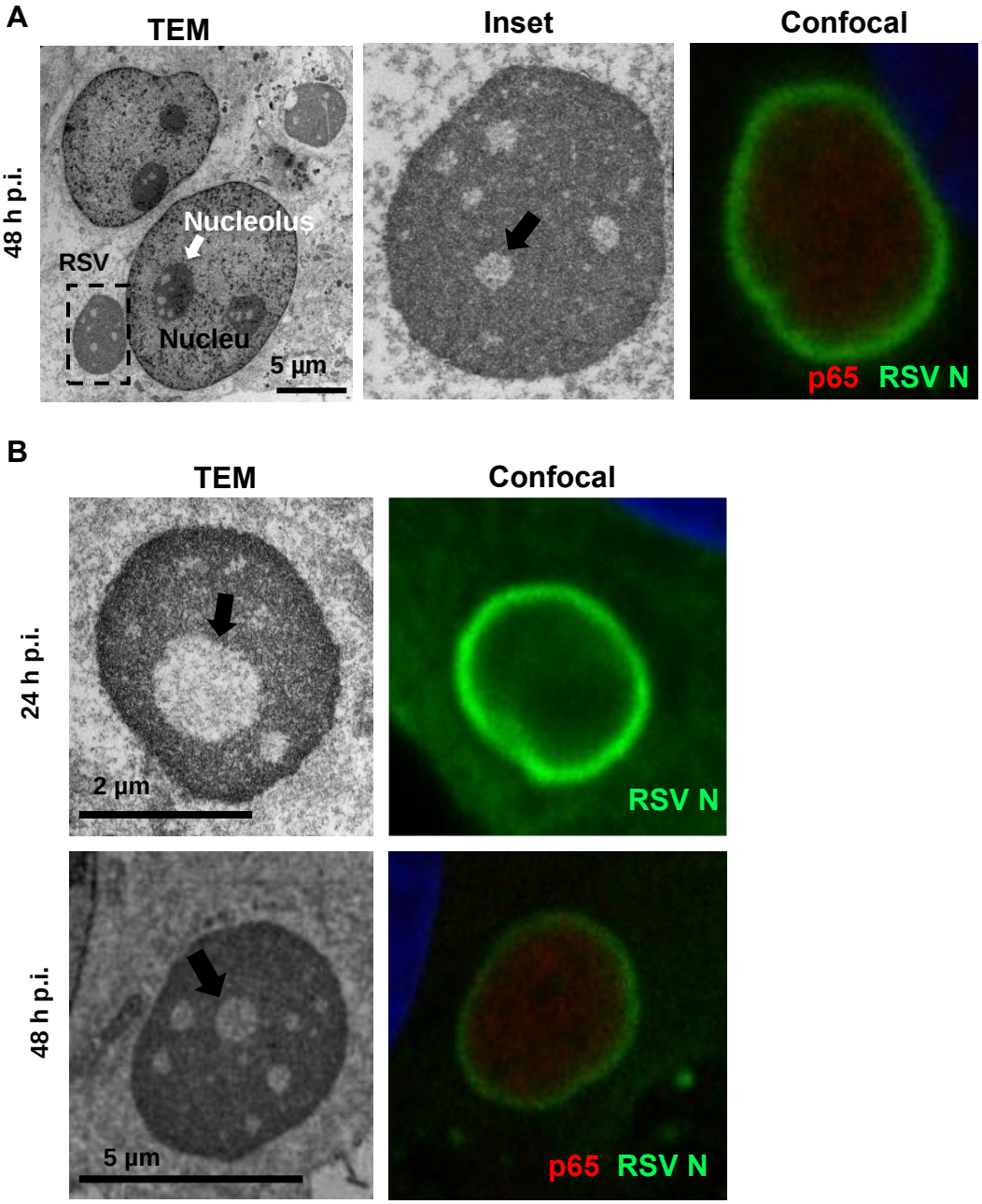

Figure 5.4 Ultrastructure of bRSV inclusion bodies by CLEM. (A) Vero and **(B)** MDBK cells infected with bRSV were fixed and stained with antibodies against RSV N (green), NF-κB p65 (red) and nuclei stained with DAPI. Following confocal imaging, cells were fixed in glutaraldehyde, sectioned and visualised by TEM. Representative confocal images of RSV IBs (right) and their corresponding electron micrographs (left) are shown. "Inset zoom" is a higher magnification of the RSV IB boxed in (A). White arrow indicates the nucleus and black arrows point to inclusion body associated granules (IBAGS). Images are representative of data from a single experiment.

has already been established that newly synthesised viral RNA interacts with M2-1 (Fig 5.3A) and another mRNA-binding protein, PolyA-binding protein 1 (PABPC1) in IBAGs (Bouillier et al., 2019). Time lapse experiments showed that IBAGs are highly dynamic and that their contents are moved out of IBs and released into the cytoplasm (Rincheval et al., 2017), possibly indicating the location of viral protein translation. I began examining viral interactions with the cellular translational machinery by investigating the localisation of proteins involved in translation initiation, specifically, proteins from the eIF4F complex. The complex (made up of eIFs 4E, 4G, 4A and 4B) together with PABP, regulates translations by recruiting mRNA to ribosomes (Gingras et al., 1999). Mock and bRSV infected cells were fixed at 24 h p.i., and co-immunostained for RSV N and eIF4G or eIF4A1. In mock infected cells, eIF4G (Fig 5.5A) and eIF4A1 (Fig 5.5B) were evenly distributed in the cytoplasm. In bRSV infected cells, although both proteins can still be seen throughout the cytoplasm, they accumulated in sub-IB compartments, similarly to that observed for M2-1 (Fig 5.3). Subsequently, co-immunostaining of infected cells for the same eIF components and M2-1 showed colocalization of both proteins with M2-1 (Fig 5.6). This data shows localisation of proteins of the translation initiation complex in IBAGs together with M2-1, possibly interacting directly with vRNA. However, identification of the final interaction of this complex with ribosomes, to uncover the site of viral mRNA translation, could not be investigated due to time limitations. This will be explored in the future work section.

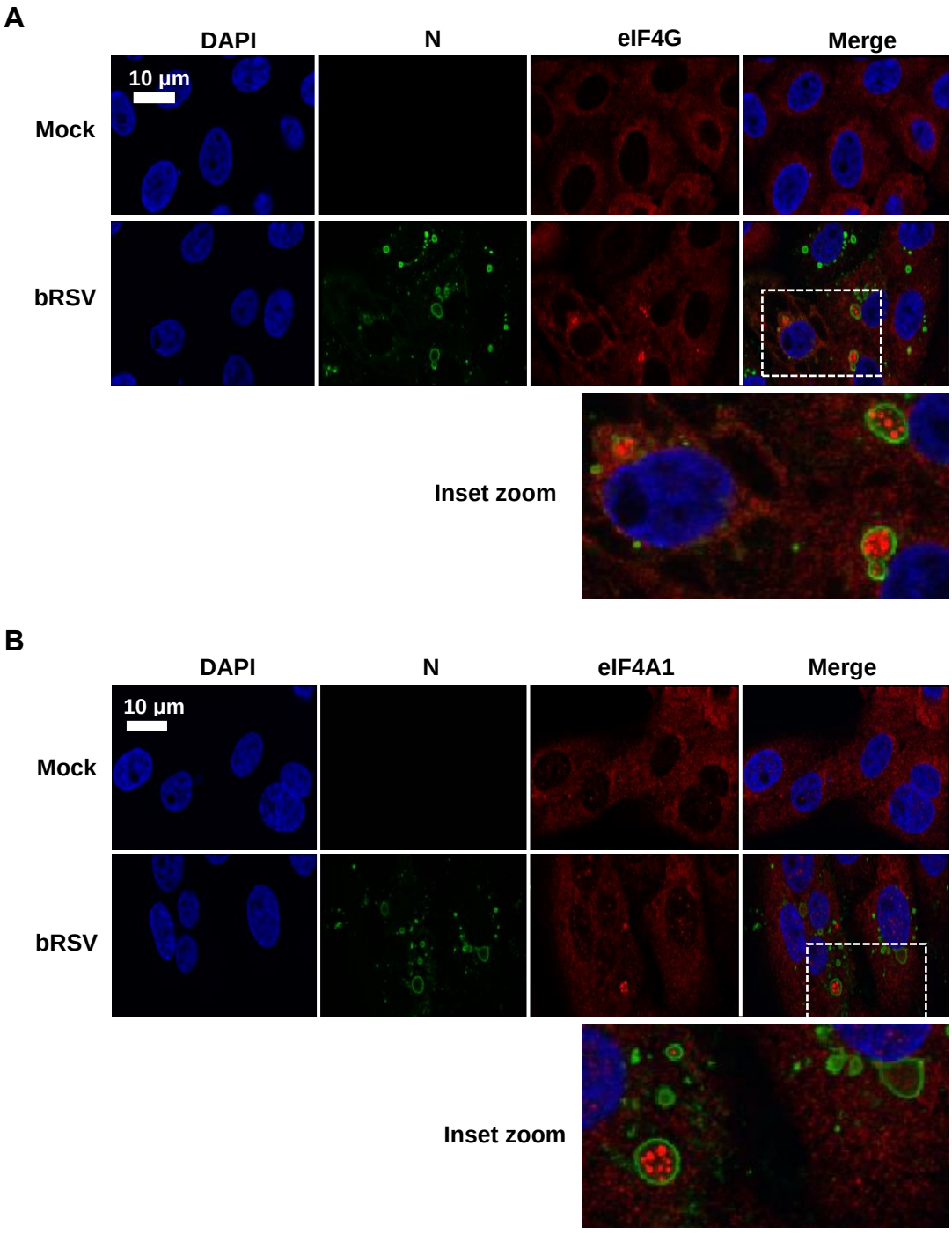

Figure 5.5 Translation initiation factors involved in mRNA activation colocalize in RSV IBs. Vero cells were infected with bRSV for 24 hrs, then fixed and immuno-stained for RSV N (green) and **(A)** eIF4G, or **(B)** eIF4A1 (red). Inset zooms show higher magnifications of boxed areas. Nuclei were stained with DAPI (blue), and images obtained using a Leica TCS SP5 confocal microscope. Images are representative of data from a single experiment.

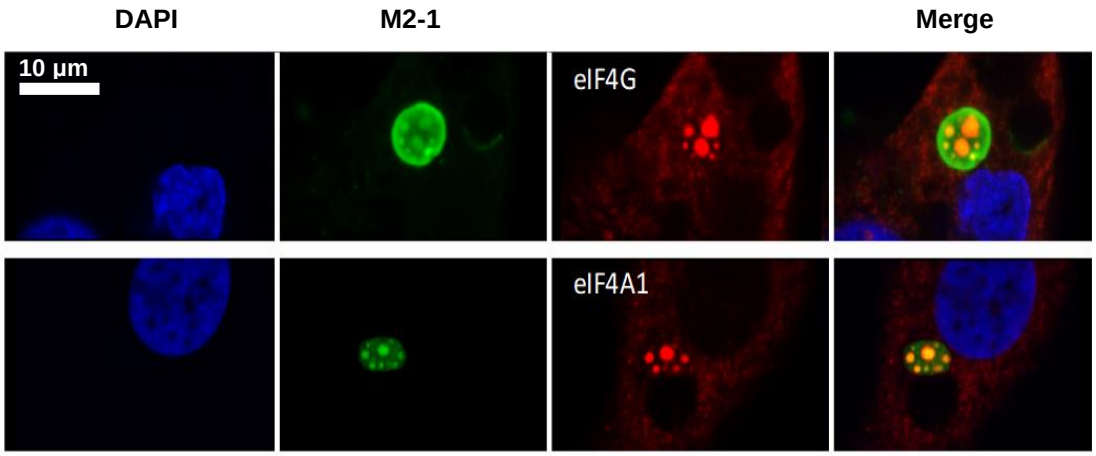

Figure 5.6 The translation initiation factors eIF4G/eIF4A1 colocalise with RSV M2-1 in IBAGs. Vero cells were infected with bRSV for 24 hrs, then fixed and immuno-stained for RSV M2-1 (green) and eIF4G or eIF4A1 (red). Nuclei were stained with DAPI (blue) and images obtained using a Leica TCS SP5 confocal microscope. Images are representative of data from a single experiment.

5.3. Discussion

Recent studies have reported that IBs of negative strand RNA viruses are specialised sites of genome replication and mRNA transcription, thus making these structures essential components of the virus lifecycle. Using 5EU incorporation into nascent viral RNA, we show, for the first time, that bRSV IBs are the sites of RNA synthesis (Fig 5.2) and describe the spatial organisation of multiple viral proteins and RNA during infection (Fig 5.1). Sub-IB domains (IBAGs) which were previously shown for hRSV to concentrate nascent viral mRNA (Rincheval et al., 2017) were identified and found to localise cellular proteins involved in the initiation of translation (Fig 5.5 and Fig 5.6). There was no conclusive colocalisation of IBAGs with intra-IB bodies concentrating p65, highlighting the possibility that multiple microdomains exist within these viral IBs.

IBs induced in the cytoplasm of RSV infected cells require further characterisation; however, they share many features with replication compartments induced by several classified members of the *Paramyxoviridae* (Zhou et al., 2019, Katoh et al., 2015b, Ringel et al., 2019), *Rhabdoviridae* (Heinrich et al., 2018, Nikolic et al., 2017) and *Filoviridae* (Hoenen et al., 2012), virus families within the *Mononegavirales* order (Nevers et al., 2020). Similar to these viruses, the processes of RSV genome replication and transcription are known to occur exclusively in the cytoplasm of infected cells, but their spatial organisation is not well defined. Aggregates of viral protein and RNA were observed in RSV infected cells as early as the 1970s (Norrby et al., 1970, Garcia et al., 1993), however, the significance of these structures in replication has only recently been uncovered (Rincheval et al., 2017, Nevers et al., 2020). Consistent with the reported findings, we observed that although the nucleocapsid components (N and P, as well as its interacting partners, M2-1 and M) can be seen diffusely distributed in the cytoplasm, they were predominantly localised in IBs (Fig 5.1). Although the location of L was not investigated due to the unavailability of antibodies, others have also observed its presence in IBs (Carromeu et al., 2007). In addition, very little RNA synthesis was detected outside of the IBs, at 24 h p.i. Thus, concentration of all components of the viral RdRP (RNA synthesis machinery) and nascent viral RNA in IBs, similar to observations in hRSV infected

cells (Rincheval et al., 2017), confirms that these cytoplasmic granules are the major sites of orthopneumovirus replication and transcription.

RNA synthesis was also observed in IBs induced during rabies (Nikolic et al., 2016, Oksayan et al., 2012, Lahaye et al., 2009), and ebola (Hoenen et al., 2012) virus infections. For rabies and hRSV, the presence of nascent genomic, antigenomic and messenger vRNA in IBs confirms they are the sites of both replication and transcription (Lahaye et al., 2009, Rincheval et al., 2017). Although this is yet to be confirmed for ebola (Hoenen et al., 2012), MeV (Zhou et al., 2019), MuV (Katoh et al., 2015b) and other related viruses, preliminary findings suggest their IBs may also carry out both processes. Interestingly, vRNA synthesis was shown to occur outside of the two structurally distinct IB populations induced in NiV infected cells (Ringel et al., 2019), which is an interesting divergence from the other mononegaviruses. Two populations of IBs were also observed during ebola virus infection – a larger subset that contained L and VP35 (the polymerase cofactor), and a VP35-positive subset lacking L which were typically smaller in size (Hoenen et al., 2012). Active viral RNA synthesis was only observed in the larger, L-containing IBs and not in the smaller L-deficient ones. The authors did not distinguish between mRNA transcription and genomic RNA synthesis but suggested that the former may occur in the cytoplasm prior to IB formation, which was detected at 10 h p.i (Hoenen et al., 2012). However, it is unclear why ebola RNA synthesis is restricted to large L-positive IBs and how the L-status of the IBs is regulated. In our studies, as infection progressed, we observed evolution of RSV IBs into a heterogenous population; a dominant IB which is likely produced from the initial infection and several intermediate and smaller sized structures which likely emerge as a result of nascent infections or due to fission of the larger structures. However, all identified structures showing characteristics of IBs exhibited similar protein and RNA composition. Using delivery of multiply labelled tetravalent imaging probes (MTRIPS) into live cells, Lifland et al. suggested that RSV RNA synthesis occurs in the small but not in large IBs (Lifland et al., 2012). In contrast, Rincheval *et al*. used immunofluorescence to detect 5EU that was actively incorporated into newly synthesised RSV RNA and observed synthesis in all IBs regardless of their size (Rincheval et al., 2017), similar to our observations with bRSV using the same protocol (Fig 5.2). We agree with the authors' suggestion that this approach, relying on metabolic labelling of nascent viral RNA, is likely unaffected by

RNA accessibility in contrast to the assay used by Lifland *et. al*. The MTRIPS seem to predominantly target vRNA diffuse in the cytoplasm, present in small punctate structures or in virus filaments, as opposed to those presumably concentrated in IBs (Lifland et al., 2012).

Although I only detected RSV RNA synthesis in IBs, I cannot rule out a more diffuse distribution of synthesis throughout the cytoplasm which may be below the detection limit of our protocol. Since I concentrated on the 24 h p.i. time point, when infection and IBs are fully established, the spatio-temporal organisation of IB formation in relation to the onset of viral protein and RNA synthesis is currently unclear. I detected viral protein expression as early as 6 h p.i. (Fig 4.5 and Fig 4.6), however the onset of RNA synthesis was not investigated. Rincheval *et al*. observed RNA synthesis at 8 h p.i. and showed that IBs were already established at this time (Rincheval et al., 2017). Interestingly, synthesis of VSV mRNA was shown to begin in the host cell cytoplasm prior to IB formation (Heinrich et al., 2010). The authors also observed that IBs formed once sufficient viral proteins were expressed, and subsequently become the predominant sites of RNA synthesis (Heinrich et al., 2010). Similar temporal organisation may be adopted by RSV since mRNA transcription and protein synthesis are known to precede genome replication (Collins et al., 2013, Bermingham and Collins, 1999). Synthesis of RSV genomic RNA is upregulated by sufficient expression of proteins such as N (Fearns et al., 1997) and M2-2 (Bermingham and Collins, 1999), at which point IBs would likely have formed to support RNA synthesis. Thus, in the early stages of infection, mRNA transcription could be initiated in the diffuse cytoplasm prior to IB formation. Unlike genomic and antigenomic RNA, viral mRNA is not protected by encapsidation with N protein and could be recognised by cytoplasmic innate single-stranded-RNA sensors. Similar phase-separated cellular structures such as stress granules and P-bodies are induced as a mechanism of excluding stalled mRNA from the translationally active pool (Zhang et al., 2019). This raises two possibilities for the process of viral IB formation: (i) it is initiated as a cellular response to restrict viral RNA which is then hijacked by the virus to support replication, or (ii) it represents an encoded viral mechanism which evolved to protect viral RNA from innate immune recognition. With regards to the former, RSV IBs were shown to be distinct from stress granules (Fig 4.9), although other cellular condensates were not interrogated. When compared to contributing viral factors the contribution

of host factors to IB biogenesis is even less clear. However, several large DNA viruses such as vaccinia virus and African swine fever virus use the cellular aggresome pathway to generate inclusions that become sites of virus replication (Wileman, 2006). In common with RSV IBs, these replication sites lie in close proximity to the MTOC and also recruit mitochondria. Thus, further investigations are required to understand the spatio-temporal organisation of viral transcription and replication, their relationship with IB formation and underlying mechanisms of biogenesis.

Aside from being the designated sites of RNA synthesis, formation of IBs provide several advantages to the virus. Random distribution of viral RNA and replication intermediaries in the cytoplasm will enhance recognition by host cell PRRs and induce activation of an antiviral response to clear the infection. As a barrier to antagonism, positive strand RNA viruses compartmentalise their replication sites in membraned structures in the cytoplasm of infected cells; a mechanism that protects viral components from immune recognition whilst also promoting replication by concentration of the machinery (Harak and Lohmann, 2015). With the exception of rabies virus IBs which become associated with membranes in the later stages of infection (Lahaye et al., 2009, Nikolic et al., 2017), mononegaviruses do not normally form membraned replication centres. However, their IBs facilitate functions orthologous to those carried out by the replication centres of positive strand RNA viruses. Spatial compartmentalisation in IBs enhances the efficiency of replication by concentrating components of the RdRp. Furthermore, although IBs allow exchange with the cytoplasm, selective control of their composition also restricts recognition of localised viral components by host cell innate sensors. To this end, IBs induced in HPIV3 infection protected viral RNA from recognition by PKR to inhibit the antiviral effects of stress granules (Hu et al., 2018). This is another strategy of immune modulation similar to the sequestration of immune sensors and antiviral proteins into IBs discussed in chapter 4. It also further highlights the importance of IBs in regulating the antiviral response and promoting infection.

Characterisation of the viral protein and RNA composition of RSV IBs, as well as spatial organisation of these components demonstrates a similar morphology to closely related RNA viruses. We observed regions of significant N and P staining at the periphery of the bRSV IBs (Fig 5.1), as has been consistently reported for rabies virus

and RSV (Nikolic et al., 2017, Rincheval et al., 2017, Lifland et al., 2012), and by CLEM analysis observed that these N- and P-rich regions have a higher electron density compared to the rest of the IB (Fig 5.4). Using fluorescence *in situ* hybridization (FISH) experiments, Rincheval *et al.* showed that genomic (g)RNA colocalized with the hRSV N and P proteins at the IB periphery while viral mRNA was found to concentrate in IBAGs, transient sites of mRNA storage (Rincheval et al., 2017). The former is not a surprising finding since both genomic and anti-genomic RNA are tightly encapsidated by N and thus expected to concentrate in regions containing N and RdRp. Although our nascent vRNA staining does not discriminate between genomic and messenger RNA, we did not observe significant concentration of vRNA at the IB periphery. Therefore, the high electron density observed at the IB periphery by TEM likely represents protein concentration rather than RNA. However, there was a significant concentration of vRNA in sub-IB domains (Fig 5.2) also concentrating M2-1 (Fig 5.3), which we believe are the IBAGs previously identified (Rincheval et al., 2017). Our findings also confirm that IBAG formation is a conserved mechanism present in multiple orthopneumoviruses. Multiple subdomains of reduced electron density were also observed by TEM which we hypothesise correspond to IBAGs. However, this will require further analysis, possibly by M2-1 CLEM. Nonetheless, differential organisation of viral protein, gRNA and mRNA in IBs shows that these structures are highly organised and contain multiple functionally compartmentalised protein-protein and protein-RNA interactions.

Consistent with previous findings for hRSV (Rincheval et al., 2017), we observed relocalisation of host cell proteins that play a role in the initiation of translation into IBAGs (Fig 5.6), likely interacting with viral mRNA. However, the location of components of the translation machinery such as the ribosomal subunits, S6 and L4, and a translation termination factor, eRF1, suggested that IBAGS or indeed IBs are not the sites of viral mRNA translation (Rincheval et al., 2017). It is currently assumed that viral mRNA is transported out of IBs into the cytoplasm to facilitate translation, however, the exact mechanism of transport, and the sites and organisation of viral protein translation require further investigation. For several viruses such as VSV (Heinrich et al., 2010), rabies (Nikolic et al., 2017), ebola (Schudt et al., 2015) and Marburg virus (Schudt et al., 2013), transportation of vRNA from IBs to elsewhere in the cell requires microtubules or the actin cytoskeleton. Of note, although viral mRNA

concentrates in IBAGs during RSV infection, it is not clear whether they are transported into IBs following synthesis in the cytoplasm or vice versa. N mRNA could be seen distributed in the cytoplasm as well as concentrated in IBAGs at 24 h p.i. (Rincheval et al., 2017). Pulse-chase analysis of viral mRNA could be carried out to identify the direction of mRNA transport at different stages of infection to confirm the spatio-temporal organisation of transcription over the time course of infection. The proteins involved in transport may also be identified by investigating the mRNA interactome. Metabolic labelling of viral proteins and single-molecule imaging may be used to identify sites of viral protein translation.

In summary, the data presented here shows that RSV IBs are highly ordered structures performing multiple roles in the virus life cycle, including the compartmentalization of viral RNA synthesis. Further characterisation of these structures, which are effectively replication complexes, is required to better understand the molecular biology of these viruses. This knowledge would potentially be applicable to other negative-sense RNA viruses that have been shown to form IBs during replication.

Chapter 6: Concluding remarks and future direction

6.1. Inhibition of innate immune signalling by targeting NF-κB subunit p65

NF-κB transcription factors are important regulators of the innate immune response induced in the early stages of virus infection. Virus detection by cellular PRRs leads to a cascade of phosphorylation and ubiquitination events that ultimately releases these transcription factors from inhibitors that normally prevent their constitutive activation, such as IκBα (Mitchell et al., 2016, Oeckinghaus et al., 2011). Activated NF-κB translocate into the nucleus where they induce the expression of several target genes, orchestrating inflammatory and antiviral responses that contribute to the clearance of infection. Therefore, to promote virus infection and spread, viruses use several strategies to inhibit activation of this ubiquitous pathway (Deng et al., 2018).

The initial objective of this project was to investigate the mechanism of NF-κB modulation by the RSV SH protein in bovine monocytes and dendritic cells (DCs), which play key roles in the immune response to virus infection. This was a follow up to previous work showing that the SH protein of RSV blocks NF-κB activation in these cells (Pollock et al., 2017), as well as in infected epithelial cells (Fuentes et al., 2007, Wilson et al., 2006, Russell et al., 2015). We hypothesised that SH interfered with the biological role of infected monocytes and DCs by impairing cytokine expression and their ability to initiate the more specific adaptive immune response. Our approach for understanding the role of the SH protein was based on the analysis of virus lacking SH expression in comparison with wild type virus and ectopic expression of the SH protein. Initially, we planned to validate research tools and establish assay protocols in Vero and THP-1 cells before moving on to more relevant primary cells. However, findings from preliminary experiments detailed in chapter 3 resulted in redirecting the objectives of the rest of our study.

We found that the RSV SH protein plays a minimal role in blocking NF-κB pathway activation through subunit p65; however, infection caused p65 to aggregate into intracytoplasmic IBs via a mechanism that was independent of the SH protein. Importantly, sequestered p65 was insensitive to exogenous NF-κB stimulation, consequently inhibiting activation of the pathway at the signalling level. NF-κB

transactivation was also reduced when assessed by reporter assay; however, analysis of NF-κB target gene expression by cytokine ELISA or qPCR will provide more robust evidence of modulation. We know from previous work that bRSV infected macrophage lines and CD14 positive primary cells do not produce significant levels of cytokines (Pollock et al., 2017). Due to the low permissivity of THP-1 cells, MDBK cells were used to investigate cytokine production by both ELISA and qPCR. However, the results obtained from these investigations were non-reproducible and inconclusive. Perhaps more relevant primary immune cells should be used for this analysis, work which we had planned but could not perform due to time limitations.

In chapter 4, we show that both hRSV and bRSV inhibit activation of the NF-κB pathway by sequestering the p65 subunit into intracytoplasmic IBs induced during infection, similar to the previously reported capture of MAVS, MDA5, MAPK and OGT (Fricke et al., 2013, Lifland et al., 2012). We postulate that the N protein has a role in this sequestration; however, further work is required to elucidate the mechanism by which p65 and other cellular proteins are recruited into IBs and to characterise this emerging immunomodulatory function of IBs. The repertoire of proteins recruited into IBs may be identified by mass spectrometry analysis of purified RSV IBs, improving our understanding of the physicochemical properties regulating IB composition. Further study of the implications of host protein sequestration will also aid the design of new antiviral therapies.

Considering the impact of the SH protein in virus pathogenesis, additional studies are also required to understand its role in infection. Identification of SH interacting partners by co-immunoprecipitation, using GFP-Trap, for example, followed by mass spectrometry analysis of pull-downs, may provide an insight into the inhibitory mechanisms exerted by SH. This may identify possible interactions with components of the NF-kB pathway, as already shown for MuV SH (Franz et al., 2017) or reveal other cellular proteins and signalling pathways regulated by SH.

Separately, an RNAseq-based comparative transcriptomics of wild type and bRSV ΔSH infected MDBK cells has been carried out by The Pirbright Institute bioinformatics department on samples I prepared. However, analysis and validation of this data was delayed by maternity leave and the Covid-19 pandemic. The plan was to identify differentially transcribed genes and proteins from this investigation in order

to improve our understanding of bRSV pathogenesis and the partial attenuation observed in the absence of SH.

6.2. The role of inclusion bodies in RSV infected cells

Inclusion bodies, granular structures induced in the cytoplasm of infected cells, are hallmarks of orthopneumovirus infection and compartmentalise several virus-virus and virus-host interactions (Rincheval et al., 2017, Garcia et al., 1993, Lifland et al., 2012, Fricke et al., 2013). They are biomolecular condensates that have been postulated to form by LLPS and share similar properties with liquid organelles (Banani et al., 2017, Nevers et al., 2020). Although they have been observed in cells infected with several mononegaviruses, their importance in infection has only recently been recognised. Inclusion bodies formed in hRSV infected cells have been shown to concentrate the N, P, L and M2-1 proteins – viral proteins essential for genome replication and transcription - and also newly synthesised viral RNA and mRNA (Rincheval et al., 2017), highlighting these structures as sites of mRNA transcription and genome replication. This work also identified the intra-organelle organisation of hRSV IBs into spatially distinct subdomains that are most likely highly regulated.

In chapters 4 and 5, using bRSV (as a model orthopneumovirus) and various microscopy tools, we characterised the structure, organisation, and function of these structures. The ultrastructure of bRSV IBs confirms that the granules are membrane-less and organised into subdomains. The N, P and M proteins, and M2-1 to a lesser extent, were found to concentrate at the boundary separating the IB from the cytoplasm. It is not clear how or whether this affects the composition of IBs or the exchange of biomolecules across the boundary. Live-cell imaging could be performed to assess the dynamics of proteins found in IBs. There is also limited mechanistic insight on the process of their formation although intrinsically disordered regions (IDRs) and RNA-binding domains in N and P, are thought to play a role (Kato et al., 2012, Banani et al., 2017, Galloux et al., 2020a). Fluorescent bioimaging techniques and truncation mutants of N and P could also be used to define the properties governing IB formation.

Using metabolic labelling of nascent viral RNA, we confirmed that IBs are the sites of RSV replication and transcription. However, RNA fluorescence in situ

hybridisation (FISH) could be carried out to discern the spatial organisation of viral genome and mRNA. Subdomains previously shown to concentrate RNA and M2-1, IBAGs (Rincheval et al., 2017), were also observed within bRSV IBs. Rincheval *et al*. suggested that IBAGs are dynamic and release their contents into the cytoplasm. This could be confirmed by single RNA imaging methods to track the fate of newly synthesised RNA. Separately, we observed that cellular proteins involved in the initiation of translation, eIF4G and eIF4A1, concentrate in IBAGs although Rincheval *et al*. suggested that RSV IBs are not the sites of viral protein translation. Therefore, we hypothesise that components essential for the initiation of translation may assemble on newly synthesised mRNA concentrated in IBAGs. These are then transported out of the IB and released into the cytoplasm where they may associate with other components of the translation machinery. The sites of RSV translation are currently unknown and may be identified by metabolic labelling of nascent viral protein.

This study has improved our basic understanding of RSV biology, in particular, the role of IBs induced in the cytoplasm of infected cells and the spatial organisation of virus replication. Of particular interest is the emerging role of IBs in innate immune modulation. We observed p65 sequestration in RSV IBs formed in a physiologically relevant model of the human bronchial epithelium, BEAS-2B cells. However, further work is required to confirm their presence in airway cells *in vivo*, and to understand the consequences of this sequestration on RSV pathogenesis.

References

ABRAHAM, M., ARROYO-DIAZ, N. M., LI, Z., ZENGEL, J., SAKAMOTO, K. & HE, B. 2018. Role of Small Hydrophobic Protein of J Paramyxovirus in Virulence. *J Virol*, 92.

AHMADIAN, G., RANDHAWA, J. S. & EASTON, A. J. 2000. Expression of the ORF-2 protein of the human respiratory syncytial virus M2 gene is initiated by a ribosomal termination-dependent reinitiation mechanism. *EMBO J,* 19**,** 2681-9.

ALBERTI, S., GLADFELTER, A. & MITTAG, T. 2019. Considerations and Challenges in Studying Liquid-Liquid Phase Separation and Biomolecular Condensates. *Cell,* 176**,** 419-434.

ALENQUER, M., VALE-COSTA, S., ETIBOR, T. A., FERREIRA, F., SOUSA, A. L. & AMORIM, M. J. 2019. Influenza A virus ribonucleoproteins form liquid organelles at endoplasmic reticulum exit sites. *Nat Commun,* 10**,** 1629.

ALVAREZ, A. E., MARSON, F. A. L., BERTUZZO, C. S., BASTOS, J. C. S., BARACAT, E. C. E., BRANDÃO, M. B., TRESOLDI, A. T., DAS NEVES ROMANELI, M. T., ALMEIDA, C. C. B., DE OLIVEIRA, T., SCHLODTMANN, P. G., CORRÊA, E., DE MIRANDA, M. L. F., DOS REIS, M. C., DE PIERI, J. V., ARNS, C. W. & RIBEIRO, J. D. 2018. Association between single nucleotide polymorphisms in TLR4, TLR2, TLR9, VDR, NOS2 and CCL5 genes with acute viral bronchiolitis. *Gene,* 645**,** 7-17.

AMANATIDOU, V., SOURVINOS, G., APOSTOLAKIS, S., TSILIMIGAKI, A. & SPANDIDOS, D. A. 2006. T280M variation of the CX3C receptor gene is associated with increased risk for severe respiratory syncytial virus bronchiolitis. *Pediatr Infect Dis J,* 25**,** 410-4.

AMARASINGHE, G. K., AYLLON, M. A., BAO, Y., BASLER, C. F., BAVARI, S., BLASDELL, K. R., BRIESE, T., BROWN, P. A., BUKREYEV, A., BALKEMA-BUSCHMANN, A., BUCHHOLZ, U. J., CHABI-JESUS, C., CHANDRAN, K., CHIAPPONI, C., CROZIER, I., DE SWART, R. L., DIETZGEN, R. G., DOLNIK, O., DREXLER, J. F., DURRWALD, R., DUNDON, W. G., DUPREX, W. P., DYE, J. M., EASTON, A. J., FOOKS, A. R., FORMENTY, P. B. H., FOUCHIER, R. A. M., FREITAS-ASTUA, J., GRIFFITHS, A., HEWSON, R., HORIE, M., HYNDMAN, T. H., JIANG, D., KITAJIMA, E. W., KOBINGER, G. P., KONDO, H., KURATH, G., KUZMIN, I. V., LAMB, R. A., LAVAZZA, A., LEE, B., LELLI, D., LEROY, E. M., LI, J., MAES, P., MARZANO, S. L., MORENO, A., MUHLBERGER, E., NETESOV, S. V., NOWOTNY, N., NYLUND, A., OKLAND, A. L., PALACIOS, G., PALYI, B., PAWESKA, J. T., PAYNE, S. L., PROSPERI, A., RAMOS-GONZALEZ, P. L., RIMA, B. K., ROTA, P., RUBBENSTROTH, D., SHI, M., SIMMONDS, P., SMITHER, S. J., SOZZI, E., SPANN, K., STENGLEIN, M. D., STONE, D. M., TAKADA, A., TESH, R. B., TOMONAGA, K., TORDO, N., TOWNER, J. S., VAN DEN HOOGEN, B., VASILAKIS, N., WAHL, V., WALKER, P. J., WANG, L. F., WHITFIELD, A. E., WILLIAMS, J. V., ZERBINI, F. M., ZHANG, T., ZHANG, Y. Z. & KUHN, J. H. 2019. Taxonomy of the order Mononegavirales: update 2019. *Arch Virol,* 164**,** 1967-1980.

ANDERSON, K., KING, A. M., LERCH, R. A. & WERTZ, G. W. 1992. Polylactosaminoglycan modification of the respiratory syncytial virus small

hydrophobic (SH) protein: a conserved feature among human and bovine respiratory syncytial viruses. *Virology,* 191**,** 417-30.

ARAUJO, G. C., SILVA, R. H., SCOTT, L. P., ARAUJO, A. S., SOUZA, F. P. & DE OLIVEIRA, R. J. 2016. Structure and functional dynamics characterization of the ion channel of the human respiratory syncytial virus (hRSV) small hydrophobic protein (SH) transmembrane domain by combining molecular dynamics with excited normal modes. *J Mol Model,* 22**,** 286.

ARNOLD, R., KONIG, B., WERCHAU, H. & KONIG, W. 2004. Respiratory syncytial virus deficient in soluble G protein induced an increased proinflammatory response in human lung epithelial cells. *Virology,* 330**,** 384-97.

ARSLANAGIC, E., MATSUMOTO, M., SUZUKI, K., NEROME, K., TSUTSUMI, H. & HUNG, T. 1996. Maturation of respiratory syncytial virus within HEp-2 cell cytoplasm. *Acta Virol,* 40**,** 209-14.

ATREYA, P. L. & KULKARNI, S. 1999. Respiratory syncytial virus strain A2 is resistant to the antiviral effects of type I interferons and human MxA. *Virology,* 261**,** 227-41.

AWOMOYI, A. A., RALLABHANDI, P., POLLIN, T. I., LORENZ, E., SZTEIN, M. B., BOUKHVALOVA, M. S., HEMMING, V. G., BLANCO, J. C. & VOGEL, S. N. 2007. Association of TLR4 polymorphisms with symptomatic respiratory syncytial virus infection in high-risk infants and young children. *J Immunol,* 179**,** 3171-7.

BAJOREK, M., CALY, L., TRAN, K. C., MAERTENS, G. N., TRIPP, R. A., BACHARACH, E., TENG, M. N., GHILDYAL, R. & JANS, D. A. 2014. The Thr205 phosphorylation site within respiratory syncytial virus matrix (M) protein modulates M oligomerization and virus production. *J Virol,* 88**,** 6380-93.

BAN, J., LEE, N. R., LEE, N. J., LEE, J. K., QUAN, F. S. & INN, K. S. 2018. Human Respiratory Syncytial Virus NS 1 Targets TRIM25 to Suppress RIG-I Ubiquitination and Subsequent RIG-I-Mediated Antiviral Signaling. *Viruses,* 10.

BANANI, S. F., LEE, H. O., HYMAN, A. A. & ROSEN, M. K. 2017. Biomolecular condensates: organizers of cellular biochemistry. *Nat Rev Mol Cell Biol,* 18**,** 285-298.

BAO, X. Y., KOLLI, D., LIU, T. S., SHAN, Y. C., GAROFALO, R. P. & CASOLA, A. 2008. Human metapneumovirus small hydrophobic protein inhibits NF-kappa B transcriptional activity. *Journal of Virology,* 82**,** 8224-8229.

BATTLES, M. B., LANGEDIJK, J. P., FURMANOVA-HOLLENSTEIN, P., CHAIWATPONGSAKORN, S., COSTELLO, H. M., KWANTEN, L., VRANCKX, L., VINK, P., JAENSCH, S., JONCKERS, T. H., KOUL, A., ARNOULT, E., PEEPLES, M. E., ROYMANS, D. & MCLELLAN, J. S. 2016. Molecular mechanism of respiratory syncytial virus fusion inhibitors. *Nat Chem Biol,* 12**,** 87-93.

BATTLES, M. B. & MCLELLAN, J. S. 2019. Respiratory syncytial virus entry and how to block it. *Nat Rev Microbiol,* 17**,** 233-245.

BAUM, A. & GARCIA-SASTRE, A. 2010. Induction of type I interferon by RNA viruses: cellular receptors and their substrates. *Amino Acids,* 38**,** 1283-99.

BAVISKAR, P. S., HOTARD, A. L., MOORE, M. L. & OOMENS, A. G. 2013. The respiratory syncytial virus fusion protein targets to the perimeter of inclusion bodies and facilitates filament formation by a cytoplasmic tail-dependent mechanism. *J Virol,* 87**,** 10730-41.

BEAURY, M., VELAGAPUDI, U. K., WEBER, S., SOTO, C., TALELE, T. T. & NICHOLS, D. B. 2017. The molluscum contagiosum virus death effector domain containing protein MC160 RxDL motifs are not required for its known viral immune evasion functions. *Virus Genes,* 53**,** 522-531.

BECKER, Y. 2006. Respiratory syncytial virus (RSV) evades the human adaptive immune system by skewing the Th1/Th2 cytokine balance toward increased levels of Th2 cytokines and IgE, markers of allergy--a review. *Virus Genes,* 33**,** 235-52.

BEHERA, A. K., MATSUSE, H., KUMAR, M., KONG, X., LOCKEY, R. F. & MOHAPATRA, S. S. 2001. Blocking intercellular adhesion molecule-1 on human epithelial cells decreases respiratory syncytial virus infection. *Biochem Biophys Res Commun,* 280**,** 188-95.

BERMINGHAM, A. & COLLINS, P. L. 1999. The M2-2 protein of human respiratory syncytial virus is a regulatory factor involved in the balance between RNA replication and transcription. *Proc Natl Acad Sci U S A,* 96**,** 11259-64.

BISWAS, S. & SHISLER, J. L. 2017. Molluscum Contagiosum Virus MC159 Abrogates cIAP1-NEMO Interactions and Inhibits NEMO Polyubiquitination. *J Virol,* 91.

BISWAS, S., SMITH, G. L., ROY, E. J., WARD, B. & SHISLER, J. L. 2018. A comparison of the effect of molluscum contagiosum virus MC159 and MC160 proteins on vaccinia virus virulence in intranasal and intradermal infection routes. *J Gen Virol,* 99**,** 246-252.

BITKO, V., GARMON, N. E., CAO, T., ESTRADA, B., OAKES, J. E., LAUSCH, R. N. & BARIK, S. 2004. Activation of cytokines and NF-kappa B in corneal epithelial cells infected by respiratory syncytial virus: potential relevance in ocular inflammation and respiratory infection. *BMC Microbiol,* 4**,** 28.

BITKO, V., SHULYAYEVA, O., MAZUMDER, B., MUSIYENKO, A., RAMASWAMY, M., LOOK, D. C. & BARIK, S. 2007. Nonstructural proteins of respiratory syncytial virus suppress premature apoptosis by an NF-kappaB-dependent, interferon-independent mechanism and facilitate virus growth. *J Virol,* 81**,** 1786-95.

BITKO, V., VELAZQUEZ, A., YANG, L., YANG, Y. C. & BARIK, S. 1997. Transcriptional induction of multiple cytokines by human respiratory syncytial virus requires activation of NF-kappa B and is inhibited by sodium salicylate and aspirin. *Virology,* 232**,** 369-78.

BLONDOT, M. L., DUBOSCLARD, V., FIX, J., LASSOUED, S., AUMONT-NICAISE, M., BONTEMS, F., ELEOUET, J. F. & SIZUN, C. 2012. Structure and functional analysis of the RNA- and viral phosphoprotein-binding domain of respiratory syncytial virus M2-1 protein. *PLoS Pathog,* 8**,** e1002734.

BLOUNT, R. E., JR., MORRIS, J. A. & SAVAGE, R. E. 1956. Recovery of cytopathogenic agent from chimpanzees with coryza. *Proc Soc Exp Biol Med,* 92**,** 544-9.

BORCHERS, A. T., CHANG, C., GERSHWIN, M. E. & GERSHWIN, L. J. 2013. Respiratory syncytial virus--a comprehensive review. *Clin Rev Allergy Immunol,* 45**,** 331-79.

BOSSHART, H. & HEINZELMANN, M. 2016. THP-1 cells as a model for human monocytes. *Annals of Translational Medicine,* 4**,** 22.

BOUILLIER, C., COSENTINO, G., LEGER, T., RINCHEVAL, V., RICHARD, C. A., DESQUESNES, A., SITTERLIN, D., BLOUQUIT-LAYE, S., ELEOUET, J. F., GAULT, E. & RAMEIX-WELTI, M. A. 2019. The Interactome analysis of the Respiratory Syncytial Virus protein M2-1 suggests a new role in viral mRNA metabolism post-transcription. *Sci Rep,* 9**,** 15258.

BOYAPALLE, S., WONG, T., GARAY, J., TENG, M., SAN JUAN-VERGARA, H., MOHAPATRA, S. & MOHAPATRA, S. 2012. Respiratory syncytial virus NS1 protein colocalizes with mitochondrial antiviral signaling protein MAVS following infection. *PLoS One,* 7**,** e29386.

BRADY, G., HAAS, D. A., FARRELL, P. J., PICHLMAIR, A. & BOWIE, A. G. 2015. Poxvirus Protein MC132 from Molluscum Contagiosum Virus Inhibits NF-B Activation by Targeting p65 for Degradation. *J Virol,* 89**,** 8406-15.

BRADY, G., HAAS, D. A., FARRELL, P. J., PICHLMAIR, A. & BOWIE, A. G. 2017. Molluscum Contagiosum Virus Protein MC005 Inhibits NF-kappaB Activation by Targeting NEMO-Regulated IkappaB Kinase Activation. *J Virol,* 91.

BRAULT, C., LEVY, P. L. & BARTOSCH, B. 2013. Hepatitis C virus-induced mitochondrial dysfunctions. *Viruses,* 5**,** 954-80.

BROADBENT, L., GROVES, H., SHIELDS, M. D. & POWER, U. F. 2015. Respiratory syncytial virus, an ongoing medical dilemma: an expert commentary on respiratory syncytial virus prophylactic and therapeutic pharmaceuticals currently in clinical trials. *Influenza Other Respir Viruses,* 9**,** 169-78.

BRODERSEN, B. W. 2010. Bovine respiratory syncytial virus. *Vet Clin North Am Food Anim Pract,* 26**,** 323-33.

BROWN, G., RIXON, H. W., STEEL, J., MCDONALD, T. P., PITT, A. R., GRAHAM, S. & SUGRUE, R. J. 2005. Evidence for an association between heat shock protein 70 and the respiratory syncytial virus polymerase complex within lipid-raft membranes during virus infection. *Virology,* 338**,** 69-80.

BUCHHOLZ, U. J., FINKE, S. & CONZELMANN, K. K. 1999. Generation of bovine respiratory syncytial virus (BRSV) from cDNA: BRSV NS2 is not essential for virus replication in tissue culture, and the human RSV leader region acts as a functional BRSV genome promoter. *J Virol,* 73**,** 251-9.

BUCHHOLZ, U. J., GRANZOW, H., SCHULDT, K., WHITEHEAD, S. S., MURPHY, B. R. & COLLINS, P. L. 2000. Chimeric bovine respiratory syncytial virus with glycoprotein gene substitutions from human respiratory syncytial virus (HRSV): effects on host range and evaluation as a live-attenuated HRSV vaccine. *J Virol,* 74**,** 1187-99.

BUCHWALD, A. G., TAMBOURA, B., TENNANT, S. M., HAIDARA, F. C., COULIBALY, F., DOUMBIA, M., DIALLO, F., KEITA, A. M., SOW, S. O., KOTLOFF, K. L., LEVINE, M. M. & TAPIA, M. D. 2020. Epidemiology, Risk Factors, and Outcomes of Respiratory Syncytial Virus Infections in Newborns in Bamako, Mali. *Clin Infect Dis,* 70**,** 59-66.

BUKREYEV, A., WHITEHEAD, S. S., MURPHY, B. R. & COLLINS, P. L. 1997. Recombinant respiratory syncytial virus from which the entire SH gene has been deleted grows efficiently in cell culture and exhibits site-specific attenuation in the respiratory tract of the mouse. *J Virol,* 71**,** 8973-82.

BUKREYEV, A., YANG, L., FRICKE, J., CHENG, L., WARD, J. M., MURPHY, B. R. & COLLINS, P. L. 2008. The secreted form of respiratory syncytial virus G glycoprotein helps the virus evade antibody-mediated restriction of replication by acting as an antigen decoy and through effects on Fc receptor-bearing leukocytes. *J Virol,* 82**,** 12191-204.

BYKOV, Y. S., CORTESE, M., BRIGGS, J. A. & BARTENSCHLAGER, R. 2016. Correlative light and electron microscopy methods for the study of virus-cell interactions. *FEBS Lett,* 590**,** 1877-95.

CAI, H., ZHANG, Y., LU, M., LIANG, X., JENNINGS, R., NIEWIESK, S. & LI, J. 2016. Phosphorylation of Human Metapneumovirus M2-1 Protein Upregulates Viral Replication and Pathogenesis. *J Virol,* 90**,** 7323-7338.

CAI, H., ZHANG, Y., MA, Y., SUN, J., LIANG, X. & LI, J. 2015. Zinc binding activity of human metapneumovirus M2-1 protein is indispensable for viral replication and pathogenesis in vivo. *J Virol,* 89**,** 6391-405.

CARPENTER, L. R., MOY, J. N. & ROEBUCK, K. A. 2002. Respiratory syncytial virus and TNF alpha induction of chemokine gene expression involves differential activation of Rel A and NF-kappa B1. *BMC Infect Dis,* 2**,** 5.

CARROMEU, C., SIMABUCO, F. M., TAMURA, R. E., FARINHA ARCIERI, L. E. & VENTURA, A. M. 2007. Intracellular localization of human respiratory syncytial virus L protein. *Arch Virol,* 152**,** 2259-63.

CARTER, S. D., DENT, K. C., ATKINS, E., FOSTER, T. L., VEROW, M., GORNY, P., HARRIS, M., HISCOX, J. A., RANSON, N. A., GRIFFIN, S. & BARR, J. N. 2010. Direct visualization of the small hydrophobic protein of human respiratory syncytial virus reveals the structural basis for membrane permeability. *FEBS Lett,* 584**,** 2786-90.

CHALLA, S., WOELFEL, M., GUILDFORD, M., MOQUIN, D. & CHAN, F. K. 2010. Viral cell death inhibitor MC159 enhances innate immunity against vaccinia virus infection. *J Virol,* 84**,** 10467-76.

CHANOCK, R., ROIZMAN, B. & MYERS, R. 1957. Recovery from infants with respiratory illness of a virus related to chimpanzee coryza agent (CCA). I. Isolation, properties and characterization. *Am J Hyg,* 66**,** 281-90.

CHEN, M. D., VAZQUEZ, M., BUONOCORE, L. & KAHN, J. S. 2000. Conservation of the respiratory syncytial virus SH gene. *J Infect Dis,* 182**,** 1228-33.

CHEN, Y., DENG, X., DENG, J., ZHOU, J., REN, Y., LIU, S., PRUSAK, D. J., WOOD, T. G. & BAO, X. 2016. Functional motifs responsible for human metapneumovirus M2-2-mediated innate immune evasion. *Virology,* 499**,** 361-368.

CHEN, Y., HE, L., PENG, Y., SHI, X., CHEN, J., ZHONG, J., CHEN, X., CHENG, G. & DENG, H. 2015. The hepatitis C virus protein NS3 suppresses TNF-alpha-stimulated activation of NF-kappaB by targeting LUBAC. *Sci Signal,* 8**,** ra118.

CHEN, Z., HAGLER, J., PALOMBELLA, V. J., MELANDRI, F., SCHERER, D., BALLARD, D. & MANIATIS, T. 1995. Signal-induced site-specific phosphorylation targets I kappa B alpha to the ubiquitin-proteasome pathway. *Genes Dev,* 9**,** 1586-97.

CHIANG, H. S. & LIU, H. M. 2018. The Molecular Basis of Viral Inhibition of IRF- and STAT-Dependent Immune Responses. *Front Immunol,* 9**,** 3086.
CHIRKOVA, T., LIN, S., OOMENS, A. G. P., GASTON, K. A., BOYOGLU-BARNUM, S., MENG, J., STOBART, C. C., COTTON, C. U., HARTERT, T. V., MOORE, M. L., ZIADY, A. G. & ANDERSON, L. J. 2015. CX3CR1 is an important surface molecule for respiratory syncytial virus infection in human airway epithelial cells. *J Gen Virol,* 96**,** 2543-2556.
CIFUENTES-MUNOZ, N., BRANTTIE, J., SLAUGHTER, K. B. & DUTCH, R. E. 2017. Human Metapneumovirus Induces Formation of Inclusion Bodies for Efficient Genome Replication and Transcription. *J Virol,* 91.
COLLINS, P. L., FEARNS, R. & GRAHAM, B. S. 2013. Respiratory syncytial virus: virology, reverse genetics, and pathogenesis of disease. *Curr Top Microbiol Immunol,* 372**,** 3-38.
COLLINS, P. L. & GRAHAM, B. S. 2008. Viral and host factors in human respiratory syncytial virus pathogenesis. *J Virol,* 82**,** 2040-55.
COLLINS, P. L., HILL, M. G., CAMARGO, E., GROSFELD, H., CHANOCK, R. M. & MURPHY, B. R. 1995. Production of infectious human respiratory syncytial virus from cloned cDNA confirms an essential role for the transcription elongation factor from the 5' proximal open reading frame of the M2 mRNA in gene expression and provides a capability for vaccine development. *Proc Natl Acad Sci U S A,* 92**,** 11563-7.
COLLINS, P. L., HILL, M. G., CRISTINA, J. & GROSFELD, H. 1996. Transcription elongation factor of respiratory syncytial virus, a nonsegmented negative-strand RNA virus. *Proc Natl Acad Sci U S A,* 93**,** 81-5.
COLLINS, P. L. & MELERO, J. A. 2011. Progress in understanding and controlling respiratory syncytial virus: still crazy after all these years. *Virus Res,* 162**,** 80-99.
COLLINS, P. L. & MOTTET, G. 1993. Membrane orientation and oligomerization of the small hydrophobic protein of human respiratory syncytial virus. *J Gen Virol,* 74 (Pt 7)**,** 1445-50.
COLLINS, P. L., OLMSTED, R. A., SPRIGGS, M. K., JOHNSON, P. R. & BUCKLER-WHITE, A. J. 1987. Gene overlap and site-specific attenuation of transcription of the viral polymerase L gene of human respiratory syncytial virus. *Proc Natl Acad Sci U S A,* 84**,** 5134-8.
COLLINS, P. L. & WERTZ, G. W. 1983. cDNA cloning and transcriptional mapping of nine polyadenylylated RNAs encoded by the genome of human respiratory syncytial virus. *Proc Natl Acad Sci U S A,* 80**,** 3208-12.
CROWE, J. E., JR., BUI, P. T., FIRESTONE, C. Y., CONNORS, M., ELKINS, W. R., CHANOCK, R. M. & MURPHY, B. R. 1996. Live subgroup B respiratory syncytial virus vaccines that are attenuated, genetically stable, and immunogenic in rodents and nonhuman primates. *J Infect Dis,* 173**,** 829-39.
CUESTA, I., GENG, X., ASENJO, A. & VILLANUEVA, N. 2000. Structural phosphoprotein M2-1 of the human respiratory syncytial virus is an RNA binding protein. *J Virol,* 74**,** 9858-67.
CUI, G., ZHU, R., QIAN, Y., DENG, J., ZHAO, L., SUN, Y. & WANG, F. 2013. Genetic variation in attachment glycoprotein genes of human respiratory syncytial virus subgroups a and B in children in recent five consecutive years. *PLoS One,* 8**,** e75020.

CURRIER, M. G., LEE, S., STOBART, C. C., HOTARD, A. L., VILLENAVE, R., MENG, J., PRETTO, C. D., SHIELDS, M. D., NGUYEN, M. T., TODD, S. O., CHI, M. H., HAMMONDS, J., KRUMM, S. A., SPEARMAN, P., PLEMPER, R. K., SAKAMOTO, K., PEEBLES, R. S., JR., POWER, U. F. & MOORE, M. L. 2016. EGFR Interacts with the Fusion Protein of Respiratory Syncytial Virus Strain 2-20 and Mediates Infection and Mucin Expression. *PLoS Pathog,* 12**,** e1005622.

DE GRAAFF, P. M., DE JONG, E. C., VAN CAPEL, T. M., VAN DIJK, M. E., ROHOLL, P. J., BOES, J., LUYTJES, W., KIMPEN, J. L. & VAN BLEEK, G. M. 2005. Respiratory syncytial virus infection of monocyte-derived dendritic cells decreases their capacity to activate CD4 T cells. *J Immunol,* 175**,** 5904-11.

DE JONG, J. C. & HARMSEN, M. 1973. Stimulated growth of respiratory syncytial virus in the presence of actinomycin D. *Antonie Van Leeuwenhoek,* 39**,** 409-13.

DEDIEGO, M. L., NIETO-TORRES, J. L., JIMENEZ-GUARDENO, J. M., REGLA-NAVA, J. A., ALVAREZ, E., OLIVEROS, J. C., ZHAO, J., FETT, C., PERLMAN, S. & ENJUANES, L. 2011. Severe acute respiratory syndrome coronavirus envelope protein regulates cell stress response and apoptosis. *PLoS Pathog,* 7**,** e1002315.

DEDIEGO, M. L., NIETO-TORRES, J. L., REGLA-NAVA, J. A., JIMENEZ-GUARDENO, J. M., FERNANDEZ-DELGADO, R., FETT, C., CASTANO-RODRIGUEZ, C., PERLMAN, S. & ENJUANES, L. 2014. Inhibition of NF-kappaB-mediated inflammation in severe acute respiratory syndrome coronavirus-infected mice increases survival. *J Virol,* 88**,** 913-24.

DEN BOON, J. A. & AHLQUIST, P. 2010. Organelle-like membrane compartmentalization of positive-strand RNA virus replication factories. *Annu Rev Microbiol,* 64**,** 241-56.

DENG, L., ZENG, Q., WANG, M., CHENG, A., JIA, R., CHEN, S., ZHU, D., LIU, M., YANG, Q., WU, Y., ZHAO, X., ZHANG, S., LIU, Y., YU, Y., ZHANG, L. & CHEN, X. 2018. Suppression of NF-kappaB Activity: A Viral Immune Evasion Mechanism. *Viruses,* 10.

DERDOWSKI, A., PETERS, T. R., GLOVER, N., QIAN, R., UTLEY, T. J., BURNETT, A., WILLIAMS, J. V., SPEARMAN, P. & CROWE, J. E. 2008. Human metapneumovirus nucleoprotein and phosphoprotein interact and provide the minimal requirements for inclusion body formation. *J Gen Virol,* 89**,** 2698-2708.

DETALLE, L., STOHR, T., PALOMO, C., PIEDRA, P. A., GILBERT, B. E., MAS, V., MILLAR, A., POWER, U. F., STORTELERS, C., ALLOSERY, K., MELERO, J. A. & DEPLA, E. 2016. Generation and Characterization of ALX-0171, a Potent Novel Therapeutic Nanobody for the Treatment of Respiratory Syncytial Virus Infection. *Antimicrob Agents Chemother,* 60**,** 6-13.

DIEL, D. G., LUO, S., DELHON, G., PENG, Y., FLORES, E. F. & ROCK, D. L. 2011. Orf virus ORFV121 encodes a novel inhibitor of NF-kappaB that contributes to virus virulence. *J Virol,* 85**,** 2037-49.

DINWIDDIE, D. L. & HARROD, K. S. 2008. Human metapneumovirus inhibits IFN-alpha signaling through inhibition of STAT1 phosphorylation. *Am J Respir Cell Mol Biol,* 38**,** 661-70.

DOMACHOWSKE, J. B., KHAN, A. A., ESSER, M. T., JENSEN, K., TAKAS, T., VILLAFANA, T., DUBOVSKY, F. & GRIFFIN, M. P. 2018. Safety, Tolerability and Pharmacokinetics of MEDI8897, an Extended Half-life Single-dose Respiratory Syncytial Virus Prefusion F-targeting Monoclonal Antibody Administered as a Single Dose to Healthy Preterm Infants. *Pediatr Infect Dis J,* 37**,** 886-892.

EASTON, A. J., DOMACHOWSKE, J. B. & ROSENBERG, H. F. 2004. Animal pneumoviruses: molecular genetics and pathogenesis. *Clin Microbiol Rev,* 17**,** 390-412.

EL NAJJAR, F., SCHMITT, A. P. & DUTCH, R. E. 2014. Paramyxovirus glycoprotein incorporation, assembly and budding: a three way dance for infectious particle production. *Viruses,* 6**,** 3019-54.

ELAWAR, F., ORABY, A. K., KIESER, Q., JENSEN, L. D., CULP, T., WEST, F. G. & MARCHANT, D. J. 2021. Pharmacological targets and emerging treatments for respiratory syncytial virus bronchiolitis. *Pharmacol Ther,* 220**,** 107712.

ELLIS, J. A. 2017. How efficacious are vaccines against bovine respiratory syncytial virus in cattle? *Vet Microbiol,* 206**,** 59-68.

ENNACIRI, J., AHMAD, R. & MENEZES, J. 2007. Interaction of monocytic cells with respiratory syncytial virus results in activation of NF-kappaB and PKC-alpha/beta leading to up-regulation of IL-15 gene expression. *J Leukoc Biol,* 81**,** 625-31.

ESNEAU, C., RAYNAL, B., ROBLIN, P., BRÛLÉ, S., RICHARD, C. A., FIX, J., ELÉOUËT, J. F. & GALLOUX, M. 2019. Biochemical characterization of the respiratory syncytial virus N. *J Biol Chem,* 294**,** 3647-3660.

ESPERANTE, S. A., NOVAL, M. G., ALTIERI, T. A., DE OLIVEIRA, G. A., SILVA, J. L. & DE PRAT-GAY, G. 2013. Fine modulation of the respiratory syncytial virus M2-1 protein quaternary structure by reversible zinc removal from its Cys(3)-His(1) motif. *Biochemistry,* 52**,** 6779-89.

EVERETT, H. & MCFADDEN, G. 1999. Apoptosis: an innate immune response to virus infection. *Trends Microbiol,* 7**,** 160-5.

EWART, G. D., SUTHERLAND, T., GAGE, P. W. & COX, G. B. 1996. The Vpu protein of human immunodeficiency virus type 1 forms cation-selective ion channels. *J Virol,* 70**,** 7108-15.

FALSEY, A. R., HENNESSEY, P. A., FORMICA, M. A., COX, C. & WALSH, E. E. 2005. Respiratory syncytial virus infection in elderly and high-risk adults. *N Engl J Med,* 352**,** 1749-59.

FARAG, N. S., BREITINGER, U., BREITINGER, H. G. & EL AZIZI, M. A. 2020. Viroporins and inflammasomes: A key to understand virus-induced inflammation. *Int J Biochem Cell Biol,* 122**,** 105738.

FARAG, N. S., BREITINGER, U., EL-AZIZI, M. & BREITINGER, H. G. 2017. The p7 viroporin of the hepatitis C virus contributes to liver inflammation by stimulating production of Interleukin-1beta. *Biochim Biophys Acta Mol Basis Dis,* 1863**,** 712-720.

FARLEY, K. I., SUROVTSEVA, Y., MERKEL, J. & BASERGA, S. J. 2015. Determinants of mammalian nucleolar architecture. *Chromosoma,* 124**,** 323-31.

FEARNS, R. & COLLINS, P. L. 1999a. Model for polymerase access to the overlapped L gene of respiratory syncytial virus. *J Virol,* 73**,** 388-97.

FEARNS, R. & COLLINS, P. L. 1999b. Role of the M2-1 transcription antitermination protein of respiratory syncytial virus in sequential transcription. *J Virol,* 73**,** 5852-64.
FEARNS, R., COLLINS, P. L. & PEEPLES, M. E. 2000. Functional analysis of the genomic and antigenomic promoters of human respiratory syncytial virus. *J Virol,* 74**,** 6006-14.
FEARNS, R., PEEPLES, M. E. & COLLINS, P. L. 1997. Increased expression of the N protein of respiratory syncytial virus stimulates minigenome replication but does not alter the balance between the synthesis of mRNA and antigenome. *Virology,* 236**,** 188-201.
FEARNS, R., PEEPLES, M. E. & COLLINS, P. L. 2002. Mapping the transcription and replication promoters of respiratory syncytial virus. *J Virol,* 76**,** 1663-72.
FELDMAN, S. A., AUDET, S. & BEELER, J. A. 2000. The fusion glycoprotein of human respiratory syncytial virus facilitates virus attachment and infectivity via an interaction with cellular heparan sulfate. *J Virol,* 74**,** 6442-7.
FELDMAN, S. A., HENDRY, R. M. & BEELER, J. A. 1999. Identification of a linear heparin binding domain for human respiratory syncytial virus attachment glycoprotein G. *J Virol,* 73**,** 6610-7.
FERIC, M., VAIDYA, N., HARMON, T. S., MITREA, D. M., ZHU, L., RICHARDSON, T. M., KRIWACKI, R. W., PAPPU, R. V. & BRANGWYNNE, C. P. 2016. Coexisting Liquid Phases Underlie Nucleolar Subcompartments. *Cell,* 165**,** 1686-1697.
FIEDLER, M. A. & WERNKE-DOLLRIES, K. 1999. Incomplete regulation of NF-kappaB by IkappaBalpha during respiratory syncytial virus infection in A549 cells. *J Virol,* 73**,** 4502-7.
FINK, K., DUVAL, A., MARTEL, A., SOUCY-FAULKNER, A. & GRANDVAUX, N. 2008. Dual role of NOX2 in respiratory syncytial virus- and sendai virus-induced activation of NF-kappaB in airway epithelial cells. *J Immunol,* 180**,** 6911-22.
FITZPATRICK, T., MCNALLY, J. D., STUKEL, T. A., LU, H., FISMAN, D., KWONG, J. C. & GUTTMANN, A. 2021. Family and Child Risk Factors for Early-Life RSV Illness. *Pediatrics,* 147.
FORSTER, A., MAERTENS, G. N., FARRELL, P. J. & BAJOREK, M. 2015. Dimerization of matrix protein is required for budding of respiratory syncytial virus. *J Virol,* 89**,** 4624-35.
FRANZ, S., RENNERT, P., WOZNIK, M., GRUTZKE, J., LUDDE, A., ARRIERO PAIS, E. M., FINSTERBUSCH, T., GEYER, H., MANKERTZ, A. & FRIEDRICH, N. 2017. Mumps Virus SH Protein Inhibits NF-kappaB Activation by Interacting with Tumor Necrosis Factor Receptor 1, Interleukin-1 Receptor 1, and Toll-Like Receptor 3 Complexes. *J Virol,* 91.
FRICKE, J., KOO, L. Y., BROWN, C. R. & COLLINS, P. L. 2013. p38 and OGT sequestration into viral inclusion bodies in cells infected with human respiratory syncytial virus suppresses MK2 activities and stress granule assembly. *J Virol,* 87**,** 1333-47.
FRIES, L., SHINDE, V., STODDARD, J. J., THOMAS, D. N., KPAMEGAN, E., LU, H., SMITH, G., HICKMAN, S. P., PIEDRA, P. & GLENN, G. M. 2017. Immunogenicity and safety of a respiratory syncytial virus fusion protein (RSV F) nanoparticle vaccine in older adults. *Immun Ageing,* 14**,** 8.

FUENTES, S., TRAN, K. C., LUTHRA, P., TENG, M. N. & HE, B. 2007. Function of the respiratory syncytial virus small hydrophobic protein. *Journal of Virology,* 81**,** 8361-8366.

FULGINITI, V. A., ELLER, J. J., SIEBER, O. F., JOYNER, J. W., MINAMITANI, M. & MEIKLEJOHN, G. 1969. Respiratory virus immunization. I. A field trial of two inactivated respiratory virus vaccines; an aqueous trivalent parainfluenza virus vaccine and an alum-precipitated respiratory syncytial virus vaccine. *Am J Epidemiol,* 89**,** 435-48.

GALLOUX, M., GABIANE, G., SOURIMANT, J., RICHARD, C. A., ENGLAND, P., MOUDJOU, M., AUMONT-NICAISE, M., FIX, J., RAMEIX-WELTI, M. A. & ELEOUET, J. F. 2015. Identification and characterization of the binding site of the respiratory syncytial virus phosphoprotein to RNA-free nucleoprotein. *J Virol,* 89**,** 3484-96.

GALLOUX, M., RISSO-BALLESTER, J., RICHARD, C. A., FIX, J., RAMEIX-WELTI, M. A. & ELEOUET, J. F. 2020a. Minimal Elements Required for the Formation of Respiratory Syncytial Virus Cytoplasmic Inclusion Bodies In Vivo and In Vitro. *mBio,* 11.

GALLOUX, M., RISSO-BALLESTER, J., RICHARD, C. A., FIX, J., RAMEIX-WELTI, M. A. & ELÉOUËT, J. F. 2020b. Minimal Elements Required for the Formation of Respiratory Syncytial Virus Cytoplasmic Inclusion Bodies In Vivo and In Vitro. *mBio,* 11.

GALLOUX, M., TARUS, B., BLAZEVIC, I., FIX, J., DUQUERROY, S. & ELÉOUËT, J. F. 2012. Characterization of a viral phosphoprotein binding site on the surface of the respiratory syncytial nucleoprotein. *J Virol,* 86**,** 8375-87.

GAN, S.-W., TAN, E., LIN, X., YU, D., WANG, J., TAN, G. M.-Y., VARARATTANAVECH, A., YEO, C. Y., SOON, C. H., SOONG, T. W., PERVUSHIN, K. & TORRES, J. 2012. The Small Hydrophobic Protein of the Human Respiratory Syncytial Virus Forms Pentameric Ion Channels. *Journal of Biological Chemistry,* 287**,** 24671-24689.

GAN, S. W., NG, L., LIN, X., GONG, X. & TORRES, J. 2008. Structure and ion channel activity of the human respiratory syncytial virus (hRSV) small hydrophobic protein transmembrane domain. *Protein Sci,* 17**,** 813-20.

GARCIA, J., GARCIA-BARRENO, B., VIVO, A. & MELERO, J. A. 1993. Cytoplasmic inclusions of respiratory syncytial virus-infected cells: formation of inclusion bodies in transfected cells that coexpress the nucleoprotein, the phosphoprotein, and the 22K protein. *Virology,* 195**,** 243-7.

GEOGHEGAN, S., ERVITI, A., CABALLERO, M. T., VALLONE, F., ZANONE, S. M., LOSADA, J. V., BIANCHI, A., ACOSTA, P. L., TALARICO, L. B., FERRETTI, A., GRIMALDI, L. A., SANCILIO, A., DUEÑAS, K., SASTRE, G., RODRIGUEZ, A., FERRERO, F., BARBOZA, E., GAGO, G. F., NOCITO, C., FLAMENCO, E., PEREZ, A. R., REBEC, B., FEROLLA, F. M., LIBSTER, R., KARRON, R. A., BERGEL, E. & POLACK, F. P. 2017. Mortality due to Respiratory Syncytial Virus. Burden and Risk Factors. *Am J Respir Crit Care Med,* 195**,** 96-103.

GHILDYAL, R., BAULCH-BROWN, C., MILLS, J. & MEANGER, J. 2003. The matrix protein of Human respiratory syncytial virus localises to the nucleus of infected cells and inhibits transcription. *Arch Virol,* 148**,** 1419-29.

GHILDYAL, R., HO, A. & JANS, D. A. 2006. Central role of the respiratory syncytial virus matrix protein in infection. *FEMS Microbiol Rev,* 30**,** 692-705.

GHILDYAL, R., LI, D., PEROULIS, I., SHIELDS, B., BARDIN, P. G., TENG, M. N., COLLINS, P. L., MEANGER, J. & MILLS, J. 2005. Interaction between the respiratory syncytial virus G glycoprotein cytoplasmic domain and the matrix protein. *J Gen Virol,* 86**,** 1879-1884.

GHILDYAL, R., MILLS, J., MURRAY, M., VARDAXIS, N. & MEANGER, J. 2002. Respiratory syncytial virus matrix protein associates with nucleocapsids in infected cells. *J Gen Virol,* 83**,** 753-7.

GILMAN, M. S. A., LIU, C., FUNG, A., BEHERA, I., JORDAN, P., RIGAUX, P., YSEBAERT, N., TCHERNIUK, S., SOURIMANT, J., ELEOUET, J. F., SUTTO-ORTIZ, P., DECROLY, E., ROYMANS, D., JIN, Z. & MCLELLAN, J. S. 2019. Structure of the Respiratory Syncytial Virus Polymerase Complex. *Cell,* 179**,** 193-204 e14.

GINGRAS, A. C., RAUGHT, B. & SONENBERG, N. 1999. eIF4 initiation factors: effectors of mRNA recruitment to ribosomes and regulators of translation. *Annu Rev Biochem,* 68**,** 913-63.

GLENN, G. M., SMITH, G., FRIES, L., RAGHUNANDAN, R., LU, H., ZHOU, B., THOMAS, D. N., HICKMAN, S. P., KPAMEGAN, E., BODDAPATI, S. & PIEDRA, P. A. 2013. Safety and immunogenicity of a Sf9 insect cell-derived respiratory syncytial virus fusion protein nanoparticle vaccine. *Vaccine,* 31**,** 524-32.

GOMES, E. & SHORTER, J. 2019. The molecular language of membraneless organelles. *J Biol Chem,* 294**,** 7115-7127.

GONZALEZ, M. E. 2015. Vpu Protein: The Viroporin Encoded by HIV-1. *Viruses,* 7**,** 4352-68.

GONZALEZ, M. E. & CARRASCO, L. 2003. Viroporins. *FEBS Lett,* 552**,** 28-34.

GORITZKA, M., MAKRIS, S., KAUSAR, F., DURANT, L. R., PEREIRA, C., KUMAGAI, Y., CULLEY, F. J., MACK, M., AKIRA, S. & JOHANSSON, C. 2015. Alveolar macrophage-derived type I interferons orchestrate innate immunity to RSV through recruitment of antiviral monocytes. *J Exp Med,* 212**,** 699-714.

GOSWAMI, R., MAJUMDAR, T., DHAR, J., CHATTOPADHYAY, S., BANDYOPADHYAY, S. K., VERBOVETSKAYA, V., SEN, G. C. & BARIK, S. 2013. Viral degradasome hijacks mitochondria to suppress innate immunity. *Cell Res,* 23**,** 1025-42.

GOULD, P. S. & EASTON, A. J. 2007. Coupled translation of the second open reading frame of M2 mRNA is sequence dependent and differs significantly within the subfamily Pneumovirinae. *J Virol,* 81**,** 8488-96.

GRAHAM, B. S., HENDERSON, G. S., TANG, Y. W., LU, X., NEUZIL, K. M. & COLLEY, D. G. 1993. Priming immunization determines T helper cytokine mRNA expression patterns in lungs of mice challenged with respiratory syncytial virus. *J Immunol,* 151**,** 2032-40.

GRIFFITHS, C. D., BILAWCHUK, L. M., MCDONOUGH, J. E., JAMIESON, K. C., ELAWAR, F., CEN, Y., DUAN, W., LIN, C., SONG, H., CASANOVA, J. L., OGG, S., JENSEN, L. D., THIENPONT, B., KUMAR, A., HOBMAN, T. C., PROUD, D., MORAES, T. J. & MARCHANT, D. J. 2020. IGF1R is an entry receptor for respiratory syncytial virus. *Nature,* 583**,** 615-619.

GROOTHUIS, J. R. & NISHIDA, H. 2002. Prevention of respiratory syncytial virus infections in high-risk infants by monoclonal antibody (palivizumab). *Pediatr Int,* 44**,** 235-41.

GUSEVA, S., MILLES, S., JENSEN, M. R., SALVI, N., KLEMAN, J. P., MAURIN, D., RUIGROK, R. W. H. & BLACKLEDGE, M. 2020. Measles virus nucleo- and phosphoproteins form liquid-like phase-separated compartments that promote nucleocapsid assembly. *Sci Adv,* 6**,** eaaz7095.

GUZMAN, E. & TAYLOR, G. 2015. Immunology of bovine respiratory syncytial virus in calves. *Mol Immunol,* 66**,** 48-56.

HABIBI, M. S., JOZWIK, A., MAKRIS, S., DUNNING, J., PARAS, A., DEVINCENZO, J. P., DE HAAN, C. A. M., WRAMMERT, J., OPENSHAW, P. J. M., CHIU, C. & INFLUENZA, M. S. A. 2015. Impaired Antibody-mediated Protection and Defective IgA B-Cell Memory in Experimental Infection of Adults with Respiratory Syncytial Virus. *American Journal of Respiratory and Critical Care Medicine,* 191**,** 1040-1049.

HABIBI, M. S., THWAITES, R. S., CHANG, M., JOZWIK, A., PARAS, A., KIRSEBOM, F., VARESE, A., OWEN, A., CUTHBERTSON, L., JAMES, P., TUNSTALL, T., NICKLE, D., HANSEL, T. T., MOFFATT, M. F., JOHANSSON, C., CHIU, C. & OPENSHAW, P. J. M. 2020. Neutrophilic inflammation in the respiratory mucosa predisposes to RSV infection. *Science,* 370.

HAEBERLE, H. A., TAKIZAWA, R., CASOLA, A., BRASIER, A. R., DIETERICH, H. J., VAN ROOIJEN, N., GATALICA, Z. & GAROFALO, R. P. 2002. Respiratory syncytial virus-induced activation of nuclear factor-kappaB in the lung involves alveolar macrophages and toll-like receptor 4-dependent pathways. *J Infect Dis,* 186**,** 1199-206.

HANLEY, L. L., MCGIVERN, D. R., TENG, M. N., DJANG, R., COLLINS, P. L. & FEARNS, R. 2010. Roles of the respiratory syncytial virus trailer region: effects of mutations on genome production and stress granule formation. *Virology,* 406**,** 241-52.

HARAK, C. & LOHMANN, V. 2015. Ultrastructure of the replication sites of positive-strand RNA viruses. *Virology,* 479-480**,** 418-33.

HARCOURT, J., ALVAREZ, R., JONES, L. P., HENDERSON, C., ANDERSON, L. J. & TRIPP, R. A. 2006. Respiratory syncytial virus G protein and G protein CX3C motif adversely affect CX3CR1+ T cell responses. *J Immunol,* 176**,** 1600-8.

HARDY, R. W. & WERTZ, G. W. 2000. The Cys(3)-His(1) motif of the respiratory syncytial virus M2-1 protein is essential for protein function. *J Virol,* 74**,** 5880-5.

HASTINGS, A. K., AMATO, K. R., WEN, S. C., PETERSON, L. S. & WILLIAMS, J. V. 2016. Human metapneumovirus small hydrophobic (SH) protein downregulates type I IFN pathway signaling by affecting STAT1 expression and phosphorylation. *Virology,* 494**,** 248-56.

HAYDEN, M. S. & GHOSH, S. 2008. Shared principles in NF-kappaB signaling. *Cell,* 132**,** 344-62.

HAYNES, L. M., MOORE, D. D., KURT-JONES, E. A., FINBERG, R. W., ANDERSON, L. J. & TRIPP, R. A. 2001. Involvement of toll-like receptor 4 in innate immunity to respiratory syncytial virus. *J Virol,* 75**,** 10730-7.

HEINRICH, B. S., CURETON, D. K., RAHMEH, A. A. & WHELAN, S. P. 2010. Protein expression redirects vesicular stomatitis virus RNA synthesis to cytoplasmic inclusions. *PLoS Pathog,* 6**,** e1000958.

HEINRICH, B. S., MALIGA, Z., STEIN, D. A., HYMAN, A. A. & WHELAN, S. P. J. 2018. Phase Transitions Drive the Formation of Vesicular Stomatitis Virus Replication Compartments. *mBio,* 9.

HEMINWAY, B. R., YU, Y., TANAKA, Y., PERRINE, K. G., GUSTAFSON, E., BERNSTEIN, J. M. & GALINSKI, M. S. 1994. Analysis of respiratory syncytial virus F, G, and SH proteins in cell fusion. *Virology,* 200**,** 801-5.

HEMMI, H., TAKEUCHI, O., SATO, S., YAMAMOTO, M., KAISHO, T., SANJO, H., KAWAI, T., HOSHINO, K., TAKEDA, K. & AKIRA, S. 2004. The roles of two IkappaB kinase-related kinases in lipopolysaccharide and double stranded RNA signaling and viral infection. *J Exp Med,* 199**,** 1641-50.

HENDERSON, G., MURRAY, J. & YEO, R. P. 2002. Sorting of the respiratory syncytial virus matrix protein into detergent-resistant structures is dependent on cell-surface expression of the glycoproteins. *Virology,* 300**,** 244-54.

HERNANDEZ-VERDUN, D. 2006. Nucleolus: from structure to dynamics. *Histochem Cell Biol,* 125**,** 127-37.

HOENEN, T., SHABMAN, R. S., GROSETH, A., HERWIG, A., WEBER, M., SCHUDT, G., DOLNIK, O., BASLER, C. F., BECKER, S. & FELDMANN, H. 2012. Inclusion bodies are a site of ebolavirus replication. *J Virol,* 86**,** 11779-88.

HOGAN, A. B., GLASS, K., MOORE, H. C. & ANDERSSEN, R. S. 2016. Exploring the dynamics of respiratory syncytial virus (RSV) transmission in children. *Theoretical Population Biology,* 110**,** 78-85.

HU, M., BOGOYEVITCH, M. A. & JANS, D. A. 2019a. Subversion of Host Cell Mitochondria by RSV to Favor Virus Production is Dependent on Inhibition of Mitochondrial Complex I and ROS Generation. *Cells,* 8.

HU, M., LI, H. M., BOGOYEVITCH, M. A. & JANS, D. A. 2017. Mitochondrial protein p32/HAPB1/gC1qR/C1qbp is required for efficient respiratory syncytial virus production. *Biochem Biophys Res Commun,* 489**,** 460-465.

HU, M., SCHULZE, K. E., GHILDYAL, R., HENSTRIDGE, D. C., KOLANOWSKI, J. L., NEW, E. J., HONG, Y., HSU, A. C., HANSBRO, P. M., WARK, P. A., BOGOYEVITCH, M. A. & JANS, D. A. 2019b. Respiratory syncytial virus co-opts host mitochondrial function to favour infectious virus production. *Elife,* 8.

HU, Z., WANG, Y., TANG, Q., YANG, X., QIN, Y. & CHEN, M. 2018. Inclusion bodies of human parainfluenza virus type 3 inhibit antiviral stress granule formation by shielding viral RNAs. *PLoS Pathog,* 14**,** e1006948.

HUANG, S., WEI, W. & YUN, Y. 2009. Upregulation of TLR7 and TLR3 gene expression in the lung of respiratory syncytial virus infected mice. *Wei Sheng Wu Xue Bao,* 49**,** 239-45.

ICHINOHE, T., PANG, I. K. & IWASAKI, A. 2010. Influenza virus activates inflammasomes via its intracellular M2 ion channel. *Nat Immunol,* 11**,** 404-10.

IWANASZKO, M. & KIMMEL, M. 2015. NF-κB and IRF pathways: cross-regulation on target genes promoter level. *BMC Genomics,* 16**,** 307.

JAMALUDDIN, M., TIAN, B., BOLDOGH, I., GAROFALO, R. P. & BRASIER, A. R. 2009. Respiratory syncytial virus infection induces a reactive oxygen

species-MSK1-phospho-Ser-276 RelA pathway required for cytokine expression. *J Virol,* 83**,** 10605-15.

JANSSEN, R., BONT, L., SIEZEN, C. L., HODEMAEKERS, H. M., ERMERS, M. J., DOORNBOS, G., VAN 'T SLOT, R., WIJMENGA, C., GOEMAN, J. J., KIMPEN, J. L., VAN HOUWELINGEN, H. C., KIMMAN, T. G. & HOEBEE, B. 2007. Genetic susceptibility to respiratory syncytial virus bronchiolitis is predominantly associated with innate immune genes. *J Infect Dis,* 196**,** 826-34.

JEFFREE, C. E., BROWN, G., AITKEN, J., SU-YIN, D. Y., TAN, B. H. & SUGRUE, R. J. 2007. Ultrastructural analysis of the interaction between F-actin and respiratory syncytial virus during virus assembly. *Virology,* 369**,** 309-23.

JEONG, K. I., PIEPENHAGEN, P. A., KISHKO, M., DINAPOLI, J. M., GROPPO, R. P., ZHANG, L., ALMOND, J., KLEANTHOUS, H., DELAGRAVE, S. & PARRINGTON, M. 2015. CX3CR1 Is Expressed in Differentiated Human Ciliated Airway Cells and Co-Localizes with Respiratory Syncytial Virus on Cilia in a G Protein-Dependent Manner. *PLoS One,* 10**,** e0130517.

JIN, H., CHENG, X., ZHOU, H. Z., LI, S. & SEDDIQUI, A. 2000a. Respiratory syncytial virus that lacks open reading frame 2 of the M2 gene (M2-2) has altered growth characteristics and is attenuated in rodents. *J Virol,* 74**,** 74-82.

JIN, H., ZHOU, H., CHENG, X., TANG, R., MUNOZ, M. & NGUYEN, N. 2000b. Recombinant respiratory syncytial viruses with deletions in the NS1, NS2, SH, and M2-2 genes are attenuated in vitro and in vivo. *Virology,* 273**,** 210-8.

JOBE, F., SIMPSON, J., HAWES, P., GUZMAN, E. & BAILEY, D. 2020. Respiratory syncytial virus sequesters NF-kappaB subunit p65 to cytoplasmic inclusion bodies to inhibit innate immune signalling. *J Virol*.

JOHNSON, J. E., GONZALES, R. A., OLSON, S. J., WRIGHT, P. F. & GRAHAM, B. S. 2007. The histopathology of fatal untreated human respiratory syncytial virus infection. *Mod Pathol,* 20**,** 108-19.

JOHNSON, S. M., MCNALLY, B. A., IOANNIDIS, I., FLANO, E., TENG, M. N., OOMENS, A. G., WALSH, E. E. & PEEPLES, M. E. 2015. Respiratory Syncytial Virus Uses CX3CR1 as a Receptor on Primary Human Airway Epithelial Cultures. *PLoS Pathog,* 11**,** e1005318.

JONES, A., MORTON, I., HOBSON, L., EVANS, G. S. & EVERARD, M. L. 2006. Differentiation and immune function of human dendritic cells following infection by respiratory syncytial virus. *Clin Exp Immunol,* 143**,** 513-22.

KARGER, A., SCHMIDT, U. & BUCHHOLZ, U. J. 2001. Recombinant bovine respiratory syncytial virus with deletions of the G or SH genes: G and F proteins bind heparin. *J Gen Virol,* 82**,** 631-40.

KARRON, R. A., BUONAGURIO, D. A., GEORGIU, A. F., WHITEHEAD, S. S., ADAMUS, J. E., CLEMENTS-MANN, M. L., HARRIS, D. O., RANDOLPH, V. B., UDEM, S. A., MURPHY, B. R. & SIDHU, M. S. 1997. Respiratory syncytial virus (RSV) SH and G proteins are not essential for viral replication in vitro: clinical evaluation and molecular characterization of a cold-passaged, attenuated RSV subgroup B mutant. *Proc Natl Acad Sci U S A,* 94**,** 13961-6.

KARRON, R. A., LUONGO, C., MATEO, J. S., WANIONEK, K., COLLINS, P. L. & BUCHHOLZ, U. J. 2020. Safety and Immunogenicity of the Respiratory Syncytial Virus Vaccine RSV/ΔNS2/Δ1313/I1314L in RSV-Seronegative Children. *J Infect Dis,* 222**,** 82-91.

KARRON, R. A., LUONGO, C., THUMAR, B., LOEHR, K. M., ENGLUND, J. A., COLLINS, P. L. & BUCHHOLZ, U. J. 2015. A gene deletion that up-regulates viral gene expression yields an attenuated RSV vaccine with improved antibody responses in children. *Sci Transl Med,* 7**,** 312ra175.

KATO, M., HAN, T. W., XIE, S., SHI, K., DU, X., WU, L. C., MIRZAEI, H., GOLDSMITH, E. J., LONGGOOD, J., PEI, J., GRISHIN, N. V., FRANTZ, D. E., SCHNEIDER, J. W., CHEN, S., LI, L., SAWAYA, M. R., EISENBERG, D., TYCKO, R. & MCKNIGHT, S. L. 2012. Cell-free formation of RNA granules: low complexity sequence domains form dynamic fibers within hydrogels. *Cell,* 149**,** 753-67.

KATOH, H., KUBOTA, T., KITA, S., NAKATSU, Y., AOKI, N., MORI, Y., MAENAKA, K., TAKEDA, M. & KIDOKORO, M. 2015a. Heat shock protein 70 regulates degradation of the mumps virus phosphoprotein via the ubiquitin-proteasome pathway. *J Virol,* 89**,** 3188-99.

KATOH, H., NAKATSU, Y., KUBOTA, T., SAKATA, M., TAKEDA, M. & KIDOKORO, M. 2015b. Mumps Virus Is Released from the Apical Surface of Polarized Epithelial Cells, and the Release Is Facilitated by a Rab11-Mediated Transport System. *J Virol,* 89**,** 12026-34.

KE, Z., DILLARD, R. S., CHIRKOVA, T., LEON, F., STOBART, C. C., HAMPTON, C. M., STRAUSS, J. D., RAJAN, D., ROSTAD, C. A., TAYLOR, J. V., YI, H., SHAH, R., JIN, M., HARTERT, T. V., PEEBLES, R. S., JR., GRAHAM, B. S., MOORE, M. L., ANDERSON, L. J. & WRIGHT, E. R. 2018. The Morphology and Assembly of Respiratory Syncytial Virus Revealed by Cryo-Electron Tomography. *Viruses,* 10.

KELLY, J. T., HUMAN, S., ALDERMAN, J., JOBE, F., LOGAN, L., RIX, T., GONCALVES-CARNEIRO, D., LEUNG, C., THAKUR, N., BIRCH, J. & BAILEY, D. 2019. BST2/Tetherin Overexpression Modulates Morbillivirus Glycoprotein Production to Inhibit Cell-Cell Fusion. *Viruses,* 11.

KHATIWADA, S., DELHON, G., NAGENDRAPRABHU, P., CHAULAGAIN, S., LUO, S., DIEL, D. G., FLORES, E. F. & ROCK, D. L. 2017. A parapoxviral virion protein inhibits NF-kappaB signaling early in infection. *PLoS Pathog,* 13**,** e1006561.

KIM, H. W., CANCHOLA, J. G., BRANDT, C. D., PYLES, G., CHANOCK, R. M., JENSEN, K. & PARROTT, R. H. 1969. Respiratory syncytial virus disease in infants despite prior administration of antigenic inactivated vaccine. *Am J Epidemiol,* 89**,** 422-34.

KIM, S., KIM, H. Y., LEE, S., KIM, S. W., SOHN, S., KIM, K. & CHO, H. 2007. Hepatitis B virus x protein induces perinuclear mitochondrial clustering in microtubule- and Dynein-dependent manners. *J Virol,* 81**,** 1714-26.

KIM, T. H. & LEE, H. K. 2014. Innate immune recognition of respiratory syncytial virus infection. *BMB Rep,* 47**,** 184-91.

KISS, G., HOLL, J. M., WILLIAMS, G. M., ALONAS, E., VANOVER, D., LIFLAND, A. W., GUDHETI, M., GUERRERO-FERREIRA, R. C., NAIR, V., YI, H., GRAHAM, B. S., SANTANGELO, P. J. & WRIGHT, E. R. 2014. Structural analysis of respiratory syncytial virus reveals the position of M2-1 between the matrix protein and the ribonucleoprotein complex. *J Virol,* 88**,** 7602-17.

KITAGAWA, Y., SAKAI, M., FUNAYAMA, M., ITOH, M. & GOTOH, B. 2017. Human Metapneumovirus M2-2 Protein Acts as a Negative Regulator of Alpha Interferon Production by Plasmacytoid Dendritic Cells. *J Virol,* 91.

KOGA, R., SUGITA, Y., NODA, T., YANAGI, Y. & OHNO, S. 2015. Actin-Modulating Protein Cofilin Is Involved in the Formation of Measles Virus Ribonucleoprotein Complex at the Perinuclear Region. *J Virol,* 89**,** 10524-31.

KOLOKOLTSOV, A. A., DENIGER, D., FLEMING, E. H., ROBERTS, N. J., JR., KARPILOW, J. M. & DAVEY, R. A. 2007. Small interfering RNA profiling reveals key role of clathrin-mediated endocytosis and early endosome formation for infection by respiratory syncytial virus. *J Virol,* 81**,** 7786-800.

KOTELKIN, A., BELYAKOV, I. M., YANG, L., BERZOFSKY, J. A., COLLINS, P. L. & BUKREYEV, A. 2006. The NS2 protein of human respiratory syncytial virus suppresses the cytotoxic T-cell response as a consequence of suppressing the type I interferon response. *J Virol,* 80**,** 5958-67.

KRUSAT, T. & STRECKERT, H. J. 1997. Heparin-dependent attachment of respiratory syncytial virus (RSV) to host cells. *Arch Virol,* 142**,** 1247-54.

KRZYZANIAK, M. A., ZUMSTEIN, M. T., GEREZ, J. A., PICOTTI, P. & HELENIUS, A. 2013. Host cell entry of respiratory syncytial virus involves macropinocytosis followed by proteolytic activation of the F protein. *PLoS Pathog,* 9**,** e1003309.

KUMAR, H., KAWAI, T. & AKIRA, S. 2011. Pathogen recognition by the innate immune system. *Int Rev Immunol,* 30**,** 16-34.

KUO, L., FEARNS, R. & COLLINS, P. L. 1996a. The structurally diverse intergenic regions of respiratory syncytial virus do not modulate sequential transcription by a dicistronic minigenome. *J Virol,* 70**,** 6143-50.

KUO, L., GROSFELD, H., CRISTINA, J., HILL, M. G. & COLLINS, P. L. 1996b. Effects of mutations in the gene-start and gene-end sequence motifs on transcription of monocistronic and dicistronic minigenomes of respiratory syncytial virus. *J Virol,* 70**,** 6892-901.

KURT-JONES, E. A., POPOVA, L., KWINN, L., HAYNES, L. M., JONES, L. P., TRIPP, R. A., WALSH, E. E., FREEMAN, M. W., GOLENBOCK, D. T., ANDERSON, L. J. & FINBERG, R. W. 2000. Pattern recognition receptors TLR4 and CD14 mediate response to respiratory syncytial virus. *Nat Immunol,* 1**,** 398-401.

LAHAYE, X., VIDY, A., FOUQUET, B. & BLONDEL, D. 2012. Hsp70 protein positively regulates rabies virus infection. *J Virol,* 86**,** 4743-51.

LAHAYE, X., VIDY, A., POMIER, C., OBIANG, L., HARPER, F., GAUDIN, Y. & BLONDEL, D. 2009. Functional characterization of Negri bodies (NBs) in rabies virus-infected cells: Evidence that NBs are sites of viral transcription and replication. *J Virol,* 83**,** 7948-58.

LAMA, J. & CARRASCO, L. 1992. Expression of poliovirus nonstructural proteins in Escherichia coli cells. Modification of membrane permeability induced by 2B and 3A. *J Biol Chem,* 267**,** 15932-7.

LAMBERT, D. M., HAMBOR, J., DIEBOLD, M. & GALINSKI, B. 1988. Kinetics of synthesis and phosphorylation of respiratory syncytial virus polypeptides. *J Gen Virol,* 69 (Pt 2)**,** 313-23.

LANGER, S., HAMMER, C., HOPFENSPERGER, K., KLEIN, L., HOTTER, D., DE JESUS, P. D., HERBERT, K. M., PACHE, L., SMITH, N., VAN DER MERWE, J. A., CHANDA, S. K., FELLAY, J., KIRCHHOFF, F. & SAUTER, D. 2019. HIV-1 Vpu is a potent transcriptional suppressor of NF-kappaB-elicited antiviral immune responses. *Elife,* 8.

LANGLEY, J. M., AGGARWAL, N., TOMA, A., HALPERIN, S. A., MCNEIL, S. A., FISSETTE, L., DEWÉ, W., LEYSSEN, M., TOUSSAINT, J. F. &

DIEUSSAERT, I. 2017. A Randomized, Controlled, Observer-Blinded Phase 1 Study of the Safety and Immunogenicity of a Respiratory Syncytial Virus Vaccine With or Without Alum Adjuvant. *J Infect Dis,* 215**,** 24-33.

LAY, M. K., GONZALEZ, P. A., LEON, M. A., CESPEDES, P. F., BUENO, S. M., RIEDEL, C. A. & KALERGIS, A. M. 2013. Advances in understanding respiratory syncytial virus infection in airway epithelial cells and consequential effects on the immune response. *Microbes Infect,* 15**,** 230-42.

LAZEAR, H. M., SCHOGGINS, J. W. & DIAMOND, M. S. 2019. Shared and Distinct Functions of Type I and Type III Interferons. *Immunity,* 50**,** 907-923.

LE NOUEN, C., HILLYER, P., BROCK, L. G., WINTER, C. C., RABIN, R. L., COLLINS, P. L. & BUCHHOLZ, U. J. 2014. Human Metapneumovirus SH and G Glycoproteins Inhibit Macropinocytosis-Mediated Entry into Human Dendritic Cells and Reduce CD4(+) T Cell Activation. *Journal of Virology,* 88**,** 6453-6469.

LI, D., JANS, D. A., BARDIN, P. G., MEANGER, J., MILLS, J. & GHILDYAL, R. 2008. Association of respiratory syncytial virus M protein with viral nucleocapsids is mediated by the M2-1 protein. *J Virol,* 82**,** 8863-70.

LI, Q., ZHENG, Z., LIU, Y., ZHANG, Z., LIU, Q., MENG, J., KE, X., HU, Q. & WANG, H. 2016. 2C Proteins of Enteroviruses Suppress IKKbeta Phosphorylation by Recruiting Protein Phosphatase 1. *J Virol,* 90**,** 5141-51.

LI, Y., JAIN, N., LIMPANAWAT, S., TO, J., QUISTGAARD, E. M., NORDLUND, P., THANABALU, T. & TORRES, J. 2015. Interaction between human BAP31 and respiratory syncytial virus small hydrophobic (SH) protein. *Virology,* 482**,** 105-10.

LI, Y., TO, J., VERDIA-BAGUENA, C., DOSSENA, S., SURYA, W., HUANG, M., PAULMICHL, M., LIU, D. X., AGUILELLA, V. M. & TORRES, J. 2014. Inhibition of the human respiratory syncytial virus small hydrophobic protein and structural variations in a bicelle environment. *J Virol,* 88**,** 11899-914.

LI, Z., XU, J., PATEL, J., FUENTES, S., LIN, Y., ANDERSON, D., SAKAMOTO, K., WANG, L. F. & HE, B. 2011. Function of the small hydrophobic protein of J paramyxovirus. *J Virol,* 85**,** 32-42.

LIFLAND, A. W., JUNG, J., ALONAS, E., ZURLA, C., CROWE, J. E., JR. & SANTANGELO, P. J. 2012. Human respiratory syncytial virus nucleoprotein and inclusion bodies antagonize the innate immune response mediated by MDA5 and MAVS. *J Virol,* 86**,** 8245-58.

LILJEROOS, L., KRZYZANIAK, M. A., HELENIUS, A. & BUTCHER, S. J. 2013. Architecture of respiratory syncytial virus revealed by electron cryotomography. *Proc Natl Acad Sci U S A,* 110**,** 11133-8.

LIN, Y., PROTTER, D. S., ROSEN, M. K. & PARKER, R. 2015. Formation and Maturation of Phase-Separated Liquid Droplets by RNA-Binding Proteins. *Mol Cell,* 60**,** 208-19.

LIN, Y. A., BRIGHT, A. C., ROTHERMEL, T. A. & HE, B. A. 2003. Induction of apoptosis by paramyxovirus Simian virus 5 lacking a small hydrophobic gene. *Journal of Virology,* 77**,** 3371-3383.

LINDQUIST, M. E., LIFLAND, A. W., UTLEY, T. J., SANTANGELO, P. J. & CROWE, J. E., JR. 2010. Respiratory syncytial virus induces host RNA stress granules to facilitate viral replication. *J Virol,* 84**,** 12274-84.

LINDQUIST, M. E., MAINOU, B. A., DERMODY, T. S. & CROWE, J. E., JR. 2011. Activation of protein kinase R is required for induction of stress

granules by respiratory syncytial virus but dispensable for viral replication. *Virology,* 413**,** 103-10.
LING, Z., TRAN, K. C. & TENG, M. N. 2009. Human respiratory syncytial virus nonstructural protein NS2 antagonizes the activation of beta interferon transcription by interacting with RIG-I. *J Virol,* 83**,** 3734-42.
LIU, P., JAMALUDDIN, M., LI, K., GAROFALO, R. P., CASOLA, A. & BRASIER, A. R. 2007. Retinoic acid-inducible gene I mediates early antiviral response and Toll-like receptor 3 expression in respiratory syncytial virus-infected airway epithelial cells. *J Virol,* 81**,** 1401-11.
LIU, P., LI, K., GAROFALO, R. P. & BRASIER, A. R. 2008. Respiratory syncytial virus induces RelA release from cytoplasmic 100-kDa NF-kappa B2 complexes via a novel retinoic acid-inducible gene-I{middle dot}NF- kappa B-inducing kinase signaling pathway. *J Biol Chem,* 283**,** 23169-78.
LO, M. S., BRAZAS, R. M. & HOLTZMAN, M. J. 2005. Respiratory syncytial virus nonstructural proteins NS1 and NS2 mediate inhibition of Stat2 expression and alpha/beta interferon responsiveness. *J Virol,* 79**,** 9315-9.
LONGHI, S., BLOYET, L. M., GIANNI, S. & GERLIER, D. 2017. How order and disorder within paramyxoviral nucleoproteins and phosphoproteins orchestrate the molecular interplay of transcription and replication. *Cell Mol Life Sci,* 74**,** 3091-3118.
LOO, Y. M., FORNEK, J., CROCHET, N., BAJWA, G., PERWITASARI, O., MARTINEZ-SOBRIDO, L., AKIRA, S., GILL, M. A., GARCIA-SASTRE, A., KATZE, M. G. & GALE, M., JR. 2008. Distinct RIG-I and MDA5 signaling by RNA viruses in innate immunity. *J Virol,* 82**,** 335-45.
LU, W., ZHENG, B. J., XU, K., SCHWARZ, W., DU, L., WONG, C. K., CHEN, J., DUAN, S., DEUBEL, V. & SUN, B. 2006. Severe acute respiratory syndrome-associated coronavirus 3a protein forms an ion channel and modulates virus release. *Proc Natl Acad Sci U S A,* 103**,** 12540-5.
LUKACS, N. W., SMIT, J. J., MUKHERJEE, S., MORRIS, S. B., NUNEZ, G. & LINDELL, D. M. 2010. Respiratory virus-induced TLR7 activation controls IL-17-associated increased mucus via IL-23 regulation. *J Immunol,* 185**,** 2231-9.
MA, D., GEORGE, C. X., NOMBURG, J. L., PFALLER, C. K., CATTANEO, R. & SAMUEL, C. E. 2018. Upon Infection, Cellular WD Repeat-Containing Protein 5 (WDR5) Localizes to Cytoplasmic Inclusion Bodies and Enhances Measles Virus Replication. *J Virol,* 92.
MAKRIS, S., BAJOREK, M., CULLEY, F. J., GORITZKA, M. & JOHANSSON, C. 2016. Alveolar Macrophages Can Control Respiratory Syncytial Virus Infection in the Absence of Type I Interferons. *J Innate Immun,* 8**,** 452-63.
MALHOTRA, R., WARD, M., BRIGHT, H., PRIEST, R., FOSTER, M. R., HURLE, M., BLAIR, E. & BIRD, M. 2003. Isolation and characterisation of potential respiratory syncytial virus receptor(s) on epithelial cells. *Microbes Infect,* 5**,** 123-33.
MARR, N. & TURVEY, S. E. 2012. Role of human TLR4 in respiratory syncytial virus-induced NF-kappaB activation, viral entry and replication. *Innate Immun,* 18**,** 856-65.
MARTY, A., MEANGER, J., MILLS, J., SHIELDS, B. & GHILDYAL, R. 2004. Association of matrix protein of respiratory syncytial virus with the host cell membrane of infected cells. *Arch Virol,* 149**,** 199-210.

MASANTE, C., EL NAJJAR, F., CHANG, A., JONES, A., MONCMAN, C. L. & DUTCH, R. E. 2014. The human metapneumovirus small hydrophobic protein has properties consistent with those of a viroporin and can modulate viral fusogenic activity. *J Virol,* 88**,** 6423-33.

MASON, S. W., ABERG, E., LAWETZ, C., DELONG, R., WHITEHEAD, P. & LIUZZI, M. 2003. Interaction between human respiratory syncytial virus (RSV) M2-1 and P proteins is required for reconstitution of M2-1-dependent RSV minigenome activity. *J Virol,* 77**,** 10670-6.

MCDONALD, T. P., PITT, A. R., BROWN, G., RIXON, H. W. & SUGRUE, R. J. 2004. Evidence that the respiratory syncytial virus polymerase complex associates with lipid rafts in virus-infected cells: a proteomic analysis. *Virology,* 330**,** 147-57.

MCFARLAND, E. J., KARRON, R. A., MURESAN, P., CUNNINGHAM, C. K., LIBOUS, J., PERLOWSKI, C., THUMAR, B., GNANASHANMUGAM, D., MOYE, J., SCHAPPELL, E., BARR, E., REXROAD, V., FEARN, L., SPECTOR, S. A., AZIZ, M., CIELO, M., BENERI, C., WIZNIA, A., LUONGO, C., COLLINS, P. & BUCHHOLZ, U. J. 2020a. Live Respiratory Syncytial Virus Attenuated by M2-2 Deletion and Stabilized Temperature Sensitivity Mutation 1030s Is a Promising Vaccine Candidate in Children. *J Infect Dis,* 221**,** 534-543.

MCFARLAND, E. J., KARRON, R. A., MURESAN, P., CUNNINGHAM, C. K., PERLOWSKI, C., LIBOUS, J., OLIVA, J., JEAN-PHILIPPE, P., MOYE, J., SCHAPPELL, E., BARR, E., REXROAD, V., FEARN, L., CIELO, M., WIZNIA, A., DEVILLE, J. G., YANG, L., LUONGO, C., COLLINS, P. L. & BUCHHOLZ, U. J. 2020b. Live-Attenuated Respiratory Syncytial Virus Vaccine With M2-2 Deletion and With Small Hydrophobic Noncoding Region Is Highly Immunogenic in Children. *J Infect Dis,* 221**,** 2050-2059.

MCFARLAND, E. J., KARRON, R. A., MURESAN, P., CUNNINGHAM, C. K., VALENTINE, M. E., PERLOWSKI, C., THUMAR, B., GNANASHANMUGAM, D., SIBERRY, G. K., SCHAPPELL, E., BARR, E., REXROAD, V., YOGEV, R., SPECTOR, S. A., AZIZ, M., PATEL, N., CIELO, M., LUONGO, C., COLLINS, P. L., BUCHHOLZ, U. J. & INTERNATIONAL MATERNAL PEDIATRIC ADOLESCENT, A. C. T. S. T. 2018. Live-Attenuated Respiratory Syncytial Virus Vaccine Candidate With Deletion of RNA Synthesis Regulatory Protein M2-2 is Highly Immunogenic in Children. *J Infect Dis,* 217**,** 1347-1355.

MCLELLAN, J. S., RAY, W. C. & PEEPLES, M. E. 2013. Structure and function of respiratory syncytial virus surface glycoproteins. *Curr Top Microbiol Immunol,* 372**,** 83-104.

MCNAMARA, P. S., FLANAGAN, B. F., HART, C. A. & SMYTH, R. L. 2005. Production of chemokines in the lungs of infants with severe respiratory syncytial virus bronchiolitis. *J Infect Dis,* 191**,** 1225-32.

MCNAMARA, P. S., RITSON, P., SELBY, A., HART, C. A. & SMYTH, R. L. 2003. Bronchoalveolar lavage cellularity in infants with severe respiratory syncytial virus bronchiolitis. *Arch Dis Child,* 88**,** 922-6.

MCSWIGGEN, D. T., MIR, M., DARZACQ, X. & TJIAN, R. 2019. Evaluating phase separation in live cells: diagnosis, caveats, and functional consequences. *Genes Dev,* 33**,** 1619-1634.

MELERO, J. A., GARCÍA-BARRENO, B., MARTÍNEZ, I., PRINGLE, C. R. & CANE, P. A. 1997. Antigenic structure, evolution and immunobiology of

human respiratory syncytial virus attachment (G) protein. *J Gen Virol,* 78 (Pt 10)**,** 2411-8.
MERCIE, P., SEIGNEUR, M., BILHOU-NABERA, C., BOISSEAU, M. R. & BERNARD, P. 1998. [Nuclear transcription factor kappa B (NF-kappa B)]. *Rev Med Interne,* 19**,** 945-7.
MESHRAM, C. D., BAVISKAR, P. S., OGNIBENE, C. M. & OOMENS, A. G. P. 2016. The Respiratory Syncytial Virus Phosphoprotein, Matrix Protein, and Fusion Protein Carboxy-Terminal Domain Drive Efficient Filamentous Virus-Like Particle Formation. *J Virol,* 90**,** 10612-10628.
MITCHELL, S., VARGAS, J. & HOFFMANN, A. 2016. Signaling via the NFkappaB system. *Wiley Interdiscip Rev Syst Biol Med,* 8**,** 227-41.
MITRA, R., BAVISKAR, P., DUNCAN-DECOCQ, R. R., PATEL, D. & OOMENS, A. G. 2012. The human respiratory syncytial virus matrix protein is required for maturation of viral filaments. *J Virol,* 86**,** 4432-43.
MIYAIRI, I. & DEVINCENZO, J. P. 2008. Human genetic factors and respiratory syncytial virus disease severity. *Clin Microbiol Rev,* 21**,** 686-703.
MONEY, V. A., MCPHEE, H. K., MOSELY, J. A., SANDERSON, J. M. & YEO, R. P. 2009. Surface features of a Mononegavirales matrix protein indicate sites of membrane interaction. *Proc Natl Acad Sci U S A,* 106**,** 4441-6.
MOSHE, A. & GOROVITS, R. 2012. Virus-induced aggregates in infected cells. *Viruses,* 4**,** 2218-32.
MOULD, J. A., DRURY, J. E., FRINGS, S. M., KAUPP, U. B., PEKOSZ, A., LAMB, R. A. & PINTO, L. H. 2000. Permeation and activation of the M2 ion channel of influenza A virus. *J Biol Chem,* 275**,** 31038-50.
MUDOGO, C. N., FALKE, S., BROGNARO, H., DUSZENKO, M. & BETZEL, C. 2019. Protein phase separation and determinants of in cell crystallization. *Traffic*.
MURAO, L. E. & SHISLER, J. L. 2005. The MCV MC159 protein inhibits late, but not early, events of TNF-alpha-induced NF-kappaB activation. *Virology,* 340**,** 255-64.
MURATA, Y. 2009. Respiratory syncytial virus vaccine development. *Clin Lab Med,* 29**,** 725-39.
MURAWSKI, M. R., BOWEN, G. N., CERNY, A. M., ANDERSON, L. J., HAYNES, L. M., TRIPP, R. A., KURT-JONES, E. A. & FINBERG, R. W. 2009. Respiratory syncytial virus activates innate immunity through Toll-like receptor 2. *J Virol,* 83**,** 1492-500.
MURTHY, A. C. & FAWZI, N. L. 2020. The (un)structural biology of biomolecular liquid-liquid phase separation using NMR spectroscopy. *J Biol Chem*.
NAIR, H., SIMOES, E. A., RUDAN, I., GESSNER, B. D., AZZIZ-BAUMGARTNER, E., ZHANG, J. S. F., FEIKIN, D. R., MACKENZIE, G. A., MOIISI, J. C., ROCA, A., BAGGETT, H. C., ZAMAN, S. M., SINGLETON, R. J., LUCERO, M. G., CHANDRAN, A., GENTILE, A., COHEN, C., KRISHNAN, A., BHUTTA, Z. A., ARGUEDAS, A., CLARA, A. W., ANDRADE, A. L., OPE, M., RUVINSKY, R. O., HORTAL, M., MCCRACKEN, J. P., MADHI, S. A., BRUCE, N., QAZI, S. A., MORRIS, S. S., EL ARIFEEN, S., WEBER, M. W., SCOTT, J. A. G., BROOKS, W. A., BREIMAN, R. F., CAMPBELL, H. & SEVERE ACUTE LOWER RESPIRATORY INFECTIONS WORKING, G. 2013. Global and regional burden of hospital admissions for severe acute lower respiratory infections in young children in 2010: a systematic analysis. *Lancet,* 381**,** 1380-1390.

NEGASH, A. A., RAMOS, H. J., CROCHET, N., LAU, D. T., DOEHLE, B., PAPIC, N., DELKER, D. A., JO, J., BERTOLETTI, A., HAGEDORN, C. H. & GALE, M., JR. 2013. IL-1beta production through the NLRP3 inflammasome by hepatic macrophages links hepatitis C virus infection with liver inflammation and disease. *PLoS Pathog,* 9**,** e1003330.

NEILSON, K. A. & YUNIS, E. J. 1990. Demonstration of respiratory syncytial virus in an autopsy series. *Pediatr Pathol,* 10**,** 491-502.

NEVERS, Q., ALBERTINI, A. A., LAGAUDRIERE-GESBERT, C. & GAUDIN, Y. 2020. Negri bodies and other virus membrane-less replication compartments. *Biochim Biophys Acta Mol Cell Res,* 1867**,** 118831.

NEWTON, A. H., CARDANI, A. & BRACIALE, T. J. 2016. The host immune response in respiratory virus infection: balancing virus clearance and immunopathology. *Semin Immunopathol,* 38**,** 471-82.

NICHOLS, D. B. & SHISLER, J. L. 2006. The MC160 protein expressed by the dermatotropic poxvirus molluscum contagiosum virus prevents tumor necrosis factor alpha-induced NF-kappaB activation via inhibition of I kappa kinase complex formation. *J Virol,* 80**,** 578-86.

NICHOLS, D. B. & SHISLER, J. L. 2009. Poxvirus MC160 protein utilizes multiple mechanisms to inhibit NF-kappaB activation mediated via components of the tumor necrosis factor receptor 1 signal transduction pathway. *J Virol,* 83**,** 3162-74.

NIETO-TORRES, J. L., DEDIEGO, M. L., VERDIA-BAGUENA, C., JIMENEZ-GUARDENO, J. M., REGLA-NAVA, J. A., FERNANDEZ-DELGADO, R., CASTANO-RODRIGUEZ, C., ALCARAZ, A., TORRES, J., AGUILELLA, V. M. & ENJUANES, L. 2014. Severe acute respiratory syndrome coronavirus envelope protein ion channel activity promotes virus fitness and pathogenesis. *PLoS Pathog,* 10**,** e1004077.

NIKOLIC, J., CIVAS, A., LAMA, Z., LAGAUDRIERE-GESBERT, C. & BLONDEL, D. 2016. Rabies Virus Infection Induces the Formation of Stress Granules Closely Connected to the Viral Factories. *PLoS Pathog,* 12**,** e1005942.

NIKOLIC, J., LAGAUDRIERE-GESBERT, C., SCRIMA, N., BLONDEL, D. & GAUDIN, Y. 2018. [Rabies virus factories are formed by liquid-liquid phase separation]. *Med Sci (Paris),* 34**,** 203-205.

NIKOLIC, J., LE BARS, R., LAMA, Z., SCRIMA, N., LAGAUDRIERE-GESBERT, C., GAUDIN, Y. & BLONDEL, D. 2017. Negri bodies are viral factories with properties of liquid organelles. *Nat Commun,* 8**,** 58.

NORRBY, E., MARUSYK, H. & ORVELL, C. 1970. Morphogenesis of respiratory syncytial virus in a green monkey kidney cell line (Vero). *J Virol,* 6**,** 237-42.

NOTON, S. L. & FEARNS, R. 2015. Initiation and regulation of paramyxovirus transcription and replication. *Virology,* 479-480**,** 545-54.

OECKINGHAUS, A., HAYDEN, M. S. & GHOSH, S. 2011. Crosstalk in NF-kappa B signaling pathways. *Nature Immunology,* 12**,** 695-708.

OKSAYAN, S., ITO, N., MOSELEY, G. & BLONDEL, D. 2012. Subcellular trafficking in rhabdovirus infection and immune evasion: a novel target for therapeutics. *Infect Disord Drug Targets,* 12**,** 38-58.

OLMSTED, R. A. & COLLINS, P. L. 1989. The 1A protein of respiratory syncytial virus is an integral membrane protein present as multiple, structurally distinct species. *J Virol,* 63**,** 2019-29.

ONOMOTO, K., YONEYAMA, M., FUNG, G., KATO, H. & FUJITA, T. 2014. Antiviral innate immunity and stress granule responses. *Trends Immunol,* 35**,** 420-8.
PANUSKA, J. R., CIRINO, N. M., MIDULLA, F., DESPOT, J. E., MCFADDEN, E. R., JR. & HUANG, Y. T. 1990. Productive infection of isolated human alveolar macrophages by respiratory syncytial virus. *J Clin Invest,* 86**,** 113-9.
PARKS, G. D. & ALEXANDER-MILLER, M. A. 2013. Paramyxovirus activation and inhibition of innate immune responses. *J Mol Biol,* 425**,** 4872-92.
PATEL, A., MALINOVSKA, L., SAHA, S., WANG, J., ALBERTI, S., KRISHNAN, Y. & HYMAN, A. A. 2017. ATP as a biological hydrotrope. *Science,* 356**,** 753-756.
PEREIRA, N., CARDONE, C., LASSOUED, S., GALLOUX, M., FIX, J., ASSRIR, N., LESCOP, E., BONTEMS, F., ELEOUET, J. F. & SIZUN, C. 2017. New Insights into Structural Disorder in Human Respiratory Syncytial Virus Phosphoprotein and Implications for Binding of Protein Partners. *J Biol Chem,* 292**,** 2120-2131.
PEREZ, M., GARCIA-BARRENO, B., MELERO, J. A., CARRASCO, L. & GUINEA, R. 1997. Membrane permeability changes induced in Escherichia coli by the SH protein of human respiratory syncytial virus. *Virology,* 235**,** 342-51.
PEREZ-PEPE, M., FERNANDEZ-ALVAREZ, A. J. & BOCCACCIO, G. L. 2018. Life and Work of Stress Granules and Processing Bodies: New Insights into Their Formation and Function. *Biochemistry,* 57**,** 2488-2498.
PFALLER, C. K., CATTANEO, R. & SCHNELL, M. J. 2015. Reverse genetics of Mononegavirales: How they work, new vaccines, and new cancer therapeutics. *Virology,* 479-480**,** 331-44.
PINTO, L. H., HOLSINGER, L. J. & LAMB, R. A. 1992. Influenza virus M2 protein has ion channel activity. *Cell,* 69**,** 517-28.
PLOUBIDOU, A. & WAY, M. 2001. Viral transport and the cytoskeleton. *Curr Opin Cell Biol,* 13**,** 97-105.
POLLOCK, N., TAYLOR, G., JOBE, F. & GUZMAN, E. 2017. Modulation of the transcription factor NF-kappaB in antigen-presenting cells by bovine respiratory syncytial virus small hydrophobic protein. *J Gen Virol,* 98**,** 1587-1599.
POWELL, M. L. 2010. Translational termination-reinitiation in RNA viruses. *Biochem Soc Trans,* 38**,** 1558-64.
PRINCE, G. A., JENSON, A. B., HEMMING, V. G., MURPHY, B. R., WALSH, E. E., HORSWOOD, R. L. & CHANOCK, R. M. 1986. Enhancement of respiratory syncytial virus pulmonary pathology in cotton rats by prior intramuscular inoculation of formalin-inactiva ted virus. *J Virol,* 57**,** 721-8.
QIN, Z. 2012. The use of THP-1 cells as a model for mimicking the function and regulation of monocytes and macrophages in the vasculature. *Atherosclerosis,* 221**,** 2-11.
RANDALL, C. M., JOKELA, J. A. & SHISLER, J. L. 2012. The MC159 protein from the molluscum contagiosum poxvirus inhibits NF-kappaB activation by interacting with the IkappaB kinase complex. *J Immunol,* 188**,** 2371-9.
REN, J., LIU, G., GO, J., KOLLI, D., ZHANG, G. & BAO, X. 2014. Human metapneumovirus M2-2 protein inhibits innate immune response in monocyte-derived dendritic cells. *PLoS One,* 9**,** e91865.

REN, J., LIU, T., PANG, L., LI, K., GAROFALO, R. P., CASOLA, A. & BAO, X. 2011. A novel mechanism for the inhibition of interferon regulatory factor-3-dependent gene expression by human respiratory syncytial virus NS1 protein. *J Gen Virol,* 92**,** 2153-2159.

REN, J., WANG, Q., KOLLI, D., PRUSAK, D. J., TSENG, C. T., CHEN, Z. J., LI, K., WOOD, T. G. & BAO, X. 2012. Human metapneumovirus M2-2 protein inhibits innate cellular signaling by targeting MAVS. *J Virol,* 86**,** 13049-61.

RICHARD, C. A., RINCHEVAL, V., LASSOUED, S., FIX, J., CARDONE, C., ESNEAU, C., NEKHAI, S., GALLOUX, M., RAMEIX-WELTI, M. A., SIZUN, C. & ELEOUET, J. F. 2018. RSV hijacks cellular protein phosphatase 1 to regulate M2-1 phosphorylation and viral transcription. *PLoS Pathog,* 14**,** e1006920.

RIFFAULT, S., HÄGGLUND, S., GUZMAN, E., NÄSLUND, K., JOUNEAU, L., DUBUQUOY, C., PIETRALUNGA, V., LAUBRETON, D., BOULESTEIX, O., GAUTHIER, D., REMOT, A., BOUKARIDI, A., FALK, A., SHEVCHENKO, G., LIND, S. B., VARGMAR, K., ZHANG, B., KWONG, P. D., RODRIGUEZ, M. J., DURAN, M. G., SCHWARTZ-CORNIL, I., ELÉOUËT, J. F., TAYLOR, G. & VALARCHER, J. F. 2020. A Single Shot Pre-fusion-Stabilized Bovine RSV F Vaccine is Safe and Effective in Newborn Calves with Maternally Derived Antibodies. *Vaccines (Basel),* 8.

RIMA, B., COLLINS, P., EASTON, A., FOUCHIER, R., KURATH, G., LAMB, R. A., LEE, B., MAISNER, A., ROTA, P., WANG, L. & ICTV REPORT, C. 2017. ICTV Virus Taxonomy Profile: Pneumoviridae. *J Gen Virol,* 98**,** 2912-2913.

RINCHEVAL, V., LELEK, M., GAULT, E., BOUILLIER, C., SITTERLIN, D., BLOUQUIT-LAYE, S., GALLOUX, M., ZIMMER, C., ELEOUET, J. F. & RAMEIX-WELTI, M. A. 2017. Functional organization of cytoplasmic inclusion bodies in cells infected by respiratory syncytial virus. *Nat Commun,* 8**,** 563.

RINGEL, M., HEINER, A., BEHNER, L., HALWE, S., SAUERHERING, L., BECKER, N., DIETZEL, E., SAWATSKY, B., KOLESNIKOVA, L. & MAISNER, A. 2019. Nipah virus induces two inclusion body populations: Identification of novel inclusions at the plasma membrane. *PLoS Pathog,* 15**,** e1007733.

RIXON, H. W. M., BROWN, G., AITKEN, J., MCDONALD, T., GRAHAM, S. & SUGRUE, R. J. 2004. The small hydrophobic (SH) protein accumulates within lipid-raft structures of the Golgi complex during respiratory syncytial virus infection. *J Gen Virol,* 85**,** 1153-1165.

RODRIGUEZ, W. J., GRUBER, W. C., GROOTHUIS, J. R., SIMOES, E. A., ROSAS, A. J., LEPOW, M., KRAMER, A. & HEMMING, V. 1997. Respiratory syncytial virus immune globulin treatment of RSV lower respiratory tract infection in previously healthy children. *Pediatrics,* 100**,** 937-42.

ROTHE, M., SARMA, V., DIXIT, V. M. & GOEDDEL, D. V. 1995. TRAF2-mediated activation of NF-kappa B by TNF receptor 2 and CD40. *Science,* 269**,** 1424-7.

RUCKWARDT, T. J., MORABITO, K. M. & GRAHAM, B. S. 2019. Immunological Lessons from Respiratory Syncytial Virus Vaccine Development. *Immunity,* 51**,** 429-442.

RUDD, B. D., BURSTEIN, E., DUCKETT, C. S., LI, X. & LUKACS, N. W. 2005. Differential role for TLR3 in respiratory syncytial virus-induced chemokine expression. *J Virol,* 79**,** 3350-7.

RUIGROK, R. W. & CRÉPIN, T. 2010. Nucleoproteins of negative strand RNA viruses; RNA binding, oligomerisation and binding to polymerase co-factor. *Viruses,* 2**,** 27-32.

RUSSELL, C. J., SIMOES, E. A. F. & HURWITZ, J. L. 2018. Vaccines for the Paramyxoviruses and Pneumoviruses: Successes, Candidates, and Hurdles. *Viral Immunol,* 31**,** 133-141.

RUSSELL, R. F., MCDONALD, J. U., IVANOVA, M., ZHONG, Z., BUKREYEV, A. & TREGONING, J. S. 2015. Partial Attenuation of Respiratory Syncytial Virus with a Deletion of a Small Hydrophobic Gene Is Associated with Elevated Interleukin-1beta Responses. *J Virol,* 89**,** 8974-81.

SABBAH, A., CHANG, T. H., HARNACK, R., FROHLICH, V., TOMINAGA, K., DUBE, P. H., XIANG, Y. & BOSE, S. 2009. Activation of innate immune antiviral responses by Nod2. *Nat Immunol,* 10**,** 1073-80.

SACCO, R. E., MCGILL, J. L., PILLATZKI, A. E., PALMER, M. V. & ACKERMANN, M. R. 2014. Respiratory syncytial virus infection in cattle. *Vet Pathol,* 51**,** 427-36.

SAMAL, S. K. & PASTEY, M. K. 1997. Role of envelope glycoproteins of bovine respiratory syncytial virus in cell fusion. *Indian J Biochem Biophys,* 34**,** 181-5.

SAMAL, S. K. & ZAMORA, M. 1991. Nucleotide sequence analysis of a matrix and small hydrophobic protein dicistronic mRNA of bovine respiratory syncytial virus demonstrates extensive sequence divergence of the small hydrophobic protein from that of human respiratory syncytial virus. *J Gen Virol,* 72 (Pt 7)**,** 1715-20.

SAUTER, D., HOTTER, D., VAN DRIESSCHE, B., STURZEL, C. M., KLUGE, S. F., WILDUM, S., YU, H., BAUMANN, B., WIRTH, T., PLANTIER, J. C., LEOZ, M., HAHN, B. H., VAN LINT, C. & KIRCHHOFF, F. 2015. Differential regulation of NF-kappaB-mediated proviral and antiviral host gene expression by primate lentiviral Nef and Vpu proteins. *Cell Rep,* 10**,** 586-99.

SCHLENDER, J., BOSSERT, B., BUCHHOLZ, U. & CONZELMANN, K. K. 2000. Bovine respiratory syncytial virus nonstructural proteins NS1 and NS2 cooperatively antagonize alpha/beta interferon-induced antiviral response. *J Virol,* 74**,** 8234-42.

SCHMITZ, M. L. 1995. Function and activation of the transcription factor NF-kappa B in the response to toxins and pathogens. *Toxicol Lett,* 82-83**,** 407-11.

SCHUDT, G., DOLNIK, O., KOLESNIKOVA, L., BIEDENKOPF, N., HERWIG, A. & BECKER, S. 2015. Transport of Ebolavirus Nucleocapsids Is Dependent on Actin Polymerization: Live-Cell Imaging Analysis of Ebolavirus-Infected Cells. *J Infect Dis,* 212 Suppl 2**,** S160-6.

SCHUDT, G., KOLESNIKOVA, L., DOLNIK, O., SODEIK, B. & BECKER, S. 2013. Live-cell imaging of Marburg virus-infected cells uncovers actin-dependent transport of nucleocapsids over long distances. *Proc Natl Acad Sci U S A,* 110**,** 14402-7.

SEDEYN, K., SCHEPENS, B. & SAELENS, X. 2019. Respiratory syncytial virus nonstructural proteins 1 and 2: Exceptional disrupters of innate immune responses. *PLoS Pathog,* 15**,** e1007984.

SEGOVIA, J., SABBAH, A., MGBEMENA, V., TSAI, S.-Y., CHANG, T.-H., BERTON, M. T., MORRIS, I. R., ALLEN, I. C., TING, J. P. Y. & BOSE, S. 2012a. TLR2/MyD88/NF-kappa B Pathway, Reactive Oxygen Species, Potassium Efflux Activates NLRP3/ASC Inflammasome during Respiratory Syncytial Virus Infection. *Plos One,* 7.

SEGOVIA, J., SABBAH, A., MGBEMENA, V., TSAI, S. Y., CHANG, T. H., BERTON, M. T., MORRIS, I. R., ALLEN, I. C., TING, J. P. & BOSE, S. 2012b. TLR2/MyD88/NF-κB pathway, reactive oxygen species, potassium efflux activates NLRP3/ASC inflammasome during respiratory syncytial virus infection. *PLoS One,* 7**,** e29695.

SHAHRIARI, S., WEI, K. J. & GHILDYAL, R. 2018. Respiratory Syncytial Virus Matrix (M) Protein Interacts with Actin In Vitro and in Cell Culture. *Viruses,* 10.

SHAIKH, F. Y., COX, R. G., LIFLAND, A. W., HOTARD, A. L., WILLIAMS, J. V., MOORE, M. L., SANTANGELO, P. J. & CROWE, J. E., JR. 2012a. A critical phenylalanine residue in the respiratory syncytial virus fusion protein cytoplasmic tail mediates assembly of internal viral proteins into viral filaments and particles. *mBio,* 3.

SHAIKH, F. Y. & CROWE, J. E., JR. 2013. Molecular mechanisms driving respiratory syncytial virus assembly. *Future Microbiol,* 8**,** 123-31.

SHAIKH, F. Y., UTLEY, T. J., CRAVEN, R. E., ROGERS, M. C., LAPIERRE, L. A., GOLDENRING, J. R. & CROWE, J. E., JR. 2012b. Respiratory syncytial virus assembles into structured filamentous virion particles independently of host cytoskeleton and related proteins. *PLoS One,* 7**,** e40826.

SHAN, J., BRITTON, P. N., KING, C. L. & BOOY, R. 2021. The immunogenicity and safety of respiratory syncytial virus vaccines in development: A systematic review. *Influenza Other Respir Viruses,* 15**,** 539-551.

SHI, T., MCALLISTER, D. A., O'BRIEN, K. L., SIMOES, E. A. F., MADHI, S. A., GESSNER, B. D., POLACK, F. P., BALSELLS, E., ACACIO, S., AGUAYO, C., ALASSANI, I., ALI, A., ANTONIO, M., AWASTHI, S., AWORI, J. O., AZZIZ-BAUMGARTNER, E., BAGGETT, H. C., BAILLIE, V. L., BALMASEDA, A., BARAHONA, A., BASNET, S., BASSAT, Q., BASUALDO, W., BIGOGO, G., BONT, L., BREIMAN, R. F., BROOKS, W. A., BROOR, S., BRUCE, N., BRUDEN, D., BUCHY, P., CAMPBELL, S., CAROSONE-LINK, P., CHADHA, M., CHIPETA, J., CHOU, M., CLARA, W., COHEN, C., DE CUELLAR, E., DANG, D. A., DASH-YANDAG, B., DELORIA-KNOLL, M., DHERANI, M., EAP, T., EBRUKE, B. E., ECHAVARRIA, M., DE FREITAS LAZARO EMEDIATO, C. C., FASCE, R. A., FEIKIN, D. R., FENG, L., GENTILE, A., GORDON, A., GOSWAMI, D., GOYET, S., GROOME, M., HALASA, N., HIRVE, S., HOMAIRA, N., HOWIE, S. R. C., JARA, J., JROUNDI, I., KARTASASMITA, C. B., KHURI-BULOS, N., KOTLOFF, K. L., KRISHNAN, A., LIBSTER, R., LOPEZ, O., LUCERO, M. G., LUCION, F., LUPISAN, S. P., MARCONE, D. N., MCCRACKEN, J. P., MEJIA, M., MOISI, J. C., MONTGOMERY, J. M., MOORE, D. P., MORALEDA, C., MOYES, J., MUNYWOKI, P., MUTYARA, K., NICOL, M. P., NOKES, D. J., NYMADAWA, P., DA COSTA OLIVEIRA, M. T., OSHITANI, H., PANDEY, N., PARANHOS-BACCALA, G., PHILLIPS, L. N., PICOT, V. S., RAHMAN, M., RAKOTO-ANDRIANARIVELO, M., RASMUSSEN, Z. A., RATH, B. A., ROBINSON, A., ROMERO, C., RUSSOMANDO, G.,

SALIMI, V., SAWATWONG, P., SCHELTEMA, N., SCHWEIGER, B., et al. 2017. Global, regional, and national disease burden estimates of acute lower respiratory infections due to respiratory syncytial virus in young children in 2015: a systematic review and modelling study. *Lancet,* 390**,** 946-958.

SHIN, Y., BERRY, J., PANNUCCI, N., HAATAJA, M. P., TOETTCHER, J. E. & BRANGWYNNE, C. P. 2017. Spatiotemporal Control of Intracellular Phase Transitions Using Light-Activated optoDroplets. *Cell,* 168**,** 159-171 e14.

SHRIVASTAVA, S., MUKHERJEE, A., RAY, R. & RAY, R. B. 2013. Hepatitis C virus induces interleukin-1beta (IL-1beta)/IL-18 in circulatory and resident liver macrophages. *J Virol,* 87**,** 12284-90.

SIEZEN, C. L., BONT, L., HODEMAEKERS, H. M., ERMERS, M. J., DOORNBOS, G., VAN'T SLOT, R., WIJMENGA, C., HOUWELINGEN, H. C., KIMPEN, J. L., KIMMAN, T. G., HOEBEE, B. & JANSSEN, R. 2009. Genetic susceptibility to respiratory syncytial virus bronchiolitis in preterm children is associated with airway remodeling genes and innate immune genes. *Pediatr Infect Dis J,* 28**,** 333-5.

SMYTH, R. L. & OPENSHAW, P. J. 2006. Bronchiolitis. *Lancet,* 368**,** 312-22.

SPANN, K. M., TRAN, K. C., CHI, B., RABIN, R. L. & COLLINS, P. L. 2004. Suppression of the induction of alpha, beta, and lambda interferons by the NS1 and NS2 proteins of human respiratory syncytial virus in human epithelial cells and macrophages [corrected]. *J Virol,* 78**,** 4363-9.

SPANN, K. M., TRAN, K. C. & COLLINS, P. L. 2005. Effects of nonstructural proteins NS1 and NS2 of human respiratory syncytial virus on interferon regulatory factor 3, NF-kappaB, and proinflammatory cytokines. *J Virol,* 79**,** 5353-62.

SUN, S. C., GANCHI, P. A., BALLARD, D. W. & GREENE, W. C. 1993. NF-kappa B controls expression of inhibitor I kappa B alpha: evidence for an inducible autoregulatory pathway. *Science,* 259**,** 1912-5.

SUN, Y. & LOPEZ, C. B. 2016. The innate immune response to RSV: Advances in our understanding of critical viral and host factors. *Vaccine*.

SWEDAN, S., MUSIYENKO, A. & BARIK, S. 2009. Respiratory syncytial virus nonstructural proteins decrease levels of multiple members of the cellular interferon pathways. *J Virol,* 83**,** 9682-93.

TAL, G., MANDELBERG, A., DALAL, I., CESAR, K., SOMEKH, E., TAL, A., ORON, A., ITSKOVICH, S., BALLIN, A., HOURI, S., BEIGELMAN, A., LIDER, O., RECHAVI, G. & AMARIGLIO, N. 2004. Association between common Toll-like receptor 4 mutations and severe respiratory syncytial virus disease. *J Infect Dis,* 189**,** 2057-63.

TALEB, S. A., AL THANI, A. A., AL ANSARI, K. & YASSINE, H. M. 2018. Human respiratory syncytial virus: pathogenesis, immune responses, and current vaccine approaches. *Eur J Clin Microbiol Infect Dis,* 37**,** 1817-1827.

TANG, R. S., NGUYEN, N., CHENG, X. & JIN, H. 2001. Requirement of cysteines and length of the human respiratory syncytial virus M2-1 protein for protein function and virus viability. *J Virol,* 75**,** 11328-35.

TAPIA, L. I., SHAW, C. A., AIDEYAN, L. O., JEWELL, A. M., DAWSON, B. C., HAQ, T. R. & PIEDRA, P. A. 2014. Gene sequence variability of the three surface proteins of human respiratory syncytial virus (HRSV) in Texas. *PLoS One,* 9**,** e90786.

TAYLOR, G. 2017. Animal models of respiratory syncytial virus infection. *Vaccine,* 35**,** 469-480.
TAYLOR, G., STOTT, E. J., BEW, M., FERNIE, B. F., COTE, P. J., COLLINS, A. P., HUGHES, M. & JEBBETT, J. 1984. Monoclonal antibodies protect against respiratory syncytial virus infection in mice. *Immunology,* 52**,** 137-42.
TAYLOR, G., STOTT, E. J., FURZE, J., FORD, J. & SOPP, P. 1992. Protective epitopes on the fusion protein of respiratory syncytial virus recognized by murine and bovine monoclonal antibodies. *J Gen Virol,* 73 (Pt 9)**,** 2217-23.
TAYLOR, G., WYLD, S., VALARCHER, J.-F., GUZMAN, E., THOM, M., WIDDISON, S. & BUCHHOLZ, U. J. 2014. Recombinant bovine respiratory syncytial virus with deletion of the SH gene induces increased apoptosis and pro-inflammatory cytokines in vitro, and is attenuated and induces protective immunity in calves. *Journal of General Virology,* 95**,** 1244-1254.
TAYYARI, F., MARCHANT, D., MORAES, T. J., DUAN, W., MASTRANGELO, P. & HEGELE, R. G. 2011. Identification of nucleolin as a cellular receptor for human respiratory syncytial virus. *Nat Med,* 17**,** 1132-5.
TECHAARPORNKUL, S., BARRETTO, N. & PEEPLES, M. E. 2001. Functional analysis of recombinant respiratory syncytial virus deletion mutants lacking the small hydrophobic and/or attachment glycoprotein gene. *J Virol,* 75**,** 6825-34.
TECHAARPORNKUL, S., COLLINS, P. L. & PEEPLES, M. E. 2002. Respiratory syncytial virus with the fusion protein as its only viral glycoprotein is less dependent on cellular glycosaminoglycans for attachment than complete virus. *Virology,* 294**,** 296-304.
TENG, M. N., WHITEHEAD, S. S. & COLLINS, P. L. 2001. Contribution of the respiratory syncytial virus G glycoprotein and its secreted and membrane-bound forms to virus replication in vitro and in vivo. *Virology,* 289**,** 283-96.
THE UNIPROT, C. 2017. UniProt: the universal protein knowledgebase. *Nucleic Acids Res,* 45**,** D158-D169.
TIAN, B., ZHANG, Y., LUXON, B. A., GAROFALO, R. P., CASOLA, A., SINHA, M. & BRASIER, A. R. 2002. Identification of NF-kappaB-dependent gene networks in respiratory syncytial virus-infected cells. *J Virol,* 76**,** 6800-14.
TO, J. & TORRES, J. 2018. Beyond Channel Activity: Protein-Protein Interactions Involving Viroporins. *Subcell Biochem,* 88**,** 329-377.
TRAN, T. L., CASTAGNE, N., DUBOSCLARD, V., NOINVILLE, S., KOCH, E., MOUDJOU, M., HENRY, C., BERNARD, J., YEO, R. P. & ELEOUET, J. F. 2009. The respiratory syncytial virus M2-1 protein forms tetramers and interacts with RNA and P in a competitive manner. *J Virol,* 83**,** 6363-74.
TREVISAN, M., DI ANTONIO, V., RADEGHIERI, A., PALU, G., GHILDYAL, R. & ALVISI, G. 2018. Molecular Requirements for Self-Interaction of the Respiratory Syncytial Virus Matrix Protein in Living Mammalian Cells. *Viruses,* 10.
TRIANTAFILOU, K., KAR, S., VAKAKIS, E., KOTECHA, S. & TRIANTAFILOU, M. 2013. Human respiratory syncytial virus viroporin SH: a viral recognition pathway used by the host to signal inflammasome activation. *Thorax,* 68**,** 66-75.
TRIPP, R. A., JONES, L. P., HAYNES, L. M., ZHENG, H., MURPHY, P. M. & ANDERSON, L. J. 2001. CX3C chemokine mimicry by respiratory syncytial virus G glycoprotein. *Nat Immunol,* 2**,** 732-8.

TRIPP, R. A., MOORE, D., JONES, L., SULLENDER, W., WINTER, J. & ANDERSON, L. J. 1999. Respiratory syncytial virus G and/or SH protein alters Th1 cytokines, natural killer cells, and neutrophils responding to pulmonary infection in BALB/c mice. *J Virol,* 73**,** 7099-107.

TSUCHIYA, S., YAMABE, M., YAMAGUCHI, Y., KOBAYASHI, Y., KONNO, T. & TADA, K. 1980. Establishment and characterization of a human acute monocytic leukemia cell line (THP-1). *Int J Cancer,* 26**,** 171-6.

ULLOA, L., SERRA, R., ASENJO, A. & VILLANUEVA, N. 1998. Interactions between cellular actin and human respiratory syncytial virus (HRSV). *Virus Res,* 53**,** 13-25.

UTLEY, T. J., DUCHARME, N. A., VARTHAKAVI, V., SHEPHERD, B. E., SANTANGELO, P. J., LINDQUIST, M. E., GOLDENRING, J. R. & CROWE, J. E., JR. 2008. Respiratory syncytial virus uses a Vps4-independent budding mechanism controlled by Rab11-FIP2. *Proc Natl Acad Sci U S A,* 105**,** 10209-14.

UVERSKY, V. N. 2017. Intrinsically disordered proteins in overcrowded milieu: Membrane-less organelles, phase separation, and intrinsic disorder. *Curr Opin Struct Biol,* 44**,** 18-30.

VALARCHER, J.-F. & TAYLOR, G. 2007. Bovine respiratory syncytial virus infection. *Veterinary Research,* 38**,** 153-180.

VALARCHER, J. F., FURZE, J., WYLD, S., COOK, R., CONZELMANN, K. K. & TAYLOR, G. 2003. Role of alpha/beta interferons in the attenuation and immunogenicity of recombinant bovine respiratory syncytial viruses lacking NS proteins. *J Virol,* 77**,** 8426-39.

VALARCHER, J. F., HÄGGLUND, S., NÄSLUND, K., JOUNEAU, L., MALMSTRÖM, E., BOULESTEIX, O., PINARD, A., LEGUÉRÉ, D., DESLIS, A., GAUTHIER, D., DUBUQUOY, C., PIETRALUNGA, V., RÉMOT, A., FALK, A., SHEVCHENKO, G., BERGSTRÖM LIND, S., VON BRÖMSSEN, C., VARGMAR, K., ZHANG, B., KWONG, P. D., RODRIGUEZ, M. J., GARCIA DURAN, M., SCHWARTZ-CORNIL, I., TAYLOR, G. & RIFFAULT, S. 2021. Single-Shot Vaccines against Bovine Respiratory Syncytial Virus (BRSV): Comparative Evaluation of Long-Term Protection after Immunization in the Presence of BRSV-Specific Maternal Antibodies. *Vaccines (Basel),* 9.

VAN DRUNEN LITTEL-VAN DEN HURK, S. & WATKISS, E. R. 2012. Pathogenesis of respiratory syncytial virus. *Curr Opin Virol,* 2**,** 300-5.

VANOVER, D., SMITH, D. V., BLANCHARD, E. L., ALONAS, E., KIRSCHMAN, J. L., LIFLAND, A. W., ZURLA, C. & SANTANGELO, P. J. 2017. RSV glycoprotein and genomic RNA dynamics reveal filament assembly prior to the plasma membrane. *Nat Commun,* 8**,** 667.

WALSH, E. E. & HRUSKA, J. 1983. Monoclonal antibodies to respiratory syncytial virus proteins: identification of the fusion protein. *J Virol,* 47**,** 171-7.

WANG, K., XIE, S. & SUN, B. 2011. Viral proteins function as ion channels. *Biochim Biophys Acta,* 1808**,** 510-5.

WHELAN, J. N., REDDY, K. D., UVERSKY, V. N. & TENG, M. N. 2016. Functional correlations of respiratory syncytial virus proteins to intrinsic disorder. *Mol Biosyst,* 12**,** 1507-26.

WHELAN, S. P., BARR, J. N. & WERTZ, G. W. 2004. Transcription and replication of nonsegmented negative-strand RNA viruses. *Curr Top Microbiol Immunol,* 283**,** 61-119.

WHITE, J. P. & LLOYD, R. E. 2012. Regulation of stress granules in virus systems. *Trends Microbiol,* 20**,** 175-83.
WHITEHEAD, S. S., BUKREYEV, A., TENG, M. N., FIRESTONE, C. Y., ST CLAIRE, M., ELKINS, W. R., COLLINS, P. L. & MURPHY, B. R. 1999. Recombinant respiratory syncytial virus bearing a deletion of either the NS2 or SH gene is attenuated in chimpanzees. *J Virol,* 73**,** 3438-42.
WILEMAN, T. 2006. Aggresomes and autophagy generate sites for virus replication. *Science,* 312**,** 875-8.
WILLIAMS, K., BASTIAN, A. R., FELDMAN, R. A., OMORUYI, E., DE PAEPE, E., HENDRIKS, J., VAN ZEEBURG, H., GODEAUX, O., LANGEDIJK, J. P. M., SCHUITEMAKER, H., SADOFF, J. & CALLENDRET, B. 2020. Phase 1 Safety and Immunogenicity Study of a Respiratory Syncytial Virus Vaccine With an Adenovirus 26 Vector Encoding Prefusion F (Ad26.RSV.preF) in Adults Aged ≥60 Years. *J Infect Dis,* 222**,** 979-988.
WILSON, L., MCKINLAY, C., GAGE, P. & EWART, G. 2004. SARS coronavirus E protein forms cation-selective ion channels. *Virology,* 330**,** 322-31.
WILSON, R. L., FUENTES, S. M., WANG, P., TADDEO, E. C., KLATT, A., HENDERSON, A. J. & HE, B. 2006. Function of small hydrophobic proteins of paramyxovirus. *Journal of Virology,* 80**,** 1700-1709.
XU, P., LI, Z., SUN, D., LIN, Y., WU, J., ROTA, P. A. & HE, B. 2011. Rescue of wild-type mumps virus from a strain associated with recent outbreaks helps to define the role of the SH ORF in the pathogenesis of mumps virus. *Virology,* 417**,** 126-36.
YANG, Y., CONG, H., DU, N., HAN, X., SONG, L., ZHANG, W., LI, C. & TIEN, P. 2019. Mitochondria Redistribution in Enterovirus A71 Infected Cells and Its Effect on Virus Replication. *Virol Sin,* 34**,** 397-411.
YOBOUA, F., MARTEL, A., DUVAL, A., MUKAWERA, E. & GRANDVAUX, N. 2010. Respiratory syncytial virus-mediated NF-kappa B p65 phosphorylation at serine 536 is dependent on RIG-I, TRAF6, and IKK beta. *J Virol,* 84**,** 7267-77.
ZENG, R., CUI, Y., HAI, Y. & LIU, Y. 2012. Pattern recognition receptors for respiratory syncytial virus infection and design of vaccines. *Virus Res,* 167**,** 138-45.
ZHANG, L., BUKREYEV, A., THOMPSON, C. I., WATSON, B., PEEPLES, M. E., COLLINS, P. L. & PICKLES, R. J. 2005a. Infection of ciliated cells by human parainfluenza virus type 3 in an in vitro model of human airway epithelium. *J Virol,* 79**,** 1113-24.
ZHANG, L., PEEPLES, M. E., BOUCHER, R. C., COLLINS, P. L. & PICKLES, R. J. 2002. Respiratory syncytial virus infection of human airway epithelial cells is polarized, specific to ciliated cells, and without obvious cytopathology. *J Virol,* 76**,** 5654-66.
ZHANG, Q., MA, J. & YOO, D. 2017. Inhibition of NF-kappaB activity by the porcine epidemic diarrhea virus nonstructural protein 1 for innate immune evasion. *Virology,* 510**,** 111-126.
ZHANG, Q., SHARMA, N. R., ZHENG, Z. M. & CHEN, M. 2019. Viral Regulation of RNA Granules in Infected Cells. *Virol Sin,* 34**,** 175-191.
ZHANG, X., BOURHIS, J. M., LONGHI, S., CARSILLO, T., BUCCELLATO, M., MORIN, B., CANARD, B. & OGLESBEE, M. 2005b. Hsp72 recognizes a P binding motif in the measles virus N protein C-terminus. *Virology,* 337**,** 162-74.

ZHOU, H., CHENG, X. & JIN, H. 2003. Identification of amino acids that are critical to the processivity function of respiratory syncytial virus M2-1 protein. *J Virol,* 77**,** 5046-53.
ZHOU, Y., SU, J. M., SAMUEL, C. E. & MA, D. 2019. Measles Virus Forms Inclusion Bodies with Properties of Liquid Organelles. *J Virol,* 93.

Appendices

Appendix A RSV purification and examination by western blotting

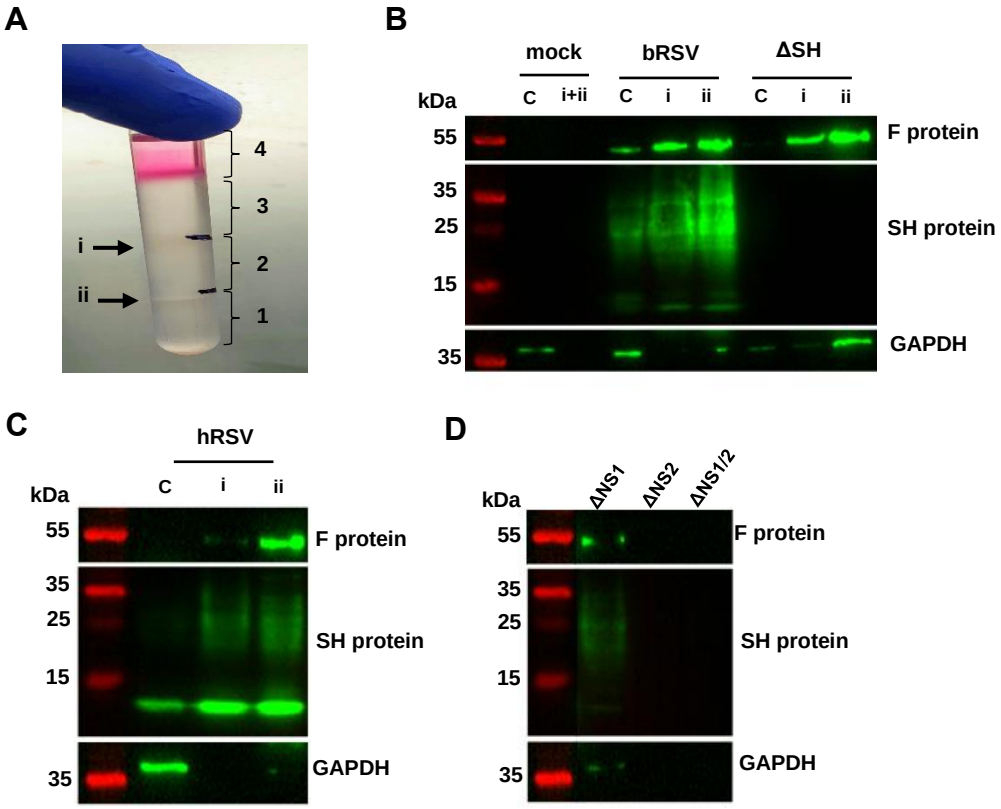

Figure A.1 RSV purification and examination by western blot. (A) Viral particles were purified by ultracentrifugation in a discontinuous sucrose density gradient (1: 60% (w/v) sucrose; 2: 45%; and 3: 30%) at 32,000 rpm for 1.5 hrs. 4 is the added PEG-precipitated virus layer. The black arrows represent collected fractions, i: top band; ii: bottom band. Examination of **(B)** wild type and ΔSH bRSV, and **(C)** hRSV by western blot analysis. C: unpurified virus/cell lysates; i: top band fraction; ii: bottom band fraction. **(D)** Purified ΔNS bRSV. No bands were visible; therefore, fractions were collected from both sucrose interfaces and combined.

Appendix B Examination of cytopathy induced by wild type bRSV and bRSV ΔSH

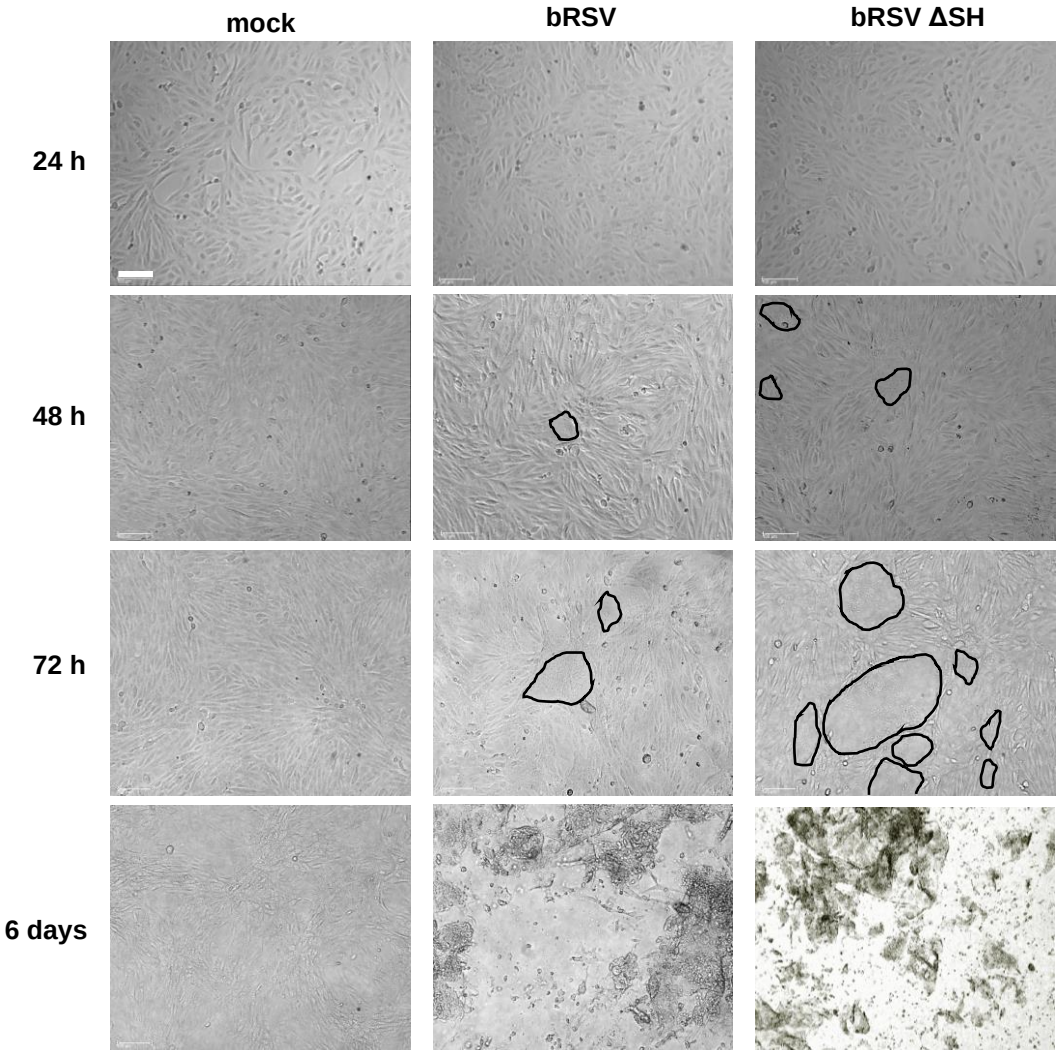

Figure B.1 Cytopathy induction by bRSV and bRSV ΔSH. Vero cells were mock infected, infected with bRSV or bRSV ΔSH viruses at MOI of 0.1. The presence of cpe was monitored and images of cells taken at 24, 48, 72 h and 6 days p.i (magnification, x10). White bar represents 100 μm and black borders indicate syncytia.

Appendix C Publication

AMERICAN SOCIETY FOR MICROBIOLOGY | Journal of Virology®

VIRUS-CELL INTERACTIONS

Respiratory Syncytial Virus Sequesters NF-κB Subunit p65 to Cytoplasmic Inclusion Bodies To Inhibit Innate Immune Signaling

Fatoumatta Jobe,[a] Jennifer Simpson,[a] Philippa Hawes,[a] Efrain Guzman,[a]* Dalan Bailey[a]

[a]The Pirbright Institute, Guildford, Surrey, United Kingdom

ABSTRACT Viruses routinely employ strategies to prevent the activation of innate immune signaling in infected cells. Respiratory syncytial virus (RSV) is no exception, as it encodes two accessory proteins (NS1 and NS2) which are well established to block interferon signaling. However, RSV-encoded mechanisms for inhibiting NF-κB signaling are less well characterized. In this study, we identified RSV-mediated antagonism of this pathway, independent of the NS1 and NS2 proteins and indeed distinct from other known viral mechanisms of NF-κB inhibition. In both human and bovine RSV-infected cells, we demonstrated that the p65 subunit of NF-κB is rerouted to perinuclear puncta in the cytoplasm, which are synonymous with viral inclusion bodies (IBs), the site for viral RNA replication. Captured p65 was unable to translocate to the nucleus or transactivate a NF-κB reporter following tumor necrosis factor alpha (TNF-α) stimulation, confirming the immune-antagonistic nature of this sequestration. Subsequently, we used correlative light electron microscopy (CLEM) to colocalize the RSV N protein and p65 within bovine RSV (bRSV) IBs, which are granular, membraneless regions of cytoplasm with liquid organelle-like properties. Additional characterization of bRSV IBs indicated that although they are likely formed by liquid-liquid phase separation (LLPS), they have a differential sensitivity to hypotonic shock proportional to their size. Together, these data identify a novel mechanism for viral antagonism of innate immune signaling which relies on sequestration of the NF-κB subunit p65 to a biomolecular condensate—a mechanism conserved across the *Orthopneumovirus* genus and not host-cell specific. More generally, they provide additional evidence that RNA virus IBs are important immunomodulatory complexes within infected cells.

IMPORTANCE Many viruses replicate almost entirely in the cytoplasm of infected cells; however, how these pathogens are able to compartmentalize their life cycle to provide favorable conditions for replication and to avoid the litany of antiviral detection mechanisms in the cytoplasm remains relatively uncharacterized. In this manuscript, we show that bovine respiratory syncytial virus (bRSV), which infects cattle, does this by generating inclusion bodies in the cytoplasm of infected cells. We confirm that both bRSV and human RSV viral RNA replication takes place in these inclusion bodies, likely meaning these organelles are a functionally conserved feature of this group of viruses (the orthopneumoviruses). Importantly, we also showed that these organelles are able to capture important innate immune transcription factors (in this case NF-KB), blocking the normal signaling processes that tell the nucleus the cell is infected, which may help us to understand how these viruses cause disease.

KEYWORDS innate immunity, LLPS, NF-κB, RSV, inclusion bodies, orthopneumovirus, respiratory syncytial virus, virology

Citation Jobe F, Simpson J, Hawes P, Guzman E, Bailey D. 2020. Respiratory syncytial virus sequesters NF-κB subunit p65 to cytoplasmic inclusion bodies to inhibit innate immune signaling. J Virol 94:e01380-20. https://doi.org/10.1128/JVI.01380-20.

Editor Susana López, Instituto de Biotecnologia/UNAM

Address correspondence to Dalan Bailey, dalan.bailey@pirbright.ac.uk.

* Present address: Efrain Guzman, Oxford Biomedica (UK) Ltd., Oxford, United Kingdom.

Received 15 July 2020
Accepted 28 August 2020
Accepted manuscript posted online 2 September 2020
Published 27 October 2020

Bovine and human respiratory syncytial virus (bRSV and hRSV, respectively) are closely related viruses that cause acute respiratory illness in cattle and humans, respectively. The viruses infect all ages, but severe illness associated with bronchiolitis and pneumonia is more common in calves (for bRSV) and infants, the elderly, and immunocompromised (for hRSV) (1, 2). Although the process is poorly understood, immune responses to RSV infections are incomplete, leading to reinfection, even in healthy adults (3). In high-risk groups, hRSV infection can be fatal; however, there is no approved vaccine and only a single therapeutic option, namely, monoclonal antibodies against the F protein. While there are available bRSV vaccines, they are mildly protective, and there is evidence for an exacerbation of natural infection (4). Both viruses were recently taxonomically reclassified as species *Bovine* and *Human orthopneumovirus* within the *Orthopneumovirus* genus of the *Pneumoviridae* family (5).

bRSV and hRSV are enveloped viruses with a single-stranded negative-sense RNA genome, ~15 kb long, which encodes 11 proteins from 10 mRNAs. Although bRSV and hRSV are restricted to their individual hosts, the viruses and the diseases they cause are similar, making bRSV an excellent model for studying hRSV-host interactions. Virus infection and replication within the cell trigger pattern recognition receptors (PRRs), such as Toll-like receptors (TLRs) and cytoplasmic nucleic acid receptors (RIG-I and MDA5), which in turn induce NF-κB- and IRF-dependent signaling (6–8). NF-κB and IRF are two families of transcription factors that exist as homo- or heterodimers, and their activation is regulated at multiple levels. For example, NF-κB p65/p50 dimers are sequestered in the cytoplasm bound to the inhibitor IκBα (9, 10). Phosphorylation of IκBα by the IκB kinase (IKK) complex targets it for proteasomal degradation releasing p65/p50 for phosphorylation and translocation into the nucleus. Activation and nuclear translocation of IRF-3 homodimers also depend on phosphorylation, through the kinases TBK1/IKKε (11). Upon activation, these critical transcription factors regulate host cell innate responses, e.g., by inducing cytokines with antiviral activity, including type 1 interferons (IFNs), tumor necrosis factor alpha (TNF-α), and interleukin-1 (IL-1). Importantly, the mechanisms by which RSV induce or inhibit these signaling pathways are not fully understood.

To overcome this ubiquitous first line of defense, viruses have evolved various inhibitors to modulate these pathways. Viral immune evasion mechanisms include the targeting of receptors, adaptor proteins, and/or intracellular kinases in the signaling pathways described above or indeed directly targeting the transcription factors and their regulators (12, 13); and in this regard, RSV is no exception. The RSV SH protein has been shown to be involved in inhibiting NF-κB activation (14, 15), although the exact mechanism of this antagonism is yet to be characterized. As an alternative strategy the RSV NS1 and NS2 proteins have been shown to antagonize IFN-mediated host responses by targeting both type I and III IFN induction (16–18) and signaling (19). In addition, NS2 interacts with RIG-I inhibiting its interaction with the mitochondrial antiviral-signaling protein (MAVS) (20). Similarly, NS1 can inhibit phosphorylation of IRF-3 by interacting with MAVS (21). Recently, the NS proteins have also been shown to be involved in the formation of an "NS-degradasome" that promotes the degradation of components of IFN induction or signaling, including RIG-I, IRF-3, IRF-7, TBK1, and STAT2 (22). Consequently, activation of the cytotoxic T lymphocyte component of the adaptive immune response is also suppressed (23). hRSV has also been shown to employ an additional mechanism of innate immune antagonism whereby MAVS and MDA5 are sequestered into inclusion bodies (IBs), likely through interaction with the RSV nucleoprotein (N protein) (24). Other cellular proteins involved in the cellular response to viral infection, such as p38 mitogen-activated protein kinase (MAPK) and O-linked *N*-acetylglucosamine transferase (OGT), have also been shown to be recruited into IBs (25).

The cytoplasmic inclusion bodies induced by hRSV infection share many characteristics with liquid organelles or biomolecular condensates (24–26) having similarity to stress granules, P-bodies, and nucleoli. They are also structurally and functionally similar to viral inclusions formed by rabies, human metapneumovirus, and measles viruses

(27–30) and likely represent an essential component of the life cycle of many negative-sense RNA viruses. The term inclusion bodies is actually quite misleading since this phrase is also widely used in biology to describe misfolded recombinant protein or aggregates. For viral IBs from negative-sense RNA viruses, it will be useful moving forward to either rename these structures or alternatively to define them based on the presence of an identifiable marker. For the pneumoviruses, these membraneless organelles have been shown to contain N, P, L, and M2-1 (26, 29–31), which are viral proteins involved in viral genome replication and mRNA transcription, together with the M protein. The nucleocapsid protein likely represents the most appropriate marker, and therefore, throughout the manuscript when we refer to RSV IBs, we are referring to N-positive inclusions with properties of a biomolecular condensate. Importantly, the presence of viral genomic RNA and mRNA within the IB strongly suggests that these organelles are functional and are the primary site for viral RNA replication within the infected cell (26), although this does not appear to be universal a trend since viral RNA replication of Nipah virus (NiV) was recently shown to occur outside both its structurally distinct IB populations (32). For RSV and related viruses, ectopic coexpression of the N and P proteins alone results in the formation of IB-like structures, indicating a evolutionarily conserved mechanism for IB formation (24, 26, 28, 30, 31). Collectively, these data provide strong evidence that events in the bRSV life cycle are not randomly distributed throughout the cell cytoplasm; instead, components of the viral genome, replication machinery, and its intermediates are likely to be sequestered, away from innate immune sensors, in intracellular compartments which are *de facto* viral replication complexes. However, to date there is no evidence on the formation of IBs in bRSV-infected cells nor, more broadly, any detailed characterization of the immunomodulatory effects of the RSV IB on two integral innate immunity transcription factors, namely, NF-κB and IRF3.

Here, we show that in both hRSV- and bRSV-infected cells, the NF-κB subunit p65 is rapidly sequestered into perinuclear intracytoplasmic puncta. Consequently, activation and nuclear translocation of sequestered NF-κB p65 in response to virus infection and TNF-α stimulation are both inhibited. Using both immunofluorescence confocal microscopy and correlative light electron microscopy (CLEM), these puncta were found to be synonymous with the RSV inclusion bodies induced by virus infection. Transmission electron microscopy confirmed that bRSV IBs are not membrane bound but instead are liquid organelles, likely formed following liquid-liquid phase separation (LLPS). Interestingly, IBs formed by ectopic N and P coexpression were also proficient in colocalizing p65. In addition, p65 recruitment was not host-range specific, with both human and bovine RSV being capable of sequestering p65, regardless of host cell origin. In addition, we present the first detailed evidence of IB formation in bRSV-infected cells, confirming that these viral organelles are the sites of viral RNA replication. Taken together, our data show an evolutionarily conserved mechanism by which RSV IBs function to compartmentalize viral replication and actively antagonize the innate immune response to infection.

RESULTS

bRSV infection induces IRF3, but not NF-κB, nuclear translocation. Given the established role of NF-κB and IRF3 signaling pathways in the cell's innate response and clearance of viral infection, we used multiple approaches to examine the activation of these transcription factors following bRSV infection. Vero cells were infected with bRSV at a multiplicity of infection (MOI) of 1 for 24 h. Cells were then immunostained for bRSV F as a marker for infection as well as for the NF-κB subunit p65 or, separately, IRF3. Immunofluorescence (IF) analysis of mock-infected cells confirmed that both transcription factors are normally located in the cytoplasm (Fig. 1A). When the NF-κB and IRF3 pathways were stimulated in mock-infected cells with agonist treatment [human TNF-α (hTNF-α) and poly(I:C), respectively], both the NF-κB subunit p65 and IRF3 translocated from the cytoplasm to the nucleus, as expected (Fig. 1A, top, inset zooms). However, although infection with bRSV induced similar levels of IRF3 nuclear translocation

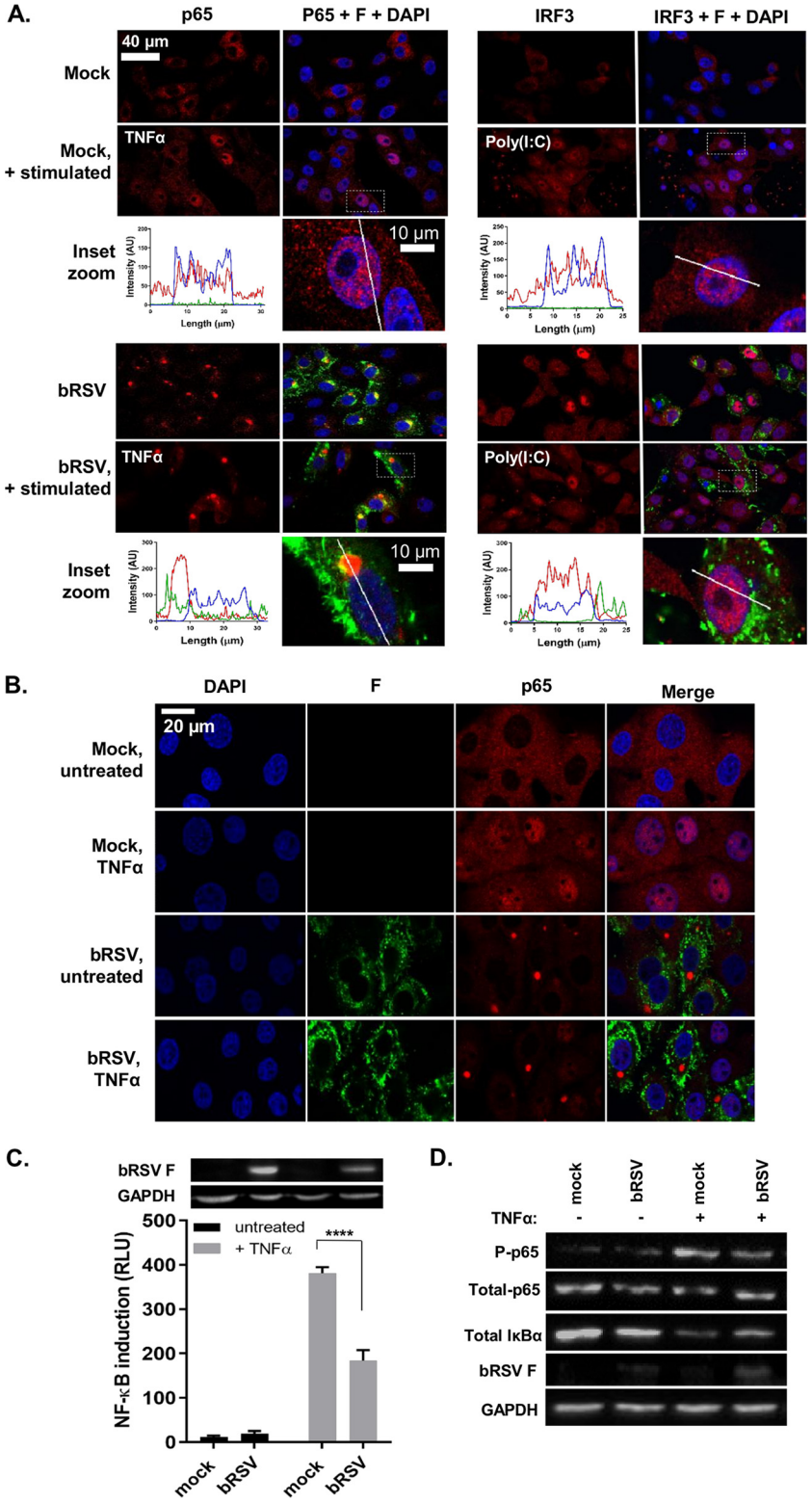

FIG 1 bRSV infection induces IRF3, but not NF-κB, nuclear translocation. (A) Vero cells uninfected (mock) or infected with bRSV at an MOI of 1 for 24 h were left untreated, stimulated with 20 ng/ml hTNF-α for 30 min, or transfected with 2.5 μg/ml poly(I:C) and incubated for 6 h at 37°C. Cells were then fixed and immunostained with anti-RSV F (green) and anti-NF-κB p65 or anti-IRF3 (red) antibodies. Cell nuclei were stained with DAPI (blue) and images obtained using a Leica TCS SP5 confocal microscope. The boxed areas are shown magnified in the panels below (inset zoom). Graphs show fluorescent line intensity profiles along the respective white lines within these inset zooms. (B) NF-κB activation in bRSV-infected MDBK cells. MDBK cells mock infected or infected with bRSV at an MOI of 1 for 24 h were left untreated

(Continued on next page)

(Fig. 1A, bottom right), significantly, the NF-κB subunit p65 remained cytoplasmic, coalescing into intracytoplasmic puncta, mostly perinuclear, and present only in infected cells (Fig. 1A, bottom left). Fluorophore intensity profile analysis was then performed to assess the relative accumulation of both p65 and IRF3 in infected and/or stimulated cells. For IRF3, poly(I:C) stimulation of infected cells enhanced its nuclear translocation, relative to uninfected cells (Fig. 1A, bottom right, inset zoom). However, IF and intensity profile analysis revealed that, even in the case of hTNF-α stimulation, p65 nuclear translocation in bRSV-infected cells was absent and that most p65 remained in the observed perinuclear puncta (Fig. 1A, bottom left, inset zoom). bRSV can infect a broad range of host cells *in vitro*—growing to similar titers in both Vero and Madin-Darby bovine kidney (MDBK) cells (data not shown). To examine the apparent innate immune antagonism in bovine cells, equivalent infections were performed in MDBK cells. These experiments confirmed the same p65 sequestration into perinuclear puncta following bRSV infection, as well as the related insensitivity to TNF-α stimulation (Fig. 1B), indicating a conserved mechanism of antagonism active in both primate and ruminant cells.

To examine the effect of this sequestration on NF-κB signaling, we next employed a luciferase reporter assay to assess NF-κB transactivation. HEK293T cells were infected with bRSV at an MOI of 1, before being transfected with the NF-κB reporter and subsequently treated with or without TNF-α (Fig. 1C). Interestingly, infection without TNF-α treatment did not result in any significant activation of the reporter, despite demonstrable viral protein production (Fig. 1C, black bars and RSV F Western blot), indicating that even in the presence of active viral replication there is little to no activation of the NF-κB signaling pathway in bRSV-infected cells. Indeed, activation of the NF-κB reporter was seen only following the addition of 20 ng/ml of exogenous hTNF-α; however, this activation was significantly less in infected cells than in the mock cells (Fig. 1C, gray bars). Separately, we also examined protein levels of p65 (total and transiently phosphorylated) and IκBα, components of NF-κB signal transduction, in infected Vero cells with and without TNF-α stimulation. As expected, TNF-α treatment of mock-infected cells resulted in an increase in p65 phosphorylation and a decrease in total IκBα (presumably the result of proteasomal degradation following its own phosphorylation) (Fig. 1D, mock −/+ TNF-α) (9). The detected levels of phospho-NF-κB p65 and total IκBα in infected cells (Fig. 1D, infected −/+ TNF-α) confirmed the lack of activation during infection and also the modest NF-κB activation induced by bRSV infection with subsequent TNF-α treatment observed in Fig. 1C. Together, the data strongly suggest that NF-κB signaling is inhibited by bRSV infection due to its sequestration into intracytoplasmic puncta. Importantly, these data also indicate that the sequestered p65 is not in a transcriptionally active state since infection did not result in a marked increase in p65 phosphorylation or demonstrable IκBα degradation.

bRSV replication induces the recruitment of the NF-κB subunit p65 into intracytoplasmic bodies distinct from stress granules. NF-κB p65 puncta were only observed in bRSV-infected cells showing detectable levels of F protein, indicating a correlation between productive infection and sequestration (Fig. 1A). To examine this

FIG 1 Legend (Continued)
or stimulated with 20 ng/ml hTNF-α for 30 min. Cells were then fixed and immunostained with anti-RSV F (green) or anti-NF-κB p65 (red) antibodies. Cell nuclei were stained with DAPI (blue) and images obtained using a Leica TCS SP5 confocal microscope. (C) 293T cells were mock infected or infected with bRSV at an MOI of 1. At 6 h p.i., cells were transfected with 100-ng NF-κB FLuc reporter and 10-ng TK-renilla luciferase and incubated at 37°C. At 18 h posttreatment (p.t.), cells were left untreated or stimulated for 16 h with 20 ng/ml hTNF-α. Cells were then lysed and analyzed for firefly and renilla luciferase activities. Graph depicts means ± SD of three replicates from the same experiment. As controls, the levels of RSV F and glyceraldehyde-3-phosphate dehydrogenase (GAPDH) were analyzed by Western blotting on a fourth replicate. Statistical significance determined by ANOVA as described in the Materials and Methods; ****, $P < 0.0001$. (D) Vero cells mock infected or infected with bRSV at an MOI of 2 for 24 h were left untreated or stimulated with 20 ng/ml hTNF-α for 10 min. Cells were then lysed and analyzed by Western blotting for phosphorylation of p65 using phospho-specific forms of the antibody, total p65, IκBα, and RSV F. GAPDH was detected as a loading control.

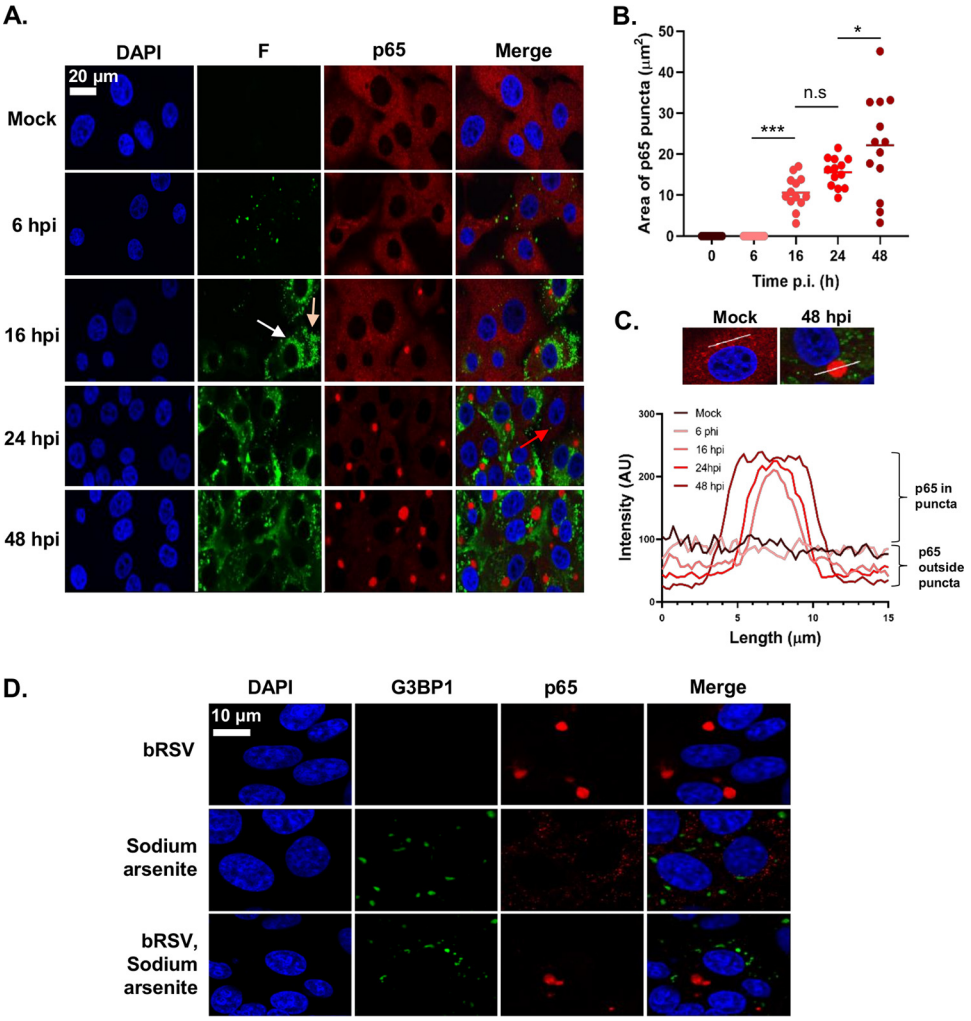

FIG 2 BRSV replication induces the recruitment of the NF-κB subunit p65 into intracytoplasmic bodies distinct from stress granules. (A) MDBK cells were mock infected or infected with bRSV. At the indicated times p.i. cells were fixed and immunostained with anti-RSV F (green) and anti-NF-κB p65 (red) antibodies. Nuclei were stained with DAPI (blue) and images obtained using a Leica TCS SP5 confocal microscope. (B and C) Quantification of p65 puncta in A obtained using the quantify tool of Leica LAS AF Lite software as described in the Materials and Methods. (B) Surface area of 13 p65 puncta per time point and mean area are indicated. Statistical significance determined by ANOVA as described in the Materials and Methods; n.s, nonsignificant; *, $P < 0.05$; ***, $P < 0.001$. (C) Graph showing the line intensity profiles along chosen 15-μm lines of interest (example micrographs: 15 μm drawn across a puncta or across the cytoplasm in mock cells) of an average of five puncta per time point. (D) Vero cells were infected with bRSV or mock infected. At 24 h p.i., cells were treated with 500 μM sodium arsenite or mock treated for 1 h. Cells were then fixed and immunostained with anti-G3BP1 (green) and anti-NF-κB p65 (red) antibodies. Nuclei were stained with DAPI (blue) and images obtained using a Leica TCS SP5 confocal microscope.

correlation and define the kinetics of p65 sequestration over time, MDBK cells were infected at an MOI of 1 and fixed at different times postinfection (p.i.), before being permeabilized and before the distribution of p65 and RSV F was analyzed by IF. Detectable NF-κB p65 puncta (>3 μm²) were apparent in infected cells by 16 h p.i. (Fig. 2B), correlating with significant levels of F expression (Fig. 2A). Interestingly, two populations of F protein were present at this stage, a perinuclear, presumably endoplasmic reticulum (ER)- or vesicle-associated population (Fig. 2A, white arrow) and a peripheral more filamentous-like population, possibly the site of virion biogenesis (Fig. 2A, beige arrow)—neither of which appeared to colocalize in any significant way with p65. By 24 h p.i., all infected cells contained at least one p65 punctum, with none being observed in nearby uninfected cells (Fig. 2A, red arrow). Using fluorophore line of interest analysis, we were also able to assess the ratio of cytoplasmic- to punctum-

localized p65 as well as the increasing diameter of these aggregates. As infection proceeded, the intensity of p65 in the puncta increased as the level of disperse p65 in the cytoplasm decreased (Fig. 2C, "p65 in puncta" versus "p65 outside puncta"), indicating coalescence and supporting our observations in Fig. 1D that the total amount of p65 in cells does not dramatically change during infection, only its subcellular localization. Average punctum size increased as infection progressed, with p65 aggregations at 48 h p.i. having a mean area of 22.18 μm^2 (Fig. 2B). Smaller p65 puncta (<10 μm^2) were also observed at 48 h p.i., most likely the result of nascent infections in nearby cells. By this time, F protein expression was markedly different, with less distinct populations of protein; however, there was still no obvious colocalization with the p65 puncta. A similar pattern of results was also observed in Vero cells (data not shown).

Our first line of inquiry following the identification of p65 puncta in bRSV-infected cells was based on their visual similarity to protein and mRNA aggregations that form in cells in response to cellular stress and viral infections, so-called stress granules (SGs). A wide range of viruses have been shown to either induce or inhibit SG formation to their advantage (33); however, there are contradictory findings on SG induction by RSV (25, 34–36). To examine the potential relationship between these p65 puncta and SG, we induced SG formation in bRSV-infected cells with sodium arsenite treatment and performed coimmunostaining for p65 and G3BP1 (an SG marker) in fixed cells. Although we were able to successfully stimulate the production of SGs in Vero cells, our analysis showed that the p65 puncta were entirely distinct from these granules (Fig. 2D). Tangentially, this experiment also demonstrated that bRSV infection does not significantly induce SG formation.

The NF-κB subunit p65 colocalizes with viral inclusion bodies independently of RSV-encoded immunomodulators. RSV has a relatively small genome, encoding 11 proteins from 10 genes (Fig. 3A). Recent work has demonstrated that hRSV infection induces the formation of inclusion bodies (IBs) which contain components of the RNA polymerase complex and ribonucleoprotein (RNP), notably N and P (26); however, to our knowledge, similar IBs have not been identified, or functionally characterized, in bRSV-infected cells. To examine the presence of IBs, the distribution of bRSV proteins, and, collectively, their subcellular localization in relation to the observed p65 puncta, we infected Vero cells and fixed them, along with mock-infected cells, for IF analysis at 24 h p.i. These cells were then coimmunostained for p65 and bRSV N, P, M, or F proteins. As expected, neither p65 puncta nor bRSV proteins were detected in mock-infected cells (Fig. 3B). Similarly, as described in Fig. 1 and 2, RSV F did not colocalize with p65 or show evidence of subcellular localization with IB-like structures. In contrast, in infected cells, three of the viral proteins (N, P, and M) predominately localized to large intracytoplasmic organelles, characteristic of viral inclusion bodies (Fig. 3B, green panels), although smaller, spherical N-positive IBs were also present (see below). Although there was a various degree of cytoplasmic signal for N, P, and M outside the IBs, most of the IF signal was found within these structures (Fig. 3B, zoomed inset and line of interest plots). The sub-IB localization of bRSV N and P was similar to that previously described for hRSV, with N and P being found on the periphery of the organelle (26). The significant intra-IB localization of the M protein at 24 h p.i., as well as its partial nuclear localization, is consistent with previously reported IF in RSV-infected cells (37, 38). However, the role of M in RNA virus IBs reflects an interesting point of divergence; with some viral IBs being M positive (e.g., RSV) and others negative (e.g., rabies) (39). Significantly, the larger N-, P-, or M-positive IBs were, in the majority of cases, also p65 positive (Fig. 3B, red IF panels) identifying, for the first time, that this NF-κB component was being recruited to RSV inclusion bodies in infected cells. To examine this in detail, we next characterized the number, size, and p65 status of N-positive IBs in infected cells, observing that they were numerous and mostly localized in the median section of the cell. We therefore obtained images from multiple planes in this section to assemble max intensity z-stacks to aid quantification. From 16 h p.i., N- and p65-positive IBs were evident throughout the cell in a conserved pattern

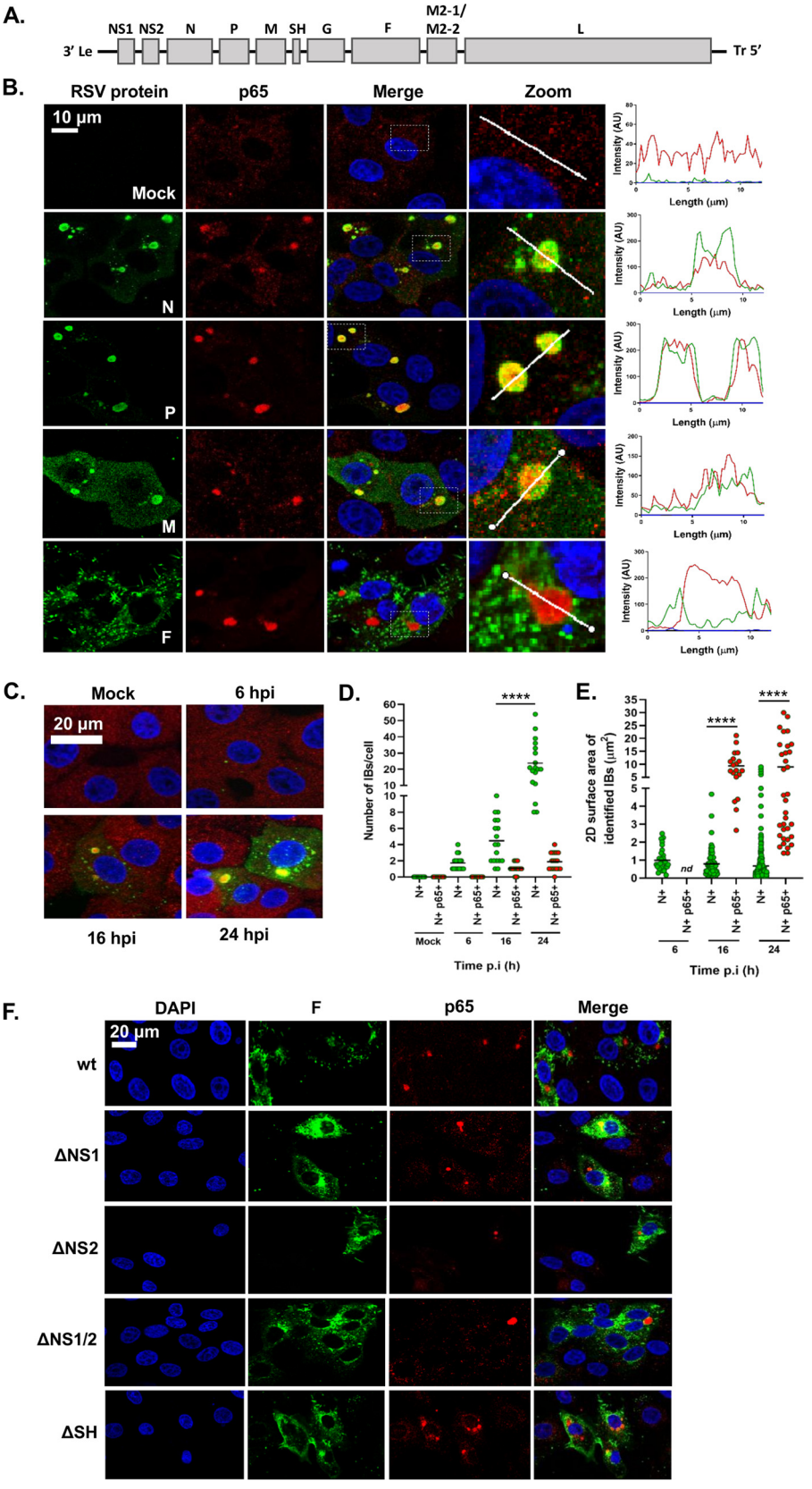

FIG 3 The NF-κB subunit p65 colocalizes with viral inclusion bodies independently of RSV-encoded immunomodulators. (A) Schematic depiction of the bRSV genome showing organization of the encoded genes. (B) Vero cells, mock infected or infected with bRSV for 24 h, were fixed and immunostained with

(Continued on next page)

consisting of a single, large, and perinuclear IB with multiple smaller inclusions more evenly distributed through the cytoplasm (Fig. 3C; see Videos S1 and S2 in the supplemental material). Using z-stacks, we quantified the number per cell (counting 18 cells per sample, per time point) and surface area of N- and/or p65-positive structures of >0.1 μm^2, observing them both increasing as infection progressed. The average number of IBs of >0.1 μm^2 grew from 1.7 per cell at 6 h p.i. to 23.8 at 24 h p.i. (Fig. 3D). Their mean area also increased to 8.99 μm^2 by 24 h p.i. (Fig. 3E), significantly influenced by the presence and growth of the larger IB. p65-positive IBs were detected from 16 h p.i.; however, p65 was only detected in larger IBs (>1.39 μm^2) (Fig. 3E) with up to 4 of them being evident per cell (Fig. 3D). In conclusion, although multiple N-positive IBs are present in infected cells, it is predominantly the larger IBs which contain the sequestered p65. Together, these data suggest that bRSV infection induces the formation of IBs in the cytoplasm of infected cells, which are organelles also involved in sequestering cellular proteins to effect immunomodulation. To our knowledge, this represents an entirely novel mechanism of viral inhibition of NF-κB signaling since it is the sequestration of signaling components to a viral organelle, rather than the degradation commonly seen (12, 22), which leads to the innate immune antagonism described in Fig. 1.

We next examined whether the established bRSV-encoded immunomodulatory proteins NS1, NS2 (18), and SH (14, 15) are responsible for this p65 sequestration. We infected cells with wild-type (wt) bRSV or recombinant bRSVs which do not express these proteins (ΔNS1, ΔNS2, ΔNS1/2 [a double knockout], or ΔSH) (15, 40). IF analysis of these samples identified p65 puncta in all infected cells (Fig. 3F), suggesting that these bRSV-encoded immunoantagonists do not play a significant role in either the formation of IBs or the sequestration of p65 to these structures.

bRSV IBs are sites of RNA replication, but p65 does not specifically colocalize with M2-1 or nascent viral RNA in IBAGs. hRSV inclusion bodies have previously been shown to be the sites of virus transcription and replication (25, 26, 41). To confirm bRSV IBs are also the site of viral RNA replication, we carried out nascent RNA labeling using 5-ethynyl-uridine (5EU) incorporation. Mock-infected MDBK cells, incubated with 5EU for 1 h, revealed, as expected, 5EU incorporation into cellular RNA in the nucleus (Fig. 4A, top row). When cellular transcription was inhibited following preincubation of mock-infected cells with actinomycin D (Act D) for 1 h, this signal was lost. 5EU labeling performed on bRSV-infected cells without Act D treatment did not reveal significant evidence for viral replication in IBs, perhaps due to overrepresentation of cellular RNA synthesis. However, in the presence of Act D, labeled, newly synthesized RNA could only be seen in the N-positive IBs, presumably the result of viral replication. This colocalization of 5EU incorporation and N protein within IBs provides strong evidence that bRSV IBs are the sites of viral RNA replication. A more detailed look at the IBs (Fig. 4A, inset zoom and line of interest plot—asterisks) revealed partial sub-IB organization to the RNA within these structures. Interestingly, a recent study on hRSV IBs identified similar functional compartments within IBs termed inclusion body-associated granules (IBAGs) (26). They were shown to concentrate newly synthesized viral mRNA and the

FIG 3 Legend (Continued)
rabbit anti-NF-κB p65 (red) and mouse monoclonal anti-RSV N, P, M, or F antibodies (green). Nuclei were stained with DAPI (blue) and images obtained using a Leica TCS SP5 confocal microscope. Zoom panel shows magnification of IBs boxed in the merge panel. Graphs shows fluorescent intensity profiles along the indicated white lines drawn across one or two IBs. (C) MDBK cells were mock infected or infected with bRSV. At the indicated times p.i., cells were fixed and immunostained with anti-RSV N (green) and anti-NF-κB p65 (red) antibodies. Images are max intensity Z-stacks of 8 planes 0.5 μm apart. Cytoplasmic bodies (area, >0.1 μm^2) from the Z-stacks were quantified in a total of 18 infected cells per time point as detailed in the Materials and Methods. (D) Number of N- and N- and p65-positive bodies per cell at the indicated time points. (E) Surface area of identified N- and N- and p65-positive IBs. Statistical significance determined by ANOVA as described in the Materials and Methods; ****, $P < 0.0001$. (F) Vero cells were infected with wt bRSV, ΔNS1, ΔNS2, ΔNS1ΔNS2, or ΔSH bRSV. At 24 h p.i., cells were fixed and immunostained with rabbit anti-NF-κB p65 (red) and mouse anti-RSV F (green) antibodies. Cell nuclei were stained with DAPI (blue) and images obtained using a Leica TCS SP5 confocal microscope.

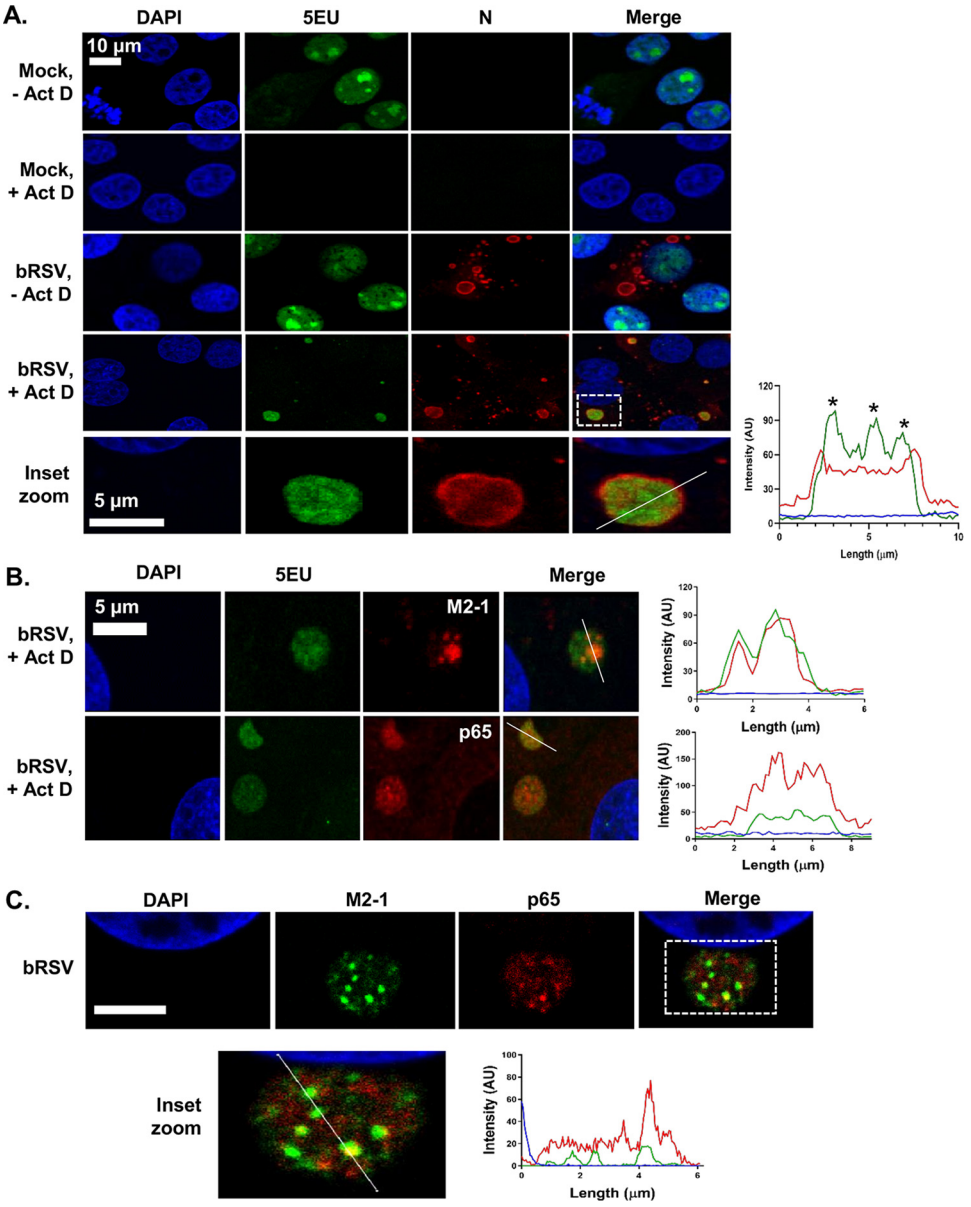

FIG 4 bRSV IBs are sites of RNA replication, but p65 does not specifically colocalize with M2-1 or nascent viral RNA in IB-associated granules (IBAGs). **(A** and **B)** MDBK cells were mock infected or infected with bRSV. After 24 h, cells were incubated with vehicle or 20 μg/ml actinomycin D (Act D) for 1 h to inhibit cellular transcription. 5-Ethynyl uridine (5EU) was then added for another 1 h and the cells fixed. 5EU incorporated into newly synthesized RNA was detected using Alexa Fluor 488-azide (green) as described in the Materials and Methods. Cells were then immunostained with anti-RSV N, M2-1, or anti-NF-κB p65 antibodies (red). Cell nuclei were stained with DAPI (blue) and images obtained using a Leica TCS SP5 confocal microscope. Bottom of A (inset zoom) shows the boxed area (in merge of bRSV, +Act D) magnified. Graphs show fluorescent intensity profiles along the indicated white lines drawn across the IBs. Asterisks in A indicate areas of increased 5EU staining within the IB. (C) Vero cells infected with bRSV for 24 h were fixed and immunostained with rabbit anti-NF-κB p65 (red) and mouse anti-M2-1 (green) antibodies. Cell nuclei were stained with DAPI (blue) and images obtained using a Leica TCS SP5 confocal microscope. Bottom image shows a higher magnification of the boxed area; scale bar corresponds to 4 μm. Graphs show fluorescent intensity profiles along the indicated white line.

viral M2-1 protein but not genomic RNA or the N, P, and L proteins. To confirm the presence of IBAGs in bRSV IBs, we immunostained bRSV-infected cells for M2-1 following nascent viral RNA labeling, observing colocalization of both these components (Fig. 4B). The intra-IB organization of RNA replication and M2-1 protein into IBAGs appears, therefore, to be a structurally conserved aspect of orthopneumovirus IBs. We next examined the potential colocalization of p65 with these sites of nascent viral RNA

(vRNA) localization (IBAGs). Although we observed partial sub-IB localization signals for p65, this did not always colocalize with vRNA (Fig. 4B) or, in subsequent experiments, M2-1 (Fig. 4C). These findings suggest that there are multiple subcompartments within bRSV IBs, in addition to IBAGs, which potentially carry out a distinct range of functions.

bRSV IBs are membraneless liquid organelles. IBs and IB-like structures form by liquid-liquid phase separation (LLPS) which favors macromolecule-macromolecule over macromolecule-water interactions (42–44). The resulting biomolecular condensates are not surrounded or compartmentalized by a membrane, distinguishing them from many other organelles found in the cytoplasm (44, 45). To examine the ultrastructural properties of the bRSV IBs, we first performed standard transmission electron microscopy (TEM) of infected cells. Vero cells were infected with bRSV at an MOI of 1 and fixed for TEM analysis at 24 and 48 h p.i. Granular structures with high electron density, characteristic of RNA virus inclusion bodies, were identified at both time points, often in close proximity to the nucleus (Fig. 5A). Smaller structures (1 to 2 μm in diameter) were predominately rounder in nature than their larger ($>$3 μm in diameter), more pleomorphic counterparts (Fig. 5A). As expected, these structures were not membrane bound or directly associated with subcellular organelles; however, rough endoplasmic reticulum (RER) and mitochondria were frequently found in close proximity (Fig. 5A). These structures are similar to those previously reported for other RNA viruses (28, 39), supporting our conclusion that bRSV also forms membraneless IBs in infected cells.

Various reports have also demonstrated that IBs can rapidly change their size due to fusion or fission while remaining spherical in nature, a characteristic feature of these liquid organelles (42). Rabies virus inclusion bodies, termed negri bodies, have been shown to rapidly dissolve and reform in response to hypotonic shock, demonstrating the dynamic nature of these structures (27, 28, 46). To assess the sensitivity of bRSV IBs to hypotonic shock, Vero cells, infected with bRSV for 24 h, were incubated with Dulbecco's modified Eagle's medium (DMEM; diluted to 20% in H_2O) for 20 min. Cells were then fixed and immunostained for the N protein. Many of the smaller spherical IBs showed evidence of dissolution following hypotonic shock (Fig. 5B, iv); however, unlike rabies virus negri bodies, the larger bRSV IBs remained intact following this significant period of cellular osmotic shock (Fig. 5B, iii). Of note, incubation beyond 20 min was not possible because of the associated cytotoxicity. In addition, a large percentage of the sequestered p65 in these larger IBs remained tightly associated with the intact structure (Fig. 5C). Recently, Zhou et al., demonstrated that larger measles IBs had lower rates of fluorescence recovery after photobleaching (FRAP) than that of their smaller counterparts, postulating that these structures had acquired a more gel-like property. The acquisition of this gel-like status, which is also less likely to exchange molecules with the surrounding cytoplasm, has been linked to aging of phase-separated organelles—a continuum which ends with the formation of irreversible aggregates (47). The insensitivity of large bRSV IBs to osmotic shock, and the maintenance of p65 within the IB even under these harsh conditions, is perhaps the result of them acquiring gel-like status, a property which may be linked to the age and size of individual IBs within infected cells.

Finally, to examine the sub-IB localization of RSV N and p65 in relation to our ultrastructural analysis of IBs, we performed correlative light electron microscopy (CLEM). Vero cells were infected at an MOI of 1 and analyzed at 24 and 48 h p.i., first by confocal microscopy using N and p65 antibodies to immunolabel these proteins (Fig. 5D). The same cells, identified by grid reference, were then isolated, embedded, and sectioned with their ultrastructure subsequently analyzed by TEM. Importantly, these CLEM data confirmed that the electron dense granular structures seen by TEM (Fig. 5A) are synonymous with the N, P, M, and p65 stained IBs seen in IF microscopy (Fig. 3B). To our knowledge, this is the first CLEM to be performed on an RNA virus IB. An overlay of the two images confirmed that bRSV IBs had retained the electron-dense granular structure characteristic of liquid organelles, even with the chemical permeabilization required for IF antibody labeling (Fig. 5C). Our CLEM data also confirmed the

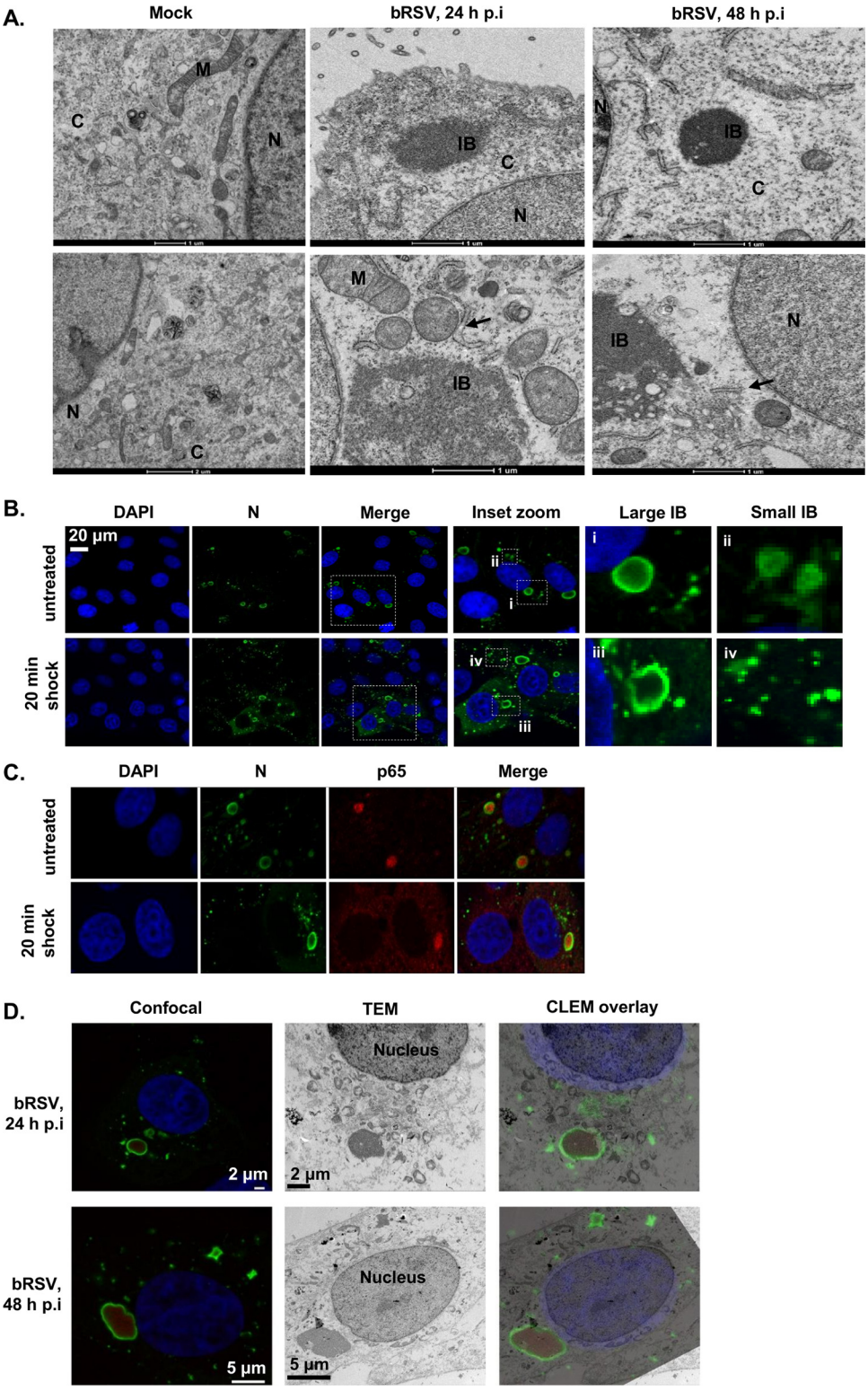

FIG 5 bRSV IBs are membraneless liquid organelles. (A) High-power transmission electron microscopy (TEM) of mock- or bRSV-infected Vero cells fixed in glutaraldehyde at 24 and 48 h p.i and prepared for TEM as detailed in the Materials and Methods. N, nucleus; M, mitochondria; C, cytoplasm; IB, inclusion body; ER is indicated with black arrow. Two representative images are shown per time point. Scale bars correspond to 1 μm. (B and C) Vero cells were infected with bRSV at an MOI of 1 and incubated at 37°C for 24 h. Hypotonic shock was applied for 20 min before the cells were fixed. Confocal analysis was performed following immunostaining for bRSV N (green) and nucleus stained with DAPI (and also p65 for C). Inset zooms demonstrate the observed effects of hypotonic shock on large (i and iii) and small (ii and iv) IBs—representative images shown. (D) Correlative light electron microscopy

(Continued on next page)

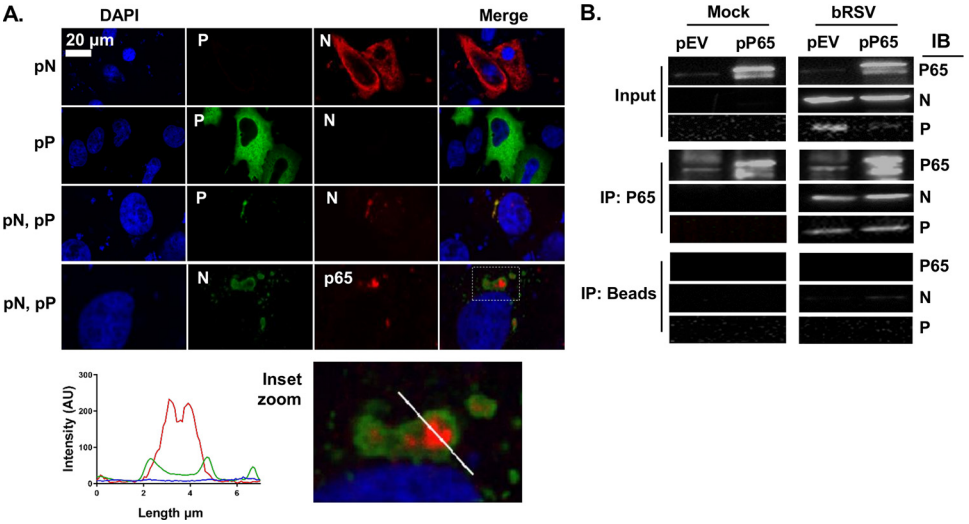

FIG 6 Coexpression of bRSV N and P proteins induces the formation of IB-like structures which can sequester p65. (A) Vero cells were cotransfected with equimolar concentrations of plasmids expressing bRSV N (pN) and/or P (pP) proteins as indicated. Following 24 h of incubation, cells were fixed and stained with anti-RSV N (green/red) and anti-RSV P (green) or anti-NF-κB p65 (red) antibodies. Bottom image shows a higher magnification of the boxed area. Graph shows fluorescent intensity profiles along the indicated white line. (B) Coimmunoprecipitation of p65. 293T cells were transfected with plasmids expressing NF-κB p65 (pP65) or empty vector (pEV) and 6 h later infected with bRSV at an MOI of 1. At 24 h p.i., cell lysates were immunoprecipitated (IP) with anti-p65 antibody or beads alone as a control. Pulldowns were analyzed by SDS-PAGE and immunoblotting (IB) using anti-p65, anti-N, or anti-P antibodies.

p65 and N proteins localizing to the IB, with p65 present within the structure and N around the periphery. At 24 h p.i., the p65-positive IB structures were mostly spherical, becoming larger and more irregularly shaped by 48 h p.i., possibly as a result of transition into a more gel-like status, as discussed above. A similar pattern of immunostaining and IB morphology was also observed in bRSV-infected MDBK cells analyzed by CLEM (data not shown).

Coexpression of bRSV N and P proteins induces the formation of IB-like structures which can sequester p65. In the absence of infection, ectopic coexpression of many *Mononegavirales* N and P proteins has been shown to result in the formation of IB-like structures (24, 26, 28, 30)—a finding which has been linked to their potential to induce LLPS independently of viral infection. Although there has been broad discussion that this is related to the presence of intrinsically disordered regions within the N and P proteins, a definitive functional mechanism for this viral-induced LLPS remains uncharacterized. In addition, whether these infection-independent IB-like structures retain all the properties of viral IBs is not entirely clear. For hRSV, it was shown that IBAGs do not form within these visually orthologous bodies (26); however, the recruitment of MDA5 and MAVS to IB-like structures, following N and P overexpression, was maintained (24). To address similar questions for bRSV IBs and to examine the related sequestration of p65, Vero cells transiently transfected with plasmids expressing bRSV N (pN) and bRSV P (pP) were fixed and stained at 24 h posttransfection and examined by IF. As has been reported previously, the expression of N or P alone did not lead to the formation of IB-like structures; however, coexpression did, resulting in the formation of inclusions up to 6.9 μm^2 in area (Fig. 6A). Examination of the subcellular localization of p65 in this system also confirmed that the N- and P-induced inclusions were proficient in sequestering p65, independent of viral replication, with a

FIG 5 Legend (Continued)
(CLEM) of confocal microscopy immunostaining and TEM showing bRSV IBs. Vero cells infected with bRSV at an MOI of 1 were fixed at 24 or 48 h p.i., stained with antibodies against RSV N (green) and NF-κB p65 (red) and nuclei stained with DAPI. Following confocal imaging, cells were fixed in glutaraldehyde, sectioned, and visualized by TEM. Confocal (left) and TEM (middle) images of the same cells were overlaid (right) as CLEM images.

pattern of expression mirroring that seen in infected cells (Fig. 6A, inset zoom and fluorescent line of interest analysis).

To examine the mechanism of p65 recruitment to, and sequestration within, the bRSV IB, we next investigated whether there was evidence for direct protein-protein interactions between this protein and N or P. Endogenous p65 or p65 expressed from a plasmid (pP65) were immunoprecipitated from bRSV-infected or mock-infected 293T cells (at 24 h p.i.) using an anti-p65 antibody. When these immunoprecipitates were analyzed by Western blot, both bRSV N and P were found to coimmunoprecipitate (co-IP) with endogenous or overexpressed p65 in infected cell lysates, providing evidence of direct interactions being maintained postlysis (Fig. 6B). Experiments with beads alone did show a small amount of co-IP N protein; however, this amount was markedly lower than that in the p65 antibody experiment and may be background signal which we believe may be the consequence of the high levels of N protein in infected cells at 24 h p.i. In summary, our results indicate that p65 recruitment into bRSV IBs is maintained even in IB-like structures formed after N and P overexpression. Furthermore, the recruitment of p65 to IBs is likely due to specific interactions with the N and/or P proteins. Since RSV N and P are known to interact and yet the IB does not form without both proteins being expressed together, it is technically challenging to define the true binding partner, either N or P. As a result, more detailed characterization of this interaction is required to elucidate the mechanism of p65 sequestration.

The sequestration of the NF-κB subunit p65 to cytoplasmic IBs is a conserved mechanism of orthopneumovirus immunomodulation. Having established structural and functional similarity between bRSV and hRSV IBs, we finally examined the regulation and subcellular localization of the NF-κB subunit p65 in hRSV-infected cells. Beginning with the NF-κB luciferase reporter assay, we uncovered a pattern of signaling inhibition similar to bRSV. Infection with hRSV in the presence of the NF-κB reporter did not lead to robust activation compared with mock-infected cells, highlighting a lack of activation of this pathway in infected cells (Fig. 7A, black bars). Again, similar to bRSV, infected 293T cells (24 h with hRSV) which were stimulated for 6 h with hTNF-α induced significantly less NF-κB transactivation, compared with equivalently treated mock-infected cells (Fig. 7A, gray bars). This finding correlated well with an examination, by IF, of hRSV replication in Vero cells, with and without hTNF-α treatment, where again we did not observe significant levels of p65 nuclear translocation (Fig. 7B). Indeed, as observed in bRSV-infected cells, p65 was recruited into intracytoplasmic puncta. These puncta were subsequently shown to be synonymous with viral IBs (Fig. 7C) in a set of experiments which also confirmed that IB formation and the recruitment of p65 is host cell independent. bRSV- or hRSV-infected MDBK (bovine) or Hep2 (human) cells demonstrated the presence of p65-containing IBs in all scenarios, highlighting that the mechanisms underpinning RSV IB formation, and the sequestration of p65 to these bodies, are likely highly conserved (Fig. 7C). We concluded this examination of host-range specificity with a more physiologically relevant model of the human bronchial epithelium, BEAS-2B cells, which are derived from normal human tissues taken following autopsy of noncancerous individuals, identifying again the formation of IBs and sequestration of p65, regardless of RSV species. Finally, we confirmed that IB-like structures formed by ectopic hRSV N and P coexpression recruited p65 to their core (Fig. 7D). Taken together, these data indicate that the formation of IBs during viral replication, together with the sequestration of the transcription factor NF-κB subunit p65 to these bodies, is a common feature of orthopneumoviruses.

DISCUSSION

Recognition of viral pathogen-associated molecular patterns (PAMPs) by RIG-I or MDA5 can lead to activation of NF-κB transcription factors through the IKK complex or IRFs through TBK-1/IKKε (9, 11, 48). Activation of these innate responses is essential for inducing a robust adaptive response, first to clear viral infections and second to elicit the establishment of a memory response (4, 48). However, *in vivo*, the various immune-evasion strategies employed by RSV combine to generate only a short-lived response

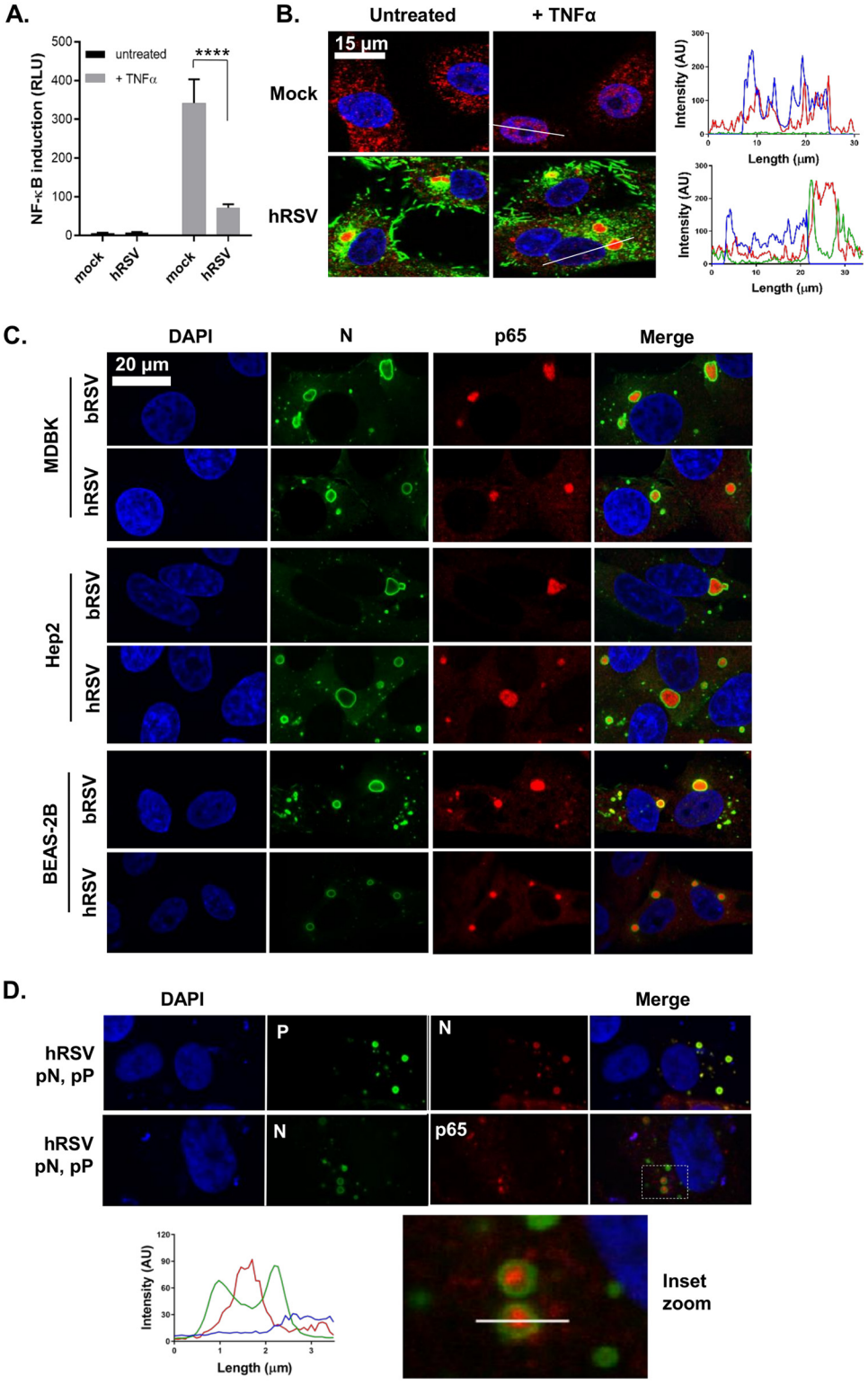

FIG 7 The sequestration of the NF-κB subunit p65 to cytoplasmic IBs is a conserved mechanism of orthopneumovirus immunomodulation. (A) 293T cells were mock-infected or infected with hRSV at an MOI of 1. At 6 h p.i., cells were transfected with 100-ng NF-κB FLuc reporter and 10-ng TK-renilla luciferase and incubated at 37°C. At 18 h p.t., cells were left untreated or stimulated for 16 h with 20 ng/ml hTNF-α. Cells were then lysed and analyzed for firefly and renilla luciferase activities. Graph depicts means ± SD of three replicates from the same experiment. Statistical significance determined by ANOVA as described in the Materials and Methods; ****, $P < 0.0001$. (B) Vero cells mock infected or infected with hRSV at an MOI of 1 for 24 h were left untreated or stimulated with 20 ng/ml hTNF-α for 30 min. Cells were then fixed and immunostained with anti-RSV F (green) or anti-NF-κB p65 (red) antibodies. Cell

(Continued on next page)

(4, 19, 20, 23, 48). For instance, there is strong evidence that the downregulation of key signaling molecules by the NS proteins suppresses IRF3 activation and type I IFN induction (17–20, 22, 23), although interestingly, we did see significant IRF3 nuclear translocation in our infected cells. As a key innate immune pathway, NF-κB signaling is often a target for viral antagonism; however, to date, RSV modulation of its activation has remained less well defined. Although RSV lacking the *SH* gene was shown to enhance NF-κB activation, the exact mechanisms employed are unclear (14, 15, 49, 50). To address this, we monitored NF-κB p65 activation in RSV-infected cells at multiple steps in the signaling pathway, namely, IκBα degradation, p65 phosphorylation (at Ser536), p65 nuclear translocation, and more broadly NF-κB transactivation. We present a novel mechanism of immune evasion wherein RSV infection results in the sequestration of the NF-κB subunit p65 into viral inclusion bodies (Fig. 3B), a process which is independent of the known RSV immunomodulatory proteins NS1, NS2, and SH (Fig. 3F) and was confirmed in BEAS-2B bronchial epithelial cells for both hRSV and bRSV. The possibility that there is mechanistic redundancy between the RSV NS1, NS2, and SH accessory proteins cannot however be excluded at this time. We also demonstrate that as a result, activation of NF-κB p65 is suppressed in infected cells, even with exogenous TNF-α stimulation (Fig. 1). Although small IBs were observed as early as 6 h p.i. ($\leq$2.5 μm^2), they did not colocalize with detectable levels of p65 (Fig. 3E). This may reflect a technical limitation of our IF or alternatively that IBs need to grow in size before they can begin to sequester p65. It remains to be determined if p65 is actively recruited to IBs by viral proteins or if its sequestration is a result of the IB's position in the cell and that it captures p65 by an indirect mechanism, perhaps involving trafficking. In addition, it is currently not clear what proportion of the IB-sequestered p65 is IκBα associated, the elucidation of which might explain the partial protection of IκBα from degradation seen following TNF-α treatment (Fig. 1D, mock versus bRSV +TNF-α). Interestingly, the lack of p65 activation prior to IB formation and p65 aggregation highlights that RSV may employ additional mechanisms for NF-κB inhibition which remain uncharacterized. Other groups have reported more robust activation of NF-κB in response to RSV infection (7, 51, 52) which could indicate that the cell line and viral strain play a role in RSV-mediated NF-κB activation. This being said, the sequestration of p65 appears to be an orthopneumovirus-conserved strategy active in physiologically relevant cells, such as BEAS-2Bs. From a wider perspective, this mechanism of immunomodulation might be a common strategy utilized by RSV and other viruses that induce IB formation. MAVS and MDA5 were similarly both found to be recruited into RSV IBs as a mechanism of suppressing IFN signaling (24). Similarly, p38 MAPK and OGT sequestration into RSV IBs suppressed MAPK-activated protein kinase 2 signaling and stress granule formation, respectively, enhancing virus replication (25). Whether viruses such as Ebola, Nipah, or rabies adopt similar mechanisms of immunomodulation remains to be determined.

From a mechanistic perspective, our results also showed that the N and P proteins are essential for the formation of bRSV IBs. As has been reported for rabies (28) and measles (30) viruses, ectopic expression of these proteins resulted in the formation of IB-like structures (Fig. 6A and 7D). They were mostly spherical and, at 24 h posttransfection, measured up to 6.9 μm^2 which is considerably less than that of the conventional IBs observed in infected cells. We hypothesize that both pseudo-IBs and viral IBs form by biomolecular condensation but that their maturation into larger structures is

FIG 7 Legend (Continued)
nuclei were stained with DAPI (blue) and images obtained using a Leica TCS SP5 confocal microscope. Graphs show line fluorescent intensity profiles along the indicated white lines. (C) MDBK, Hep2, and BEAS-2B cells were infected with b/hRSV for 24 h, fixed, and immunostained for RSV N (green) or NF-κB p65 (red). (D) Vero cells were cotransfected with equimolar concentrations of plasmids expressing hRSV N (pN) and/or P (pP) proteins as indicated. Following 24 h of incubation, cells were fixed and stained with anti-RSV N (green/red) and anti-RSV P (green) or anti-NF-κB p65 (red) antibodies. Cell nuclei were stained with DAPI (blue) and confocal analysis performed. The bottom image shows a higher magnification of the boxed area, and the graph shows the fluorescent intensity profiles along the indicated white line.

dependent on other factors present only in infected cells. That these pseudo-IBs could also recruit p65 suggested a direct interaction between p65 and RSV N or P, which we confirmed by co-IP (Fig. 6B). Interestingly, our IF data were somewhat contradictory, with the staining patterns and line intensity profiles showing p65 concentrated in the middle of IBs with N and P at the periphery, separating the IB contents from the cytoplasm. It is possible that the exchange of biomolecules across the boundary, e.g., during the sequestration of p65, may require transient N or P interactions. Intriguingly, Lifland et al. also suggested that MAVS and MDA5 are recruited into IBs by interacting with N and P in a macromolecular complex (24). We propose that this recruitment may involve low-affinity interactions with N and/or P and that maintenance within the IB is enhanced by the same physicochemical properties of the IBs which enable them to induce LLPS, namely, macromolecule-macromolecule interactions. The RSV P protein has been shown to bind and recruit M2-1 to IBs, potentially through intrinsically disordered regions within P that allow it to form multiple interactions (53). Although further work is required to identify the exact mechanism of p65, MAVS, and MDA5 recruitment into IBs, we postulate that the physicochemical properties of these proteins may also be an important factor. Of note, in order to definitively identify the bRSV IBs as liquid organelles, fluorescence recovery after photobleaching (FRAP) experiments could be performed to assess the acquisition of tagged N or P over time. In addition, the fusion and fission of these organelles could be monitored in real time. Both of these experimental approaches are areas of continued investigation in our laboratory; however, the dissolution of the smaller IBs in response to hypotonic shock still provides strong evidence for the LLPS nature of these structures (Fig. 5B). The stability of larger IBs to extended periods of hypotonic shock was surprising—a finding we attribute to the larger IBs gaining hydrogel- or even aggregate-like status. This might also explain the loss of their spherical nature, as the biophysical constraints on this organelle might be relaxed by this transition.

Electron micrograph analysis of our RSV IBs showed greater electron density in the IBs than in the cytoplasm, a characteristic of biomolecular condensates (Fig. 5A). These data also highlighted the structural complexity of the phase-separated structure. Although we observed some association with the ER and RER, RSV IBs were not membrane bound, unlike rabies virus negri bodies which acquire a membrane boundary later in infection, presumably derived from the ER (28, 39). Interestingly, our CLEM analysis confirmed previous IF data from the field that the IB boundary is surrounded by N protein (Fig. 5D). A debate remains in the field as to whether this is an artifact of disrupted antibody epitope accessibility to N since GFP-tagged N proteins were shown to have a diffuse pattern throughout the IB (24); however, we would only note that we used an antibody developed in-house for this staining. Nevertheless, the presence of viral RNA-associated proteins N, P, and M2-1 in IBs (Fig. 3B and 4C) strongly suggested the presence of RNA replication and transcription within these structures. Building on previous work for hRSV and rabies virus (26, 39), we used 5EU incorporation to confirm RNA synthesis in the IBs (Fig. 4A and B). Using fluorescence *in situ* hybridization (FISH) experiments, Rincheval et al. showed that genomic RNA colocalized with the hRSV N and P proteins at the periphery, while viral mRNA was found to concentrate in IBAGs, transient sites of mRNA storage (26). Our data showed the formation of similar structures, confirming IBAGs are found in multiple orthopneumoviruses; however, there was no conclusive colocalization with p65. However, this sequestered cellular protein did localize to distinct intra-IB bodies (Fig. 4B and C), raising the intriguing possibility that multiple microdomains exist within what is, by TEM, an apparently uniform granular biomolecular condensate.

In summary, our data show that RSV IBs are highly ordered structures performing multiple roles in the virus life cycle, including the compartmentalization of virus replication and transcription and the sequestration of cellular proteins involved in the antiviral response. This mechanistic characterization is potentially applicable to other negative-sense RNA viruses that have been shown to form IBs during replication.

MATERIALS AND METHODS

Cells and viruses. All cells were cultured at 37°C in a 5% CO_2 atmosphere. Madin-Darby bovine kidney (MDBK), Vero (monkey kidney epithelial), 293T (human embryonic kidney), and Hep-2 (human epithelial type 2) cells were obtained from the Pirbright Institute Central Services Unit and maintained in Dulbecco's modified Eagle's medium (DMEM) supplemented with 10% heat-inactivated fetal calf serum (FCS; TCS Biologicals), sodium pyruvate (Gibco), and penicillin and streptomycin (Sigma). Beas-2B (human bronchial epithelial) cells (ATCC) were cultured in LHC basal medium (ThermoFisher) supplemented with 10% FCS, penicillin, and streptomycin.

Wild-type recombinant bRSV (rbRSV) and deletion mutant rbRSVs ΔSH, ΔNS1, ΔNS2, and ΔNS1/2 were produced by reverse genetics from rbRSV strain A51908 variant Atue51908 (GenBank accession no. AF092942) (18, 40, 54). They were propagated in Vero cells and hRSV subtype A (A2 strain) grown in Hep-2 cells. All viruses were further purified from total cell lysates using polyethylene glycol (molecular weight, 8,000) precipitation and discontinuous sucrose gradient centrifugation.

Plasmids and transfections. All viral gene sequences were derived from bRSV A51908 (GenBank accession no. NC_038272) and hRSV A2 (GenBank accession no. KT992094). Expression plasmids (pcDNA3.1) encoding codon-optimized *N* genes at KpnI-BamHI sites referred to as pN were purchased from Bio Basic Inc. Full-length *P* genes were amplified by reverse transcriptase PCR using gene-specific primers and Superscript II reverse transcriptase (Invitrogen). They were then cloned into pcDNA3.1 at KpnI-BamHI sites and designated pP. The p65 open reading frame (ORF) was amplified from pcDNA3.1-HA-p65 (kindly provided by Carlos Maluquer de Motes, University of Surrey), inserted at the HindIII-BamHI sites of pcDNA3.1, and designated pP65. All sequences were confirmed by conventional sanger sequencing. Plasmids were transfected into cells using TransIT-X2 (Geneflow).

Antibodies and drugs. Mouse monoclonal antibodies raised against bRSV F (mAb19), N (mAb89), P (mAb12), M (mAb105), and M2-1 (mAb91) were previously described (55, 56). The rabbit polyclonal anti-bRSV SH antibody was purchased from Ingenasa. Rabbit anti-NF-κB p65 (8242) antibody, rabbit anti-IRF3 (11904), rabbit anti-phospho-NF-κB p65 (Ser536; 3033), mouse anti-IκBα (4814), and rabbit anti-GAPDH (5174) were obtained from Cell Signaling Technology (CST). Mouse anti-G3BP-1 was obtained from BD Biosciences. Secondary horseradish peroxidase-linked antibodies were obtained from CST and Alexa Fluor secondary antibodies from Life Technologies. Recombinant hTNF-α (CST), poly(I:C) (InvivoGen), sodium arsenite (Sigma), and actinomycin D (Sigma) were purchased from the indicated suppliers.

Confocal immunofluorescence microscopy. Cells were fixed with 4% paraformaldehyde (PFA; Sigma) in PBS for 15 min, permeabilized with 0.2% Triton X-100 in PBS for 5 min, and blocked with 0.5% bovine serum albumin (BSA) (Sigma) in PBS. Cells were then incubated with the indicated primary antibodies overnight at 4°C. They were then washed and incubated with Alexa Fluor secondary antibodies (Life Technologies) for 1 h at room temperature. Cells were then washed and mounted with Vectashield (Vector labs) containing 4′,6-diamidino-2-phenylindole (DAPI) for nuclei staining. Fluorescence was imaged on a Leica TCS SP5 confocal microscope using 405-nm, 488-nm, and 568-nm laser lines for the appropriate dyes and a 63× oil immersion objective.

Quantitation of bRSV-induced p65 puncta and IBs. Mock- or bRSV-infected (at an MOI of 1) MDBK cells were fixed in 4% PFA (Sigma) at 6, 16, and 24 h p.i. and labeled according to the described immunofluorescence method. Multiple Z-sections, 0.5 μm apart, were taken for each cell, by confocal microscopy and max intensity Z-stacks of 8 planes made using the Leica LAS AF Lite software. Quantifications of N- and p65-positive structures were performed using the area region of interest analysis tool. GraphPad Prism 7 was used to perform parametric one-way analysis of variance (ANOVA) and Tukey's multiple comparison tests. ImageJ was also used to make 3D projections of 9 images 0.9 μm apart.

Luciferase reporter assay. A total of 2×10^5 293T cells seeded onto 24-well plates a day prior were mock infected or infected with bRSV or hRSV at an MOI of 1. A total of 6 h later, cells were cotransfected with a 100-ng NF-κB FLuc reporter which expresses the firefly luciferase gene under the control of five NF-κB repeated transcription factor binding sites and 10-ng TK-ren control plasmid (both kindly provided by Gareth Brady; The University of Dublin) using Transit-X2 (Geneflow). A total of 24 hours later, cells were stimulated with 20 ng/ml hTNF-α for 16 hours or were left untreated. Cells were then lysed with reporter lysis buffer (Promega), and lysates were used to determine firefly and renilla luciferase activities on a Glomax luminometer using the luciferase assay system (Promega) and coeleterazine (Promega), respectively. Firefly data were normalized to renilla which was used as an internal control of transfection. GraphPad Prism 7 was used to perform parametric one-way analysis of variance (ANOVA) and Tukey's multiple comparison tests.

Western blot analysis. Following virus infection and stimulation, growth medium was removed from cells and cell extracts prepared by lysis in SDS sample buffer (Bio-Rad) supplemented with β-mercaptoethanol (Sigma), complete mini-EDTA-free protease inhibitors (Roche), and 1 mM sodium orthovanadate (New England BioLabs). Lysates were then boiled for 5 min and 30 μl resolved by SDS-PAGE on a 12% polyacrylamide gel and proteins transferred to polyvinylidene difluoride (PVDF) membranes (ThermoScientific). After being blocked for 1 h with 5% dry semiskimmed milk in 0.1% PBS Tween 20 (PBS-T), membranes were washed with PBS-T and incubated with primary antibodies overnight at 4°C. After being washed, the membranes were incubated with the corresponding horseradish peroxidase-conjugated secondary antibodies (CST). Protein bands were detected using Clarity Western ECL substrate (Bio-Rad) and imaged with the Bio-Rad ChemiDoc MP imaging system.

5-Ethynyl uridine labeling. Infected cells growing on coverslips were incubated with or without medium supplemented with 20 μg/ml actinomycin D (Act D) to inhibit cellular transcription for 1 h. Cells

were then incubated with medium containing 1 mM 5EU and 20 μg/ml Act D for another hour. Medium was then washed off and cells fixed in 4% PFA for 15 min. Cells were then washed with PBS and permeabilized with 0.2% Triton X-100 for 5 min. They were both supplemented with 0.125 U/ml RNase inhibitor (Promega). Incorporated 5EU was labeled using the Click-IT RNA imaging kit (Invitrogen) following the manufacturer's protocol. Following that step, immunofluorescence staining was done as described above.

Transmission electron microscopy. Cells seeded onto Thermanox coverslips (Thermo Scientific) were fixed at 24 h and 48 h p.i in phosphate-buffered 2% glutaraldehyde (Agar Scientific) for 1 hour followed by 1 hour in aqueous 1% osmium tetroxide (Agar Scientific). We performed the following dehydration steps in an ethanol series: 70% for 30 min, 90% for 15 min, and 100% three times for 10 min. Then, a transitional step of 10 min in propylene oxide (Agar Scientific) was undertaken before infiltration with a 50:50 mix of propylene oxide and epoxy resin (Agar Scientific) for 1 hour. After a final infiltration of 100% epoxy resin for 1 hour, the samples were embedded and polymerized overnight at 60°C. Next, 80-μm-thin sections were cut, collected onto copper grids (Agar Scientific), and grid stained using Leica EM AC20 before being imaged at 100 kV in a FEI Tecnai 12 TEM with a TVIPS F214 digital camera.

Correlative light electron microscopy. Cells seeded onto gridded glass coverslips (MatTek) were fixed at 24 h and 48 h p.i in 4% PFA (Sigma) and labeled according to the described immunofluorescence method. Selected grid squares were imaged on a Leica TCS SP8 confocal microscope using 405-nm, 488-nm, and 568-nm laser lines for the appropriate dyes. The cells were then fixed in phosphate-buffered 2% glutaraldehyde (Agar Scientific) for 1 hour followed by 1 hour in aqueous 1% osmium tetroxide (Agar Scientific). Following 15 min in 3% uranyl acetate (Agar Scientific), the cells were dehydrated in an ethanol series, as follows: 70% for 30 min, 90% for 15 min, and 100% three times for 10 min. After infiltration of 100% epoxy resin for 2 hours, the samples were embedded and polymerized overnight at 60°C. The glass coverslips were removed with liquid nitrogen and the appropriate grid squares located. Next, 80-μm-thin sections were cut, collected onto copper grids (Agar Scientific), and grid stained using a Leica EM AC20 instrument. The specific cells imaged in the confocal were identified and imaged at 100 kV in a FEI Tecnai 12 TEM with a TVIPS F214 digital camera.

Coimmunoprecipitation. A total of 1×10^5 293T cells cultured overnight in 12-well plates were transfected with pcDNA3.1-empty vector (pEV) or pcDNA3.1-p65 (pP65) using the TransIT-X2 reagent (Geneflow). After 24 h, cells were infected with bRSV at an MOI of 1 or mock infected and incubated for another 24 h. Cells were then lysed on ice with radioimmunoprecipitation assay (RIPA) lysis buffer (EMB Millipore) and cell debris removed by centrifugation. Cell lysates precleared with protein A-coated magnetic beads (CST) were incubated with rabbit anti-p65 antibodies overnight at 4°C. Lysates were then incubated with protein A-coated magnetic beads for 20 min at room temperature with rotation. Following five washes with PBS-T, immunoprecipitates were eluted with Laemmli sample buffer and subjected to SDS-PAGE and Western blot analysis as already described.

Ethics statement. This research did not use any primary human or animal tissue. BEAS-2B cells were procured from ATCC.

SUPPLEMENTAL MATERIAL

Supplemental material is available online only.

SUPPLEMENTAL FILE 1, AVI file, 0.3 MB.

SUPPLEMENTAL FILE 2, AVI file, 1.4 MB.

SUPPLEMENTAL FILE 3, PDF file, 0.01 MB.

ACKNOWLEDGMENTS

This work was supported by a UK Research and Innovation (UKRI; www.ukri.org) Medical Research Council (MRC) New Investigator Research Grant to D.B. (MR/P021735/1) as well as a UKRI Biotechnology and Biological Sciences Research Council (BBSRC; www.ukri.org) Institute Strategic Program Grant (ISPG) to The Pirbright Institute and D.B. (BBS/E/I/00007034 and BBS/E/I/00007030). The funders had no role in study design, data collection and analysis, decision to publish, or preparation of the manuscript.

We acknowledge the support of Geraldine Taylor (The Pirbright Institute), Ursula Buchholz (NIAID, NIH), Karl-Klaus Conzelmann (Max-von-Pettenkofer Institut), Andrew Broadbent (The Pirbright Institute), Gareth Brady (Trinity College, Dublin, Ireland), Carlos Maluquer de Motes (University of Surrey), and Helena Maier (The Pirbright Institute) for the provision of valuable reagents, recombinant viruses, and technical advice.

F.J. performed all experiments, apart from the EM and CLEM which were performed by J.S. and P.H. E.G. was involved in training F.J. F.J. and D.B. analyzed the data, designed the experiments, compiled the figures, and wrote the manuscript.

REFERENCES

1. Hogan AB, Glass K, Moore HC, Anderssen RS. 2016. Exploring the dynamics of respiratory syncytial virus (RSV) transmission in children. Theor Popul Biol 110:78–85. https://doi.org/10.1016/j.tpb.2016.04.003.
2. Falsey AR, Hennessey PA, Formica MA, Cox C, Walsh EE. 2005. Respiratory syncytial virus infection in elderly and high-risk adults. N Engl J Med 352:1749–1759. https://doi.org/10.1056/NEJMoa043951.
3. Habibi MS, Jozwik A, Makris S, Dunning J, Paras A, Mechanisms of Severe Acute Influenza Consortium Investigators, DeVincenzo JP, de Haan CAM, Wrammert J, Openshaw PJM, Chiu C. 2015. Impaired antibody-mediated protection and defective IgA B-cell memory in experimental infection of adults with respiratory syncytial virus. Am J Respir Crit Care Med 191:1040–1049. https://doi.org/10.1164/rccm.201412-2256OC.
4. Guzman E, Taylor G. 2015. Immunology of bovine respiratory syncytial virus in calves. Mol Immunol 66:48–56. https://doi.org/10.1016/j.molimm.2014.12.004.
5. Amarasinghe GK, Bào Y, Basler CF, Bavari S, Beer M, Bejerman N, Blasdell KR, Bochnowski A, Briese T, Bukreyev A, Calisher CH, Chandran K, Collins PL, Dietzgen RG, Dolnik O, Dürrwald R, Dye JM, Easton AJ, Ebihara H, Fang Q, Formenty P, Fouchier RAM, Ghedin E, Harding RM, Hewson R, Higgins CM, Hong J, Horie M, James AP, Jiāng D, Kobinger GP, Kondo H, Kurath G, Lamb RA, Lee B, Leroy EM, Li M, Maisner A, Mühlberger E, Netesov SV, Nowotny N, Patterson JL, Payne SL, Paweska JT, Pearson MN, Randall RE, Revill PA, Rima BK, Rota P, Rubbenstroth D, Schwellme M, Smither SJ, Song Q, Stone DM, Takada A, Terregino C, Tesh RB, Tomonaga K, Tordo N, Towner JS, Vasilakis N, Volchknov VE, Wahl-Jensen V, Walker PJ, Wang B, Wang D, Wang F, Wang L-F, Werren JH, Whitfield AE, Yan Z, Ye G, Kuhn JH. 2017. Taxonomy of the order Mononegavirales: update 2017. Arch Virol 162:2493–2504. https://doi.org/10.1007/s00705-017-3311-7.
6. Liu P, Jamaluddin M, Li K, Garofalo RP, Casola A, Brasier AR. 2007. Retinoic acid-inducible gene I mediates early antiviral response and Toll-like receptor 3 expression in respiratory syncytial virus-infected airway epithelial cells. J Virol 81:1401–1411. https://doi.org/10.1128/JVI.01740-06.
7. Yoboua F, Martel A, Duval A, Mukawera E, Grandvaux N. 2010. Respiratory syncytial virus-mediated NF-kappa B p65 phosphorylation at serine 536 is dependent on RIG-I, TRAF6, and IKK beta. J Virol 84:7267–7277. https://doi.org/10.1128/JVI.00142-10.
8. Baum A, García-Sastre A. 2010. Induction of type I interferon by RNA viruses: cellular receptors and their substrates. Amino Acids 38:1283–1299. https://doi.org/10.1007/s00726-009-0374-0.
9. Mitchell S, Vargas J, Hoffmann A. 2016. Signaling via the NFkappaB system. Wiley Interdiscip Rev Syst Biol Med 8:227–241. https://doi.org/10.1002/wsbm.1331.
10. Kanarek N, Ben-Neriah Y. 2012. Regulation of NF-kappaB by ubiquitination and degradation of the IkappaBs. Immunol Rev 246:77–94. https://doi.org/10.1111/j.1600-065X.2012.01098.x.
11. Hemmi H, Takeuchi O, Sato S, Yamamoto M, Kaisho T, Sanjo H, Kawai T, Hoshino K, Takeda K, Akira S. 2004. The roles of two IkappaB kinase-related kinases in lipopolysaccharide and double stranded RNA signaling and viral infection. J Exp Med 199:1641–1650. https://doi.org/10.1084/jem.20040520.
12. Deng L, Zeng Q, Wang M, Cheng A, Jia R, Chen S, Zhu D, Liu M, Yang Q, Wu Y, Zhao X, Zhang S, Liu Y, Yu Y, Zhang L, Chen X. 2018. Suppression of NF-kappaB activity: a viral immune evasion mechanism. Viruses 10:409. https://doi.org/10.3390/v10080409.
13. Chiang H-S, Liu HM. 2018. The molecular basis of viral inhibition of IRF- and STAT-Dependent immune responses. Front Immunol 9:3086. https://doi.org/10.3389/fimmu.2018.03086.
14. Pollock N, Taylor G, Jobe F, Guzman E. 2017. Modulation of the transcription factor NF-kappaB in antigen-presenting cells by bovine respiratory syncytial virus small hydrophobic protein. J Gen Virol 98:1587–1599. https://doi.org/10.1099/jgv.0.000855.
15. Taylor G, Wyld S, Valarcher J-F, Guzman E, Thom M, Widdison S, Buchholz UJ. 2014. Recombinant bovine respiratory syncytial virus with deletion of the SH gene induces increased apoptosis and pro-inflammatory cytokines in vitro, and is attenuated and induces protective immunity in calves. J Gen Virol 95:1244–1254. https://doi.org/10.1099/vir.0.064931-0.
16. Spann KM, Tran KC, Chi B, Rabin RL, Collins PL. 2004. Suppression of the induction of alpha, beta, and lambda interferons by the NS1 and NS2 proteins of human respiratory syncytial virus in human epithelial cells and macrophages. J Virol 78:4363–4369. https://doi.org/10.1128/jvi.78.8.4363-4369.2004.
17. Spann KM, Tran KC, Collins PL. 2005. Effects of nonstructural proteins NS1 and NS2 of human respiratory syncytial virus on interferon regulatory factor 3, NF-kappaB, and proinflammatory cytokines. J Virol 79:5353–5362. https://doi.org/10.1128/JVI.79.9.5353-5362.2005.
18. Schlender J, Bossert B, Buchholz U, Conzelmann KK. 2000. Bovine respiratory syncytial virus nonstructural proteins NS1 and NS2 cooperatively antagonize alpha/beta interferon-induced antiviral response. J Virol 74:8234–8242. https://doi.org/10.1128/jvi.74.18.8234-8242.2000.
19. Lo MS, Brazas RM, Holtzman MJ. 2005. Respiratory syncytial virus nonstructural proteins NS1 and NS2 mediate inhibition of Stat2 expression and alpha/beta interferon responsiveness. J Virol 79:9315–9319. https://doi.org/10.1128/JVI.79.14.9315-9319.2005.
20. Ling Z, Tran KC, Teng MN. 2009. Human respiratory syncytial virus nonstructural protein NS2 antagonizes the activation of beta interferon transcription by interacting with RIG-I. J Virol 83:3734–3742. https://doi.org/10.1128/JVI.02434-08.
21. Boyapalle S, Wong T, Garay J, Teng M, San Juan-Vergara H, Mohapatra S, Mohapatra S. 2012. Respiratory syncytial virus NS1 protein colocalizes with mitochondrial antiviral signaling protein MAVS following infection. PLoS One 7:e29386. https://doi.org/10.1371/journal.pone.0029386.
22. Goswami R, Majumdar T, Dhar J, Chattopadhyay S, Bandyopadhyay SK, Verbovetskaya V, Sen GC, Barik S. 2013. Viral degradasome hijacks mitochondria to suppress innate immunity. Cell Res 23:1025–1042. https://doi.org/10.1038/cr.2013.98.
23. Kotelkin A, Belyakov IM, Yang L, Berzofsky JA, Collins PL, Bukreyev A. 2006. The NS2 protein of human respiratory syncytial virus suppresses the cytotoxic T-cell response as a consequence of suppressing the type I interferon response. J Virol 80:5958–5967. https://doi.org/10.1128/JVI.00181-06.
24. Lifland AW, Jung J, Alonas E, Zurla C, Crowe JE, Jr, Santangelo PJ. 2012. Human respiratory syncytial virus nucleoprotein and inclusion bodies antagonize the innate immune response mediated by MDA5 and MAVS. J Virol 86:8245–8258. https://doi.org/10.1128/JVI.00215-12.
25. Fricke J, Koo LY, Brown CR, Collins PL. 2013. p38 and OGT sequestration into viral inclusion bodies in cells infected with human respiratory syncytial virus suppresses MK2 activities and stress granule assembly. J Virol 87:1333–1347. https://doi.org/10.1128/JVI.02263-12.
26. Rincheval V, Lelek M, Gault E, Bouillier C, Sitterlin D, Blouquit-Laye S, Galloux M, Zimmer C, Eleouet JF, Rameix-Welti MA. 2017. Functional organization of cytoplasmic inclusion bodies in cells infected by respiratory syncytial virus. Nat Commun 8:563. https://doi.org/10.1038/s41467-017-00655-9.
27. Nikolic J, Civas A, Lama Z, Lagaudriere-Gesbert C, Blondel D. 2016. Rabies virus infection induces the formation of stress granules closely connected to the viral factories. PLoS Pathog 12:e1005942. https://doi.org/10.1371/journal.ppat.1005942.
28. Nikolic J, Le Bars R, Lama Z, Scrima N, Lagaudriere-Gesbert C, Gaudin Y, Blondel D. 2017. Negri bodies are viral factories with properties of liquid organelles. Nat Commun 8:58. https://doi.org/10.1038/s41467-017-00102-9.
29. Cifuentes-Muñoz N, Branttie J, Slaughter KB, Dutch RE. 2017. Human metapneumovirus induces formation of inclusion bodies for efficient genome replication and transcription. J Virol 91:e01282-17. https://doi.org/10.1128/JVI.01282-17.
30. Zhou Y, Su JM, Samuel CE, Ma D. 2019. Measles virus forms inclusion bodies with properties of liquid organelles. J Virol 93:e00948-19. https://doi.org/10.1128/JVI.00948-19.
31. Garcia J, Garcia-Barreno B, Vivo A, Melero JA. 1993. Cytoplasmic inclusions of respiratory syncytial virus-infected cells: formation of inclusion bodies in transfected cells that coexpress the nucleoprotein, the phosphoprotein, and the 22K protein. Virology 195:243–247. https://doi.org/10.1006/viro.1993.1366.
32. Ringel M, Heiner A, Behner L, Halwe S, Sauerhering L, Becker N, Dietzel E, Sawatsky B, Kolesnikova L, Maisner A. 2019. Nipah virus induces two inclusion body populations: identification of novel inclusions at the plasma membrane. PLoS Pathog 15:e1007733. https://doi.org/10.1371/journal.ppat.1007733.
33. White JP, Lloyd RE. 2012. Regulation of stress granules in virus systems. Trends Microbiol 20:175–183. https://doi.org/10.1016/j.tim.2012.02.001.
34. Lindquist ME, Lifland AW, Utley TJ, Santangelo PJ, Crowe JE, Jr. 2010.

Respiratory syncytial virus induces host RNA stress granules to facilitate viral replication. J Virol 84:12274–12284. https://doi.org/10.1128/JVI.00260-10.
35. Hanley LL, McGivern DR, Teng MN, Djang R, Collins PL, Fearns R. 2010. Roles of the respiratory syncytial virus trailer region: effects of mutations on genome production and stress granule formation. Virology 406:241–252. https://doi.org/10.1016/j.virol.2010.07.006.
36. Lindquist ME, Mainou BA, Dermody TS, Crowe JE, Jr. 2011. Activation of protein kinase R is required for induction of stress granules by respiratory syncytial virus but dispensable for viral replication. Virology 413:103–110. https://doi.org/10.1016/j.virol.2011.02.009.
37. Ghildyal R, Mills J, Murray M, Vardaxis N, Meanger J. 2002. Respiratory syncytial virus matrix protein associates with nucleocapsids in infected cells. J Gen Virol 83:753–757. https://doi.org/10.1099/0022-1317-83-4-753.
38. Shahriari S, Wei KJ, Ghildyal R. 2018. Respiratory syncytial virus matrix (M) protein interacts with actin in vitro and in cell culture. Viruses 10:535. https://doi.org/10.3390/v10100535.
39. Lahaye X, Vidy A, Pomier C, Obiang L, Harper F, Gaudin Y, Blondel D. 2009. Functional characterization of Negri bodies (NBs) in rabies virus-infected cells: evidence that NBs are sites of viral transcription and replication. J Virol 83:7948–7958. https://doi.org/10.1128/JVI.00554-09.
40. Buchholz UJ, Finke S, Conzelmann KK. 1999. Generation of bovine respiratory syncytial virus (BRSV) from cDNA: BRSV NS2 is not essential for virus replication in tissue culture, and the human RSV leader region acts as a functional BRSV genome promoter. J Virol 73:251–259. https://doi.org/10.1128/JVI.73.1.251-259.1999.
41. Carromeu C, Simabuco FM, Tamura RE, Farinha Arcieri LE, Ventura AM. 2007. Intracellular localization of human respiratory syncytial virus L protein. Arch Virol 152:2259–2263. https://doi.org/10.1007/s00705-007-1048-4.
42. Alberti S, Gladfelter A, Mittag T. 2019. Considerations and challenges in studying liquid-liquid phase separation and biomolecular condensates. Cell 176:419–434. https://doi.org/10.1016/j.cell.2018.12.035.
43. Murthy AC, Fawzi NL. 2020. The (un)structural biology of biomolecular liquid-liquid phase separation using NMR spectroscopy. J Biol Chem 295:2375–2384. https://doi.org/10.1074/jbc.REV119.009847.
44. Mudogo CN, Falke S, Brognaro H, Duszenko M, Betzel C. 2020. Protein phase separation and determinants of in cell crystallization. Traffic 21:220–230. https://doi.org/10.1111/tra.12711.
45. Perez-Pepe M, Fernandez-Alvarez AJ, Boccaccio GL. 2018. Life and work of stress granules and processing bodies: new insights into their formation and function. Biochemistry 57:2488–2498. https://doi.org/10.1021/acs.biochem.8b00025.
46. Nikolic J, Lagaudriere-Gesbert C, Scrima N, Blondel D, Gaudin Y. 2018. [Rabies virus factories are formed by liquid-liquid phase separation]. Med Sci (Paris) 34:203–205. https://doi.org/10.1051/medsci/20183403004.
47. Shin Y, Berry J, Pannucci N, Haataja MP, Toettcher JE, Brangwynne CP. 2017. Spatiotemporal control of intracellular phase transitions using light-activated optoDroplets. Cell 168:159–171.e14. https://doi.org/10.1016/j.cell.2016.11.054.
48. Sun Y, Lopez CB. 2017. The innate immune response to RSV: advances in our understanding of critical viral and host factors. Vaccine 35:481–488. https://doi.org/10.1016/j.vaccine.2016.09.030.
49. Russell RF, McDonald JU, Ivanova M, Zhong Z, Bukreyev A, Tregoning JS. 2015. Partial attenuation of respiratory syncytial virus with a deletion of a small hydrophobic gene is associated with elevated interleukin-1beta responses. J Virol 89:8974–8981. https://doi.org/10.1128/JVI.01070-15.
50. Fuentes S, Tran KC, Luthra P, Teng MN, He B. 2007. Function of the respiratory syncytial virus small hydrophobic protein. J Virol 81:8361–8366. https://doi.org/10.1128/JVI.02717-06.
51. Bitko V, Garmon NE, Cao T, Estrada B, Oakes JE, Lausch RN, Barik S. 2004. Activation of cytokines and NF-kappa B in corneal epithelial cells infected by respiratory syncytial virus: potential relevance in ocular inflammation and respiratory infection. BMC Microbiol 4:28. https://doi.org/10.1186/1471-2180-4-28.
52. Carpenter LR, Moy JN, Roebuck KA. 2002. Respiratory syncytial virus and TNF alpha induction of chemokine gene expression involves differential activation of Rel A and NF-kappa B1. BMC Infect Dis 2:5. https://doi.org/10.1186/1471-2334-2-5.
53. Richard CA, Rincheval V, Lassoued S, Fix J, Cardone C, Esneau C, Nekhai S, Galloux M, Rameix-Welti MA, Sizun C, Eleouet JF. 2018. RSV hijacks cellular protein phosphatase 1 to regulate M2-1 phosphorylation and viral transcription. PLoS Pathog 14:e1006920. https://doi.org/10.1371/journal.ppat.1006920.
54. Karger A, Schmidt U, Buchholz UJ. 2001. Recombinant bovine respiratory syncytial virus with deletions of the G or SH genes: G and F proteins bind heparin. J Gen Virol 82:631–640. https://doi.org/10.1099/0022-1317-82-3-631.
55. Taylor G, Stott EJ, Bew M, Fernie BF, Cote PJ, Collins AP, Hughes M, Jebbett J. 1984. Monoclonal antibodies protect against respiratory syncytial virus infection in mice. Immunology 52:137–142.
56. Taylor G, Stott EJ, Furze J, Ford J, Sopp P. 1992. Protective epitopes on the fusion protein of respiratory syncytial virus recognized by murine and bovine monoclonal antibodies. J Gen Virol 73:2217–2223. https://doi.org/10.1099/0022-1317-73-9-2217.